Cell type specific complex formation of key transcription factors regulates stem cell homeostasis in the root of *Arabidopsis thaliana*

Inaugural-Dissertation

Zur Erlangung des Doktorgrades der

Mathematisch-Naturwissenschaftlichen Fakultät der

Heinrich-Heine-Universität Düsseldorf

vorgelegt von

Vivien Ingeborg Strotmann

aus Greven (Westfalen)

Düsseldorf, April 2024

Aus dem Institut für Entwicklungsgenetik der
Heinrich-Heine-Universität Düsseldorf

Gedruckt mit der Genehmigung der
Mathematisch-Naturwissenschaftlichen Fakultät der
Heinrich-Heine-Universität Düsseldorf

Berichterstatter:

1. Prof. Dr. Yvonne Stahl
2. Prof. Dr. Rüdiger Simon

Tag der mündlichen Prüfung: 10.07.2024

Eidesstattliche Erklärung zur Dissertation mit dem Titel:

Cell type specific complex formation of key transcription factors regulates stem cell homeostasis in the root of *Arabidopsis thaliana*

Ich versichere an Eides Statt, dass diese Dissertation von mir selbstständig und ohne unzulässige fremde Hilfe unter Beachtung der „Grundsätze zur Sicherung guter wissenschaftlicher Praxis an der Heinrich-Heine-Universität Düsseldorf“ erstellt worden ist.

Außerdem versichere ich, dass ich diese Dissertation nur in diesem und keinem anderen Promotionsverfahren eingereicht habe und dass diesem Promotionsverfahren kein gescheitertes Promotionsverfahren vorausgegangen ist.

Ort, Datum Unterschrift

Content

Preface

In this dissertation novel aspects of the intricate interplay of the key transcription factors (TFs) BRASSINOSTEROID AT VASCULAR AND ORGANIZING CENTRE (BRAVO), PLETHORA 3 (PLT3) and WUSCHEL-RELATED HOMEOBOX 5 (WOX5) in the regulation of stem cell quiescence and replenishment in the root of *Arabidopsis thaliana* (*A. thaliana*) are uncovered. The main body of this thesis consists of five publications and one submitted manuscript. First, three reviews provide a comprehensive introduction about the relevant topics discussed in the subsequent research articles, which comprises the second part of this dissertation.

1. **Review: At the root of quiescence: function and regulation of the quiescent center**

   Vivien I. Strotmann and Yvonne Stahl

Higher plants harbour a pool of rarely dividing stem cells, termed the quiescent center (QC), within the root apical meristem (RAM), which is located at the root tip. The QC maintains the surrounding more frequently dividing initials, that together form the stem cell niche (SCN). The initials, following numerous rounds of division and differentiation, give rise to nearly all tissues of the root. Hence, QC establishment, maintenance, and function are crucial for the development of the whole root system, which is fundamental to plant growth and productivity. Although the concept of the QC has been known for many years, much of its molecular regulations and intricate connections remain elusive. In *A. thaliana*, many different molecular factors such as phytohormones, small signaling peptides and their receptors, as well as key TFs, interact in a complex and intertwined regulatory network to maintain the QC. The first publication of this dissertation provides an overview about molecular factors that contribute to the fine-tuned regulation of QC maintenance in the *Arabidopsis* root.

2. **Review: Unlocking nature's (sub)cellular symphony: Phase separation in plant meristems**

   Ali Eljebbawi, Anika Dolata, Vivien I. Strotmann and Yvonne Stahl

The balance of stem cell maintenance and differentiation in the root meristem not only involves the interplay of many different molecular factors, but also depends on dynamic compartmentalization strategies which includes liquid-liquid phase separation (LLPS), allowing the formation of membrane-less compartments. In this part of the dissertation, significant findings about the emerging research field of LLPS in the plant meristems are reviewed.

3. Review: Visualization of *in vivo* protein-protein interactions in plants

Vivien I. Strotmann and Yvonne Stahl

Molecular processes, such as the regulation of stem cell balance, often depend on the collaborative and dynamic interaction of proteins. This includes the assembly of two proteins of interest (POI), whether identical or different, as well as the formation of larger protein complexes that can consist of a multitude of different proteins. Precise (subcellular-) localization, as well as protein concentration and timing are crucial to specifically trigger the correct downstream processes. Understanding these complex regulatory mechanisms *in vivo* requires preservation of the spatio-temporal information of the POIs. In this publication, methods to detect protein-protein-interactions (PPIs) in plants are summarized, particularly emphasizing *in vivo* fluorescent microscopy imaging techniques. Here, the unique characteristics of these methods are described and benefits and potential pitfalls are discussed.

4. Research article: *One Pattern Analysis* (*OPA*) for the quantitative determination of protein interactions in plant cells

Jan E. Maika, Benedikt Krämer, Vivien I. Strotmann, Frank Wellmer, Stefanie Weidtkamp-Peters, Yvonne Stahl and Rüdiger Simon

In this publication, a novel fitting routine for quantitative Förster resonance energy transfer fluorescence lifetime imaging microscopy (FRET-FLIM) data is established, termed ‘One Pattern Analysis’ (OPA). While deciphering differences in protein affinities and complex dynamics is trivial for monoexponentially decaying donor fluorophores, OPA, for the first time, offers this practicability for multi-exponentially-decaying donors. As a proof of principle, the hetero- and homomerization potential of several MADS-domain TFs crucial for flower development in *A. thaliana* are reassessed.

5. **Research article: PLETHORA-WOX5 interaction and subnuclear localization control *Arabidopsis* root stem cell maintenance**
   Rebecca C Burkart, Vivien I. Strotmann, Gwendolyn K. Kirschner, Abdullah Akinci, Laura Czempik, Anika Dolata, Alexis Maizel, Stefanie Weidtkamp-Peters and Yvonne Stahl

In the following publication the joint function of the auxin-regulated TFs PLT3 and WOX5 in the regulation of root stem cell maintenance is described. The use of fluorescent reporters uncovers their mutual transcriptional regulation, and phenotypic analysis of several multiple mutants employing a novel SCN staining method reveals their joint control of QC quiescence and columella stem cell (CSC) fate decisions. FRET-FLIM measurements disclose an interaction of WOX5 and PLT3 predominantly occurring in subnuclear microdomains referred to as nuclear bodies (NBs). NB formation is facilitated by prion-like domains (PrDs) found in PLT3. These PLT3 NBs are hypothesized to occur via LLPS and control stem cell fate determination in CSCs.

6. **Research article: Stem cell homeostasis in the root of *Arabidopsis* involves cell-type specific complex formation of key transcription factors**
   Vivien I. Strotmann, Monica L. Garcia-Gomez and Yvonne Stahl

In this manuscript, the interplay of the key TFs PLT3 and WOX5 in maintaining stem cell homeostasis in the root of *Arabidopsis* is extended by the TF BRAVO. By assessing phenotypical defects in several multiple mutants, their joint function in QC maintenance and CSC fate decisions is determined. Additionally, quantitative experimental data on protein abundance in the *Arabidopsis* root, as well as heterodimerization and -oligomerization data, are combined in a mathematical modelling approach. Here, the integration of experimental and computational approaches suggests that distinct cell type specific profiles of protein complexes are formed. Furthermore, it is hypothesized that these unique cell type specific profiles of complexes and unbound proteins could serve as a read-out for cell fate specificity necessary for root stem cell maintenance.

Further publications I contributed to:

7. Review: Eljebbawi, A., Dolata, A., Strotmann, V.I., Stahl, Y., (2024). Stem Cell Quiescence and Dormancy in Plant Meristems. Under revision for publication in Journal of Experimental Botany.

I contributed to editing the manuscript as well as by producing the figures and tables for the revision.

8. Research article: Hutin, S., Kumita, J.R., Strotmann, V.I., Dolata, A., Ling, W.L., Louafi, N., Popov, A., Milhiet, P.-E., Blackledge, M., Nanao, M.H., et al. (2023). Phase separation and molecular ordering of the prion-like domain of the Arabidopsis thermosensory protein EARLY FLOWERING 3. Proceedings of the National Academy of Sciences of the United States of America *120*, e2304714120. https://doi.org/10.1073/pnas.2304714120

I contributed to this publication with my expertise in Fluorescence Recovery after Photobleaching (FRAP) microscopy and analysis.

9. Research article: Zhang, Y., Chen, M., Siemiatkowska, B., Toleco, M.R., Jing, Y., Strotmann, V., Zhang, J., Stahl, Y. and Fernie, A.R. (2020). A Highly Efficient Agrobacterium-Mediated Method for Transient Gene Expression and Functional Studies in Multiple Plant Species. Plant communications *1*, 100028. https://doi.org/10.1016/j.xplc.2020.100028

I contributed to this publication by testing and improving the developed method and by showing that it can be used in (advanced) fluorescence microscopy experiments.

10. Research article: Alexander, R.D., Castillejo-Pons, P., Melzer, N., Alsaif, O., Strotmann, V.I., Stahl, Y., Seale, M. and Morris, P.C. (2020) The conserved Arabidopsis PM19L1 protein functions as an osmosensor and regulator of dormancy and germination. bioRxiv. https://doi.org/10.1101/2020.08.10.244889

I contributed to this manuscript with my expertise in vivo fluorescence microscopy of Arabidopsis roots.

Manuscripts in preparation for submission I contributed to

11. Research article: Marquès-Bueno M.M., Herrero I., Blasco-Escámez D, Gupta A., Lozano-Elena F., Karampelias M., Fàbregas N., Strotmann V. I., Stahl Y., Caño-Delgado A. I. (2024) Dehydrin ERD14 chaperones brassinosteroid receptor kinase BRL3 to confer drought resistance in plants. *In preparation for submission.*

I contributed to this manuscript with my expertise in advanced FRET-FLIM microscopy.

12. Research article: Burkart R. C., Eljebbawi A., Czempik L, Strotmann V. I., Wuthenow P., Stahl Y. (2024) A novel role for EARLY FLOWERING 3 (ELF3) links circadian/light signalling and root stem cell maintenance by microdomain formation. *In preparation for submission.*

I contributed to performing experiments and the generation of plasmids as well as transgenic Arabidopsis lines.

Chapter 1

At the root of quiescence: function and regulation of the quiescent center

This manuscript was published in the *Journal of Experimental Botany* in June 2021.

https://doi.org/10.1093/jxb/erab275

Authors

Vivien I. Strotmann[1] and Yvonne Stahl[1]*

Affiliation

[1]Institute for Developmental Genetics, Heinrich-Heine-University, Universitätsstr. 1, 40225 Düsseldorf

*corresponding author

Author contribution

I contributed to this work by writing the chapters ‘Molecular factors regulating the QC in Arabidopsis’, ‘Phytohormonal regulation of the Arabidopsis QC’ and ‘The role of ROS in Arabidopsis QC regulation’ as well as by conceptualizing and designing Figure 2.

Journal of Experimental Botany
https://doi.org/10.1093/jxb/erab275 Advance Access Publication 10 June, 2021

REVIEW

At the root of quiescence: function and regulation of the quiescent center

Vivien I. Strotmann and Yvonne Stahl*

Institute for Developmental Genetics, Heinrich-Heine University, Universitätsstr. 1, 40225 Düsseldorf, Germany

* Correspondence: yvonne.stahl@hhu.de

Received 26 March 2021; Editorial decision 7 June 2021; Accepted 8 June 2021

Editor: Kris Vissenberg, University of Antwerp, Belgium

Abstract

The quiescent center (QC) of roots consists of a rarely dividing pool of stem cells within the root apical meristem (RAM). The QC maintains the surrounding more frequently dividing initials, together constituting the stem cell niche of the RAM. The initials, after several rounds of division and differentiation, give rise to nearly all tissues necessary for root function. Hence, QC establishment, maintenance, and function are key for producing the whole plant root system and are therefore at the foundation of plant growth and productivity. Although the concept of the QC has been known since the 1950s, much of its molecular regulations and their intricate interconnections, especially in more complex root systems such as cereal RAMs, remain elusive. In Arabidopsis, molecular factors such as phytohormones, small signaling peptides and their receptors, and key transcription factors play important roles in a complex and intertwined regulatory network. In cereals, homologs of these factors are present; however, QC maintenance in the larger RAMs of cereals might also require more complex control of QC cell regulation by a combination of asymmetric and symmetric divisions. Here, we summarize current knowledge on QC maintenance in Arabidopsis and compare it with that of agriculturally relevant cereal crops.

Keywords: Quiescent center, quiescent center maintenance, root apical meristem, stem cell homeostasis, stem cell niche.

Introduction

As sessile organisms, higher plants must adapt their growth and development in response to internal and external cues such as light and nutrient availability, and biotic and abiotic stresses. Plant roots provide anchorage in the soil and are necessary for the uptake of nutrients and water, and the plasticity of plant root development in response to such cues is therefore essential to maintain plant vigor and fertility. Plant development, in contrast to animal development, takes place mainly after embryogenesis and depends on the maintenance of pools of pluripotent stem cells in structures called meristems. In both animals and plants, stem cells are defined as undifferentiated cells with a self-renewing capacity that produce progenitor cells that replenish and regenerate the tissues of multicellular organisms (Barlow, 1978, 1997; Sánchez Alvarado and Yamanaka, 2014). The stem cells within the two main meristems at the shoot apex [the shoot apical meristem (SAM)] and at the root apex [the root apical meristem (RAM)] give rise to all above- and below-ground organs of a plant, respectively.

The concept of a multicellular "cytogenerative center" within the RAM, from which most of the root cells derive and which functions as a source of regeneration in wounded plant root tips, was first formulated by F.A.L. Clowes in 1953 based on his observations on *Fagus sylvatica* and *Vicia faba* roots. He later renamed it the "quiescent center" (QC) due to its proliferative quiescence, which he observed in the RAM of *Zea mays* (Clowes, 1953, 1956; Barlow, 1978, 1997; Dubrovsky and Barlow, 2015). In doing so, he presented one of the first conceptualizations of a population of pluripotent stem cells within the RAM serving as long-term progenitors for most root cells. This fundamental work provided the foundation of many decades of research to understand the regulation of this important stem cell pool in plant roots (Clowes, 1953, 1953, 1956; Barlow, 1978, 1997; Jiang and Feldman, 2005; Dubrovsky and Barlow, 2015).

In this review, we summarize the information about molecular regulators of QC positioning, maintenance, and function, and hypothesize how stem cell pools can be maintained depending on their size in different roots. To date, most of the knowledge about QC function and its regulation by molecular factors has been acquired by studying the root of the eudicot model plant *Arabidopsis thaliana*.

The root stem cell niche of Arabidopsis

Stem cell niches (SCNs) in multicellular organisms are thought to provide the necessary microenvironment to regulate the balance of stem cell maintenance and renewal, and the production of daughter cells that produce differentiated tissues (Spradling *et al.*, 2001; Heidstra and Sabatini, 2014). In the Arabidopsis RAM, the SCN consists of the, on average, four rarely dividing QC cells and the adjacent, shorter-lived, proliferating stem cells, which are also called initials. The initials are produced by asymmetric divisions of the QC cells and are maintained by the QC in a non-cell-autonomous manner (Dolan *et al.*, 1993; van den Berg *et al.*, 1997; Benfey and Scheres, 2000). Future cell fates are defined by the fixed position of the initials and their descendants during plant development. This results in the production of concentrically organized clonal cell lineages that form distinct tissue layers representing a spatiotemporal developmental gradient along a longitudinal axis. Here, the youngest cells are closest to the SCN and more differentiated cells are displaced by new daughter cells originating from the dividing initials. From the outside to the inside of the root, the resulting concentric cell layers are the epidermis, cortex and endodermis (together also referred to as ground tissue), and stele (consisting of the pericycle and vasculature), as well as the columella and lateral root cap at the root tip (Fig. 1A).

The root SCN can be divided into two distinct groups of stem cells on the basis of their different frequencies of cell division. These groups are the slowly dividing QC cells and the surrounding, more rapidly dividing initials, which have also been named structural and functional initials, respectively (Barlow, 1997; Jiang and Feldman, 2005). The appearance of two populations of stem cells with different proliferative and generative capacities at distinct but neighboring locations is a common characteristic of SCN organization not only in plants but also in animals (Barlow, 1978, 1997; Schofield, 1978; Jiang and Feldman, 2005; Li and Clevers, 2010). In Arabidopsis, most QC divisions are periclinal and produce, after some days, columella stem cell (CSC) initials (Cruz-Ramírez *et al.*, 2013). However, other initials are produced, albeit at a slower rate, by anticlinal divisions, such as the cortex/endodermis initials (CEIs), which subsequently divide periclinally to produce the cortex and endodermis cell layers (Cruz-Ramírez *et al.*, 2013).

The QC cells play a pivotal role in the maintenance of the root SCN both by maintaining themselves and by producing or regenerating the surrounding initials that serve as progenitor cells of all the different cell types of the root (Heyman *et al.*, 2014). Because of their low mitotic activity, QC cells are thought to be protected from DNA damage, which thereby enables them to act as a long-term reservoir or stem cell pool for all the different abutting initials with a higher proliferation rate (Cruz-Ramírez *et al.*, 2013; Vilarrasa-Blasi *et al.*, 2014).

A complex interplay of molecular factors is involved in maintaining the delicate balance between stem cell maintenance and the generation of differentiating descendants in the root SCN, with the QC acting as a "signaling center" repressing the differentiation of the surrounding initials (van den Berg *et al.*, 1997). Key players are phytohormones such as auxin and cytokinins, conserved signaling modules involving small secreted peptide ligands and their receptors, as well as certain transcription factors (TFs), which are described in the next section (Aida *et al.*, 2004; Blilou *et al.*, 2005; Sarkar *et al.*, 2007; Stahl *et al.*, 2009, 2013; Zhang *et al.*, 2013; Drisch and Stahl, 2015; Burkart *et al.*, 2019, Preprint).

Molecular factors regulating the QC in Arabidopsis

Molecular factors that regulate Arabidopsis root stem cell homeostasis have either a promoting or an inhibiting effect on QC divisions. One of the best-studied molecular factors known to inhibit QC divisions while at the same time maintaining stem cell fate in the surrounding initials is the homeodomain TF WUSCHEL-RELATED HOMEOBOX 5 (WOX5). WOX5 is the closest homolog of WUSCHEL (WUS), which regulates stem cell homeostasis in the SAM as part of a negative feedback loop. Here, the dodecapeptide CLAVATA3 (CLV3) is expressed by the stem cells at the central zone at the tip of the SAM. *CLV3* expression is positively regulated in a non-cell-autonomous manner by WUS, which moves from its expression domain in the organizing centre upward to the central zone. CLV3 signal perception

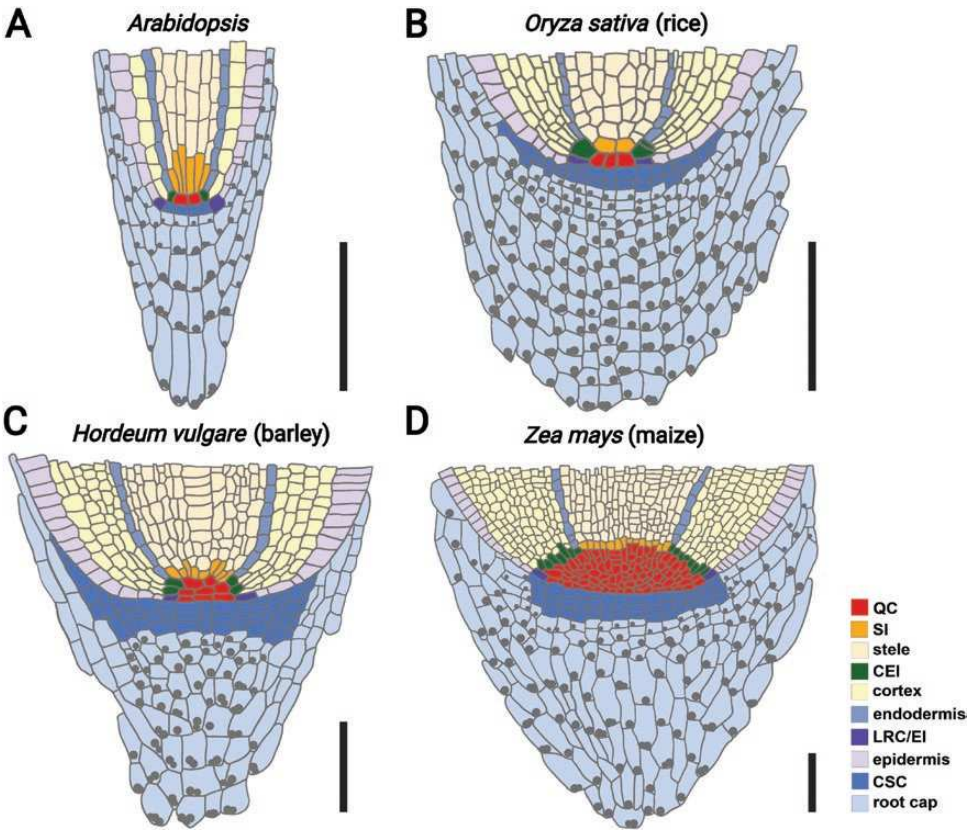

Fig. 1. The RAMs of (A) Arabidopsis, (B) rice, (C) barley, and (D) maize. Schematic representations of longitudinal sections of RAMs. Different root tissues are color coded (see legend). Grey dots represent starch granules. The (putative) QC region is marked in red. The (putative) initials are color coded (see legend). CEI, cortex/endodermis initial; CSC, columella stem cells; LRC/EI, lateral root cap/epidermis initial; SI, stele initial. Scale bars=100 μm. Modified from Kirschner *et al.* (2017).

by the leucine-rich repeat receptor-like kinase (LRR RLK) CLV1, or a heterodimer composed of CLV2 and CORYNE (CRN), in turn negatively regulates *WUS* expression. This ultimately results in reduced expression of *CLV3*, creating a negative feedback loop (Brand *et al.*, 2000; Schoof *et al.*, 2000; Müller *et al.*, 2008; Guo *et al.*, 2010; Bleckmann *et al.*, 2010).

In the RAM, analyses of transcriptional and translational reporter lines showed that *WOX5* expression is confined to the QC but the WOX5 protein can move to the adjacent CSC layer, hereby non-cell-autonomously preserving the undifferentiated status of these distal stem cells (Sarkar *et al.*, 2007; Pi *et al.*, 2015). Even though the necessity of the observed WOX5 mobility for CSC fate is under debate (Berckmans *et al.*, 2020), WOX5 is a key regulator in root SCN maintenance. The SCN in the RAM is also under the control of negative feedback regulation. Here, the CLV3 homolog CLAVATA3/EMBRYOSURROUNDING REGION 40 (CLE40) is putatively perceived by a receptor kinase heterodimer formed by ARABIDOPSIS CRINKLY 4 (ACR4) and CLV1, repressing *WOX5* expression and thereby promoting CSC differentiation (Fig. 2) (Stahl *et al.*, 2009, 2013). WOX5 itself represses the expression of the TF gene *CYCLING DOF FACTOR 4* (*CDF4*), by recruiting the co-repressor TOPLESS (TPL) and HISTONE DEACETYLASE 19 (HDA19) (Krogan *et al.*, 2012), which promotes terminal differentiation of columella cells. This leads to lower expression of *CDF4* in the CSCs and no expression in the QC, as well as higher expression levels in the upper differentiated columella cells. This generates an inverse protein gradient of CDF4 compared to WOX5 protein levels that is necessary to maintain CSC fate (Pi *et al.*, 2015). At the same time, WOX5 also inhibits cell divisions in the QC by suppressing the D-type cyclins CYCLIND3;3 (CYCD3;3) and CYCLIND1;1 (CYCD1;1) (Forzani *et al.*, 2014). This could explain why the roots of *wox5-1* loss-of-function mutants, as a consequence of the relieved repression of *CYCD3;3*, *CYCD1;1*, and *CDF4* expression, show increased QC division rates and lack the subjacent CSC layers (Pi *et al.*, 2015; Burkart *et al.*, 2019, Preprint). The expression of *WOX5* is repressed and restricted to the QC by the plant hormone auxin, mediated by AUXIN RESPONSE FACTOR 10 (ARF10) and ARF16 (Ding and Friml, 2010) and by the PHD domain-containing protein REPRESSOR OF WUSCHEL 1 (ROW1) (Zhang *et al.*, 2015). On the other hand, the glutamine-rich SEUSS (SEU) protein is physically recruited to the *WOX5* promoter by SCARECROW

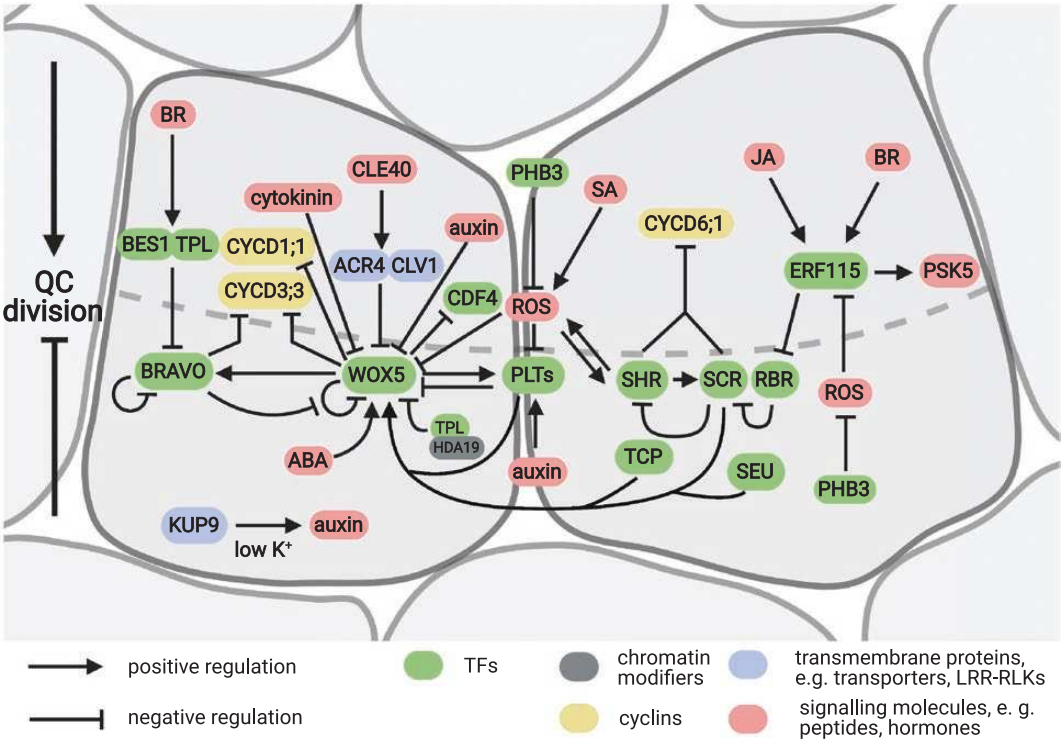

Fig. 2. A model of the intricate regulatory network of molecular factors involved in QC division control in Arabidopsis. Not all of the molecular factors shown in this scheme are expressed in the QC, but nevertheless, they have been shown to inhibit or promote QC divisions (indicated by their position below or above the dashed line, respectively). All transcription factors (TFs) (green) below the dashed line inhibit QC divisions per se, whereas all TFs above the dotted line positively influence QC divisions per se. These TFs are themselves influenced and regulated by other factors, such as hormones, other TFs, signaling molecules, cyclins, and chromatin modifiers. Arrows indicate positive regulations; barred lines indicate negative regulations. Green, TFs; grey, chromatin modifiers; yellow, cyclins; blue, transmembrane proteins (e.g. transporters or LRR-RLKs); red, signaling molecules (e.g. peptides or hormones).

(SCR) and induces *WOX5* expression (Zhai *et al.*, 2020). Furthermore, WOX5 activity is necessary to induce another key TF family in the QC, the PLETHORAs (PLTs), which are highly expressed in the root SCN (Aida *et al.*, 2004; Galinha *et al.*, 2007).

The AP2-type TF family of the PLTs consists of six family members, which are master regulators of root formation and development (Aida *et al.*, 2004; Galinha *et al.*, 2007). PLTs [PLT1, 2, 3 and 4 (also known as BABYBOOM; BBM)] are induced by auxin (Aida *et al.*, 2004) and form instructive protein gradients balancing stem cell differentiation and replenishment within the Arabidopsis RAM (Galinha *et al.*, 2007; Mähönen *et al.*, 2014). The highest PLT levels can be found in the root SCN, maintaining its low mitotic activity; medium protein levels in the meristematic zone promote cell proliferation, while low PLT protein concentrations cause differentiation (Mähönen *et al.*, 2014). Recent findings also directly link PLT2 and PLT3 to QC maintenance. Here, analysis of *plt2* and *plt3* single mutants and *plt2, plt3* double mutants revealed increased QC division rates, indicating an inhibiting role of PLTs on QC divisions. Interestingly, the frequency of QC division increases further in the *plt2, plt3, wox5* triple mutant. This suggests that parallel pathways operate in WOX5- and PLT-mediated regulation of QC division, although WOX5 and PLTs were shown to interact (Burkart *et al.*, 2019, Preprint). Another interesting observation is that PLT3 can form nuclear bodies in some of the CSCs and in developing lateral root primordia. This distinct subcellular compartmentalization seems to depend on the presence of prion-like domains and might provide a mechanism to dynamically integrate external and internal cues into SCN regulation, possibly by liquid–liquid phase separation (Burkart *et al.*, 2019, Preprint).

In addition to the PLT pathway, a network based on SCARECROW (SCR) and SHORT-ROOT (SHR), two members of the GRAS family of TFs, is essential for the correct positioning of the QC (Sabatini *et al.*, 2003) and for the regulation of the formative asymmetric cell divisions of the CEIs (Di Laurenzio *et al.*, 1996; Helariutta *et al.*, 2000). *SHR* is expressed in the stele but the encoded protein moves to the outer adjacent cell layer including the QC, endodermis, and CEI (Nakajima *et al.*, 2001). Here, SHR activates the expression of *SCR*, which in turn prevents further movement of SHR toward the outer cell layers, thereby defining a single layer of endodermis (Cui *et al.*, 2007). Together, SHR and SCR regulate the expression of *CYCLIND6;1* (*CYCD6;1*) in order to induce the asymmetric periclinal cell divisions that will later

give rise to the cortical and endodermal cell layers (Sozzani *et al.*, 2010; Koizumi *et al.*, 2012).

Furthermore, SCR, together with RETINOBLASTOMA-RELATED (RBR) protein, down-regulates the asymmetric QC divisions that give rise to all initial cell types, also referred to as short-term stem cells (Wildwater *et al.*, 2005; Cruz-Ramírez *et al.*, 2013). Recently, it was shown that PLTs and SCR genetically and physically interact with plant-specific teosinte-branched cycloidea PCNA (TCP) TFs to maintain QC cells post-embryonically (Shimotohno *et al.*, 2018).

SHR and SCR are known to form distinct protein complexes with JACKDAW (JKD) in different initials and the QC in the Arabidopsis SCN (Moreno-Risueno *et al.*, 2015; Long *et al.*, 2017; Clark *et al.*, 2020). This variation in complex composition is suggested to provide specificity in SHR-regulated genes, thereby regulating cell-fate separation within the RAM (Long *et al.*, 2015, 2017). Furthermore, it was reported that, depending on its stoichiometry, the SHR–SCR complex promotes the more frequently occurring CEI divisions and at the same time inhibits the less frequent QC divisions (Clark *et al.*, 2020).

Phytohormonal regulation of the Arabidopsis QC

Auxin is the key phytohormone necessary for QC establishment and, as mentioned above, regulates other important molecular factors involved in QC maintenance. Differentially localized efflux carriers of the PIN-FORMED family, such as PIN1, mediate unidirectional auxin transport from the shoot to the root, resulting in a defined auxin peak at the root tip that specifies QC identity (Gälweiler *et al.*, 1998; Grieneisen *et al.*, 2007). As described above, some of the most important molecular factors regulating the root SCN, such as WOX5 and PLTs, are directly regulated by auxin and act as a read-out of auxin distribution, which is important for QC specification and the regulation of cell proliferation rates within the RAM (Blilou *et al.*, 2005; Ding and Friml, 2010). However, the regulatory effect of auxin on WOX5 is quite contradictory: on the one hand, WOX5 is positively regulated by MONOPTEROS/AUXIN RESPONSE FACTOR 5 (MP/ARF5) but on the other hand, it is repressed by ARF10/16 (Sarkar *et al.*, 2007; Ding and Friml, 2010). These ambivalent effects of auxin and other hormones on TFs might in part be due to their spatial or temporal distribution within the root; for example, MP is expressed in the QC, but ARF10 and ARF16 are not (Rademacher *et al.*, 2011). In addition, a dose-dependent effect of auxin on cell proliferation is suggested by the low mitotic activity and high auxin levels in the QC but higher cell division rates and lower auxin levels in the surrounding tissue (Ding and Friml, 2010). To fully understand the regulatory impact of auxin on stem cell homeostasis, further investigations are necessary. So far, all information about auxin distribution is based on visualizing irreversible auxin responses, by using auxin reporters such as DR5::ER-GFP (Friml *et al.*, 2003), or auxin-dependent degradation, by using DII:VENUS or the R2D2 reporter (Brunoud *et al.*, 2012; Liao *et al.*, 2015). A recently designed Förster resonance energy transfer (FRET)-based biosensor is able to directly visualize changes in auxin distribution in a reversible manner (Herud-Sikimić *et al.*, 2021). This tool will allow a deeper understanding of the regulatory mechanisms of auxin and of how spatial and temporal distribution might affect auxin response regulators.

In the past decade, the brassinosteroid (BR) signaling pathway was also found to play a role in stem cell maintenance in the Arabidopsis RAM (González-García *et al.*, 2011). Regarding QC divisions, BRs act via the R2R3-MYB TF BRASSINOSTEROIDS AT VASCULAR AND ORGANIZING CENTER (BRAVO) (Fig. 2) (Vilarrasa-Blasi *et al.*, 2014). BRAVO expression in the RAM is restricted to the vasculature initials and the QC. Loss of BRAVO function, as in the *bravo-1* and *bravo-2* mutants, leads to an increased frequency of QC division, a phenomenon also observed in *wox5-1* mutants (Sarkar *et al.*, 2007; Stahl *et al.*, 2009; Pi *et al.*, 2015; Burkart *et al.*, 2019, Preprint; Betegón-Putze *et al.*, 2021). By analyzing *bravo-2, wox5-1* double mutants, recent studies revealed that, regarding the regulation of QC quiescence, WOX5 and BRAVO act in the same pathway and interact with each other (Betegón-Putze *et al.*, 2021). Additionally, both WOX5 and BRAVO are known to control the expression of *CYCD3;3*, supporting their joint role in the regulation of mitotic activity in the QC (Forzani *et al.*, 2014; Vilarrasa-Blasi *et al.*, 2014). Nevertheless, *wox5-1* mutants are insensitive to the enhanced QC proliferation effect that accompanies BR application, suggesting that WOX5 acts upstream of BR-regulated QC activity (González-García *et al.*, 2011).

Conversely, in the presence of BR, the transcriptional regulator BRI1-EMS-SUPPRESSOR1 (BES1/BZR2) is dephosphorylated, enabling its translocation to the nucleus (Yin *et al.*, 2002), where it represses BRAVO at the transcriptional and protein levels (Vilarrasa-Blasi *et al.*, 2014). The repression of BRAVO by BES1 involves the activity of the co-repressor TOPLESSS (TPL) (Espinosa-Ruiz *et al.*, 2017). TPL and its homologs, TOPLESS-RELATED proteins (TRP), are part of the Groucho/TUP1 transcriptional co-repressor family and are known to be involved in the regulation of many different developmental processes in Arabidopsis (Long *et al.*, 2006; Causier *et al.*, 2012). Transcriptional regulation is mediated by the interaction of the TPL N-terminal LisH domain with the ERF-associated amphiphilic repression (EAR) motif of different TFs, such as WUS, NINJA, BES1, and WOX5 (Kieffer *et al.*, 2006; Kagale and Rozwadowski, 2011; Causier *et al.*, 2012; Vilarrasa-Blasi *et al.*, 2014; Espinosa-Ruiz *et al.*, 2017; Betegón-Putze *et al.*, 2021).

BRs are also able to promote QC divisions by inducing the expression of *ETHYLENE RESPONSE FACTOR 115* (*ERF115*), which encodes a member of the ethylene

response factor TF family (Heyman *et al.*, 2013). ERF115 in turn regulates the expression of the peptide hormone *PHYTOSULFOKINES 5* (*PSK5*), which is known to elevate QC division rates (Fig. 2) (Heyman *et al.*, 2013). Taken together, BRs promote QC divisions via the ERF115 pathway and by suppressing the inhibitory effect of BRAVO via activation of the repressor complex BES1/TPL.

In contrast, abscisic acid (ABA) has been reported to contribute to QC maintenance, presumably by regulating known RAM regulators (Zhang *et al.*, 2010). Analyses of ABA-deficient and ABA-insensitive mutants revealed an elevated rate of QC division and increased differentiation of CSCs. Roots treated with exogenous ABA exhibited a lower frequency of QC division and reduced CSC differentiation, which correlates with the up-regulated expression of *PLT2*, *MP*, and *WOX5* (Zhang *et al.*, 2010).

A mechanism by which all plant hormones mentioned so far influence SCN regulation is the modulation of *WOX5* expression, both directly and indirectly (Sarkar *et al.*, 2007; Ding and Friml, 2010; Zhang *et al.*, 2010; Betegón-Putze *et al.*, 2021). This further demonstrates the central role of WOX5 in QC and SCN maintenance.

Besides auxin, ABA, and BRs, cytokinins and ethylene are also part of the network involved in stem cell homeostasis in the root of Arabidopsis (Ortega-Martínez *et al.*, 2007; Zhang *et al.*, 2013). The regulation of mitotic activity in the QC by cytokinin is mediated by the redistribution of auxin (Zhang *et al.*, 2013). In contrast, the contribution of ethylene to the frequency of QC division appears to be independent of auxin, even though ethylene and auxin are known to interact in several other developmental processes (Rahman *et al.*, 2002; Stepanova *et al.*, 2005; Chilley *et al.*, 2006). Therefore, the exact molecular mechanism by which ethylene affects QC division remains to be elucidated (Ortega-Martínez *et al.*, 2007).

Plant hormones such as the above-discussed BR, ABA, auxin, and cytokinin are not only essential for normal plant growth and development but, like jasmonate (JA) and ethylene, also serve as stress hormones involved in the reaction to certain environmental influences. Adaptation to environmental changes, such as reduced access to water or nutrients, is known to affect meristem activity and thereby QC size (Jiang and Feldman, 2005). For example, the potassium transporter KUP9 located in the endoplasmic reticulum was found to regulate root meristem activity in Arabidopsis in response to reduced K^+ availability (Zhang *et al.*, 2020). By maintaining K^+ and auxin homeostasis in QC cells, KUP9 maintains local auxin levels and thereby maintains QC activity (Fig. 2). A similar function has been reported for the endoplasmic reticulum-localized PIN8, even though PIN8 is not expressed in the root of Arabidopsis (Ding *et al.*, 2012). Nevertheless, PIN8 can partially take over the function of KUP9 in the QC when driven by the KUP9 promoter (Zhang *et al.*, 2020).

In addition to adapting to nutrient deficiency, plants also need to develop response and defense mechanisms to wounding, resection, or parasites. JA is a well-studied plant stress hormone involved in several stress-response processes (Pieterse *et al.*, 2012). ERF115, which is known to be regulated by BRs (Ohme-Takagi and Shinshi, 1995; Heyman *et al.*, 2013; Kong *et al.*, 2018), was also recently linked to a complex molecular stress-response network induced by JA (Zhou *et al.*, 2019). Within this network, JA induces *ERF115* expression. Subsequently, ERF115 acts together with the SCR–RBR complex to promote QC quiescence. Interestingly, the effect of ERF115 and RBR on the frequency of QC division is larger than the effect of SCR alone, indicating that RBR and ERF115 can form complexes independently of SCR and thereby act via an SCR-independent regulatory mechanism (Zhou *et al.*, 2019).

The role of ROS in Arabidopsis QC regulation

In addition to plant hormones, reactive oxygen species (ROS) are also involved in the maintenance of the Arabidopsis RAM. In the past, ROS had been regarded simply as by-products of aerobic metabolism. However, ROS are now known to act as important signaling molecules that are involved in both normal root growth (Tsukagoshi *et al.*, 2010) and responses to stresses such as heat (Zhao *et al.*, 2018) and drought (Lee *et al.*, 2012).

Recently, it was shown that ERF115 is not only a downstream factor of BR signaling but is also regulated by ROS via the spatial restriction of *PROHIBITIN 3* (*PHB3*) expression (Kong *et al.*, 2018). PHB3 has previously been linked to cell division control in the root tip (van Aken *et al.*, 2007) but the underlying molecular mechanisms remained unclear. It has now been shown that PHB3 functions via ERF109, ERF114, and ERF115 to maintain root SCN identity in Arabidopsis (Fig. 2) (Kong *et al.*, 2018). Interestingly, PHB3 also down-regulates *PLT1* and *PLT2* expression in the root SCN independently of ERFs. Taken together, these findings indicate that PHB3 suppresses ERFs and maintains the activity of PLT1 and PLT2 via ROS to control root SCN identity.

Further investigations have provided further evidence that the effect of PLTs and WOX5 on QC quiescence is linked to ROS (Wang *et al.*, 2021). Here, an overaccumulation of salicylic acid (SA) causes ROS production by the activation of respiratory burst oxidase homologs (RBOHs), which leads to supernumerary QC divisions as a result of the repression of *PLT1*, *PLT2*, and *WOX5*.

Recently, it was discovered that SHR is also able to elevate ROS levels either by the activation of the SA pathway or by the activation of RBOHD, RBOHE, and RBOHF (Li *et al.*, 2020). The regulation of ROS levels directly influences the ability of SHR to induce the periclinal divisions necessary for the formation of the cortex and endodermis.

Therefore, by maintaining ROS levels in the RAM, SHR is thought to create a microenvironment to mediate asymmetric periclinal cell divisions. Intriguingly, the activation of RBOHD and RBOHF has also been linked to SA-mediated down-regulation of *PLTs* and *WOX5* in order to induce cell divisions in the QC (Wang *et al.*, 2021). The fact that SHR was shown to be sufficient to activate *RBOHD* and *RBOHF* expression could hypothetically interconnect SHR and PLT/WOX5 in terms of ROS-mediated SCN regulation. Hence, more investigations are needed to elucidate whether the two pathways, which are known to act in parallel, are also linked regarding ROS-regulated QC quiescence. The great number of the above-described molecular factors and their intricate cross-regulations involved in QC positioning, division, and function demonstrate the complexity of the mechanisms required to control this stem cell pool in the RAM (see Fig. 2).

The QC within RAMs of larger roots

As mentioned earlier, the processes controlling QC activity and thereby RAM maintenance in the Arabidopsis root have been studied for several decades. However, to date, little is known about how the QC of plants with more complex and larger root systems, such as monocots, is controlled. The root system architecture of monocots differs considerably from the simple, well-described tap root system of Arabidopsis. The Arabidopsis root consists of one embryo-derived primary (or main) root and post-embryonically formed lateral roots. The monocot root systems of members of the agriculturally relevant Poaceae family, for example, *Hordeum vulgare* (barley), *Zea mays* (maize), and *Oryza sativa* (rice), show a more complex fibrous root system. Here, in addition to the main and lateral roots, embryo-derived seminal roots and even shoot-borne crown roots can also be found (Hochholdinger and Zimmermann, 2008; Smith and de Smet, 2012; Kirschner *et al.*, 2017).

Apart from the architectural differences of these root systems, the cereal root in general is considerably thicker than the root of the dicot model plant Arabidopsis. Recently, a correlation has been observed between the thickness (diameter) of the main root and the length of the RAM; in thicker roots (dicot and monocot roots alike), the length of the RAM is almost double the size of its diameter (Bystrova *et al.*, 2018). An increase of root diameter also usually correlates with a larger number of cortical and stele cell layers compared with the single cell layers observed in Arabidopsis (see Fig. 1). Therefore, it can be concluded that the thickness of the root depends on the number of meristematic cells present in the RAM and thus on the number of stem cells as their progenitors. Consequently, these roots would be expected to contain more QC cells as a basis for the larger number of meristematic cells and cell layers contributing to the greater root diameter.

For some cereal roots, such as barley roots (with on average 30 QC cells) and maize roots (with ~800–1200 QC cells), this has indeed been reported (Fig. 1C, D) (Jiang *et al.*, 2003; Jiang and Feldman, 2005; Kirschner *et al.*, 2017). However, in rice roots, which are also thicker than Arabidopsis roots, on average only three or four QC cells were defined based on the observed expression of the WOX5 ortholog *QUIESCENT-CENTER-SPECIFIC HOMEOBOX* (*QHB*) (Fig. 1B) (Kamiya *et al.*, 2003). It is not clear why in rice roots, despite their greater number of cortical and stele cell layers in comparison to Arabidopsis roots, so few QC cells are present, in stark contrast to roots of other Poaceae family members. One explanation might be that *QHB* expression is not the only hallmark of QC identity in these thicker roots. In maize roots, for example, *ZmWOX5* expression is found in only a fraction of the QC cells that were determined by classical [^{3}H]thymidine and BrdU assays to determine cell division rates (Clowes, 1956; Jiang *et al.*, 2003). Indeed, more than four mitotically inactive cells were found in BrdU assays on rice RAMs and, in addition, a larger *QHB* expression domain has been reported, but whether the cells in these larger areas possess QC identity is still unclear (Chu *et al.*, 2013; Ni *et al.*, 2014). Therefore, the size of the QC in rice roots might in fact be underestimated, and the exact number of QC cells remains to be determined. This could indicate that in these larger roots further subdivisions of the SCN, based on other morphological or (novel) functional markers, might be necessary. Nevertheless, based on the observed greater number of QC cells in thicker roots such as those of barley and maize, one could argue that there is a correlation between root size and SCN size. Here especially, a higher QC cell number serving as a larger stem cell pool might indeed be necessary to maintain the larger RAMs. This in turn raises the question of how the required QC divisions are regulated to provide and maintain these larger stem cell pools.

Maintenance of larger QC stem cell pools

From fundamental work on Arabidopsis, it is known that the stem cell pool of the root needs to be maintained and continually replenished by coordinated divisions of the QC cells, as stem cells are continually lost to differentiation in response to various intrinsic or external cues. It is postulated that the underlying mechanisms are the mainly asymmetric divisions of QC cells to maintain the QC and produce initial cell fate as a first step toward the future differentiation of these cell lineages. As summarized above, a multitude of factors such as phytohormones, receptors and small secreted peptides, ROS, and transcriptional regulators are known to play important roles during this process in Arabidopsis (Drisch and Stahl, 2015; García-Gómez *et al.*, 2020, 2021). However, most of the molecular players necessary for SCN regulation and maintenance within the RAM of thicker roots, especially in the agriculturally relevant monocot cereals, are still unknown.

Considering the more complex and thicker monocot roots, such as those of the cereals rice, barley, and maize, it is possible

that a more intricate SCN regulation is necessary to maintain their elaborate RAMs harboring larger stem cell pools (including more QC cells) compared with the less complex RAM in Arabidopsis. The observed increase of QC cell number could be due to more symmetric divisions of the QC cells in these bigger SCNs. This could support the model of a systemic mechanism for uncoupled stem cell division and differentiation (Fig. 3) (García-Gómez *et al.*, 2020). According to this model, the on average four QC cells in the Arabidopsis root would always divide asymmetrically, leading to one rarely dividing QC cell and one faster dividing cell (in this case an initial cell) that is already dedicated to a specific cell fate and therefore is already in a very early phase of differentiation (see Fig. 3A). In the meristems of thicker roots, such as cereal roots, a larger population of QC cells needs to be maintained, which might be achieved by the occurrence of more symmetric divisions of the QC cells and an uncoupling of these divisions from the differentiation of their descendants. In this case, a QC cell could divide and produce either two QC cells, one QC cell and one differentiating cell, or even two differentiating cells, which would allow the dynamic maintenance of a larger group of QC cells as a stem cell pool (exemplified in Fig. 3B for the barley SCN).

Still, temporal changes of the rather low QC proliferation rate within the SCN, which is around three to six times lower for QC cells in the Arabidopsis root than for the surrounding initials, also have to be considered (Fujie *et al.*, 1993; Timilsina *et al.*, 2019). It is known that under stress conditions such as temperature or genotoxic stresses the rate of QC division is enhanced (Cruz-Ramírez *et al.*, 2013). Recently, it has been observed that aging Arabidopsis roots show more QC proliferation, correlating with a decrease in the tolerance to genotoxic stress (Timilsina *et al.*, 2019). However, which underlying internal and external cues are necessary for this temporal transition of the QC division rate and how they are integrated into the complex regulations of the stem cell pool in roots remain largely elusive.

Nevertheless, there is accumulating evidence that homologs of some of the key molecular factors regulating Arabidopsis stem cell maintenance are also present in the thicker monocot RAMs, although there is only limited functional data available for QC maintenance and regulation. In rice, a CLE–WOX module regulating RAM maintenance has been postulated (Chu *et al.*, 2013). Regarding the expression of, for example, WOX5 homologs in rice, barley, and maize, both similarities and differences between these species and Arabidopsis become apparent. For instance, the expression domain of WOX5 homologs found in maize (*ZmWOX5B*) and rice *QHB* are expressed not just in the QC region of the RAM but also in the metaxylem (Nardmann *et al.*, 2007; Chu *et al.*, 2013; Ni *et al.*, 2014). This could indicate that for the regulation of the stem cell pools of these more complex roots either other factors are involved or different mechanisms are necessary, which could be a consequence of the potentially distinct regulation of stem cell pool maintenance.

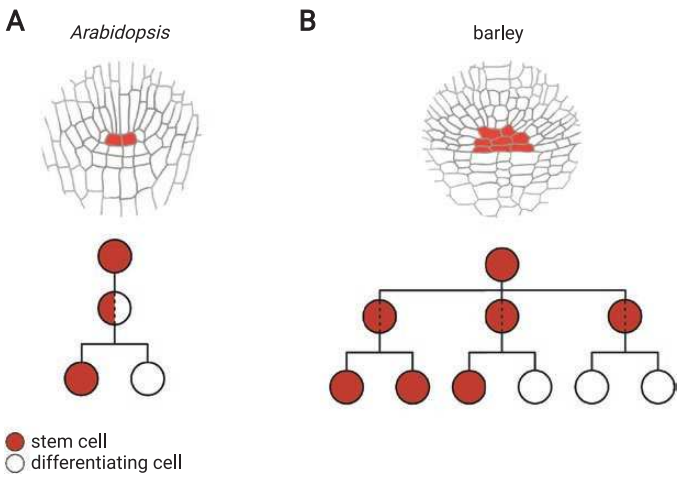

Fig. 3. Putative regulation of QC cell number in SCNs of different sizes. In the upper row, the QC cells of the root of Arabidopsis (A) and barley (B) are marked in red. Below, the putative outcomes of symmetric or asymmetric divisions of these QC cells are shown. Red circles represent QC cells; white circles represent progenitor (initial) or (early) differentiating cells. Modified from García-Gómez *et al.* (2020).

Conclusion and future perspectives

In an ever-changing world facing imminent challenges such as climate change and a growing human population, fundamental research is needed on how the plasticity of plant development is regulated on a molecular level in response to external cues. Plant roots provide anchorage in the soil and facilitate the uptake of nutrients and water essential for the development, growth, and sustainment of the whole plant. The regulation and maintenance of the QC at the centre of the SCN at the root tip is of utmost importance for root development and function. A deeper understanding of the underlying molecular mechanisms is crucial to decipher the intricate networks required for stem cell control in the root. Especially in agriculturally relevant plant species such as cereal crops, efforts to understand the maintenance of the QC as a stem cell pool will provide access to information needed to fortify plants in the expected more extreme climate conditions, to increase plant yield and improve agricultural land use to increase food security for an expanding human population.

Acknowledgements

VIS and YS were supported by the Deutsche Forschungsgemeinschaft grant STA 1212/4-1. We would like to thank Vicky Howe for critical reading. We apologize to all colleagues whose relevant work could not be mentioned due to space restrictions. Figures were created with BioRender.com.

Conflict of interest

The authors declare no competing interests.

Author contributions

YS conceptualized the review; VS and YS jointly wrote the manuscript and produced the figures.

References

Aida M, Beis D, Heidstra R, Willemsen V, Blilou I, Galinha C, Nussaume L, Noh YS, Amasino R, Scheres B. 2004. The *PLETHORA* genes mediate patterning of the *Arabidopsis* root stem cell niche. Cell **119**, 109–120.

Barlow PW. 1978. The concept of the stem cell in the context of plant growth and development. In: Lord BI, Potten CS, Cole RJ, eds. Stem cells and tissue homeostasis. Cambridge: Cambridge University Press, 87–113.

Barlow PW. 1997. Stem cells and founder zones in plants, particularly their roots. In: Potten CS, ed. Stem cells. London: Academic Press, 29–57.

Benfey PN, Scheres B. 2000. Root development. Current Biology **10**, R813–R815.

Berckmans B, Kirschner G, Gerlitz N, Stadler R, Simon R. 2020. CLE40 signaling regulates root stem cell fate. Plant Physiology **182**, 1776–1792.

Betegón-Putze I, Mercadal J, Bosch N, *et al.* 2021. Precise transcriptional control of cellular quiescence by BRAVO/WOX5 complex in *Arabidopsis* roots. Molecular Systems Biology **17**, e9864.

Bleckmann A, Weidtkamp-Peters S, Seidel CA, Simon R. 2010. Stem cell signaling in Arabidopsis requires CRN to localize CLV2 to the plasma membrane. Plant Physiology **152**, 166–176.

Blilou I, Xu J, Wildwater M, Willemsen V, Paponov I, Friml J, Heidstra R, Aida M, Palme K, Scheres B. 2005. The PIN auxin efflux facilitator network controls growth and patterning in *Arabidopsis* roots. Nature **433**, 39–44.

Brand U, Fletcher JC, Hobe M, Meyerowitz EM, Simon R. 2000. Dependence of stem cell fate in *Arabidopsis* on a feedback loop regulated by *CLV3* activity. Science **289**, 617–619.

Brunoud G, Wells DM, Oliva M, *et al.* 2012. A novel sensor to map auxin response and distribution at high spatio-temporal resolution. Nature **482**, 103–106.

Burkart RC, Strotmann VI, Kirschner GK, *et al.* 2019. PLETHORA and WOX5 interaction and subnuclear localisation regulates Arabidopsis root stem cell maintenance. bioRxiv doi: 10.1101/818187 [Preprint].

Bystrova EI, Zhukovskaya NV, Ivanov VB. 2018. Dependence of root cell growth and division on root diameter. Russian Journal of Developmental Biology **49**, 79–86.

Causier B, Ashworth M, Guo W, Davies B. 2012. The TOPLESS interactome: a framework for gene repression in Arabidopsis. Plant Physiology **158**, 423–438.

Chilley PM, Casson SA, Tarkowski P, Hawkins N, Wang KL, Hussey PJ, Beale M, Ecker JR, Sandberg GK, Lindsey K. 2006. The POLARIS peptide of *Arabidopsis* regulates auxin transport and root growth via effects on ethylene signaling. The Plant Cell **18**, 3058–3072.

Chu H, Liang W, Li J, *et al.* 2013. A CLE–WOX signalling module regulates root meristem maintenance and vascular tissue development in rice. Journal of Experimental Botany **64**, 5359–5369.

Clark NM, Fisher AP, Berckmans B, *et al.* 2020. Protein complex stoichiometry and expression dynamics of transcription factors modulate stem cell division. Proceedings of the National Academy of Sciences, USA **117**, 15332–15342.

Clowes FAL. 1953. The cytogenerative centre in roots with broad columellas. New Phytologist **52**, 48–57.

Clowes FAL. 1956. Nucleic acids in the root apical meristems of *Zea*. New Phytologist **55**, 29–34.

Cruz-Ramírez A, Díaz-Triviño S, Wachsman G, *et al.* 2013. A SCARECROW-RETINOBLASTOMA protein network controls protective quiescence in the Arabidopsis root stem cell organizer. PLoS Biology **11**, e1001724.

Cui H, Levesque MP, Vernoux T, Jung JW, Paquette AJ, Gallagher KL, Wang JY, Blilou I, Scheres B, Benfey PN. 2007. An evolutionarily conserved mechanism delimiting SHR movement defines a single layer of endodermis in plants. Science **316**, 421–425.

Di Laurenzio L, Wysocka-Diller J, Malamy JE, Pysh L, Helariutta Y, Freshour G, Hahn MG, Feldmann KA, Benfey PN. 1996. The *SCARECROW* gene regulates an asymmetric cell division that is essential for generating the radial organization of the Arabidopsis root. Cell **86**, 423–433.

Ding Z, Friml J. 2010. Auxin regulates distal stem cell differentiation in *Arabidopsis* roots. Proceedings of the National Academy of Sciences, USA **107**, 12046–12051.

Ding Z, Wang B, Moreno I, *et al.* 2012. ER-localized auxin transporter PIN8 regulates auxin homeostasis and male gametophyte development in *Arabidopsis*. Nature Communications **3**, 941.

Dolan L, Janmaat K, Willemsen V, Linstead P, Poethig S, Roberts K, Scheres B. 1993. Cellular organisation of the *Arabidopsis thaliana* root. Development **119**, 71–84.

Drisch RC, Stahl Y. 2015. Function and regulation of transcription factors involved in root apical meristem and stem cell maintenance. Frontiers in Plant Science **6**, 505.

Dubrovsky JG, Barlow PW. 2015. The origins of the quiescent centre concept. New Phytologist **206**, 493–496.

Espinosa-Ruiz A, Martínez C, de Lucas M, Fàbregas N, Bosch N, Caño-Delgado AI, Prat S. 2017. TOPLESS mediates brassinosteroid control of shoot boundaries and root meristem development in *Arabidopsis thaliana*. Development **144**, 1619–1628.

Forzani C, Aichinger E, Sornay E, Willemsen V, Laux T, Dewitte W, Murray JA. 2014. WOX5 suppresses *CYCLIN D* activity to establish quiescence at the center of the root stem cell niche. Current Biology **24**, 1939–1944.

Friml J, Vieten A, Sauer M, Weijers D, Schwarz H, Hamann T, Offringa R, Jürgens G. 2003. Efflux-dependent auxin gradients establish the apical–basal axis of *Arabidopsis*. Nature **426**, 147–153.

Fujie M, Kuroiwa H, Suzuki T, Kawano S, Kuroiwa T. 1993. Organelle DNA synthesis in the quiescent centre of *Arabidopsis thaliana* (Col.). Journal of Experimental Botany **44**, 689–693.

Galinha C, Hofhuis H, Luijten M, Willemsen V, Blilou I, Heidstra R, Scheres B. 2007. PLETHORA proteins as dose-dependent master regulators of *Arabidopsis* root development. Nature **449**, 1053–1057.

Gälweiler L, Guan C, Müller A, Wisman E, Mendgen K, Yephremov A, Palme K. 1998. Regulation of polar auxin transport by AtPIN1 in *Arabidopsis* vascular tissue. Science **282**, 2226–2230.

García-Gómez ML, Garay-Arroyo A, García-Ponce B, Sánchez MP, Álvarez-Buylla ER. 2021. Hormonal regulation of stem cell proliferation at the *Arabidopsis thaliana* root stem cell niche. Frontiers in Plant Science **12**, 628491.

García-Gómez ML, Ornelas-Ayala D, Garay-Arroyo A, García-Ponce B, Sánchez MP, Álvarez-Buylla ER. 2020. A system-level mechanistic explanation for asymmetric stem cell fates: *Arabidopsis thaliana* root niche as a study system. Scientific Reports **10**, 3525.

González-García MP, Vilarrasa-Blasi J, Zhiponova M, Divol F, Mora-García S, Russinova E, Caño-Delgado AI. 2011. Brassinosteroids control meristem size by promoting cell cycle progression in *Arabidopsis* roots. Development **138**, 849–859.

Grieneisen VA, Xu J, Marée AF, Hogeweg P, Scheres B. 2007. Auxin transport is sufficient to generate a maximum and gradient guiding root growth. Nature **449**, 1008–1013.

Guo Y, Han L, Hymes M, Denver R, Clark SE. 2010. CLAVATA2 forms a distinct CLE-binding receptor complex regulating Arabidopsis stem cell specification. The Plant Journal **63**, 889–900.

Heidstra R, Sabatini S. 2014. Plant and animal stem cells: similar yet different. Nature Reviews. Molecular Cell Biology **15**, 301–312.

Helariutta Y, Fukaki H, Wysocka-Diller J, Nakajima K, Jung J, Sena G, Hauser MT, Benfey PN. 2000. The *SHORT-ROOT* gene controls radial patterning of the *Arabidopsis* root through radial signaling. Cell **101**, 555–567.

Herud-Sikimić O, Stiel AC, Kolb M, Shanmugaratnam S, Berendzen KW, Feldhaus C, Höcker B, Jürgens G. 2021. A biosensor for the direct visualization of auxin. Nature **592**, 768–772.

Heyman J, Cools T, Vandenbussche F, *et al.* 2013. ERF115 controls root quiescent center cell division and stem cell replenishment. Science **342**, 860–863.

Heyman J, Kumpf RP, De Veylder L. 2014. A quiescent path to plant longevity. Trends in Cell Biology **24**, 443–448.

Hochholdinger F, Zimmermann R. 2008. Conserved and diverse mechanisms in root development. Current Opinion in Plant Biology **11**, 70–74.

Jiang K, Feldman LJ. 2005. Regulation of root apical meristem development. Annual Review of Cell and Developmental Biology **21**, 485–509.

Jiang K, Meng YL, Feldman LJ. 2003. Quiescent center formation in maize roots is associated with an auxin-regulated oxidizing environment. Development **130**, 1429–1438.

Kagale S, Rozwadowski K. 2011. EAR motif-mediated transcriptional repression in plants: an underlying mechanism for epigenetic regulation of gene expression. Epigenetics **6**, 141–146.

Kamiya N, Nagasaki H, Morikami A, Sato Y, Matsuoka M. 2003. Isolation and characterization of a rice *WUSCHEL*-type homeobox gene that is specifically expressed in the central cells of a quiescent center in the root apical meristem. The Plant Journal **35**, 429–441.

Kieffer M, Stern Y, Cook H, Clerici E, Maulbetsch C, Laux T, Davies B. 2006. Analysis of the transcription factor WUSCHEL and its functional homologue in *Antirrhinum* reveals a potential mechanism for their roles in meristem maintenance. The Plant Cell **18**, 560–573.

Kirschner GK, Stahl Y, Von Korff M, Simon R. 2017. Unique and conserved features of the barley root meristem. Frontiers in Plant Science **8**, 1240.

Koizumi K, Hayashi T, Gallagher KL. 2012. SCARECROW reinforces SHORT-ROOT signaling and inhibits periclinal cell divisions in the ground tissue by maintaining SHR at high levels in the endodermis. Plant Signaling & Behavior **7**, 1573–1577.

Kong X, Tian H, Yu Q, *et al.* 2018. PHB3 maintains root stem cell niche identity through ROS-responsive AP2/ERF transcription factors in *Arabidopsis*. Cell Reports **22**, 1350–1363.

Krogan NT, Hogan K, Long JA. 2012. APETALA2 negatively regulates multiple floral organ identity genes in *Arabidopsis* by recruiting the co-repressor TOPLESS and the histone deacetylase HDA19. Development **139**, 4180–4190.

Lee S, Seo PJ, Lee HJ, Park CM. 2012. A NAC transcription factor NTL4 promotes reactive oxygen species production during drought-induced leaf senescence in Arabidopsis. The Plant Journal **70**, 831–844.

Li L, Clevers H. 2010. Coexistence of quiescent and active adult stem cells in mammals. Science **327**, 542–545.

Li P, Cai Q, Wang H, *et al.* 2020. Hydrogen peroxide homeostasis provides beneficial micro-environment for SHR-mediated periclinal division in *Arabidopsis* root. New Phytologist **228**, 1926–1938.

Liao CY, Smet W, Brunoud G, Yoshida S, Vernoux T, Weijers D. 2015. Reporters for sensitive and quantitative measurement of auxin response. Nature Methods **12**, 207–10, 2 p following 210.

Long JA, Ohno C, Smith ZR, Meyerowitz EM. 2006. TOPLESS regulates apical embryonic fate in *Arabidopsis*. Science **312**, 1520–1523.

Long Y, Stahl Y, Weidtkamp-Peters S, *et al.* 2017. *In vivo* FRET–FLIM reveals cell-type-specific protein interactions in *Arabidopsis* roots. Nature **548**, 97–102.

Mähönen AP, Ten Tusscher K, Siligato R, Smetana O, Díaz-Triviño S, Salojärvi J, Wachsman G, Prasad K, Heidstra R, Scheres B. 2014. PLETHORA gradient formation mechanism separates auxin responses. Nature **515**, 125–129.

Moreno-Risueno MA, Sozzani R, Yardımcı GG, *et al.* 2015. Transcriptional control of tissue formation throughout root development. Science **350**, 426–430.

Müller R, Bleckmann A, Simon R. 2008. The receptor kinase CORYNE of Arabidopsis transmits the stem cell-limiting signal CLAVATA3 independently of CLAVATA1. The Plant Cell **20**, 934–946.

Nakajima K, Sena G, Nawy T, Benfey PN. 2001. Intercellular movement of the putative transcription factor SHR in root patterning. Nature **413**, 307–311.

Nardmann J, Zimmermann R, Durantini D, Kranz E, Werr W. 2007. *WOX* gene phylogeny in *Poaceae*: a comparative approach addressing leaf and embryo development. Molecular Biology and Evolution **24**, 2474–2484.

Ni J, Shen Y, Zhang Y, Wu P. 2014. Definition and stabilisation of the quiescent centre in rice roots. Plant Biology **16**, 1014–1019.

Ohme-Takagi M, Shinshi H. 1995. Ethylene-inducible DNA binding proteins that interact with an ethylene-responsive element. The Plant Cell **7**, 173–182.

Ortega-Martínez O, Pernas M, Carol RJ, Dolan L. 2007. Ethylene modulates stem cell division in the *Arabidopsis thaliana* root. Science **317**, 507–510.

Pi L, Aichinger E, van der Graaff E, Llavata-Peris CI, Weijers D, Hennig L, Groot E, Laux T. 2015. Organizer-derived WOX5 signal maintains root columella stem cells through chromatin-mediated repression of *CDF4* expression. Developmental Cell **33**, 576–588.

Pieterse CM, Van der Does D, Zamioudis C, Leon-Reyes A, Van Wees SC. 2012. Hormonal modulation of plant immunity. Annual Review of Cell and Developmental Biology **28**, 489–521.

Rademacher EH, Möller B, Lokerse AS, Llavata-Peris CI, van den Berg W, Weijers D. 2011. A cellular expression map of the Arabidopsis *AUXIN RESPONSE FACTOR* gene family. The Plant Journal **68**, 597–606.

Rahman A, Hosokawa S, Oono Y, Amakawa T, Goto N, Tsurumi S. 2002. Auxin and ethylene response interactions during Arabidopsis root hair development dissected by auxin influx modulators. Plant Physiology **130**, 1908–1917.

Sabatini S, Heidstra R, Wildwater M, Scheres B. 2003. SCARECROW is involved in positioning the stem cell niche in the *Arabidopsis* root meristem. Genes & Development **17**, 354–358.

Sánchez Alvarado A, Yamanaka S. 2014. Rethinking differentiation: stem cells, regeneration, and plasticity. Cell **157**, 110–119.

Sarkar AK, Luijten M, Miyashima S, Lenhard M, Hashimoto T, Nakajima K, Scheres B, Heidstra R, Laux T. 2007. Conserved factors regulate signalling in *Arabidopsis thaliana* shoot and root stem cell organizers. Nature **446**, 811–814.

Schofield R. 1978. The relationship between the spleen colony-forming cell and the haemopoietic stem cell. Blood Cells **4**, 7–25.

Schoof H, Lenhard M, Haecker A, Mayer KF, Jürgens G, Laux T. 2000. The stem cell population of *Arabidopsis* shoot meristems in maintained by a regulatory loop between the *CLAVATA* and *WUSCHEL* genes. Cell **100**, 635–644.

Shimotohno A, Heidstra R, Blilou I, Scheres B. 2018. Root stem cell niche organizer specification by molecular convergence of PLETHORA and SCARECROW transcription factor modules. Genes & Development **32**, 1085–1100.

Smith S, De Smet I. 2012. Root system architecture: insights from *Arabidopsis* and cereal crops. Philosophical Transactions of the Royal Society of London. Series B, Biological Sciences **367**, 1441–1452.

Sozzani R, Cui H, Moreno-Risueno MA, Busch W, Van Norman JM, Vernoux T, Brady SM, Dewitte W, Murray JA, Benfey PN. 2010. Spatiotemporal regulation of cell-cycle genes by SHORTROOT links patterning and growth. Nature **466**, 128–132.

Spradling A, Drummond-Barbosa D, Kai T. 2001. Stem cells find their niche. Nature **414**, 98–104.

Stahl Y, Grabowski S, Bleckmann A, *et al.* 2013. Moderation of *Arabidopsis* root stemness by CLAVATA1 and ARABIDOPSIS CRINKLY4 receptor kinase complexes. Current Biology **23**, 362–371.

Stahl Y, Wink RH, Ingram GC, Simon R. 2009. A signaling module controlling the stem cell niche in *Arabidopsis* root meristems. Current Biology **19**, 909–914.

Stepanova AN, Hoyt JM, Hamilton AA, Alonso JM. 2005. A link between ethylene and auxin uncovered by the characterization of two root-specific ethylene-insensitive mutants in Arabidopsis. The Plant Cell **17**, 2230–2242.

Timilsina R, Kim JH, Nam HG, Woo HR. 2019. Temporal changes in cell division rate and genotoxic stress tolerance in quiescent center cells of Arabidopsis primary root apical meristem. Scientific Reports **9**, 3599.

Tsukagoshi H, Busch W, Benfey PN. 2010. Transcriptional regulation of ROS controls transition from proliferation to differentiation in the root. Cell **143**, 606–616.

van Aken O, Pecenková T, van de Cotte B, *et al.* 2007. Mitochondrial type-I prohibitins of *Arabidopsis thaliana* are required for supporting proficient meristem development. The Plant Journal **52**, 850–864.

van den Berg C, Willemsen V, Hendriks G, Weisbeek P, Scheres B. 1997. Short-range control of cell differentiation in the *Arabidopsis* root meristem. Nature **390**, 287–289.

Vilarrasa-Blasi J, González-García MP, Frigola D, *et al.* 2014. Regulation of plant stem cell quiescence by a brassinosteroid signaling module. Developmental Cell **30**, 36–47.

Wang Z, Rong D, Chen D, *et al.* 2021. Salicylic acid promotes quiescent center cell division through ROS accumulation and down-regulation of PLT1, PLT2, and WOX5. Journal of Integrative Plant Biology **63**, 583–596.

Wildwater M, Campilho A, Perez-Perez JM, Heidstra R, Blilou I, Korthout H, Chatterjee J, Mariconti L, Gruissem W, Scheres B. 2005. The *RETINOBLASTOMA-RELATED* gene regulates stem cell maintenance in *Arabidopsis* roots. Cell **123**, 1337–1349.

Yin Y, Wang ZY, Mora-Garcia S, Li J, Yoshida S, Asami T, Chory J. 2002. BES1 accumulates in the nucleus in response to brassinosteroids to regulate gene expression and promote stem elongation. Cell **109**, 181–191.

Zhai H, Zhang X, You Y, Lin L, Zhou W, Li C. 2020. SEUSS integrates transcriptional and epigenetic control of root stem cell organizer specification. The EMBO Journal **39**, e105047.

Zhang H, Han W, De Smet I, Talboys P, Loya R, Hassan A, Rong H, Jürgens G, Paul Knox J, Wang MH. 2010. ABA promotes quiescence of the quiescent centre and suppresses stem cell differentiation in the Arabidopsis primary root meristem. The Plant Journal **64**, 764–774.

Zhang ML, Huang PP, Ji Y, Wang S, Wang SS, Li Z, Guo Y, Ding Z, Wu WH, Wang Y. 2020. KUP9 maintains root meristem activity by regulating K^+ and auxin homeostasis in response to low K. EMBO Reports **21**, e50164.

Zhang W, Swarup R, Bennett M, Schaller GE, Kieber JJ. 2013. Cytokinin induces cell division in the quiescent center of the *Arabidopsis* root apical meristem. Current Biology **23**, 1979–1989.

Zhang Y, Jiao Y, Liu Z, Zhu YX. 2015. ROW1 maintains quiescent centre identity by confining *WOX5* expression to specific cells. Nature Communications **6**, 6003.

Zhao Q, Zhou L, Liu J, *et al.* 2018. Involvement of CAT in the detoxification of HT-induced ROS burst in rice anther and its relation to pollen fertility. Plant Cell Reports **37**, 741–757.

Zhou W, Lozano-Torres JL, Blilou I, Zhang X, Zhai Q, Smant G, Li C, Scheres B. 2019. A jasmonate signaling network activates root stem cells and promotes regeneration. Cell **177**, 942–956.e14.

Chapter 2

Unlocking nature's (sub)cellular symphony: Phase separation in plant meristems

This manuscript was published in *Current Opinion in Plant Biology* in October 2023.

https://doi.org/10.1016/j.pbi.2023.102480

Authors

Ali Eljebbawi[1], Anika Dolata[1], Vivien I. Strotmann[1] and Yvonne Stahl[1,2]*

Affiliation

[1]Institute for Developmental Genetics, Heinrich-Heine-University, Universitätsstr. 1, 40225 Düsseldorf

[2]Cluster of Excellence on Plant Sciences (CEPLAS), Heinrich-Heine-University, Universitätsstr. 1, 40225 Düsseldorf

*corresponding author

Author contribution

I contributed to writing the chapter 'LLPS in the aboveground tissues' as well as designing and producing the tables and figures.

Available online at www.sciencedirect.com

ScienceDirect

Current Opinion in Plant Biology

Unlocking nature's (sub)cellular symphony: Phase separation in plant meristems

Ali Eljebbawi[1], Anika Dolata[1], Vivien I. Strotmann[1] and Yvonne Stahl[1,2]

Abstract

Plant development is based on the balance of stem cell maintenance and differentiation in the shoot and root meristems. The necessary cell fate decisions are regulated by intricate networks of proteins and biomolecules within plant cells and require robust and dynamic compartmentalization strategies, including liquid-liquid phase separation (LLPS), which allows the formation of membrane-less compartments. This review summarizes the current knowledge about the emerging field of LLPS in plant development, with a particular focus on the shoot and root meristems. LLPS regulates not only floral transition and flowering time while integrating environmental signals in the shoots but also influences auxin signalling and is putatively involved in maintaining the stem cell niche (SCN) in the roots. Therefore, LLPS has the potential to play a crucial role in the plasticity of plant development, necessitating further research for a comprehensive understanding.

Addresses

[1] Institute for Developmental Genetics, Heinrich-Heine University Duesseldorf, Germany

[2] Cluster of Excellence on Plant Sciences (CEPLAS), Heinrich-Heine University Duesseldorf, Germany

Corresponding author: Stahl, Yvonne (Yvonne.Stahl@hhu.de)

Current Opinion in Plant Biology 2023, **76:**102480

This review comes from a themed issue on **Growth and development 2023**

Edited by **Zachary L Nimchuk** and **Ikram Blilou**

For a complete overview see the Issue and the Editorial

Available online xxx

https://doi.org/10.1016/j.pbi.2023.102480

Keywords

Phase separation, Cellular compartmentalization, Shoot apical meristem, Root apical meristem, Stem cell maintenance.

Introduction

During their development, plants maintain niches of stem cells within their shoot apex (shoot apical meristem, SAM) and root apex (root apical meristem, RAM) to ensure postembryonic growth and *de novo* formation of organs throughout their lifecycle [1]. Within the meristems, stem cells are renewed as they divide, giving rise to daughter cells, which eventually differentiate into the various tissues and organs [2]. The homeostasis between SCN maintenance and differentiation is tightly controlled by proteins and other biomolecules in an intricate regulatory network. Consequently, plant cells, which are the fundamental building blocks of all tissues and organs, must undergo various structural [3], biochemical [4], and transcriptional changes [5] during cell fate decisions rendering their inner environment highly dynamic [6]. At this juncture, cellular compartmentalization, such as into membrane-bound organelles, allows the coexistence and independent management of the diverse functions within isolated compartments inside the cells [7]. Moreover, cells evolved transient compartmentalization strategies, such as into non-membrane-bound compartments through liquid-liquid phase separation (LLPS), addressing their requirement for more spatiotemporally -precise and -dynamic regulating mechanisms.

LLPS is a mechanism during which membrane-less bodies of biomolecules, such as proteins and RNA, spontaneously and dynamically form as they segregate into distinct non-mixing liquid phases (Figure 1). LLPS can thus allow a dynamic compartmentalization of subcellular components into functional domains [8–10]. The different studies on LLPS refer to these subcellular domains as biomolecular "bodies", "condensates", "puncta", "foci", "speckles", or "aggregates". Over the past decade, LLPS research has experienced significant growth, particularly in the study of animals and yeast, where biomolecular condensates have emerged as key players in important processes including environmental sensing, intracellular storage, subcellular localization, and morphological shaping [11–13]. In recent years, there has been a growing focus on studying LLPS in plants, revealing its significant influence on various aspects of plant biology, including plant development, flowering, photomorphogenesis, autophagy [14] and stress tolerance [15]. [8,16].

Additionally, LLPS may be evoked by diverse abiotic and biotic factors such as temperature, salt concentration,

Figure 1

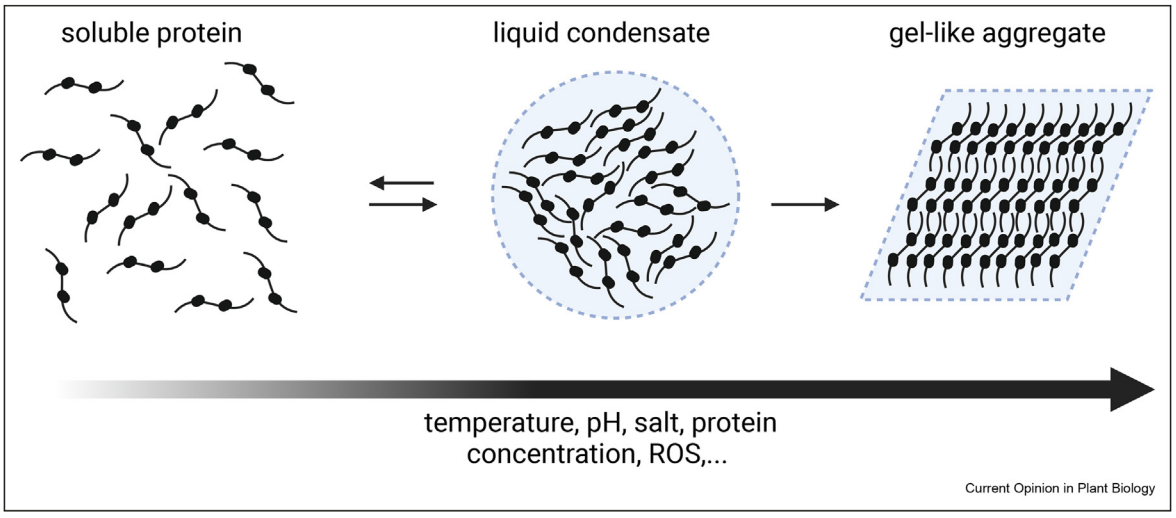

Driving forces of liquid and solid condensate formation. Variations in temperature, pH, salt levels, ROS (Reactive Oxygen Species), or protein concentrations can initiate the assembly of liquid condensates, which are predominantly reversible. Under certain conditions, gel-like condensates may potentially emerge. This figure was created using BioRender.com.

or the presence of intrinsically disordered proteins [17]. To illustrate, several proteins are characterized by intrinsically disordered regions (IDRs) within their sequences, such as low-complexity domains (LCDs) and prion-like-domains (PrDs). These IDRs which are enriched in eukaryotic transcription factors (TFs), including plants, promote LLPS due to their lack of a defined 3D-structure, their flexibility, and their conformation switching attribute, thus also allowing multivalency of interactions [18].

Lately, LLPS has become a relevant topic in plant biology as it is involved in regulating developmental and physiological processes [10,19,20]. In this review article, we highlight the latest findings about subcellular compartmentalization via LLPS in the context of plant development, with particular focus on the hormonal and transcriptional control within the above- and below-ground meristematic tissues.

LLPS and phase separation in plant development

LLPS in the aboveground tissues

In the SAM, developmental and environmental signals are integrated into the balance between stem cell maintenance in its center and the production of new organs at its periphery. In its vegetative state, the SAM produces new leaves, but after entering the reproductive state it produces flowers. This transition is crucial for reproductive success and therefore requires fine-tuned regulation [21].

Floral transition relies on phase separation

FLOWERING LOCUS C (FLC) is a well-described temperature-regulated repressor of floral transition in *Arabidopsis thaliana*. Cold-induced changes in the FLC chromatin structure are important for stable silencing and require VERNALIZATION 1 (VRN1) [22]. A combination of *in vivo* and *in vitro* studies revealed that upon binding of VRN1 to non-specific DNA fragments, phase separation is induced, leading to the formation of liquid-like droplets [23]. Droplet formation not only requires the IDR of VRN1, but also the flanking B3 DNA-binding motifs, emphasizing the DNA dependency of this mechanism (Table 1). In addition, the composition of the IDR is important as its acidic and basic patches are necessary for proper droplet size. So far, the exact molecular trigger and mechanism remain unclear, but it is very likely involving temperature.

An already described example for temperature response as a reaction to environmental changes is the recruitment of histone modifiers to the *FLC* promoter by FRIGIDA (FRI) under warm conditions (Figure 2 a) [24]. At low temperatures, FRI forms stable condensates that sequester FRI away from the *FLC* locus leading to a shutdown of its expression. The formation of FRI condensates at low temperatures is supported by COOLAIR which thereby indirectly regulates *FLC* expression (Figure 2 a′) [25]. The alternative 3' processing of *COOLAIR* is regulated by FLOWERING CONTROL LOCUS A (FCA). Recent studies have

Table 1

Body-forming developmental regulators in the shoot and root meristems. IDR: intrinsically disordered region; PrD: prion-like domain; B3: B3 DNA-binding domain; ?: uncertain/unknown.

Name	Function	Phase separation mediating domain	Reference
Floral transition/Flowering time			
VRN1	Induction of structural changes of the *FLC* chromatin to ensure stable gene silencing	IDR, B3	Zhou et al., 2019 [16]
FRI	Sequestration away from the *FLC*-locus for expression shutdown	PrDs	Zhu et al., 2021 [17]
FCA	Regulation of COOLAIR, an antisense transcript of *FLC*	PrDs	Fang et al., 2019 [18]
FLL2	Promotion of FCA phase separation and NB formation	?	Fang et al., 2019 [18]
TFAM	Carnalization mechanism to increase robustness of flower development together with TMF in tomato	IDRs	Huang et al., 2022 [20]
TMF	Repression of *AN* to regulate flower transition in tomato	cysteines in IDRs	Huang et al., 2021 [19]
ELF3	Response to temperature changes	PrDs	Jung et al., 2020 [21]
Root development			
PLT3	Determination of distal stem cell fate	PrDs	Burkart et al., 2022b [32]
ARF19	Attenuation of auxin responsiveness and modulating downstream transcriptional responses	PrD	Powers et al., 2019 [28]
SFH8	Maintenance of polarized transport of PINs at the plasma membrane	IDR	Liu et al., 2022 [30]

Figure 2

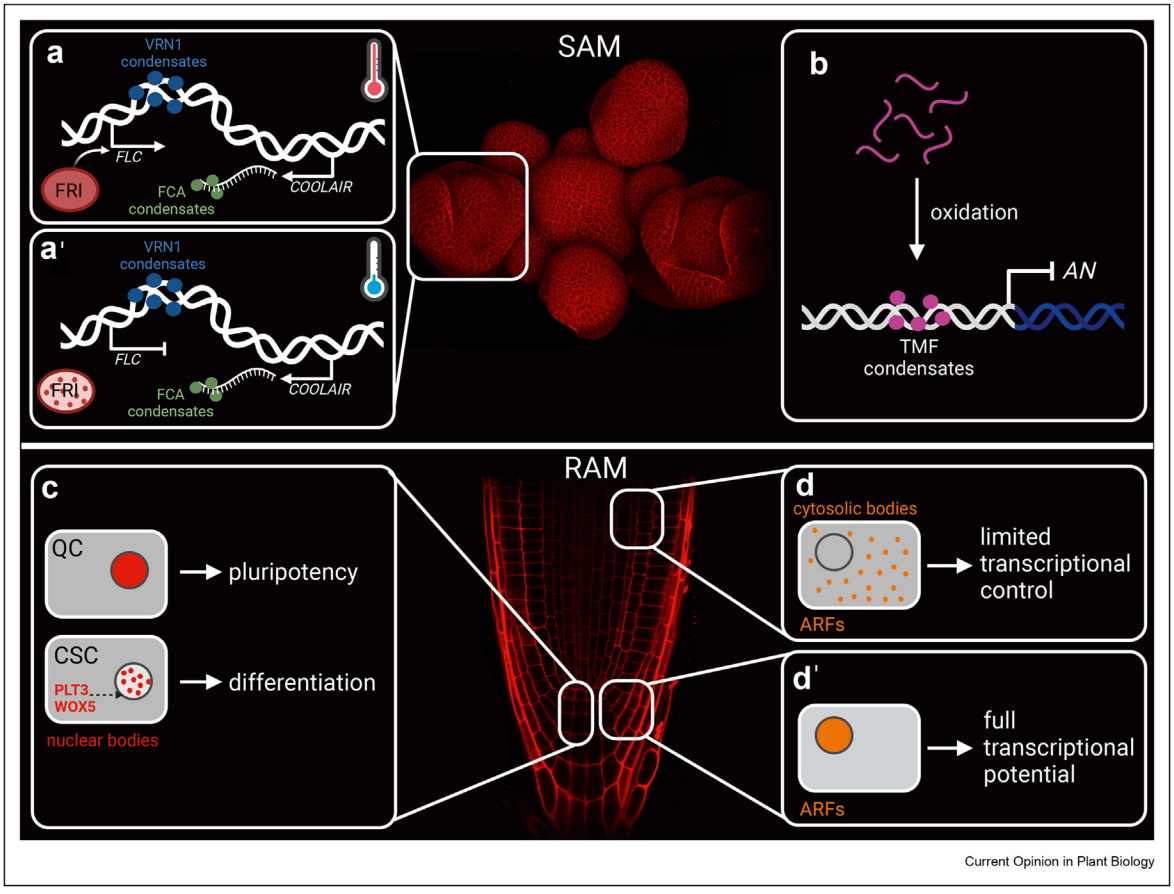

Body formation of developmental regulators in the shoot and root apical meristem. (a-a′) Vernalization in *Arabidopsis* is regulated by several transcriptional regulators that can form bodies: VRN1, FRI and FCA. (**a″**) Flower transition in tomato is controlled by the formation of ROS-dependent bodies by TMF that regulate *AN* expression. **(b, b′)** In the *Arabidopsis* root, ARFs form cell type specific cytosolic bodies to spatially control auxin response. (**b″**) PLT3 recruits WOX5 into nuclear bodies to specify stem cell fate in the *Arabidopsis* RAM. SAM: shoot apical meristem; RAM: root apical meristem; QC: quiescent center; CSC: columella stem cell. This figure was created with BioRender.com.

shown that PrDs can act as a driver for phase separation of RNA-binding proteins. FCA contains two PrDs that mediate localization to nuclear bodies with liquid-like properties, indicating LLPS. The highly disordered protein FLL*2* is required for FCA function and co-localizes to nuclear bodies (NBs) with FCA. It has been shown that FLL*2* promotes phase-separation of FCA to form NBs (Table 1) [25].

In tomato, the timing of flower transition was recently linked to the ALOG (Arabidopsis LSH1 and Oryza G1) family gene TERMINATING FLOWER (TMF) in a reactive oxygen species (ROS)-dependent mechanism [26]. *In vitro* and *in vivo* localization studies revealed that TMF forms ROS-dependent liquid-like condensates. The underlying LLPS leading to condensate formation is triggered by cysteine residues located in the IDRs. In an oxidative microenvironment, these cysteines form intermolecular disulfide bonds, promoting the homomerization of TMF which act as transcriptional repressors of *ANANTHA* (*AN*) to regulate flowering transition (Figure 2 b).

Furthermore, TMF-dependent regulation of *AN* was found to be part of a novel genetic canalization mechanism that provides developmental robustness in flower transition [27]. The genetic redundancy of TMF and TMF FAMILY MEMBERs (TFAMs) shows high variation, resulting in gradually enhanced precocious flowering and defective floral organs. TFAMs, like TMF, undergo phase separation mediated by prion-like IDRs. Modifications of these IDRs, caused by gene duplication, result in divergent phase separation capabilities accompanied by varying transcriptional abundance. Together, TMF and TFAMs form heterotypic condensates that repress *AN* to prevent precocious flowering in tomato (Table 1).

Flowering time is regulated by temperature-dependent phase separation

NB formation mediated by PrDs was also shown for EARLY FLOWERING 3 (ELF3) as a response to temperature [28]. The expression of ELF3 shows formation of speckles at high temperatures which depends on the presence of PrDs. Binding of ELF3 to its target genes decreases with increasing temperatures. However, lack of PrDs leads to a loss of this effect indicating an important function of these domains in the thermoresponsiveness of ELF3 binding target genes. ELF3 was found to exist in two conformations, an active soluble form and a multimeric form that is visible as speckles at high temperatures. The PrDs of ELF3 act as a tunable thermosensor allowing dynamic responses to temperature changes via LLPS. For instance, *elf3* mutants, which show rapid floral transition at ambient temperatures, are irresponsive to the thermal induction of flowering (Table 1).

A recent publication provided more insight on the nature of the previously described ELF3 speckles [29]. Here it was shown that the observed puncta of ELF3 consist of a mixture of mobile and immobile species, indicating LLPS. Temperature and pH have effects on the formation of puncta, increasing their number at higher temperatures. The impact of temperature on LLPS is largely reversible as shifts to cold temperatures lead to a loss of puncta. This further indicates the highly dynamic capabilities of regulating development by LLPS.

LLPS in the underground tissues

The root system of higher plants provides access to nutrients and water as well as anchorage to the soil. To ensure optimal growth and development, the quiescent center (QC) and the abutting initials located in the middle of the RAM, produce new cells for the different tissues during the entire lifespan of the plant. This process is highly regulated by a multitude of molecules, including peptides and their receptors, hormones, and transcription factors [30].

SFH8, a Nodulin Sec14-like protein, form cytoplasmic puncta in the distal meristem

Another study highlighted that PIN2 localization is controlled by the establishment of plasma membrane (PM) polar domains via the interaction between SEC FOURTEEN-HOMOLOG8 (SFH8) and kinesin-separase complex (KISC) [31]. KISC compromises EXTRA SPINDLE POLES (ESP) and three Kinesin 7 (KIN7) homologs (KIN7.1, KIN7.3, and KIN7.5) which all lack lipid binding motifs. However, KISC associates with the PM and modulates its polar domains, as ESP or KIN7.3 mutations reduce PIN delivery to the PM [32].

KISC colocalizes with SFH8, a SEC14-like lipid transfer protein, which acts as a KISC tether to the PM, and in turn, KISC promotes SFH8 polarization in the meristematic/transition zone (distal meristem), but not in the “core” or proximal meristem. SFH8 was shown to form mobile LLPS clusters inaccessible to KISC at the PM in the “core” meristem. However, it is cleaved by ESP at its R84 residue in the distal meristem, producing N-terminus cytoplasmic puncta and C-terminus filaments to which KISC associates. Indeed, the N-terminus of the SFH8 protein comprises an IDR which promotes LLPS-mediated cluster formation, thus, when it is cleaved by KISC, SFH8 undergoes cluster-to-filament transition (Table 1). The produced filaments are more stable and associate with KISC at the PM.

Consequently, subsets of polar domains are established by LLPS, allowing the delivery and association of proteins like PIN2 with the PM. These LLPS-driven regulations of auxin distributors can change the plant developmental robustness [31].

Nuclear bodies formed by PLETHORA 3 in the root SCN

The interaction of PLETHORA 3 (PLT3) and WUSCHEL-RELATED HOMEOBOX 5 (WOX5), two key transcriptional regulators of root stem cell maintenance which have been shown to act downstream of auxin, has been recently reported [33]. PLT3 contains PrDs, which facilitate the formation of nuclear bodies (NBs) and are necessary for the interaction with and translocation of WOX5 to NBs to maintain columella stem cell fate (Table 1). The PLT3 NBs also colocalize with RNA and are hypothesized to result from LLPS. Further investigations are required to verify whether LLPS is involved in the underlying mechanism (Figure 2c).

ARF7 and ARF19 assemble into cytoplasmic bodies in the upper root

Auxin acts ubiquitously as master regulator in plant development, where its polar distribution regulates many developmental processes, including growth patterning and meristematic positioning [34,35]. Lately, various actors in the auxin network were shown to undergo phase separation. AUXIN RESPONSE FACTORS (ARFs) modulate gene expression by targeting the auxin response elements (AREs) in gene promoters via their N-terminal B3-type DNA-binding domains [36]. Additionally, ARFs have a variable middle region (MR) and a C-terminal type I/II Phox and Bem1p (PB1) domain important for its interactions [37].

A recent study showed that the ARF7 and ARF19 form micron-sized cytoplasmic condensates in mature cells in the upper root via a cell-type dependent mechanism [38]. Here, ARF19 multimerizes and forms cytoplasmic assemblies, depending on its PB1 domain electrostatic asymmetries and its PrD-containing MR (Table 1). The PB1 domain associations form semi-stable filaments, providing the MR bristles a multivalence for lateral associations, and thus an extended scaffold for higher-order organizations with other ARFs. Consequently, ARFs may be sequestered into biomolecular condensates altering their nuclear-cytoplasmic partitioning, hence attenuating auxin signalling and modulating downstream transcriptional responses. This mechanism represents another link between development and phase separation (Figure 2 d-d') [38,39].

Conclusion

In conclusion, the emerging field of LLPS offers novel and exciting insights into the intricate regulation of plant development. In shoots, LLPS is involved in the regulation of floral transition and flowering time by temperature, DNA binding motifs, and oxidative microenvironments. In roots, LLPS putatively contributes to the maintenance of stem cells and auxin signalling. Nuclear bodies and cytoplasmic condensates formed by transcription factors and regulatory proteins modulate gene expression, protein localization and interactions. Indeed, further research is needed to fully understand the mechanisms and functional implications of LLPS in plants. For instance, numerous undiscovered plant-specific proteins and RNAs may play roles in LLPS, necessitating exploration of their contributions to cellular processes and functional outcomes. Additionally, the development of advanced techniques and tools can enhance our understanding of LLPS dynamics in plant cells. Further investigation is also required to determine whether LLPS exhibits conservation across plant species and to explore potential applications in agriculture, including the enhancement of crop traits and stress tolerance.

Authors' contribution

All authors contributed to writing and editing this review.

Declaration of competing interest

The authors declare the following financial interests/personal relationships which may be considered as potential competing interests: Yvonne Stahl reports financial support was provided by German Research Foundation.

Data availability

No data was used for the research described in the article.

Acknowledgements

We thank Meik Thiele for providing the image of the shoot apical meristem. We acknowledge funding by the Deutsche Forschungsgemeinschaft (DFG, German Research Foundation) under Germany's Excellence Strategy – EXC-2048/1 – project ID 390686111. We would like to apologize to all colleagues whose relevant work could not be mentioned due to space restrictions.

References

Papers of particular interest, published within the period of review, have been highlighted as:

* of special interest
** of outstanding interest

1. Su YH, Zhou C, Li YJ, *et al.*: **Integration of pluripotency pathways regulates stem cell maintenance in the Arabidopsis shoot meristem**. *Proc Natl Acad Sci U S A* 2020, **117**: 22561–22571, https://doi.org/10.1073/pnas.2015248117 [PMID: 32839309].

2. Umeda M, Ikeuchi M, Ishikawa M, *et al.*: **Plant stem cell research is uncovering the secrets of longevity and persistent growth**. *Plant J* 2021, **106**:326–335, https://doi.org/10.1111/tpj.15184 [PMID: 33533118].

3. Vaahtera L, Schulz J, Hamann T: **Cell wall integrity maintenance during plant development and interaction with the environment**. *Nat Plants* 2019, **5**:924–932, https://doi.org/10.1038/s41477-019-0502-0 [PMID: 31506641].

4. Dong N-Q, Lin H-X: **Contribution of phenylpropanoid metabolism to plant development and plant-environment interactions**. *J Integr Plant Biol* 2021, **63**:180–209, https://doi.org/10.1111/jipb.13054 [PMID: 33325112].

5. Zhao T, Zhan Z, Jiang D: **Histone modifications and their regulatory roles in plant development and environmental**

memory. *J Genet Genom* 2019, **46**:467–476, https://doi.org/10.1016/j.jgg.2019.09.005 [PMID: 31813758].

6. Roeder AHK, Otegui MS, Dixit R, *et al.*: **Fifteen compelling open questions in plant cell biology**. *Plant Cell* 2022, **34**:72–102, https://doi.org/10.1093/plcell/koab225 [PMID: 34529074].

7. Diekmann Y, Pereira-Leal JB: **Evolution of intracellular compartmentalization**. *Biochem J* 2013, **449**:319–331, https://doi.org/10.1042/BJ20120957 [PMID: 23240612].

8. Emenecker RJ, Holehouse AS, Strader LC: **Emerging roles for phase separation in plants**. *Dev Cell* 2020, **55**:69–83, https://doi.org/10.1016/j.devcel.2020.09.010 [PMID: 33049212].

9. Xu X, Zheng C, Lu D, Song C-P, Zhang L: **Phase separation in plants: new insights into cellular compartmentalization**. *J Integr Plant Biol* 2021, **63**:1835–1855, https://doi.org/10.1111/jipb.13152 [PMID: 34314106].

10. Burkart RC, Eljebbawi A, Stahl Y: **Come together now: dynamic body-formation of key regulators integrates environmental cues in plant development**. *Front Plant Sci* 2022, **13**, 1052107, https://doi.org/10.3389/fpls.2022.1052107 [PMID: 36452084].

11. Brangwynne CP, Eckmann CR, Courson DS, *et al.*: **Germline P granules are liquid droplets that localize by controlled dissolution/condensation**. *Science* 2009, **324**:1729–1732, https://doi.org/10.1126/science.1172046 [PMID: 19460965].

12. Belott C, Janis B, Menze MA: **Liquid-liquid phase separation promotes animal desiccation tolerance**. *Proc Natl Acad Sci U S A* 2020, **117**:27676–27684, https://doi.org/10.1073/pnas.2014463117 [PMID: 33077592].

13. Alberti S, Gladfelter A, Mittag T: **Considerations and challenges in studying liquid-liquid phase separation and biomolecular condensates**. *Cell* 2019, **176**:419–434, https://doi.org/10.1016/j.cell.2018.12.035 [PMID: 30682370].

14. Guan B, Xue H-W: **Arabidopsis AUTOPHAGY-RELATED3 (ATG3) facilitates the liquid-liquid phase separation of ATG8e to promote autophagy**. *Sci Bull* 2022, **67**:350–354, https://doi.org/10.1016/j.scib.2021.10.012 [PMID: 36546085].

15. Wang B, Zhang H, Huai J, *et al.*: **Condensation of SEUSS promotes hyperosmotic stress tolerance in Arabidopsis**. *Nat Chem Biol* 2022, **18**:1361–1369, https://doi.org/10.1038/s41589-022-01196-z [PMID: 36376475].

16. Emenecker RJ, Holehouse AS, Strader LC: **Biological phase separation and biomolecular condensates in plants**. *Annu Rev Plant Biol* 2021, **72**:17–46, https://doi.org/10.1146/annurev-arplant-081720-015238 [PMID: 33684296].

17. Hyman AA, Weber CA, Jülicher F: **Liquid-liquid phase separation in biology**. *Annu Rev Cell Dev Biol* 2014, **30**:39–58, https://doi.org/10.1146/annurev-cellbio-100913-013325 [PMID: 25288112].

18. Oldfield CJ, Dunker AK: **Intrinsically disordered proteins and intrinsically disordered protein regions**. *Annu Rev Biochem* 2014, **83**:553–584, https://doi.org/10.1146/annurev-biochem-072711-164947 [PMID: 24606139].

19. Cuevas-Velazquez CL, Dinneny JR: **Organization out of disorder: liquid-liquid phase separation in plants**. *Curr Opin Plant Biol* 2018, **45**(Pt A):68–74, https://doi.org/10.1016/j.pbi.2018.05.005 [PMID: 29859470].

20. Rabouille C, Alberti S: **Cell adaptation upon stress: the emerging role of membrane-less compartments**. *Curr Opin Cell Biol* 2017, **47**:34–42, https://doi.org/10.1016/j.ceb.2017.02.006 [PMID: 28342303].

21. Wang B, Smith SM, Li J: **Genetic regulation of shoot architecture**. *Annu Rev Plant Biol* 2018, **69**:437–468, https://doi.org/10.1146/annurev-arplant-042817-040422 [PMID: 29553800].

22. Levy YY, Mesnage S, Mylne JS, Gendall AR, Dean C: **Multiple roles of Arabidopsis VRN1 in vernalization and flowering time control**. *Science* 2002, **297**:243–246, https://doi.org/10.1126/science.1072147 [PMID: 12114624].

23. Zhou H, Song Z, Zhong S, *et al.*: **Mechanism of DNA-induced phase separation for transcriptional repressor VRN1**. *Angew Chem Int Ed Engl* 2019, **58**:4858–4862, https://doi.org/10.1002/anie.201810373 [PMID: 30762296].

24. * Zhu P, Lister C, Dean C: **Cold-induced Arabidopsis FRIGIDA nuclear condensates for FLC repression**. *Nature* 2021, **599**:657–661, https://doi.org/10.1038/s41586-021-04062-5 [PMID: 34732891].
The authors show regulation of FLC promoter activity by temperature response of FRIGIDA. Cold temperatures lead to a formation of FRI condensates, sequestering it away from *FLC* and therefore shutting down gene expression.

25. Fang X, Wang L, Ishikawa R, *et al.*: **Arabidopsis FLL2 promotes liquid-liquid phase separation of polyadenylation complexes**. *Nature* 2019, **569**:265–269, https://doi.org/10.1038/s41586-019-1165-8 [PMID: 31043738].

26. ** Huang X, Chen S, Li W, *et al.*: **ROS regulated reversible protein phase separation synchronizes plant flowering**. *Nat Chem Biol* 2021, **17**:549–557, https://doi.org/10.1038/s41589-021-00739-0 [PMID: 33633378].
Here, TMF was reported to form ROS-dependent condensates to control flower transition in tomato. Cysteines located within IDRs of TMF were shown to build intermolecular disulfide bonds that lead to homomerization of TMF and thereby condensate formation to repress AN.

27. * Huang X, Xiao N, Zou Y, *et al.*: **Heterotypic transcriptional condensates formed by prion-like paralogous proteins canalize flowering transition in tomato**. *Genome Biol* 2022, **23**:78, https://doi.org/10.1186/s13059-022-02646-6 [PMID: 35287709].
The authors describe a novel canalization mechanism that increases the robustness of flowering time and shoot architecture. TMF and TFAMs contain intrinsically disordered regions (IDRs) that enable them to form transcriptional condensates to repress ANANTHA, leading to synchronized flowering. The potential to form condensates and thereby the transcriptional repression potential is rooted in the variation sequence of the IDRs.

28. Jung J-H, Barbosa AD, Hutin S, *et al.*: **A prion-like domain in ELF3 functions as a thermosensor in Arabidopsis**. *Nature* 2020, **585**:256–260, https://doi.org/10.1038/s41586-020-2644-7 [PMID: 32848244].

29. * Hutin S, Kumita JR, Strotmann VI, *et al.*: **Phase separation and molecular ordering of the prion-like domain of the Arabidopsis thermosensory protein Early Flowering 3**. *Proc Natl Acad Sci U S A* 2023, **120**, e2304714120, https://doi.org/10.1073/pnas.2304714120 [PMID: 37399408].
The authors investigate the biochemical, biophysical, and structural properties of the dilute and condensed phases of ELF3 PrDs, providing insights into biomolecular condensates. ELF3 puncta show a mixture of mobile and immobile species, indicating LLPS. Puncta formation depends on temperature, pH, and polyQ length.

30. Strotmann VI, Stahl Y: **At the root of quiescence: function and regulation of the quiescent center**. *J Exp Bot* 2021, **72**:6716–6726, https://doi.org/10.1093/jxb/erab275 [PMID: 34111273].

31. * Liu C, Mentzelopoulou A, Deli A, *et al.*: *Phase separation of a nodulin sec14-like protein maintains auxin efflux carrier polarity at Arabidopsis plasma membranes*. 2022.
This preprint identifies SFH8 protein, a lipid-like transferase which phase separates at the plasma membrane of plant cells. Due to its proteolytic-induced solidification, SFH8 is important in maintaining the polarized transport of PINs.

32. Moschou PN, Gutierrez-Beltran E, Bozhkov PV, Smertenko A: **Separase promotes microtubule polymerization by activating CENP-E-related kinesin Kin7**. *Dev Cell* 2016, **37**:350–361, https://doi.org/10.1016/j.devcel.2016.04.015 [PMID: 27219063].

33. * Burkart RC, Strotmann VI, Kirschner GK, *et al.*: **PLETHORA-WOX5 interaction and subnuclear localization control Arabidopsis root stem cell maintenance**. *EMBO Rep* 2022, **23**, e54105, https://doi.org/10.15252/embr.202154105 [PMID: 35373503].
This paper describes how the two transcription factors PLT3 and WOX5 regulate the SCN within the RAM. The results suggest that the partitioning of PLT-WOX5 complexes to NBs, possibly by phase separation, is important for CSC fate determination.

34. Roychoudhry S, Kepinski S: **Auxin in root development**. *Cold Spring Harbor Perspect Biol* 2022, **14**, https://doi.org/10.1101/cshperspect.a039933 [PMID: 34312248].

35. Smet I de, Tetsumura T, Rybel B de, *et al.*: **Auxin-dependent regulation of lateral root positioning in the basal meristem of Arabidopsis**. *Development* 2007, **134**:681–690, https://doi.org/10.1242/dev.02753 [PMID: 17215297].

36. Guilfoyle TJ: **The PB1 domain in auxin response factor and Aux/IAA proteins: a versatile protein interaction module in the auxin response**. *Plant Cell* 2015, **27**:33–43, https://doi.org/10.1105/tpc.114.132753 [PMID: 25604444].

37. Korasick DA, Westfall CS, Lee SG, *et al.*: **Molecular basis for AUXIN RESPONSE FACTOR protein interaction and the control of auxin response repression**. *Proc Natl Acad Sci U S A* 2014, **111**:5427–5432, https://doi.org/10.1073/pnas.1400074111 [PMID: 24706860].

38. Powers SK, Holehouse AS, Korasick DA, *et al.*: **Nucleo-cytoplasmic partitioning of ARF proteins controls auxin responses in Arabidopsis thaliana**. *Mol Cell* 2019, **76**:177–190.e5, https://doi.org/10.1016/j.molcel.2019.06.044 [PMID: 31421981].

39. Powers SK, Strader LC: **Regulation of auxin transcriptional responses**. *Dev Dynam* 2020, **249**:483–495, https://doi.org/10.1002/dvdy.139 [PMID: 31774605].

Chapter 3

Visualization of *in vivo* protein-protein interactions in plants

This manuscript was published in the *Journal of Experimental Botany* in April 2022.

https://doi.org/10.1093/jxb/erac139

Authors

Vivien I. Strotmann[1] and Yvonne Stahl[1]*

Affiliation

[1]Institute for Developmental Genetics, Heinrich-Heine-University, Universitätsstr. 1, 40225 Düsseldorf

*corresponding author

Author contribution

I contributed to this work by writing the chapters ‘Traditional methods’, ‘Shedding light on *in vivo* PPI measurements’ as well as the paragraphs about ‘Combined BiFC and FRET’, ‘Triple FRET’ and ‘Knocksideways in plants (KSP)’ from the chapter ‘PPI measurements of higher order complexes’. Additionally, I contributed to the design of tables and figures.

Journal of Experimental Botany
https://doi.org/10.1093/jxb/erac139 Advance Access Publication 8 April, 2022
This paper is available online free of all access charges (see https://academic.oup.com/jxb/pages/openaccess for further details)

REVIEW PAPER

Visualization of *in vivo* protein–protein interactions in plants

Vivien I. Strotmann and Yvonne Stahl*

Institute for Developmental Genetics, Heinrich-Heine University, Universitätsstr. 1, D-40225 Düsseldorf, Germany

* Correspondence: Yvonne.Stahl@hhu.de

Received 28 December 2021; Editorial decision 25 March 2022; Accepted 1 April 2022

Editor: Aleksandra Skirycz, MPI for Molecular Plant Physiology, Germany

Abstract

Molecular processes depend on the concerted and dynamic interactions of proteins, either by one-on-one interactions of the same or different proteins or by the assembly of larger protein complexes consisting of many different proteins. Here, not only the protein–protein interaction (PPI) itself, but also the localization and activity of the protein of interest (POI) within the cell is essential. Therefore, in all cell biological experiments, preserving the spatio-temporal state of one POI relative to another is key to understanding the underlying complex and dynamic regulatory mechanisms *in vivo*. In this review, we examine some of the applicable techniques to measure PPIs *in planta* as well as recent combinatorial advances of PPI methods to measure the formation of higher order complexes with an emphasis on *in vivo* imaging techniques. We compare the different methods and discuss their benefits and potential pitfalls to facilitate the selection of appropriate techniques by providing a comprehensive overview of how to measure *in vivo* PPIs in plants.

Keywords: BiFC, FRET, FRET-APB, FRET-FLIM, *in planta*, *in vivo*, protein–protein interaction (PPI), splitLuc.

Introduction

In vivo protein–protein interaction (PPI) measurements are needed to understand the dynamic and complex interactions of proteins underlying a plethora of biological processes in all living organisms. The observed PPI can also help to decipher the function of the involved proteins of interest (POIs), bringing them into a wider biological context. In this review, we focus on several different techniques that are available for PPI measurements *in planta*, either in heterologous systems or in stably transformed plants.

Independent of the technique used to measure PPIs, several important prerequisites must be met for PPIs of two or more POIs to occur. Here, the most important prerequisite of PPI is the spatio-temporal co-localization of POIs at a subcellular level, for example at the plasma membrane in a certain tissue at a specific time during plant development. Depending on the plant species under investigation, information about a specific POI, for example gene expression, protein localization, and putative interaction domains, might already be available and can be utilized to design subsequent PPI experiments.

To determine whether two or more proteins are co-localized, the proteins can be visualized using different techniques such as immunolocalization with specific, fluorescent dye-labelled antibodies against the POI in fixed samples, or in living cells using genetically encoded fluorescent proteins (FPs) fused to the POI. Subsequently, (co-)localization can be assessed via fluorescence microscopy. For example, the most commonly used FP, enhanced green fluorescent protein (eGFP), is a 28 kDa protein that forms a cylinder-like structure

4.2 nm long and 2.4 nm wide (Hink *et al.*, 2000). Therefore, even when using state-of-the-art fluorescence microscopes, a mere co-localization of two POIs is no proof that they interact physically, as the lateral diffraction limit of light means the maximum resolution attainable by light microscopy is only ~250 nm. Even when super-resolution microscopy methods are applied with resolutions in the range of ~30 nm, there is still uncertainty as to whether a PPI takes place between the POIs (Won, 2009). Therefore, a number of different techniques to test for direct PPI *in vitro* and *in vivo* have been developed (Struk *et al.*, 2019). In this review, we will focus on some of the traditional and newly emerging PPI techniques, with a focus on *in vivo* imaging techniques *in planta*.

Traditionally, techniques such as co-immunoprecipitation (co-IP) or yeast two-hybrid (Y2H) experiments were used to measure PPI. These techniques allow for the identification of numerous potential interaction candidates in a short time and are thus regarded as relatively high throughput. Although the use of these methods results in the loss of spatial and temporal information about the POIs and their interaction partners, they can still serve as a starting point to identify potential interacting POIs, which can then be verified by subsequent *in vivo* PPI measurements.

Traditional methods

Co-immunoprecipitation

The *in vitro* method co-IP is still one of the most commonly used techniques to identify PPIs (Ren *et al.*, 2003; Phee *et al.*, 2006). During co-IP, an immobilized antibody against the POI isolates the POI from a cell lysate, along with other proteins that directly or indirectly interact with the POI (Ransone, 1995; Ren *et al.*, 2003; Phee *et al.*, 2006). These potential interaction partners can then be identified by mass-spectroscopy (MS) (as reviewed in Monti *et al.*, 2005). Furthermore, the precipitated complex can be tested for a specific target protein that has been identified by other experiments. Additionally, the putative interaction partner can be subsequently confirmed and visualized by a western blot using an antibody against the identified complex partner.

However, this is also one of the major limitations of this technique, as protein-specific antibodies are, at least in plant biology, often not available. Therefore, it is necessary to label the POI with one of the common protein tags available (e.g. His, FLAG, HA, or FPs), which can then be detected. Another concern is that co-IP is not well suited to detect weak or transient interactions as the experimental procedure includes several washing steps, often with detergents, to eliminate non-specific binding. Also, detection of proteins via western blot requires sufficient protein expression, which can be problematic if endogenous promoters are used, which are often only weakly or transiently expressed, or only expressed in a few cells (as reviewed in Tang and Takahashi, 2018). Another major drawback of this technique is that spatial information of the POI is lost through lysis of the cells. Here, proteins that are not present in the same cellular compartments are released into the lysate and PPIs may take place, even if they would not normally come into contact with each other in an intact cell. Additionally, when using co-IP, it remains unclear whether the discovered interaction is direct or indirect (as reviewed in Masters, 2004). Therefore, false-positive results must be considered, and PPI must be confirmed using other techniques that conserve spatial information. Furthermore, false-negative results are also possible due to the need for the POI to be soluble, which, for example in the case of membrane proteins, is not always the case. Nevertheless, co-IP with subsequent MS offers the possibility to identify a multitude of novel interaction partners which can subsequently be confirmed using other techniques as described below.

Yeast two-hybrid

A widely used high-throughput *in vivo* technique is the Y2H system, which was originally designed to identify PPIs using the yeast GAL4 transcriptional activator. GAL4 consists of two functional domains, a DNA-binding domain and an activator domain (Fields and Song, 1989). In the Y2H system, the binding of GAL4 to the upstream activation sequence triggers the transcription of an enzymatic reporter gene, for example *lacZ* coding for β-galactosidase. Separation of these two domains and fusion to two different POIs allows testing of their interaction with an easy read-out, such as a colour reaction triggered by the addition of a suitable substrate for β-galactosidase. In recent decades, several other variations of this technique have been developed, for example in *Arabidopsis thaliana* protoplasts, named protoplast two-hybrid (Ehlert *et al.*, 2006).

A Y2H screen can give an indication of whether a PPI could take place between two POIs, and it is easy to carry out without the need for any sophisticated equipment. In addition, Y2H offers the opportunity for large-scale high-throughput approaches and allows screening of thousands of proteins for potential PPIs, which has led to the availability of Y2H interactome databases (e.g. Arabidopsis Interactome Mapping Consortium, 2011 for *A. thaliana*). The analysis of such large networks of interacting proteins offers the opportunity to classify POIs into larger biological contexts and enables the discovery of novel hypothetical links and putative functions of POIs. Even though these databases, if available, are a very good starting point, one major limitation of the underlying Y2H technique is the high rate of false-positive, but also false-negative results. Here, estimates suggest 70% false-positive identifications, which are caused by the overexpression of the POI and the expression in a heterologous system (as reviewed in Deane *et al.*, 2002; Auerbach and Stagljar, 2005). Nevertheless, high-throughput Y2H screens are very useful to identify many putative POIs that could interact, even though other promising *in vivo* high-throughput methods have been developed recently.

Biotin-based proximity labelling

Within the last few years, an enzyme-catalysed proximity labelling technique was developed in which biomolecules, usually proteins or RNA, are labelled if they are in close proximity to the POI (Roux *et al.*, 2012). Here, a POI is fused to a ligase that covalently labels adjacent proteins or RNA with biotin. The biotinylated proteins can then be isolated using streptavidin which has a strong affinity for biotin. The putatively interacting proteins pulled-down in this way can then be identified by MS. The bifunctional BirA isolated from *Escherichia coli* is one of the best studied biotin ligases (Chakravartty and Cronan, 2012). Due to its high sequence specificity, BirA was not only used for protein isolation employing streptavidin, but also to analyse binary interactions. Fusing two POIs with BirA or BAP, a short biotin acceptor peptide, respectively, leads to biotinylation in the case of interaction of the POIs (as reviewed in Kim and Roux, 2016). Since the discovery of this useful mechanism, many improvements of biotin ligases have been developed. BioID is a mutated biotin ligase derived from BirA and works independently of BAP, leading to unspecific labelling of all nearby biomolecules. Recently another modification of BirA led to the development of the biotin ligase TurboID (Branon *et al.*, 2018). It combines advantages of other commonly used proximity labelling enzymes, such as APEX2 and BioID, by enabling non-toxic, fast labelling and an increased catalytic efficiency.

To date, one of the major limitations of proximity labelling in plants has been that experiments had to be carried out at 37 °C due to the temperature requirements of the labelling enzyme, which could cause heat stress in plants. However, TurboID can be successfully used at room temperature in transiently and stably transformed *Nicotiana benthamiana* and stably transformed Arabidopsis, thereby avoiding unnecessary abiotic stress in the plants (Mair *et al.*, 2019; Zhang *et al.*, 2019). In contrast to co-IP approaches, proximity labelling is also suitable to detect low-affinity or transient interactions, due to the promiscuity of the biotin ligases and the strong biotin–streptavidin affinity (as reviewed in Kim and Roux, 2016). Additionally, the labelling of the putative interaction/complex partner occurs under native spatio-temporal conditions *in vivo*; only the subsequent identification takes place *ex vivo*. Nevertheless, some caveats must be considered even when TurboID or the smaller version, called miniTurbo, are used; for example, biotin might not be accessible to some organelles such as peroxisomes and vacuoles because of their acidic environments (Mair *et al.*, 2019). Furthermore, unspecific background labelling can result in false-positive potential complex/interaction partners, and therefore appropriate negative controls must be included. In addition, as when using co-IP to monitor PPIs, isolated interaction partners must be identified by MS. Lastly, it must be taken into account that the labelling process requires a negatively charged amino acid on the surface of the protein, which could lead to false-negative results if negatively charged amino acid are not available in some POIs (as reviewed in Yang *et al.*, 2021).

All of the three above-mentioned techniques can identify a multitude of different putatively interacting proteins. Nevertheless, these interactions must be verified individually by other PPI methods, and we will focus on these PPI methods in the following sections.

Shedding light on *in vivo* PPI measurements

In vivo visualization and quantification of PPIs has greatly profited during the past decades from the use of luminescent proteins and, notably, FPs that emit photons in a specific spectral range. The high spatio-temporal resolution at which FP-tagged POIs can be detected *in vivo* without the need for further substrates or cofactors has led to the application of a multitude of different quantitative methods involving FPs *in planta* (Grossmann *et al.*, 2018). We will describe techniques that allow for *in vivo* PPI detection using fluorescence or bioluminescence and discuss potential benefits and pitfalls of the different applications. Next, we introduce two techniques to measure PPI by protein fragment complementation using either fluorescence or luminescence as a read-out.

Bimolecular fluorescence complementation (BiFC)

The *in vivo* BiFC assay is based on the complementation of an FP (Hu *et al.*, 2002; Bracha-Drori *et al.*, 2004). Here, the two POIs are fused to the N- or C-terminal part of the FP, respectively. If the two POIs are in close proximity to each other, the FP is reconstituted and its fluorescence restored, thus indicating interaction of the POIs (see Fig. 1B, B′). This technique was first described using yellow fluorescent protein (YFP), but since then other split FPs have become available (Hu *et al.*, 2002; Fan *et al.*, 2008). This opens up the possibility to simultaneously visualize several PPIs within the same cell, known as multicolour BiFC (Hu and Kerppola, 2003; Waadt *et al.*, 2008). The relatively simple principle of detecting interactions makes BiFC a widely used technique, since it does not require any specialized equipment other than a fluorescence microscope and appropriate filters for excitation and emission. Additionally, PPIs can be directly visualized in different cell compartments and, because of the cellular resolution of modern fluorescence microscopes or laser scanning microscopes, BiFC can provide information about the spatial characteristics of the investigated interaction. Because of its simplicity, many PPIs could be verified by BiFC *in vivo* (Table 2), for example in transient experiments in *N. benthamiana* and Arabidopsis leaf epidermal cells (Bracha-Drori *et al.*, 2004), mustard seedlings, and also in protoplasts of Arabidopsis (Olejnik *et al.*, 2011) and rice (Chen *et al.*, 2006).

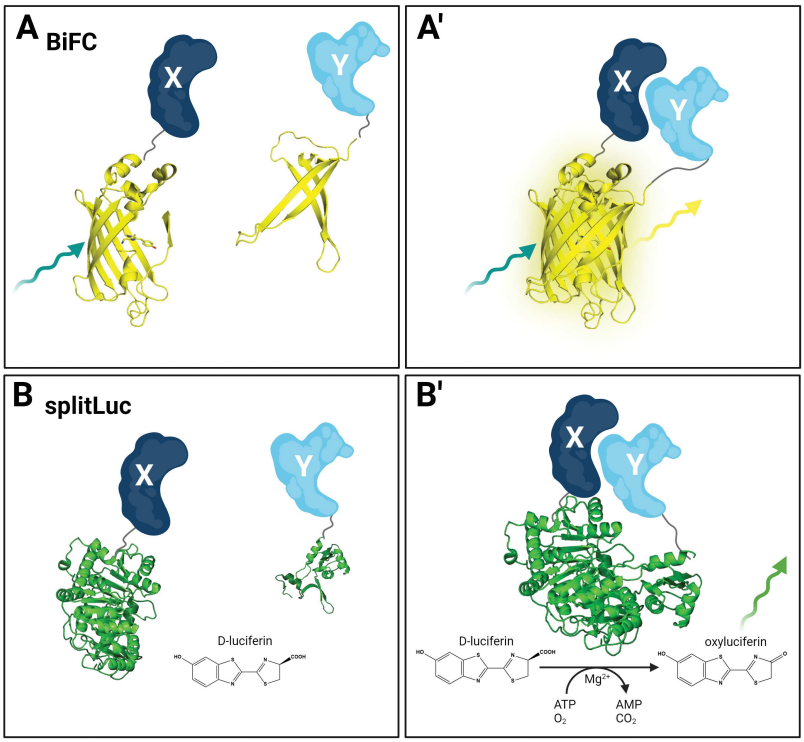

Fig. 1. Split systems for measuring PPI *in vivo*. (A) In the bimolecular fluorescence complementation (BiFC) system, two POIs (X, dark blue; Y, light blue) are fused to the N- or C-terminal part of an FP (here, 3D structures of YFP in yellow), respectively. (A′) If the two POIs interact, the two YFP parts are reconstituted and, after excitation (teal arrow), can emit light (yellow arrow). (B) In the split-luciferase (splitLuc) system, two POIs (X, dark blue; Y, light blue) are fused to the N- or C-terminal part of a luciferase (here, 3D protein structure of firefly luciferase in green). (B′) If the two POIs interact, the luciferase fragments are reconstituted and can produce light (green arrow) in the presence of the substrate D-luciferin, in an ATP- and oxygen-dependent reaction. Figure created with BioRender.com.

Nevertheless, one major limitation of BiFC is the high frequency of false-positive PPIs caused by the intrinsic affinity of the two parts of the FP for each other (see Table 1) (as reviewed in Horstman *et al.*, 2014; Romei and Boxer, 2019). This is especially problematic when the expression is driven by a constitutive promoter in a heterologous system and thus the concentration of the proteins no longer reflects the endogenous expression level. In addition, expression in a heterologous system could also lead to false (co)-localization of proteins that, under native conditions, are localized in distinct compartments; for example, a protein expressed in the cytoplasm which is highly expressed in epidermal leaf cells of *N. benthamiana* could partially co-localize with a plasma membrane protein. Additionally, several attempts to diminish self-assembly, such as by changing the split position, have been made, but none of these approaches was generally applicable in plants (as reviewed in Horstman *et al.*, 2014).

Therefore, appropriate negative controls are absolutely necessary to minimize false-positive results (Horstman *et al.*, 2014). In addition, BiFC does not give any information about the temporal dynamics of PPI since the FP is highly unlikely to dissociate after reconstitution, as FPs have a half-life >24 h (Hu *et al.*, 2002). On the other hand, this phenomenon can also be advantageous in detecting weak and/or transient PPIs (Morell *et al.*, 2007). Recently, a split fluorescence reporter has been developed that also allows monitoring of assembly and disassembly of PPIs in living cells (Tebo and Gautier, 2019). To date, this reporter has only been applied in mammalian cell culture. Another *in vivo* protein fragment complementation assay based on a split-luciferase (splitLuc) can detect dynamic changes of PPI, and has been applied in plants; this is described next.

Split-luciferase

The *in vivo* splitLuc assay is based on the complementation of two fragments of a luciferase enzyme fused to two POIs that, in the case of interaction of the POIs, leads to enzyme reconstitution and subsequent substrate conversion. The turnover of the substrate, and therefore the interaction of the POIs, can be monitored by the emission of bioluminescence (Fig. 2A, A′). *In planta*, two luciferases are most frequently used for splitLuc assays: one is obtained from the North American firefly (*Photinus pyralis*), referred to as firefly luciferase, and one from the sea pansy (*Renilla reniformis*), referred to as *Renilla* luciferase. The firefly luciferase uses D-luciferin as a substrate which is converted in a two-step ATP- and oxygen-dependent reaction to oxyluciferin, AMP, carbon dioxide, and light (de Wet *et al.*, 1987). Interestingly, the emission spectrum of the firefly

Table 1. Evaluation of PPI techniques *in planta* involving imaging

Method	Cellular resolution	Dynamics	False positives	False negatives	Applicability	Special features and characteristics
BiFC	●	○	●●	○●	●●	Suitable for weak/transient PPIs
Split-Luc	○	●	●	●	●[a]	Dynamic assembly and disassembly of PPIs can be studied
FRET-APB	●	●	○●	●	●●[b]	Fast data acquisition and analysis
FRET-FLIM	●●	●	○●	●	○●[c,d]	High quality of acquired data
BiFC and FRET	●●	○●	●●	●●	○●[d,e]	Analysis of trimeric complexes
Triple FRET	●●	○●	○●	●●	○●[c,d,e]	Analysis of trimeric complexes
Homo-FRET	●●	●●	○●	●●	○●[d]	Analysis of higher order complexes Can be combined with FRET-FLIM
FCCS	○●	●●	○	○●	○[d]	Low concentration of POI needed Simultaneous detection of PPI and dynamics
RICS and N&B	○●	●●	○●	●	●[c]	Simultaneous detection of PPI and dynamics
KSP	○●	○●	○●	○●	○●[f]	Analysis of higher order complexes. Inducible visualization of PPI. Can be added to other methods as intrinsic positive control

'O' = 'no or low', 'O ● = 'medium', '● = 'high', '● ● = 'very high'.

[a] Phosphorescence of chlorophyll can mask the signal of luciferase.

[b] Not suitable for moving proteins.

[c] Data acquisition and analysis can be time consuming.

[d] Special technical equipment might be needed,

[e] Appropriate controls needed.

[f] Rapamycin-induced effects must be considered.

luciferase peaks at 560 nm (green light), but can undergo a red shift in an acidic environment or at higher temperatures (reviewed in Fraga, 2008). The *Renilla* luciferase converts its substrate coelenterazine in an oxygen-dependent reaction to coelenteramide, carbon dioxide, and blue light, with an emission maximum at 480 nm, and is ATP independent (Matthews *et al.*, 1977). Compared with the firefly luciferase with an approximate mol. wt of 62 kDa, the *Renilla* luciferase is relatively small, measuring 37 kDa (Matthews *et al.*, 1977; de Wet *et al.*, 1987). The distinguishable emission spectra of these two different enzymes combined with a high substrate specificity allows for the simultaneous detection of the activity of both luciferases (McNabb *et al.*, 2005).

For both luciferases, a split variant is available for the detection of PPI (Ozawa *et al.*, 2001; Paulmurugan and Gambhir, 2003; Fujikawa and Kato, 2007; Chen *et al.*, 2008). These have been successfully utilized in different experimental approaches in plants, such as in transient expression in *N. benthamiana* (Liu *et al.*, 2021) or in Arabidopsis protoplasts (Li *et al.*, 2011) (see Table 2). Which luciferase is more suitable for the detection of PPI *in vivo* strongly depends on the characteristics of the putative interaction partners. For example, the enzymatic reaction catalysed by *Renilla* luciferase does not require ATP, which might be limiting in some cellular compartments. On the other hand, the substrate coelenterazine is unstable and can undergo spontaneous oxidation (Zhao *et al.*, 2004), whereas D-luciferin is more stable.

Compared with other protein fragment complementation assays, luciferase fragments do not spontaneously reconstitute, thus avoiding false-positive interactions often encountered in BiFC. Furthermore, splitLuc assays enable the investigation of dynamic changes of PPIs since the reconstitution of the firefly luciferase is reversible, as shown in large-scale approaches in Arabidopsis mesophyll protoplasts (Table 1) (Li *et al.*, 2011). The high turnover rate of reconstituted luciferase and its short half-life time allow the visualization of formation and dissociation of protein complexes (Luker *et al.*, 2004; Xing *et al.*, 2016). Although the splitLuc assays require the addition of a substrate, it can be easily applied exogenously, either by incubation or by watering (Chen *et al.*, 2008), or even through infiltration of the diluted substrate (Schatlowski *et al.*, 2010).

Despite its advantages, splitLuc assays are less commonly used than other protein fragment complementation assays. For one thing, luciferase activity can only be measured in the dark. Therefore, light-dependent processes are not suitable for this technique. Furthermore, for splitLuc assays in green tissue, for example tobacco leaves or Arabidopsis leaf protoplasts, a special filter is needed that excludes the phosphorescence of Chl *a* and *b* (reviewed in Krasnovsky and Kovalev, 2014) as this could interfere with the detection of the emitted light from the luciferase. Although splitLuc experiments can be used in quantitative high-throughput assays, such as on floating leaf discs or on protoplasts using plate readers (Chen *et al.*, 2006; Gehl *et al.*, 2011), these experiments do not provide information on the

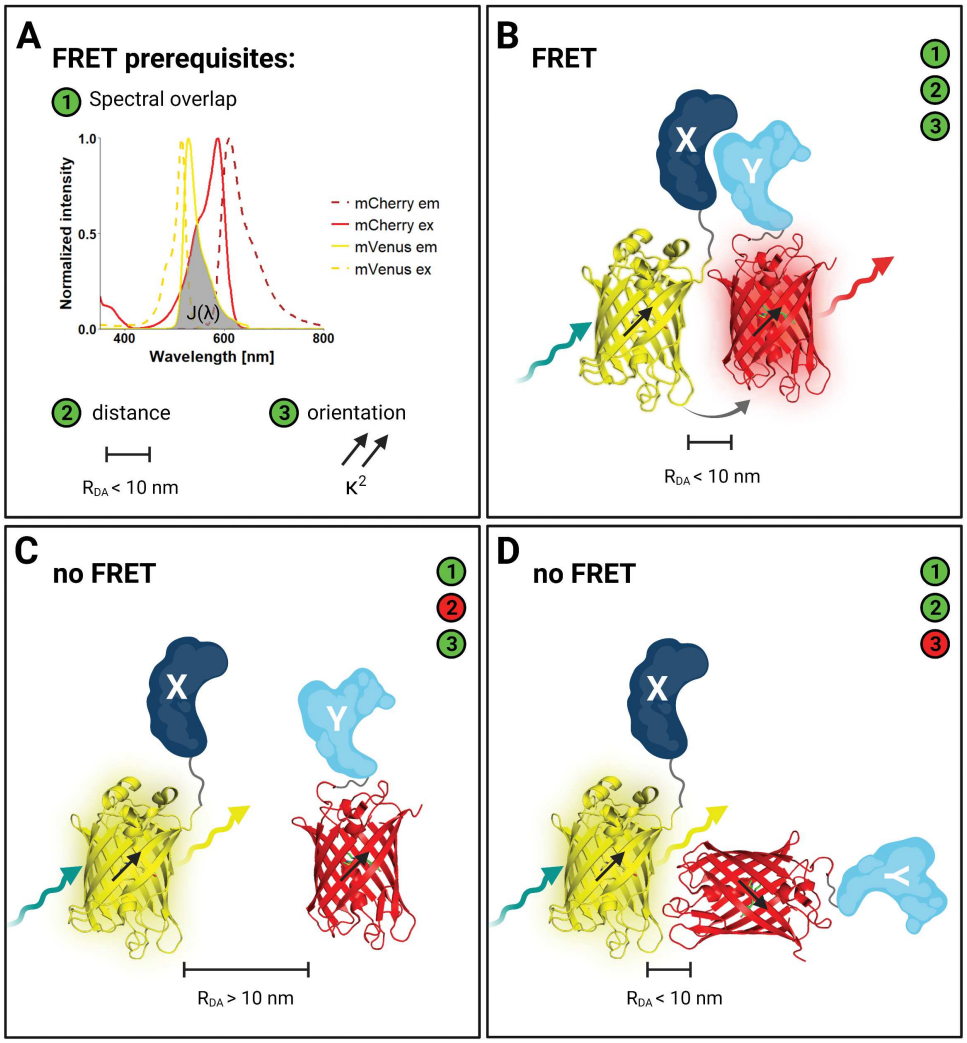

Fig. 2. FRET prerequisites and possible scenarios when measuring PPI *in vivo*. (A) Prerequisites for FRET to take place between the two fluorophores or FPs of the chosen FRET pair, in this case the FPs mVenus (yellow) and mCherry (red), are: ① spectral overlap of donor emission and acceptor excitation [$J(\lambda)$]; ② distance between the donor and acceptor is <10 nm (R_{DA}); ③ dipole orientation of the donor and acceptor are parallel (κ^2). (B) PPI of two POIs can be measured by FRET *in vivo* if the donor FP (mVenus 3D structure in yellow) and the acceptor FP (mCherry 3D structure in red) are fused to POI X (dark blue) or Y (light blue), respectively. In the case that all three FRET prerequisites are met (①–③ green), FRET takes place by the energy migration after exciting (teal arrow) the donor FP to the acceptor FP (grey arrow) which is excited and can emit light (red arrow). (C) No FRET can be measured if the distance between donor and acceptor FPs (R_{DA}) is >10 nm (red number ②). (D) No FRET can be measured if the dipole orientation (κ^2) of donor and acceptor are not parallel (red number ③). Figure created with BioRender.com.

subcellular localization of the PPI and are not suitable for low-affinity interactions (reviewed in Xing *et al.*, 2016). Another concern is that compared with commonly used fluorescent proteins, such as GFP or mCherry, the firefly luciferase is particularly large, which could cause problems when monitoring interactions of small proteins as this could sterically hinder PPIs (Matthews *et al.*, 1977; de Wet *et al.*, 1987; Cormack *et al.*, 1996; Shaner *et al.*, 2004). Recently, a smaller so-called Nano luciferase (Nluc) with a total molecular mass of 19.1 kDa was established to address this concern (Wang *et al.*, 2020).

Nonetheless, neither BiFC nor splitLuc assays can provide information on whether the interaction of the proteins is direct or indirect or whether an interaction could be considered strong or weak, thereby making the quantification of PPI of different interaction partners impossible. Additionally, either spatial or temporal resolution of PPI is lost in splitLuc or BiFC experiments, respectively. Therefore, other quantitative techniques to measure *in vivo* PPI that preserve the spatio-temporal resolution are additionally required and will be discussed in the next sections.

Measurement of PPI by energy transfer

Förster resonance energy transfer (FRET)

FRET, first described by Theodor Förster (Förster, 1948), is a physical phenomenon in which the energy of an excited donor fluorophore is transferred by a radiation-free process

Table 2. Examples of PPI measured *in planta*

Technique	Recent example and biological context	Organism	References
BiFC and FRET-FLIM	PII localizes to foci within chloroplasts where it interacts with NAGK and BCCP and thereby regulates protein degradation.	Transient expression in *N. benthamiana*	Krieger *et al.* (2021)
SplitLuc (firefly)	MKK2 and MPK2, both known to be involved in plant immunity, interact with ACO2 and with ACO2, CHH, and PBP1, respectively.	Transient expression in *N. benthamiana*	Leissing *et al*. (2021)
SplitLuc (firefly), BiFC, Y2H	OsUEV1B interaction with OsVDAC1 is suggested to be required for phosphate homeostasis in rice	Transient expression in *N. benthamiana* and Arabidopsis protoplasts	Liu *et al.* (2021)
FRET-APB	CRN and CLV2 interact at the plasma membrane, where they perceive CLV3 peptide and regulate stem cell number in the shoot apical meristem of *A. thaliana.*	Transient expression in *N. benthamiana*	Bleckmann *et al.* (2010)
FRET-FLIM	Cell type-specific interaction of the transcription factor network SHR–SCR–JKD regulates gene expression and thereby specifies cell fate in the *A. thaliana* root.	Stable expression in *A. thaliana*	Long *et al.* (2017)
FRET-FLIM, Y2H	OsFD7 involved in floral transition and panicle development in rice, was found to interact with OsFTL1, Hd3a, and RFT1.	Transient expression in onion peel cells	Kaur *et al.* (2021)
	BRAVO and WOX5 interaction is involved in quiescent centre quiescence. Both transcription factors can interact with the BES1–TPL repressor complex.	Transient expression in *N. benthamiana*	Betegón-Putze *et al.* (2021)
Triple FRET	BRI1 and BAK1 can form a trimeric complex with RLP44 which is thought to sense cell wall integrity in response to BR signalling.	Transient expression in *N. benthamiana*	Glöckner *et al.* (2020)
FRET-FLIM and homo-FRET	CLV1 and ACR4 form homo- and heteromeric complexes depending on their subcellular localization and thereby control distal root meristem maintenance in *A. thaliana*.	Transient expression in *N. benthamiana*	Stahl *et al.* (2013)
	Cluster formation of CRN, CLV2, and CLV1 at the plasma membrane in presence of CLV3 regulates shoot meristem maintenance in *A. thaliana*.	Transient expression in *N. benthamiana*	Somssich *et al.* (2015)
FCCS	Exogenous BR application leads to an increased co-localization of BRI1 and AtFlot1 and stimulation of the membrane microdomain-associated pathway of BRI1 internalization. Co-diffusion of BRI1 and CLC demonstrates that BRI1 internalization is clathrin dependent.	Stable expression in *A. thaliana*	Wang *et al*. (2015)
RICS and N&B	SHR was found to exist in a monomeric and dimeric state in the endodermis and both forms can interact with SCR, indicating a stoichiometric complex composition of 1:1 or 2:1.	Stable expression in *A. thaliana*	Clark *et al.* (2016)
KSP	Proof of concept as shown for the transcription factors: SACL and LHW; BES1 and BIN2 and the endocytosis protein complex: TPLATE and TML	Transient expression in *N. benthamiana*	Winkler *et al*. (2021)

to an acceptor chromophore, for example chlorophyll in the light-harvesting complexes necessary for plant photosynthesis. This process of energy transfer is strongly dependent on the distance between donor and acceptor fluorophores (R_{DA}) (see Fig. 2A, C), the overlap integral of donor emission and acceptor absorption spectra [$J(\lambda)$] (see Fig. 2A), as well as the parallel orientation of the donor and acceptor dipoles (κ^2) (see Fig. 2A, D). FRET efficiency (E_{FRET}) is directly dependent on the distance between the donor and acceptor fluorophores, as it is inversely proportional to the sixth power of the distance between donor and acceptor, and can be described by the following equation:

$$E_{FRET} = \frac{R_0^6}{R_0^6 + R_{DA}^6}$$

Here, R_{DA} represents the actual distance between the two fluorophores, and R_0 the so-called Förster distance between the two fluorophores, a characteristic distance between a pair of fluorophores at which the FRET efficiency (E_{FRET}) is 50%, which is usually well below 10 nm. For PPI measurements, two POIs are fused to suitable donor or acceptor fluorophores or FPs, also called FRET pairs. Widely used FP FRET pairs are: eCFP–eYFP, eGFP–mRFP, eGFP–mCherry, or mVenus–mCherry. The Förster radius (R_0) of the FRET pair eCFP–eYFP is 4.9 nm (Bajar *et al.*, 2016). Because of its strong distance dependency, FRET can be utilized to quantitatively determine PPI *in vivo*. To figure out which FRET pair is most suitable to detect PPI in a specific *in planta* experiment can be quite challenging, as it depends on several aspects, such as spectral properties, photostability, folding, localization, and activity of the labelled POI within the respective cellular context (Denay *et al.*, 2019). The development of new FPs or new variants of already established FPs starts with analysing important characteristics *in vitro*, such as photostability, pH stability, and maturation time (reviewed in Day and Davidson, 2009). For some FPs, these attributes have been at least partially characterized *in vivo*, albeit mostly in bacteria (Megerle *et al.*, 2008; Hebisch *et al.*, 2013; Balleza *et al.*, 2018) and also in yeast or mammalian cell culture (Zhong *et al.*, 2019; Lee *et al.*, 2020). Therefore, when starting with a recently developed FP, its applicability in plants first needs to be tested, as its properties can vary quite significantly in comparison with published results from other organisms (Denay *et al.*, 2019).

Furthermore, when choosing a suitable FRET pair for PPI experiments, the maturation time of the individual fluorophores should also be considered. The specific maturation time of an FP can vary between different species or even within different strains of the same species, as shown for *E. coli* (Hebisch *et al.*, 2013). As higher amounts of acceptor increase the possibility for FRET to occur, an equal or shorter maturation time for the acceptor fluorophore compared with the donor fluorophore is preferred (Bajar *et al.*, 2016; Denay *et al.*, 2019).

One important property of FRET is that it also affects the mean fluorescence intensity and lifetime of the donor fluorophore, as the fraction of excited donor fluorophores is depopulated faster in the presence of a suitable acceptor fluorophore in close proximity (Bücherl *et al.*, 2014; Weidtkamp-Peters and Stahl, 2017). The resulting decrease of donor fluorescence intensity and lifetime, also called quenching, and the consequent increase of acceptor fluorescence can be measured by different approaches.

Donor and acceptor fluorescence intensities can be simultaneously measured by either acquiring a complete spectrum covering the donor and acceptor emission or by using appropriate filter sets for acceptor and donor fluorescence, known as sensitized emission. These techniques are often applied in genetically encoded FRET-based biosensors, detecting changes of intramolecular FRET in response to specific biological stimuli, such as calcium, reactive oxygen species, pH, phytohormones, and nutrients (Walia *et al.*, 2018).

The two techniques most widely used for quantitative measurements of PPI by FRET are acceptor photobleaching (APB) and fluorescence lifetime imaging microscopy (FLIM), which we describe in more detail below.

Acceptor photobleaching (APB)

One of the most accessible FRET-based techniques to monitor PPI *in vivo* is acceptor APB. APB makes use of the differences in fluorescence intensity of the donor molecule in the presence or absence of the acceptor. Here, if FRET takes place, the energy transfer from the donor to the acceptor fluorophore is inhibited by bleaching the acceptor with a strong laser pulse (Bastiaens and Jovin, 1996; Bastiaens *et al.*, 1996; Wouters *et al.*, 1998; Kenworthy and Edidin, 1999; Kenworthy, 2001; Karpova *et al.*, 2003; Albertazzi *et al.*, 2009). Therefore, if the two POIs interact, bleaching of the acceptor leads to an increase of the donor fluorescence intensity because the energy is no longer transferred to the acceptor. This technique has successfully been applied *in planta*, for example in transiently expressing *N. benthamiana* leaf epidermal cells expressing different receptor proteins (Bleckmann *et al.*, 2010). An apparent FRET efficiency (E_{FRET}, as a percentage) can be calculated if the intensity of the donor fluorescence (I_D) is recorded before ($I_{D\ before}$) and after ($I_{D\ after}$) bleaching of the acceptor and is described by the following equation:

$$E_{FRET} = 1 - \frac{I_{D\ after} - I_{D\ before}}{I_{D\ after}} \times 100$$

This method does not require expensive or complicated equipment, and does not need time-consuming training or extensive experience (see Table 1). Additionally, data acquisition is relatively fast compared with other FRET-based methods. Drawbacks of FRET-APB are the need for high laser powers during bleaching of the acceptor fluorophore, potentially

leading to phototoxic effects, as well as low spatial resolution due to the necessary high acquisition speed and the analysis of only a small region of interest. Furthermore, filter sets and/or bandwidths should be carefully chosen to avoid possible cross-talk of donor and acceptor emission.

Another point to consider is that FRET-APB utilizes the intensity of the donor molecule fluorescence to calculate FRET efficiency and therefore is strongly affected by protein concentration. As a rule, a low donor/acceptor ratio will lead to increased FRET efficiencies whereas a high donor/acceptor ratio decreases FRET efficiency as the acceptor may be limiting. On the other hand, high expression levels of both proteins increase the possibility of the donor and acceptor fluorophore meeting by chance and could thereby artificially increase FRET efficiency. This phenomenon is known as bystander-FRET and should be taken into consideration for all FRET-based techniques. To avoid strongly differing POI concentrations in transient expression systems, both POIs can be expressed from a single T-DNA so that the preferable 1:1 ratio of donor and acceptor is achieved (Mehlhorn *et al.*, 2018; Denay *et al.*, 2019). Another point is, that depending on the cellular compartment and the mobility of the protein, the fluorescence of the acceptor could recover after the bleaching, even before an increase of the donor intensity can be detected. This effect might be enhanced by the inevitable delay between pre-bleach and post-bleach image acquisition. Therefore, highly mobile POIs and/or transient PPIs would be difficult to measure using APB. Another quantitative method to measure FRET overcoming some of the shortcomings of FRET-APB is FLIM, which is described next.

Fluorescence lifetime imaging microscopy (FLIM)

Fluorescence lifetime (τ) is defined as the average time, usually in the nanosecond range, that a fluorophore remains in the excited state after excitation before returning to the ground state by emitting a photon. If two proteins interact, the fluorescence lifetime of the donor is decreased, and its fluorescence intensity is quenched. The fluorescence lifetime is an intrinsic characteristic for each fluorophore and therefore strongly differs between different fluorophores. FRET-FLIM is a non-intensity-based imaging method in contrast to the above-described FRET-APB, largely independent of protein concentration, making it particularly suitable for the quantitative analysis of PPIs in living cells, where fluorescence intensity can vary significantly. In order to measure the fluorescence lifetime of an FP in the so-called time domain, a pulsed laser source and special equipment for time-correlated single photon counting (TCSPC) is required: single photon-sensitive detectors and photon counting electronics (Becker *et al.*, 2004). The time between the laser pulse and emission of a single photon is measured for every individual photon and plotted as a histogram, which shows an exponential decay. From fitting this decay, the average fluorescence lifetime can be deduced (Biskup *et al.*, 2007; Weidtkamp-Peters and Stahl, 2017). The resulting FRET efficiency can be determined by recording the fluorescence lifetime τ of the POI labelled with the donor fluorophore in the absence (donor only sample) or presence of the putative interactor labelled with the acceptor fluorophore (FRET sample). The following equation describes the resulting FRET efficiency (E_{FRET}, as a percentage) depending on the donor fluorescence lifetime in the presence (τ_{DA}) or absence (τ_D) of the acceptor:

$$E_{FRET} = 1 - \frac{\tau_{DA}}{\tau_D} \times 100$$

One major advantage of FRET-FLIM is the quality of the acquired data. In contrast to other methods to investigate PPIs, FLIM data can also be used to determine quantitative data that can potentially show differences in the interaction strength or binding of different POIs at a high spatial resolution (see Table 1) (Weidtkamp-Peters and Stahl, 2017). Nevertheless, this requires some expert knowledge and advanced data analyses, as well as careful control experiments. Additionally, FLIM is largely independent of protein concentration. Therefore, FRET-FLIM measurements are widely considered as more reliable than the detection of FRET by APB and spectral imaging, and have been successfully applied *in planta* (Stahl *et al.*, 2013; Bücherl *et al.*, 2014; Somssich *et al.*, 2015; Long *et al.*, 2017; Weidtkamp-Peters and Stahl, 2017; Betegón-Putze *et al.*, 2021; Kaur *et al.*, 2021).

On the other hand, time domain FLIM data acquisition and processing are time-consuming and require a significant amount of training and experience. Furthermore, the necessary equipment, such as pulsed laser sources, TCSPC electronics, etc. are a quite expensive additions to a widefield or confocal microscope setup. An alternative that does not require cost-intensive TCSPC electronics and fitting of the data is the so-called frequency domain FLIM. Here, a continuous, modulated light source and a synchronized modulated detector are required to determine the phase-shifted fluorescent lifetimes of the donor fluorophore. Frequency domain FLIM measurements can be carried out at high speed, which is advantageous for monitoring dynamic processes. Nevertheless, time domain FLIM measurements show a higher precision even at low signal to noise ratios and can be used for more complex donors (Datta *et al.*, 2020).

A more general limitation of FRET-based methods, as in FRET-APB and FRET-FLIM, is the number of false-negative results resulting from inadequate photoselection of fluorophores (Bajar *et al.*, 2016). As mentioned, the dipole orientation (κ^2) of the two fluorophores used for FRET should be (close to) parallel (Fig. 2). The more precisely the dipole orientations of the fluorophores are aligned in parallel, the more efficient the energy transfer from donor to acceptor and therefore the

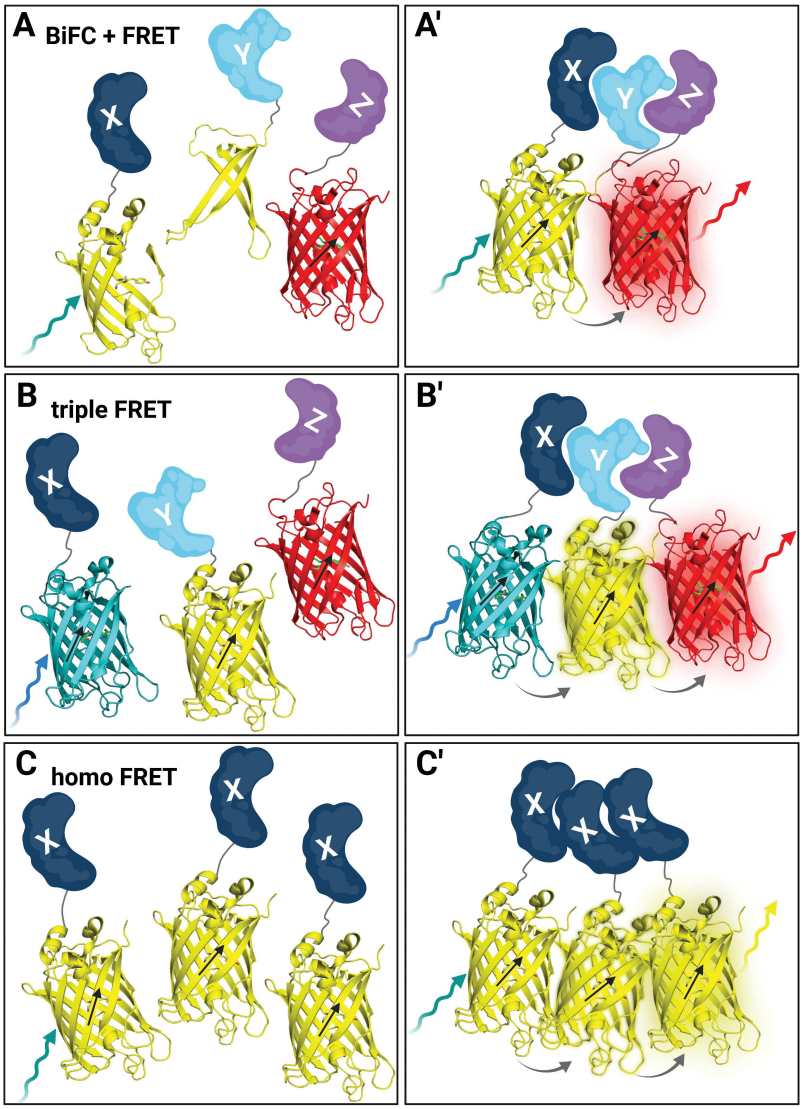

Fig. 3. Techniques to measure PPI of more than two POIs. (A) In a combined BiFC–FRET experiment, two POIs (X, dark blue; Y, light blue) are fused to the N- or C-terminal part of a split FP (here, split 3D YFP structures in yellow), and a third POI (Z, purple) is fused to an acceptor FP (here, 3D mCherry structure in red). (A′) In the case of interaction of all three POIs, the YFP parts are reconstituted and, after excitation (teal arrow), can transfer energy by FRET (grey arrow) to the acceptor FP (mCherry) which can emit light (red arrow). (B) In a triple FRET experiment, three POIs (X, dark blue; Y, light blue; Z, purple) are fused to three different FPs (here, 3D structures of CFP, cyan; YFP, yellow; and mCherry, red). (B′) In the case of interaction of all three POIs, the three FPs come close enough to allow, upon excitation of CFP by blue light (blue arrow), energy transfer (grey arrow) by FRET to YFP as acceptor which then serves also as a donor and transfers energy via FRET (grey arrow) to mCherry which can then emit light (red arrow). (C) In a homo-FRET experiment, two or more of the same POI (X, dark blue) are labelled with an FP (here, 3D structure of YFP in yellow). (C′) If the POI can form higher order complexes, energy can be transferred from one excited (teal arrow) FP to another, thereby depolarizing the emission of the FP (yellow arrow). Figure created with BioRender.com.

higher the FRET efficiency (reviewed in Weidtkamp-Peters *et al.*, 2022).

Another potentially problematic factor, apart from choosing the best possible FRET pair for the PPI experiment, is the position of the FP or enzyme at the N- or C-terminus of the POI. The protein class, the (subcellular) localization, and known functional domains can help to choose the optimal position of the reporter protein (Long *et al.*, 2018, 2020). In addition, a linker between the POI and the fluorophore could be used to improve FRET efficiency if this leads to an increased rotation of the fluorophore without increasing the distance between the two fluorophores, which could diminish FRET (Denay *et al.*, 2019).

Nevertheless, FRET-FLIM measurements are highly suited to validate PPIs in a quantitative way preserving spatio-temporal information of the POI. In addition, FRET-FLIM can also be used if PPI measurements of more than two POIs is necessary, as described below.

PPI measurements of higher order complexes

Combined BiFC and FRET

To identify and analyse putative homo- or heteromeric complex formation of more than two proteins, combinations of established methods to study PPIs are used. The combination of BiFC and FRET-FLIM offers the possibility to simultaneously test the interaction of three POIs while preserving high spatial resolution (Kwaaitaal *et al.*, 2010). Here, two POIs are fused to the N- or C-terminal part of the donor fluorophore, respectively. The third POI is fused to the acceptor fluorophore. Only in the case of complex formation of all three POIs can a reduction of the donor fluorescence lifetime or intensity be observed, for example by FRET-FLIM or FRET-APB measurements, respectively (Fig. 3B, B′). An alternative approach without BiFC is described next.

Triple FRET

Triple FRET, also referred to as three-colour FRET or two-step FRET, is another FRET-based method to simultaneously study interactions of more than two proteins, for example in higher order complexes consisting of different proteins. Here, the excited donor fluorophore (D) transfers energy to the first acceptor (A1), which at the same time serves as a donor for a second acceptor fluorophore (A2) (Horsey *et al.*, 2000). Thereby, energy can be transferred sequentially from D via A1 to A2, but also directly from D to A1 and from D to A2 (Fig. 3C, C′). For the required energy transfer, the same prerequisites must be met that were described for conventional FRET above, but in this case for three FPs. Most importantly, the emission spectrum of D must overlap with the excitation spectrum of A1, and the emission spectrum of A1 must overlap with the excitation spectrum of A2. Before triple FRET-FLIM measurements can be carried out, a series of control experiments must be performed to ensure the measured FRET effect is caused by interaction and not by an artefact, for example quantification of fluorescence emission intensity of A1 and A2 with the excitation wavelength of D, to estimate spectral bleed through and crosstalk (Table 1).

One of the first attempts of triple FRET was used *in vitro* to investigate structural changes in DNA using sensitized emission as well as donor fluorescence and lifetime quenching as a read-out for FRET (Watrob *et al.*, 2003). The first experiments using triple FRET *in planta* in Arabidopsis mesophyll protoplasts also analysed sensitized acceptor emission and showed that 2-Cys peroxiredoxin forms decamers (Seidel *et al.*, 2010). Recently, the first attempts to establish three-colour FRET-FLIM *in planta* were performed (see Table 2) (Glöckner *et al.*, 2020, Preprint). Another technique to measure PPI of higher order complexes of the same POI is described next.

Homo-FRET detection by fluorescence anisotropy measurements

FRET can also take place between members of the same kind of fluorophores because they also fulfil the requirements of FRET. This phenomenon of energy migration between identical fluorophores is called homo-FRET (Vogel *et al.*, 2009). The detection of homo-FRET can also be utilized to measure PPI between the same POIs, for example when they form dimeric or multimeric homomeric complexes. While homo-FRET does not impact fluorescence intensity or lifetime, it does affect the direction of the fluorescence emission of the examined fluorophores. This effect can be measured as fluorescence anisotropy r of a fluorophore (reviewed in Weidtkamp-Peters *et al.*, 2022). Here, a microscopic setup with a polarized light source (e.g. a laser) excites the fluorophores with a parallel dipole orientation, a process called photoselection. The steady-state fluorescence anisotropy r of the excited fluorophores can be measured by two detectors detecting the same emission bandwidth of the excited fluorophores but divided by a polarized beam splitter for detecting the intensity of the emitted light parallel ($I_{||}$) and perpendicular ($I_{\perp}$) to the polarized excitation light. Steady-state fluorescence anisotropy r can be described by the following equation:

$$r = \frac{I_{||} - I_{\perp}}{I_{||} + 2I_{\perp}}$$

The fluorescence anisotropy r decreases in the case of PPI because of energy transfer to a fluorophore with the same properties in the vicinity of the next POI with a slightly different dipole orientation, thereby depolarizing the emitted fluorescence (Fig. 3C, C′) (Weidtkamp-Peters *et al.*, 2022). Fluorescence anisotropy measurements can be combined with FRET-FLIM measurements to detect dynamic hetero- and homomeric complexes and their spatial distribution within a cell at the same time, which was shown *in planta* (Table 2) (Stahl *et al.*, 2013; Somssich *et al.*, 2015). Other spectroscopic methods described below can be used to detect PPI by correlating the fluctuations of the fluorescence of POIs as they move together.

Fluorescence fluctuation microscopy to study PPI

Fluorescence correlation spectroscopy (FCS) is an advanced fluorescence technique that measures fluctuations in fluorescence of single molecules over time to quantify the concentration and diffusion coefficients of these molecules in a very small defined volume, such as in a confocal volume (Laursen *et al.*, 2016). This is achieved by focusing excitation light on to a sample (e.g. in a confocal or two-photon microscope), and the resulting fluctuation of fluorescence due to the movement or Brownian motion of the fluorescent molecules is

statistically analysed. For FCS measurements, the number of fluorescent molecules must be relatively low (in the pico- to micromolar range) (Eigen and Rigler, 1994; Schwille *et al.*, 1999). Two POIs, if labelled with two spectrally distinct FPs, can be observed in two separate channels by fluorescence cross-correlation spectroscopy (FCCS). If the two proteins indeed interact, they will move together, as demonstrated with interacting receptor kinases in Arabidopsis roots (Table 2) (Wang *et al.*, 2015). For FCS measurements, the same specialized microscopic equipment is needed as described above for FRET-FLIM measurements, because here too a very high temporal resolution of single photons is needed. These single molecule measurements are highly dependent on a very good signal to noise ratio which can be achieved by eliminating out-of-focus fluorescence as much as possible, such as by internal reflection microscopy, in particular variable angle total internal reflection microscopy (VA-TIRF) (Wang *et al.*, 2015).

By using another FCS-based method called raster image correlation spectroscopy (RICS) which extracts fluorescence correlation from confocal image stacks combined with number and brightness analyses (N&B), two POIs labelled with spectrally different FPs can be analysed for their mobility, oligomeric state, and stoichiometry (including PPI) preserving spatio-temporal information, which has recently been successfully applied in Arabidopsis roots employing a conventional confocal microscopic setup (Table 2) (Clark *et al.*, 2016). The advantage of using RICS instead of FCCS is that no specific setup other than a conventional confocal microscope is needed (Table 1). Even though the analyses of the FCCS and RICS data is not as easy as, for example, in FRET-APB experiments, these techniques provide very valuable information on the mobility at the same time as on PPI.

Knocksideways in plants (KSP)

Recently, an exciting new technique to measure and visualize PPI in transiently expressing *N. benthamiana* leaf epidermis was described which can be compared with an intracellular co-IP (Winkler *et al.*, 2021). This technique combines the—in the animal field—well-established conditional ability of rapamycin to alter the localization of a bait protein and its interactors via the heterodimerization of FKBP and FRB domains. In KSP, this conditional heterodimerization is combined with rerouting interacting proteins to mitochondria upon rapamycin induction. The PPI of more than two POIs can thereby be directly visualized and quantified by FP-tagged POIs in conventional fluorescence microscopy (Table 2) (Winkler *et al.*, 2021). So far, KSP has been used to improve the quality of interaction data acquired with split-ubiquitin, BiFC, and FRET approaches, as the addition of FKBP and FRB domains to these well-established methods can serve as an intrinsic positive control (Andersen *et al.*, 2016). It will be very interesting to see how applicable this new technique is in stable transgenic lines in the future, as KSP also offers, aside from PPI detection, a conditional compartmentalization and thereby a protein knockout tool.

One general consideration concerning all of the above-described PPI techniques that involve imaging is that the POI must be tagged or expressed in fusion with an FP or other protein (domain), and therefore the function of the POI might be impaired. Therefore, control experiments, such as rescue experiments using stable transformants in the respective loss-of-function mutants, should be carried out to test if the labelled POI is still functioning.

Nevertheless, the outstanding benefit of all described imaging-based PPI techniques is the preservation of spatio-temporal information of the involved POI and even quantitative data on the observed PPI (Table 1).

Conclusions

In summary, many different techniques, most of them relying on the use of FPs, have been successfully applied in living plant cells, either in stably transformed plants or transiently in heterologous plant expression systems. Here, dynamic PPIs and complex formations can be investigated in a minimally invasive manner, whilst in most cases preserving the spatio-temporal characteristics of the POI. While we have summarized numerous pros and cons for each of the techniques to study PPI in this review, there is no one technique that fits all requirements. Which technique is best for a given research question depends on, for example, the expression system, POI abundance, and PPI strength and dynamics (Table 1). In the future, emerging techniques in the *in vivo* or correlative super-resolution microscopy field and/or in novel advances of data analyses could add more depth to the detection and/or quantification of PPIs. Here, novel, high-throughput techniques for improved visualization of PPI and the determination of dynamic *in vivo* binding affinities would help to decipher complex regulatory networks in plants. Additionally, the more insights into structural information on plant proteins become available, the more *in silico* predictions of PPI and even of PPI sites, such as in PlaPPISite, will become available (Ding and Kihara, 2019;Yang *et al.*, 2020), which can guide *in vivo* and *in planta* experiments. Due to the numbers of PPIs already predicted and/or verified in different plant species, computational networks of PPIs will become even more necessary to understand the complex and dynamic PPIs in a wider biological context.

Acknowledgements

We would like to thank Dr Vicky Howe for critical reading of the manuscript. We would like to apologize to all colleagues whose relevant work could not be discussed due to space restrictions.

Conflict of interest

The authors declare no conflicts of interest.

Funding

This work was supported by the Deutsche Forschungsgemeinschaft (DFG) via grant STA 1212/4-1 to YS.

References

Albertazzi L, Arosio D, Marchetti L, Ricci F, Beltram F. 2009. Quantitative FRET analysis with the EGFP–mCherry fluorescent protein pair. Photochemistry and Photobiology **85**, 287–297.

Andersen TG, Nintemann SJ, Marek M, Halkier BA, Schulz A, Burow M. 2016. Improving analytical methods for protein–protein interaction through implementation of chemically inducible dimerization. Scientific Reports **6**, 27766.

Arabidopsis Interactome Mapping Consortium. 2011. Evidence for network evolution in an Arabidopsis interactome map. Science **333**, 601–607.

Auerbach D, Stagljar I. 2005. Yeast two-hybrid protein–protein interaction networks. In: Waksman G, ed. Proteomics and protein–protein interactions. Boston, MA: Springer US, 19–31.

Bajar BT, Wang ES, Zhang S, Lin MZ, Chu J. 2016. A guide to fluorescent protein FRET pairs. Sensors **16**, 1488.

Balleza E, Kim JM, Cluzel P. 2018. Systematic characterization of maturation time of fluorescent proteins in living cells. Nature Methods **15**, 47–51.

Bastiaens PI, Jovin TM. 1996. Microspectroscopic imaging tracks the intracellular processing of a signal transduction protein: fluorescent-labeled protein kinase C beta I. Proceedings of the National Academy of Sciences, USA **93**, 8407–8412.

Bastiaens PI, Majoul IV, Verveer PJ, Söling HD, Jovin TM. 1996. Imaging the intracellular trafficking and state of the AB5 quaternary structure of cholera toxin. The EMBO Journal **15**, 4246–4253.

Becker W, Bergmann A, Hink MA, König K, Benndorf K, Biskup C. 2004. Fluorescence lifetime imaging by time-correlated single-photon counting. Microscopy Research and Technique **63**, 58–66.

Betegón-Putze I, Mercadal J, Bosch N, *et al*. 2021. Precise transcriptional control of cellular quiescence by BRAVO/WOX5 complex in Arabidopsis roots. Molecular Systems Biology **17**, e9864.

Biskup C, Zimmer T, Kelbauskas L, *et al*. 2007. Multi-dimensional fluorescence lifetime and FRET measurements. Microscopy Research and Technique **70**, 442–451.

Bleckmann A, Weidtkamp-Peters S, Seidel CAM, Simon R. 2010. Stem cell signaling in Arabidopsis requires CRN to localize CLV2 to the plasma membrane. Plant Physiology **152**, 166–176.

Bracha-Drori K, Shichrur K, Katz A, *et al*. 2004. Detection of protein–protein interactions in plants using bimolecular fluorescence complementation. The Plant Journal **40**, 419–427.

Branon TC, Bosch JA, Sanchez AD, *et al*. 2018. Efficient proximity labeling in living cells and organisms with TurboID. Nature Biotechnology **36**, 880–887.

Bücherl CA, Bader A, Westphal AH, Laptenok SP, Borst JW. 2014. FRET-FLIM applications in plant systems. Protoplasma **251**, 383–394.

Chakravartty V, Cronan JE. 2012. Altered regulation of *Escherichia coli* biotin biosynthesis in BirA superrepressor mutant strains. Journal of Bacteriology **194**, 1113–1126.

Chen S, Tao L, Zeng L, Vega-Sanchez ME, Umemura K, Wang G-L. 2006. A highly efficient transient protoplast system for analyzing defence gene expression and protein–protein interactions in rice. Molecular Plant Pathology **7**, 417–427.

Chen H, Zou Y, Shang Y, *et al*. 2008. Firefly luciferase complementation imaging assay for protein–protein interactions in plants. Plant Physiology **146**, 368–376.

Clark NM, Hinde E, Winter CM, *et al*. 2016. Tracking transcription factor mobility and interaction in Arabidopsis roots with fluorescence correlation spectroscopy. eLife **5**, e14770.

Cormack BP, Valdivia RH, Falkow S. 1996. FACS-optimized mutants of the green fluorescent protein (GFP). Gene **173**, 33–38.

Datta R, Heaster TM, Sharick JT, Gillette AA, Skala MC. 2020. Fluorescence lifetime imaging microscopy: fundamentals and advances in instrumentation, analysis, and applications. Journal of Biomedical Optics **25**, 1–43.

Day RN, Davidson MW. 2009. The fluorescent protein palette: tools for cellular imaging. Chemical Society Reviews **38**, 2887–2921.

Deane CM, Salwiński L, Xenarios I, Eisenberg D. 2002. Protein interactions: two methods for assessment of the reliability of high throughput observations. Molecular & Cellular Proteomics **1**, 349–356.

Denay G, Schultz P, Hänsch S, Weidtkamp-Peters S, Simon R. 2019. Over the rainbow: a practical guide for fluorescent protein selection in plant FRET experiments. Plant Direct **3**, e00189.

de Wet JR, Wood KV, DeLuca M, Helinski DR, Subramani S. 1987. Firefly luciferase gene: structure and expression in mammalian cells. Molecular and Cellular Biology **7**, 725–737.

Ding Z, Kihara D. 2019. Computational identification of protein–protein interactions in model plant proteomes. Scientific Reports **9**, 8740.

Ehlert A, Weltmeier F, Wang X, *et al*. 2006. Two-hybrid protein–protein interaction analysis in Arabidopsis protoplasts: establishment of a heterodimerization map of group C and group S bZIP transcription factors. The Plant Journal **46**, 890–900.

Eigen M, Rigler R. 1994. Sorting single molecules: application to diagnostics and evolutionary biotechnology. Proceedings of the National Academy of Sciences, USA **91**, 5740–5747.

Fan J-Y, Cui Z-Q, Wei H-P, *et al*. 2008. Split mCherry as a new red bimolecular fluorescence complementation system for visualizing protein–protein interactions in living cells. Biochemical and Biophysical Research Communications **367**, 47–53.

Fields S, Song O. 1989. A novel genetic system to detect protein–protein interactions. Nature **340**, 245–246.

Förster T. 1948. Zwischenmolekulare Energiewanderung und Fluoreszenz. Annalen der Physik **437**, 55–75.

Fraga H. 2008. Firefly luminescence: a historical perspective and recent developments. Photochemical & Photobiological Sciences **7**, 146–158.

Fujikawa Y, Kato N. 2007. Split luciferase complementation assay to study protein–protein interactions in Arabidopsis protoplasts. The Plant Journal **52**, 185–195.

Gehl C, Kaufholdt D, Hamisch D, *et al*. 2011. Quantitative analysis of dynamic protein–protein interactions in planta by a floated-leaf luciferase complementation imaging (FLuCI) assay using binary Gateway vectors. The Plant Journal **67**, 542–553.

Glöckner N, zur Oven-Krockhaus S, Rohr L, *et al*. 2020. Three-fluorophore FRET enables the analysis of ternary protein association in living plant cells. BioRxiv doi: https://doi.org/10.1101/722124. [Preprint].

Grossmann G, Krebs M, Maizel A, Stahl Y, Vermeer JEM, Ott T. 2018. Green light for quantitative live-cell imaging in plants. Journal of Cell Science **131**, jcs209270.

Hebisch E, Knebel J, Landsberg J, Frey E, Leisner M. 2013. High variation of fluorescence protein maturation times in closely related *Escherichia coli* strains. PLoS One **8**, e75991.

Hink MA, Griep RA, Borst JW, *et al*. 2000. Structural dynamics of green fluorescent protein alone and fused with a single chain Fv protein. Journal of Biological Chemistry **275**, 17556–17560.

Horsey I, Furey WS, Harrison JG, Osborne MA, Balasubramanian S. 2000. Double fluorescence resonance energy transfer to explore

multicomponent binding interactions: a case study of DNA mismatches. Chemical Communications **2000**, 1043–1044.

Horstman A, Tonaco IAN, Boutilier K, Immink RGH. 2014. A cautionary note on the use of split-YFP/BiFC in plant protein–protein interaction studies. International Journal of Molecular Sciences **15**, 9628–9643.

Hu C-D, Chinenov Y, Kerppola TK. 2002. Visualization of interactions among bZIP and rel family proteins in living cells using bimolecular fluorescence complementation. Molecular Cell **9**, 789–798.

Hu C-D, Kerppola TK. 2003. Simultaneous visualization of multiple protein interactions in living cells using multicolor fluorescence complementation analysis. Nature Biotechnology **21**, 539–545.

Karpova TS, Baumann CT, He L, *et al*. 2003. Fluorescence resonance energy transfer from cyan to yellow fluorescent protein detected by acceptor photobleaching using confocal microscopy and a single laser. Journal of Microscopy **209**, 56–70.

Kaur A, Nijhawan A, Yadav M, Khurana JP. 2021. OsbZIP62/OsFD7, a functional ortholog of FLOWERING LOCUS D, regulates floral transition and panicle development in rice. Journal of Experimental Botany **72**, 7826–7845.

Kenworthy AK. 2001. Imaging protein–protein interactions using fluorescence resonance energy transfer microscopy. Methods **24**, 289–296.

Kenworthy AK, Edidin M. 1999. Imaging fluorescence resonance energy transfer as probe of membrane organization and molecular associations of GPI-anchored proteins. Methods in Molecular Biology **116**, 37–49.

Kim DI, Roux KJ. 2016. Filling the void: proximity-based labeling of proteins in living cells. Trends in Cell Biology **26**, 804–817.

Krasnovsky AA, Kovalev YV. 2014. Spectral and kinetic parameters of phosphorescence of triplet chlorophyll a in the photosynthetic apparatus of plants. Biochemistry **79**, 349–361.

Krieger N, Pastryk K-F, Forchhammer K, Kolukisaoglu U. 2021. Arabidopsis PII proteins form characteristic foci in chloroplasts indicating novel properties in protein interaction and degradation. International Journal of Molecular Sciences **22**, 12666.

Kwaaitaal M, Keinath NF, Pajonk S, Biskup C, Panstruga R. 2010. Combined bimolecular fluorescence complementation and Forster resonance energy transfer reveals ternary SNARE complex formation in living plant cells. Plant Physiology **152**, 1135–1147.

Laursen T, Borch J, Knudsen C, *et al*. 2016. Characterization of a dynamic metabolon producing the defense compound dhurrin in sorghum. Science **354**, 890–893.

Lee J, Liu Z, Suzuki P, *et al*. 2020. Versatile phenotype-activated cell sorting. Science Advances **6**, eabb7438.

Leissing F, Misch NV, Wang X, *et al*. 2021. Purification of MAP-kinase protein complexes and identification of candidate components by XL-TAP-MS. Plant Physiology **187**, 2381–2392.

Li J-F, Bush J, Xiong Y, Li L, McCormack M. 2011. Large-scale protein–protein interaction analysis in Arabidopsis mesophyll protoplasts by split firefly luciferase complementation. PLoS One **6**, e27364.

Liu J, Liao W, Nie B, Zhang J, Xu W. 2021. OsUEV1B, an Ubc enzyme variant protein, is required for phosphate homeostasis in rice. The Plant Journal **106**, 706–719.

Long Y, Stahl Y, Weidtkamp-Peters S, *et al*. 2017. In vivo FRET-FLIM reveals cell-type-specific protein interactions in Arabidopsis roots. Nature **548**, 97–102.

Long Y, Stahl Y, Weidtkamp-Peters S, *et al*. 2018. Optimizing FRET-FLIM labeling conditions to detect nuclear protein interactions at native expression levels in living arabidopsis roots. Frontiers in Plant Science **9**, 639.

Long Y, Stahl Y, Weidtkamp-Peters S, Blilou I. 2020. Visualizing protein associations in living arabidopsis embryo. Methods in Molecular Biology **2122**, 167–188.

Luker KE, Smith MCP, Luker GD, Gammon ST, Piwnica-Worms H, Piwnica-Worms D. 2004. Kinetics of regulated protein–protein interactions revealed with firefly luciferase complementation imaging in cells and living animals. Proceedings of the National Academy of Sciences, USA **101**, 12288–12293.

Mair A, Xu S-L, Branon TC, Ting AY, Bergmann DC. 2019. Proximity labeling of protein complexes and cell-type-specific organellar proteomes in Arabidopsis enabled by TurboID. eLife **8**, e47864.

Masters SC. 2004. Co-immunoprecipitation from transfected cells. Methods in Molecular Biology **261**, 337–350.

Matthews JC, Hori K, Cormier MJ. 1977. Purification and properties of *Renilla reniformis* luciferase. Biochemistry **16**, 85–91.

McNabb DS, Reed R, Marciniak RA. 2005. Dual luciferase assay system for rapid assessment of gene expression in *Saccharomyces cerevisiae*. Eukaryotic Cell **4**, 1539–1549.

Megerle JA, Fritz G, Gerland U, Jung K, Rädler JO. 2008. Timing and dynamics of single cell gene expression in the arabinose utilization system. Biophysical Journal **95**, 2103–2115.

Mehlhorn DG, Wallmeroth N, Berendzen KW, Grefen C. 2018. 2in1 vectors improve in planta BiFC and FRET analyses. Methods in Molecular Biology **1691**, 139–158.

Monti M, Orrù S, Pagnozzi D, Pucci P. 2005. Interaction proteomics. Bioscience Reports **25**, 45–56.

Morell M, Espargaró A, Avilés FX, Ventura S. 2007. Detection of transient protein–protein interactions by bimolecular fluorescence complementation: the Abl–SH3 case. Proteomics **7**, 1023–1036.

Olejnik K, Bucholc M, Anielska-Mazur A, *et al*. 2011. *Arabidopsis thaliana* Nudix hydrolase AtNUDT7 forms complexes with the regulatory RACK1A protein and Ggamma subunits of the signal transducing heterotrimeric G protein. Acta Biochimica Polonica **58**, 609–616.

Ozawa T, Kaihara A, Sato M, Tachihara K, Umezawa Y. 2001. Split luciferase as an optical probe for detecting protein–protein interactions in mammalian cells based on protein splicing. Analytical Chemistry **73**, 2516–2521.

Paulmurugan R, Gambhir SS. 2003. Monitoring protein–protein interactions using split synthetic renilla luciferase protein-fragment-assisted complementation. Analytical Chemistry **75**, 1584–1589.

Phee B-K, Shin DH, Cho J-H, *et al*. 2006. Identification of phytochrome-interacting protein candidates in *Arabidopsis thaliana* by co-immunoprecipitation coupled with MALDI-TOF MS. Proteomics **6**, 3671–3680.

Ransone LJ. 1995. Detection of protein–protein interactions by coimmunoprecipitation and dimerization. Methods in Enzymology **254**, 491–497.

Ren L, Emery D, Kaboord B, Chang E, Qoronfleh MW. 2003. Improved immunomatrix methods to detect protein:protein interactions. Journal of Biochemical and Biophysical Methods **57**, 143–157.

Romei MG, Boxer SG. 2019. Split green fluorescent proteins: scope, limitations, and outlook. Annual Review of Biophysics **48**, 19–44.

Roux KJ, in Kim D, Raida M, Burke B. 2012. A promiscuous biotin ligase fusion protein identifies proximal and interacting proteins in mammalian cells. Journal of Cell Biology **196**, 801–810.

Schatlowski N, Stahl Y, Hohenstatt ML, Goodrich J, Schubert D. 2010. The CURLY LEAF interacting protein BLISTER controls expression of polycomb-group target genes and cellular differentiation of *Arabidopsis thaliana*. The Plant Cell **22**, 2291–2305.

Schwille P, Haupts U, Maiti S, Webb WW. 1999. Molecular dynamics in living cells observed by fluorescence correlation spectroscopy with one- and two-photon excitation. Biophysical Journal **77**, 2251–2265.

Seidel T, Seefeldt B, Sauer M, Dietz K-J. 2010. In vivo analysis of the 2-Cys peroxiredoxin oligomeric state by two-step FRET. Journal of Biotechnology **149**, 272–279.

Shaner NC, Campbell RE, Steinbach PA, Giepmans BNG, Palmer AE, Tsien RY. 2004. Improved monomeric red, orange and yellow fluorescent proteins derived from *Discosoma* sp. red fluorescent protein. Nature Biotechnology **22**, 1567–1572.

Somssich M, Ma Q, Weidtkamp-Peters S, *et al*. 2015. Real-time dynamics of peptide ligand-dependent receptor complex formation in planta. Science Signaling **8**, ra76.

Stahl Y, Grabowski S, Bleckmann A, *et al*. 2013. Moderation of Arabidopsis root stemness by CLAVATA1 and ARABIDOPSIS CRINKLY4 receptor kinase complexes. Current Biology **23**, 362–371.

Struk S, Jacobs A, Sánchez Martín-Fontecha E, Gevaert K, Cubas P, Goormachtig S. 2019. Exploring the protein–protein interaction landscape in plants. Plant, Cell & Environment **42**, 387–409.

Tang Z, Takahashi Y. 2018. Analysis of protein–protein interaction by co-IP in human cells. Methods in Molecular Biology **1794**, 289–296.

Tebo AG, Gautier A. 2019. A split fluorescent reporter with rapid and reversible complementation. Nature Communications **10**, 2822.

Vogel SS, Thaler C, Blank PS, Koushik SV. 2009. Time-resolved fluorescence anisotropy. In: Periasamy A, Clegg RM, eds. FLIM microscopy in biology and medicine. Chapman and Hall/CRC, 245–290.

Waadt R, Schmidt LK, Lohse M, Hashimoto K, Bock R, Kudla J. 2008. Multicolor bimolecular fluorescence complementation reveals simultaneous formation of alternative CBL/CIPK complexes in planta. The Plant Journal **56**, 505–516.

Walia A, Waadt R, Jones AM. 2018. Genetically encoded biosensors in plants: pathways to discovery. Annual Review of Plant Biology **69**, 497–524.

Wang F-Z, Zhang N, Guo Y-J, Gong B-Q, Li J-F. 2020. Split Nano luciferase complementation for probing protein–protein interactions in plant cells. Journal of Integrative Plant Biology **62**, 1065–1079.

Wang L, Li H, Lv X, *et al*. 2015. Spatiotemporal dynamics of the BRI1 receptor and its regulation by membrane microdomains in living Arabidopsis cells. Molecular Plant **8**, 1334–1349.

Watrob HM, Pan C-P, Barkley MD. 2003. Two-step FRET as a structural tool. Journal of the American Chemical Society **125**, 7336–7343.

Weidtkamp-Peters S, Rehwald S, Stahl Y. 2022. Homo-FRET imaging to study protein–protein interaction and complex formation in plants. Methods in Molecular Biology **2379**, 197–208.

Weidtkamp-Peters S, Stahl Y. 2017. The use of FRET/FLIM to study proteins interacting with plant receptor kinases. Methods in Molecular Biology **1621**, 163–175.

Winkler J, Mylle E, de Meyer A, *et al*. 2021. Visualizing protein–protein interactions in plants by rapamycin-dependent delocalization. The Plant Cell **33**, 1101–1117.

Won R. 2009. Eyes on super-resolution. Nature Photonics **3**, 368–369.

Wouters FS, Bastiaens PI, Wirtz KW, Jovin TM. 1998. FRET microscopy demonstrates molecular association of non-specific lipid transfer protein (nsL-TP) with fatty acid oxidation enzymes in peroxisomes. The EMBO Journal **17**, 7179–7189.

Xing S, Wallmeroth N, Berendzen KW, Grefen C. 2016. Techniques for the analysis of protein–protein interactions in vivo. Plant Physiology **171**, 727–758.

Yang X, Wen Z, Zhang D, *et al*. 2021. Proximity labeling: an emerging tool for probing in planta molecular interactions. Plant Communications **2**, 100137.

Yang X, Yang S, Qi H, Wang T, Li H, Zhang Z. 2020. PlaPPISite: a comprehensive resource for plant protein–protein interaction sites. BMC Plant Biology **20**, 61.

Zhang Y, Song G, Lal NK, *et al*. 2019. TurboID-based proximity labeling reveals that UBR7 is a regulator of N NLR immune receptor-mediated immunity. Nature Communications **10**, 3252.

Zhao H, Doyle TC, Wong R, *et al*. 2004. Characterization of coelenterazine analogs for measurements of Renilla luciferase activity in live cells and living animals. Molecular Imaging **3**, 43–54.

Zhong S, Rivera-Molina F, Rivetta A, Toomre D, Santos-Sacchi J, Navaratnam D. 2019. Seeing the long tail: a novel green fluorescent protein, SiriusGFP, for ultra long timelapse imaging. Journal of Neuroscience Methods **313**, 68–76.

Aims of the study

In higher plants, the root plays a pivotal role in plant fitness as it provides access to nutrients and water, as well as anchorage in the soil. In the model plant *Arabidopsis thaliana*, the main root is formed by a small group of pluripotent stem cells, called the quiescent center (QC), located in the center of the root meristem at the tip of the root. By undergoing rarely-occurring, asymmetric cell divisions, the QC produces the surrounding cell type specific stem cells and preserves their undifferentiated status non-cell-autonomously. Hence, QC maintenance and function is crucial to sustain high developmental plasticity e.g., in response to internal and external cues. The delicate balance of stem cell maintenance and replenishment is regulated by a complex regulatory network. Although the concept of root stem cells has existed for decades, many aspects of the underlying intertwined pathways remain elusive.

On the one hand, this study aims to uncover the role of the transcription factors (TFs) WUSCHEL-RELATED HOMEOBOX 5 (WOX5) and PLETHORA 3 (PLT3) in stem cell homeostasis in the *Arabidopsis* root using genetic approaches as well as advanced microscopy techniques. Furthermore, the role of the subcellular compartments termed nuclear bodies (NBs) that are mediated by prion-like domains (PrDs) found in PLT3 in columella stem cell (CSC) fate regulation should be investigated.

Furthermore, in this dissertation it is proposed that the brassinosteroid-dependent TF BRASSINOSTEROID AT VASCULAR AND ORGANIZING CENTRE (BRAVO) genetically and physically interact with WOX5 and PLT3, forming a regulatory triangle that controls QC divisions and CSC fate determination. Here, a novel analysis method provides insights into protein binding affinities of heterodimers and higher-order complexes formed by BRAVO, WOX5 and PLT3. Finally, the combination of experimental data and computational modelling suggests the formation of cell type specific TFs complexes that could serve as read-out for cell type specificity.

In summary, this study aims to highlight the importance of fully understanding the fine-tuned molecular regulation of root stem cell homeostasis in *Arabidopsis,* as well as the use of combinatory approaches, which offer great potential for future studies in all fields of research.

Chapter 4

One pattern analysis (*OPA*) for the quantitative determination of protein interactions in plant cells

This manuscript was published in *Plant Methods* in July 2023.

https://doi.org/10.1186/s13007-023-01049-3

Authors

Jan E. Maika[1], Benedikt Krämer[2], Vivien I. Strotmann[1], Frank Wellmer[3], Stefanie Weidtkamp-Peters[4], Yvonne Stahl[1]* and Rüdiger Simon[1]*

Affiliation

[1]Institute for Developmental Genetics and Cluster of Excellence on Plant Sciences (CEPLAS), Heinrich-Heine-University, Universitätsstraße 1, 40225 Düsseldorf, Germany

[2]PicoQuant GmbH, Rudower Chaussee 29 (IGZ), 12489, Berlin, Germany

[3]Smurfit Institute of Genetics, Trinity College Dublin, Dublin, Ireland

[4]Centre for Advanced Imaging, Heinrich Heine University, Universitätsstraße 1, 40225, Düsseldorf, Germany

*corresponding authors

Author contribution

I contributed to this work by providing data to test and optimize the fitting model as well as by discussing and implementing improvements of the novel fitting routine.

Plant Methods

METHODOLOGY

Open Access

One pattern analysis (*OPA*) for the quantitative determination of protein interactions in plant cells

Jan Eric Maika[1], Benedikt Krämer[2], Vivien I. Strotmann[1], Frank Wellmer[3], Stefanie Weidtkamp-Peters[4], Yvonne Stahl[1*] and Rüdiger Simon[1*]

Abstract

Background A commonly used approach to study the interaction of two proteins of interest (POIs) in vivo is measuring Förster Resonance Energy Transfer (FRET). This requires the expression of the two POIs fused to two fluorescent proteins that function as a FRET pair. A precise way to record FRET is Fluorescence Lifetime IMaging (FLIM) which generates quantitative data that, in principle, can be used to resolve both complex structure and protein affinities. However, this potential resolution is often lost in many experimental approaches. Here we introduce a novel tool for FLIM data analysis of multiexponential decaying donor fluorophores, *one pattern analysis (OPA),* which allows to obtain information about protein affinity and complex arrangement by extracting the relative amplitude of the FRET component and the FRET transfer efficiency from other FRET parameters.

Results As a proof of concept for *OPA*, we used FLIM-FRET, or FLIM-FRET in combination with BiFC to reassess the dimerization and tetramerization properties of known interacting MADS-domain transcription factors in *Nicotiana benthamiana* leaf cells and *Arabidopsis thaliana* flowers. Using the *OPA* tool and by extracting protein BINDING efficiencies from FRET parameters to dissect MADS-domain protein interactions in vivo in transient *N. benthamiana* experiments, we could show that MADS-domain proteins display similar proximities within dimeric or tetrameric complexes but bind with variable affinities. By combining FLIM with BiFC, we were able to identify SEPALLATA3 as a mediator for tetramerization between the other MADS-domain factors. *OPA* also revealed that in vivo expression from native promoters at low levels in *Arabidopsis* flower meristems, makes in situ complex formation of MADS-domain proteins barely detectable.

Conclusions We conclude that MADS-domain protein interactions are transient in situ and may involve additional, so far unknown interaction mediators. We conclude that *OPA* can be used to separate protein binding from information about proximity and orientation of the interacting proteins in their complexes. Visualization of individual protein interactions within the underlying interaction networks in the native environment is still restrained if expression levels are low and will require continuous improvements in fluorophore labelling, instrumentation set-ups and analysis tools.

*Correspondence:
Yvonne Stahl
yvonne.stahl@hhu.de
Rüdiger Simon
ruediger.simon@hhu.de
Full list of author information is available at the end of the article

Introduction

Protein interactions and the formation of higher-order protein complexes play a crucial role in a plethora of cellular and developmental processes, but the precise identification and monitoring of protein–protein interactions (PPIs) in cells remains challenging. Two common techniques to visualize and quantify protein–protein interactions in vivo are BiFC and FRET (Fig. 1A and B).

BiFC is based on the complementation of two fragments of a fluorescence protein (FP; Fig. 1B). Fluorophore functionality is regained when the fragments, fused to interacting POIs, are brought in close proximity to each other [15]. FRET describes the process of non-radiative energy transfer from an excited "donor" fluorophore to an "acceptor" molecule [9]. Occurrence of FRET depends on three specific conditions: (i) The emission spectrum of the donor and the excitation spectrum of the acceptor must sufficiently overlap. (ii) The orientation of donor and acceptor dipoles must not be oriented perpendicular to each other. (iii) Donor and acceptor molecules must be in close proximity to each other (< 10 nm or 100 Å distance). FRET is considered the more accurate method and less susceptible to false positive interactions when compared to BiFC [2, 13, 41]. Commonly, FRET is measured either by fluorescence intensity-based techniques such as FRET-Acceptor Photo Bleaching (APB) and recording of sensitized emission, or by the analysis of the fluorescence lifetime of donor fluorescence using FLIM. Intensity-based FRET usually requires strict controls and correction for spectral bleed-through, whereas lifetime acquisition by FLIM is more robust [2, 11, 31, 39, 41]. Additionally, FLIM-FRET is independent from local Donor and Acceptor concentrations and requires only relatively low irradiation of cells, and is thus considered

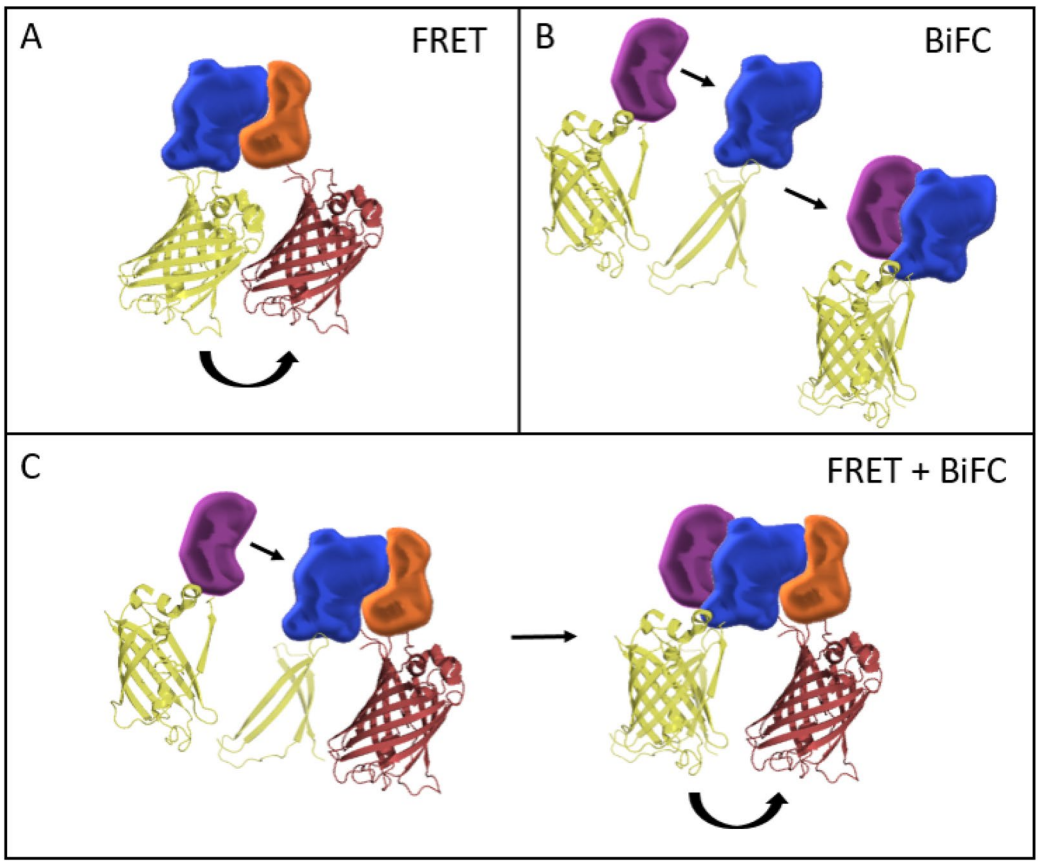

Fig. 1 FRET and BiFC can be used to investigate protein–protein interactions. **A** FRET describes the process of non-radiative energy transfer from an excited "donor" fluorophore to a non-excited "acceptor" molecule. Occurrence of FRET depends on three specific conditions: (i) the emission spectrum of the donor and the excitation spectrum of the acceptor must sufficiently overlap. (ii) The orientation of donor and acceptor dipoles must not be oriented perpendicular to each other. (iii) Donor and acceptor molecules must be in close proximity towards each other (< 1 nm or 100 Å distance). **B** BiFC is based on the complementation of two fragments of a fluorescence protein (FP). Fluorophore functionality is regained when the fragments, fused to interacting proteins, are brought in proximity to each other. **C** Combination of BiFC with FRET allows to investigate larger protein complexes. Thereby, the complemented FP can serve as a donor or acceptor

to be superior compared to intensity-based techniques [7, 10, 26, 27, 35, 40]. In time-domain FLIM experiments, arrival times of single photons after excitation with a pulsed laser are recorded and binned into a histogram, resulting in a characteristic fluorescence decay for a specific fluorophore. The fluorescence lifetime τ is the average time such fluorophore stays in its excited state, whereas during this time, its intensity decreases by ~ 64% [5]. Decaying intensity at time t is given by the summed decay functions across all components i, where τ is the lifetime and α the pre-exponential factor (amplitude) of the exponential decay function (Fig. 2A).

Occurrence of FRET leads to quenching of donor intensity and a decrease of its lifetime. Thus, in the overall decay of a bi-exponential donor fluorophore, a third component describes the effect of FRET. In this case, each of the three decay components have their own lifetime and amplitude. Thereby, the lifetimes τ_i of the individual components describe the decay rate, and the amplitudes α_i describe the contribution of each component to the overall decay (Fig. 2A'). Commonly, the average amplitude weighted lifetime τ_m of a mixture of differentially decaying components is calculated by the sum of each component's lifetime (τ_i), weighted by its respective amplitude (α_i). In case of FRET, τ_m decreases and can be used as a measure for PPI (Fig. 2B).

Importantly, reduction of τ_m can be due to either (i) high affinity between the proteins but low proximity, resulting in low energy transfer efficiency between fluorophores, or (ii) low protein affinity but high proximity, resulting in high energy transfer efficiency. Thus, the same value of τ_m can either be a result of a high number of interacting proteins but with low proximity or a lower number of interacting proteins but with high proximity and thus more effective transfer of energy between fluorophores. This crucial information about binding affinities and spatial information within the complex is in principle available within the acquired FLIM data and can be accessed by analysing amplitudes and lifetimes separately. Consequently, the relative amplitude of the FRET fraction, here termed BINDING, and the FRET efficiency, based on the reduction of the FRET component lifetime compared to the donor component lifetime can be determined. Thereby, BINDING is indicative for the relative number of molecules undergoing FRET in a sample, whereas FRET efficiency describes the efficiency of the energy transfer between the fluorophores. As energy transfer efficiency is dependent on the distance between fluorophores and the orientation of their dipoles [9], FRET efficiency can be used as a measure for proximity and orientation within the complex [4] and BINDING as an indicator for the affinity between the proteins (Fig. 2C). While calculation of BINDING (relative amplitude of the FRET fraction) is trivial for monoexponentially decaying donors and was described before [30, 50], determination of BINDING parameter from decays of multiexponential decaying donors is more difficult. As the fluorescent protein mVenus can display a biexponentially decaying behaviour [36], we here apply a newly developed analysis method, "*One Pattern Analysis* (*OPA*)" (PicoQuant, Berlin, Parts of this method is covered by a German patent application DE10 2021 107 759.1), in which the donor only decay components (Donor only lifetime components and their respective amplitudes) are pre-defined as a "pattern", allowing the calculation of BINDING from multiexponential donor decays. By discriminating between the affinity of interacting proteins and their proximity or orientation within the forming protein complex, we reassessed dimer and tetramer formation of MADS-domain transcription factors involved in the specification of floral organs *in planta*. The activities of these floral regulators is summarized in the Floral Quartet Model (FQM) [44], which posits that tetrameric complexes of MADS-domain proteins bind to proximal CArG-box sequences (CArG: C-A-rich-G; consensus: 5′-CC(A/T)$_6$GG-3′) to regulate their target genes.

Thus, for the specific development of each floral organ, different tetrameric complexes of MADS-domain

(See figure on next page.)

Fig. 2 BINDING and FRET efficiency in FLIM experiments. **A** Schematic of a multiexponential fluorescence decay when FRET occurs. Fluorescence lifetime τ is defined as the average time a fluorophore stays in its excited state. During this time, the intensity *I(t)* decreases by 63.8%. The decaying intensity at time t is given by the summed decay functions across all components i, where τ is the lifetime and α the pre-exponential factor (amplitude) of the exponential decay function. **A'** Schematic of the different components in the overall decay. The sum of the individual components would result in the overall decay curve. **B** The mean amplitude weighted lifetime τ_m of a mixture of differentially decaying components is given by the sum of each component's lifetime (τ_i) weighted by its respective amplitude (α_i). In case of FRET, τ_m decreases and can be used as a measure for protein–protein interaction. However, reduction of τ_m ccould be due to high affinity between the proteins and low energy transfer efficiency between fluorophores or vice versa. Therefore, using τ_m, one loses information which are usually included in FLIM data. **C** Using the amplitudes and the lifetimes of the exponential decay, BINDING and FRET efficiency can be calculated. BINDING is indicative of how many molecules undergo FRET in a sample, whereas FRET efficiency describes the efficiency of the energy transfer between the fluorophores. As energy transfer efficiency is dependent on the distance between fluorophores and the orientation of their dipoles, FRET efficiency can be used as a measure for proximity and orientation within the complex and BINDING as an indicator for the affinity between the proteins. Increase of BINDING correlates with more protein–protein interactions. Increase in FRET efficiency indicates higher transfer efficiency due to higher proximity of the fluorophores and similar orientation of their dipoles

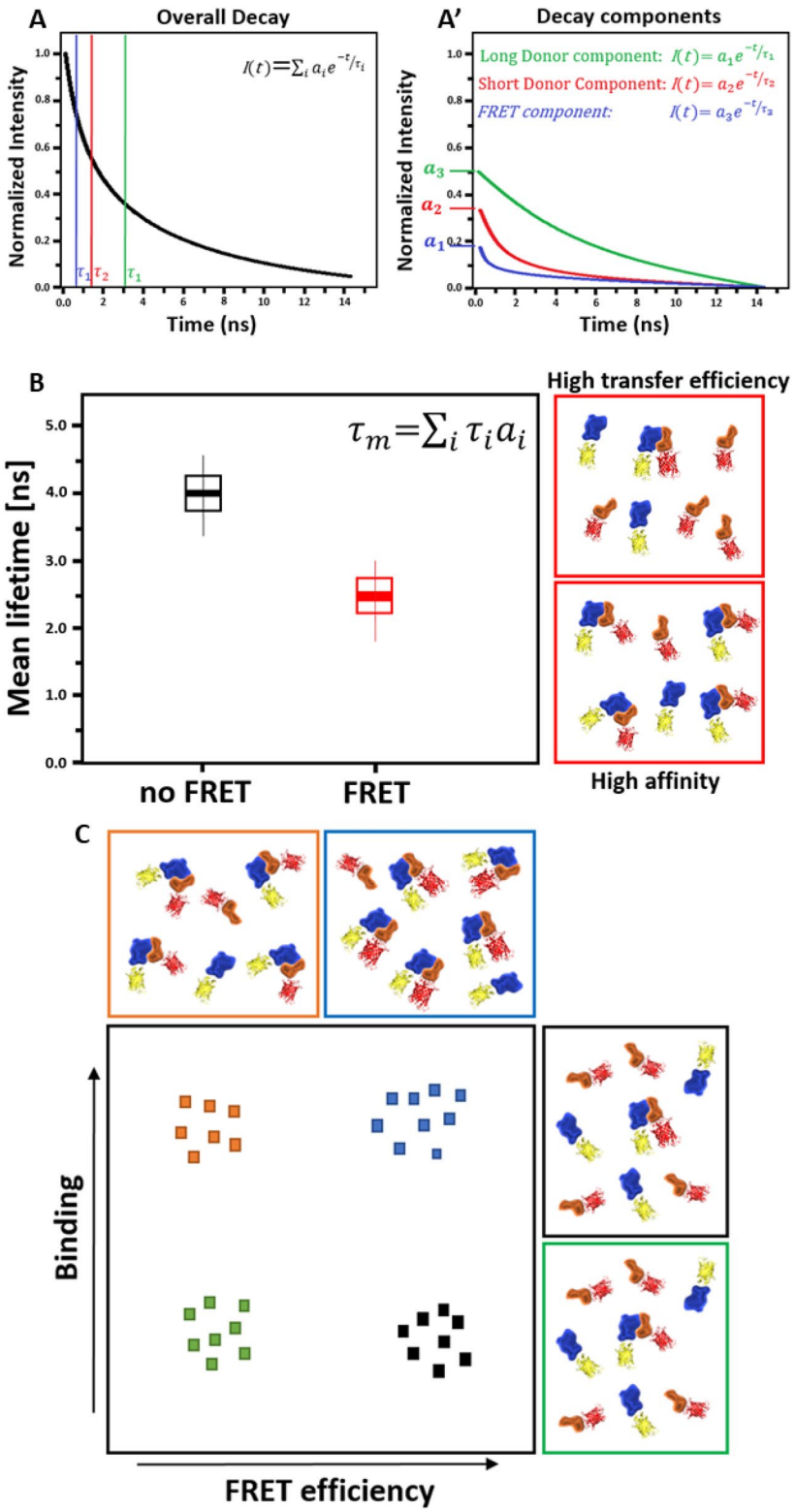

Fig. 2 (See legend on previous page.)

proteins are responsible [12, 43, 44]. However, while tetramerization seems to be characteristic for MADS-domain proteins, chromatin immunoprecipitation experiments followed by next generation sequencing also highlighted the relevance of dimers and it is assumed that both, tetramers and dimers, can occur in dynamic equilibria [21, 22, 22, 23, 23].

Over the past three decades, complex formation of plant MADS-domain proteins has been well characterised and numerous complex combinations have been reported [8, 12, 14, 16–18, 20, 28, 34, 38, 47, 49]. (A summary of Arabidopsis MADS-domain protein interactions can be found in Table 1)Thus, the FQM is well supported, but yet little is known about the stoichiometry or the presence of distinct complexes *in planta*. Although previously reported FRET assays in *N. benthamiana* leaf cells and *Arabidopsis* protoplasts support the idea of in vivo complex formation [14, 17, 18, 28], they come with the limitation that they do not resolve binding dynamics or PPI strength. Additionally, because standard two-colour FRET and BiFC are limited to investigate dimeric interactions, evidence for tetramer formation *in planta* is still sparse. Initial in situ interactions have been illustrated with BiFC experiments in developing flowers [38], but equilibria between dimers and tetramers in a cellular, tissue-specific or developmental/temporal context are still not understood. Furthermore, BiFC itself affects the nature of protein interactions so that even very transient or by-chance encounters of overexpressed proteins are stabilised, creating a background of protein interactions that are unlikely to represent the in vivo situation.

To overcome these limitations, we established a pipeline using FRET-FLIM alone or in combination with BiFC (Fig. 1C) as well as discrimination between BINDING and FRET efficiency to elucidate dimer and tetramer formation between MADS-domain transcription factors more precisely. We observed strong interactions between the MADS-domain proteins APETALA1 (AP1), SEP3, PISTILLATA (PI) and APETALA3 (AP3), and the formation of tetrameric complexes in vivo using an inducible heterologous expression system (*N. benthamiana*). We were able to dissect preferences for homo- or heteromer formation between the individual complex components and found that the interaction of AP1 with AP3 and PI in the tetrameric assembly depends on SEP3. The *OPA* approach allowed us to overcome biexponential donor-only decays, which poses a general difficulty in FLIM data fitting procedures and often results in data over interpretation or erroneous determination of FRET. We noted that currently available FLIM setups do not allow to reliably detect the aforementioned tetrameric complexes in young *Arabidopsis* flowers, where the presence of other native interaction partners, variable donor or acceptor concentrations and low photon numbers lead to a diluted FRET component. Nevertheless, the development of new labelling technologies and advancement of brighter fluorophores will allow the successful determination of multimeric protein interaction networks in vivo in the future.

Results

Observation of AP1 and SEP3 homo- and heteromeric complexes in vivo

To characterize the interaction properties of MADS-domain transcription factors in vivo, we expressed C-terminal fusions between AP1, SEP3, AP3 or PI and the fluorescent proteins (FP), mVenus (mV) and mCherry

Table 1 Overview of observed interactions between the MADS-domain proteins AP1, SEP3, PI and AP3. (Yeast 2 Hybrid (Y2H), Electrophoretic Mobility Shift Assay (EMSA), Immunoprecipitation (IP), Liquid chromatography–mass spectrometry (LC–MS)).

	Y2H	EMSA or IP	BiFC	LC–MS	FRET	Crystal structure	Literature
AP3-PI-SEP3-AG	●	●					[12, 16]
AP3-PI-SEP3-AP1					●		This study
AP3-PI-AP1	●	●			●		[12], This study
AP3-PI-SEP3	●	●			●		[12, 18], This study
PI-PI		●			●		[34], This study
AP3-PI		●	●	●	●		[34, 38, 47], This study
AP3-AP3		●			●		[34], This study
SEP3-AP3		●		●	●		[18, 38], This study
SEP3-PI		●		●	●		[18, 38], This study
SEP3-SEP3		●			●	●	[16, 18, 33], This study
AP1-AP3		●		●	●		[34, 38], This study
AP1-PI		●		●	●		[34, 38], This study
AP1-SEP3	●	●	●		●		[12, 18, 38], This study
AP1-AP1		●			●		[34], This study

(mCh), respectively, in epidermal leaf cells of transiently expressing *N. benthamiana*. When expressed individually, all fusion proteins localized to the nucleoplasm and were excluded from the nucleolus (Fig. 3A–D).

Signal of AP3-mV and PI-mV was also detected in the cytoplasm (Fig. 3C, D), as dimerization of AP3 with PI is necessary for complete nuclear localisation [17, 29]. We then measured FRET to analyse distinct complexes at a subcellular level. To this end, we acquired FLIM images of nuclei from cells expressing different combinations of the four aforementioned fusion proteins. In most cases, the measured mVenus (donor only) data displayed a bi-exponential decay consisting of a longer lifetime of ~ 3 ns and a shorter lifetime of ~ 1–2 ns. This bi-exponential decay behavior was previously described for mVenus, but also for other fluorescence proteins like YFP or GFP [1, 36, 42].Even though the amplitude of the shorter lifetime fraction is much lower compared to the amplitude of the longer lifetime fraction, we considered this as a real contribution to the decay and accordingly applied a newly developed fitting routine for multi-exponential decays to avoid artificially increased BINDING or FRET efficiencies. We applied the same fitting procedure, used for FRET samples containing both mV and mCh, to all donor only samples expressing only mVenus fused to one of the MADS-box proteins to characterize the background BINDING levels we could expect from our fitting model.

In most of the cells of the donor only sample AP1-mV we acquired apparent BINDING values between − 10 and 10% (1.2% ± 4.5; Additional file 1: Fig. S1; Fig. 4).

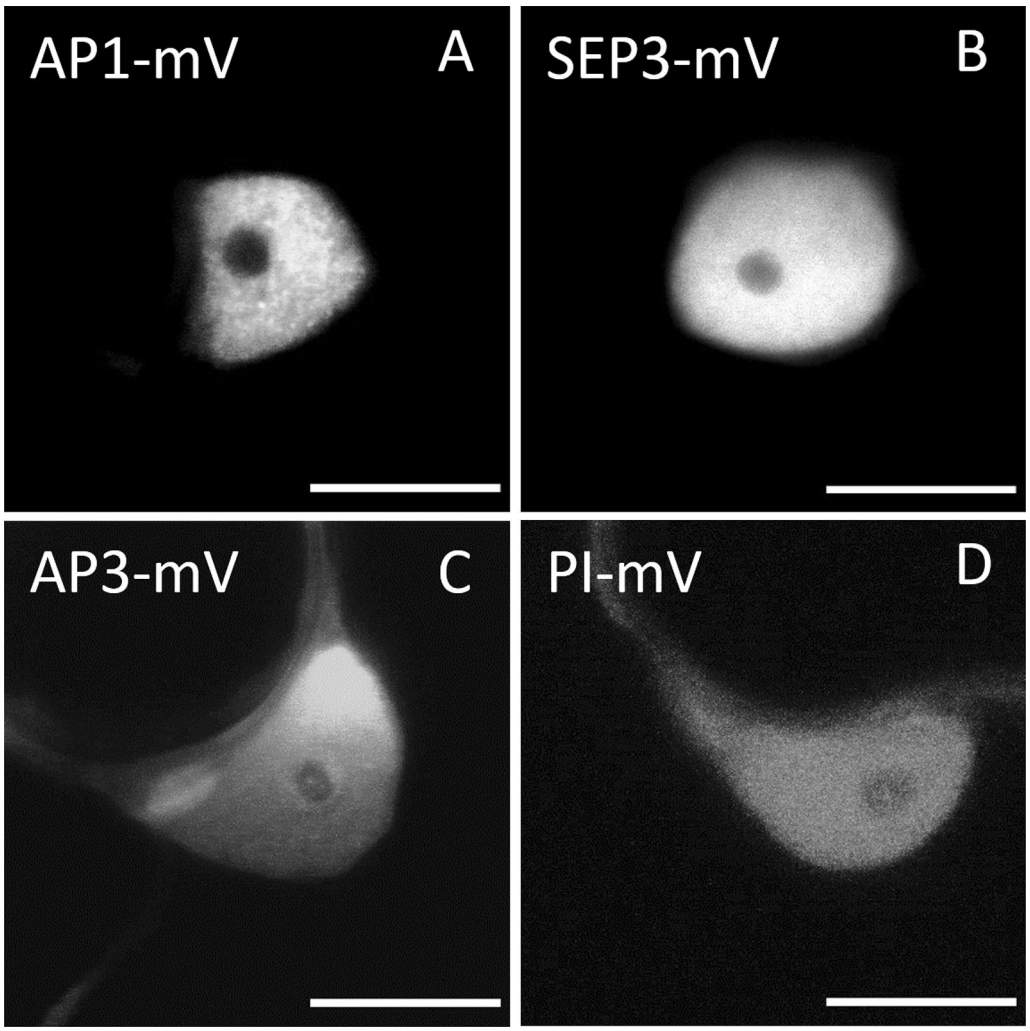

Fig. 3 Localisation of MADS-domain proteins in *N. benthamiana* leaf cells. MADS-domain proteins fused to fluorescent proteins were transiently expressed via the UBQ10 promoter in epidermis cells of *N. benthamiana* leaves. **A** Localization of AP1-mV. **B** Localisation of SEP3-mV. AP1 and SEP3 are localised to the nucleus. **C** Localisation of AP3-mV. **D** Localisation of PI-mV. Signal from AP3 and PI was selected in both nucleus and cytoplasm. All proteins were absent from the nucleolus (Scale bars: 10 µm)

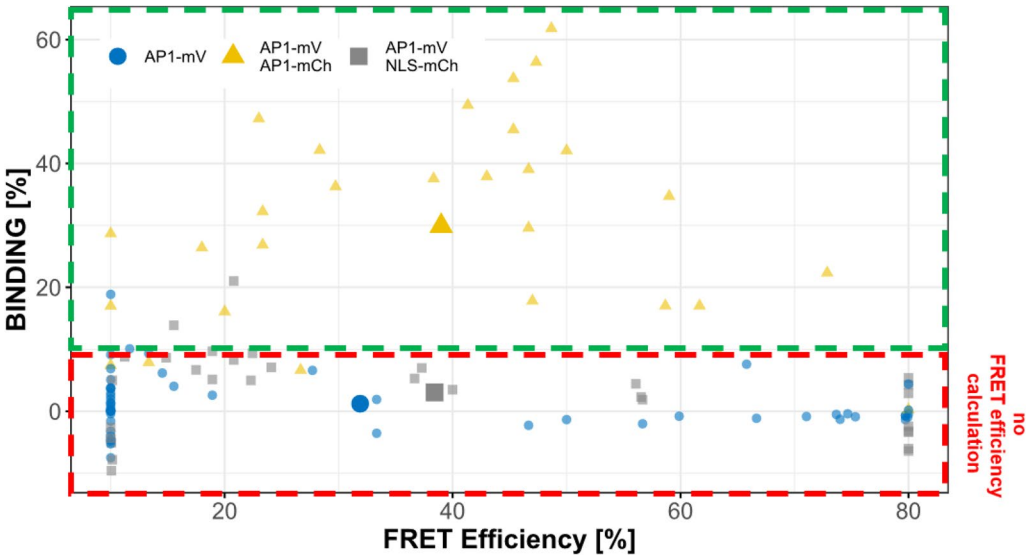

Fig. 4 BINDING versus FRET efficiencies in FRET and no-FRET samples. BINDING and FRET efficiencies for donor only (AP1-mV), negative control (AP1-mV NLS-mCh) and FRET (AP1-mV AP1-mCh) samples. In samples where molecules don't undergo FRET, acquired BINDING usually was between − 10 and 10%. We therefore defined this range below 10% as "limit for FRET efficiency calculation". When BINDING was below 10%, FRET efficiencies were highly variable and accumulated at the limits (10% and 80% FRET efficiency) which defined in the fitting model. Therefore, we excluded FRET efficiencies when BINDING was below 10% and only include them when molecules in a sample undergo FRET (BINDING above 10%)

When donor only samples AP1-mV were fitted using a model, which assumes a mono exponentially decaying donor, BINDING appeared significantly increased and in one fourth of the images BINDING was above 10% (7.6% ± 9.0; Additional file 1: Fig. S2). Donor only decays must therefore be carefully examined to avoid that a second, more rapidly decaying donor component is considered as FRET. The corresponding apparent FRET efficiencies displayed high variance (Additional file 1: Table S1), usually values close to the minimum or maximum limits of our fitting model (Additional file 1: Fig. S1; Fig. 4). As in donor only samples no photons are detected originating from the FRET process, their contribution to the overall decay cannot be fitted correctly due to low photon statistic. Therefore, we acknowledged that we cannot sufficiently calculate reliable apparent FRET efficiencies for nuclei with BINDING below 10%. Consequently, we defined a cut-off for BINDING below 10% as "limit for FRET efficiency calculation". As in this range, FRET efficiencies cannot be calculated adequately, we subsequently did not display FRET efficiencies for nuclei with lower BINDING (Fig. 5B). In nuclei displaying BINDING above the "limit for FRET efficiency calculation" of 10%, we could more reliably fit FRET efficiency and therefore subsequently display FRET efficiencies determined from these samples (Figs. 4, 5B). Indeed, when AP1-mCh was co-expressed as acceptor for AP1-mV, we measured significantly increased BINDING (29.9% ± 16.4; Fig. 5B), showing the formation of AP1 homomeric complexes (with a FRET efficiency of 39.0% ± 16.9).

Subsequent bleaching of the acceptor molecules led to a significantly decreased BINDING in the same nuclei (from 19.2% ± 4.7 to 1.17% ± 1.2; Additional file 1: Fig. S3), confirming FRET between AP1-mV and AP1-mCh. As expected, BINDING weakly correlated with the acceptor concentration (Additional file 1: Fig. S4). FRET can also occur between non-interacting proteins. This phenomenon is known as bystander FRET and is due to high protein concentrations in the analysed environment [3, 24]. To analyse a possible effect of bystander FRET in our set-up we co-expressed AP1-mV with mCh tagged to a nuclear localisation sequence (NLS). We observed a small, but not significant increase in BINDING compared to the donor only sample (from 1.2% ± 4.5 to 3.1% ± 6.8). As BINDING was not significantly elevated and in most AP1-mV NLS-mCh images below 10%, we assumed that bystander FRET could be neglected in our experimental set-up (Additional file 1: Fig. S2).

According to the FQM, a quaternary complex, consisting of a dimer formed by AP1 and SEP3 that interacts with a dimer formed by AP3 and PI is responsible for the specification of petals during floral development [12, 44]. Before analysing tetramer formation between AP1, AP3, PI and SEP3 we wanted to test the stability of the individual proposed dimeric interactions. To this end, we

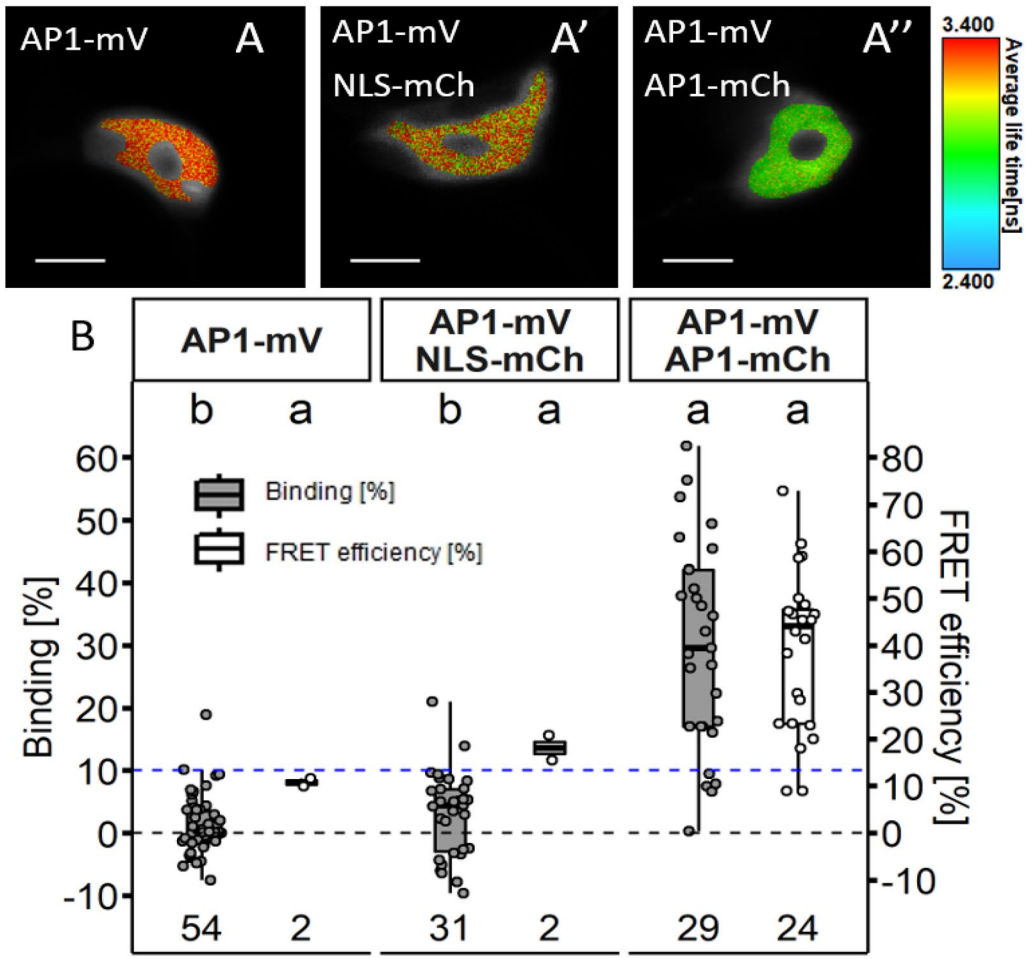

Fig. 5 FLIM analysis of AP1-mV NLS-mCh and AP1-mV Ap1-mCh in *N. benthamiana* leaf cells. FLIM experiments were performed in *N. benthamiana* leaf epidermis cells. Fusion proteins were expressed from the *UBQ10* promoter and imaged 3–4 days after infiltration. **A** Average lifetime image of individual nuclei expressing AP1-mV, AP1-mV NLS-mCh and Ap1-mV AP1-mCh (**A**′–**A**″ respectively). Nucleoli were excluded from FLIM analysis. (Scale bars: **A**–**A**″: 6 µm) **B** BINDING [%] (grey) and FRET efficiencies [%] (white) for AP1-mV, AP1-mV NLS-mCh and AP1-mV AP1-mCh. For each analysed nucleus average BINDING and a corresponding average lifetime were fitted. Mean BINDING of the donor only sample AP1-mV was 1.23% and most values were below 10%. Therefore, nuclei with BINDING below 10% were excluded from FRET efficiency calculation. Co-expression of NLS-mCh with AP1-mV did not lead to significant higher BINDING (3.06%) compared to the donor only sample, while AP1-mV AP1-mCh showed increased BINDING (29.89%) with an average FRET efficiency of 39.98%. Statistical groups were assigned after multiple comparison with Kruskal–Wallis and a Post hoc test using the criterium Fisher's least significant difference (alpha parameter is 0.05). (Dashed blue line marks the BINDING cut-off of 10%; Number of repetitions are indicated below BINDING values and number of images with BINDING above 10% are indicated below the FRET efficiency values in the bottom of the plot)

first assessed AP1/SEP3 heteromers. Subcellular localisation of AP1 and SEP3 did not change upon co-expression (Fig. 6A–A").

BINDING values of AP/SEP3 (36.1% ± 10.0; Fig. 6B) showed high affinity between the two proteins, suggesting stable dimer or even tetramer formation. Mean FRET efficiency of AP1/SEP3 (42.6% ± 6.3) was comparable to the mean FRET efficiency measured for AP1/AP1 (39.0% ± 16.9), but less variable (Additional file 1: Table S1). We also tested for SEP3 homomerization (Fig. 6B). As shown before, SEP3 can form homomeric complexes [33], although average BINDING (28.2% ± 9.7) was lower than detected for AP1/SEP3, but similar to AP1/AP1 (Additional file 1: Table S1). Hence, heteromer formation of AP1 with SEP3 appears to be preferential over the formation of individual homomeric complexes.

AP3/PI heteromerization is dominant over AP3 or PI homomerization

Formation of AP3/PI heterodimers was previously characterised *in planta* by FRET-FLIM, BiFC and immunoprecipitation (IP) [18, 38]. We also detected

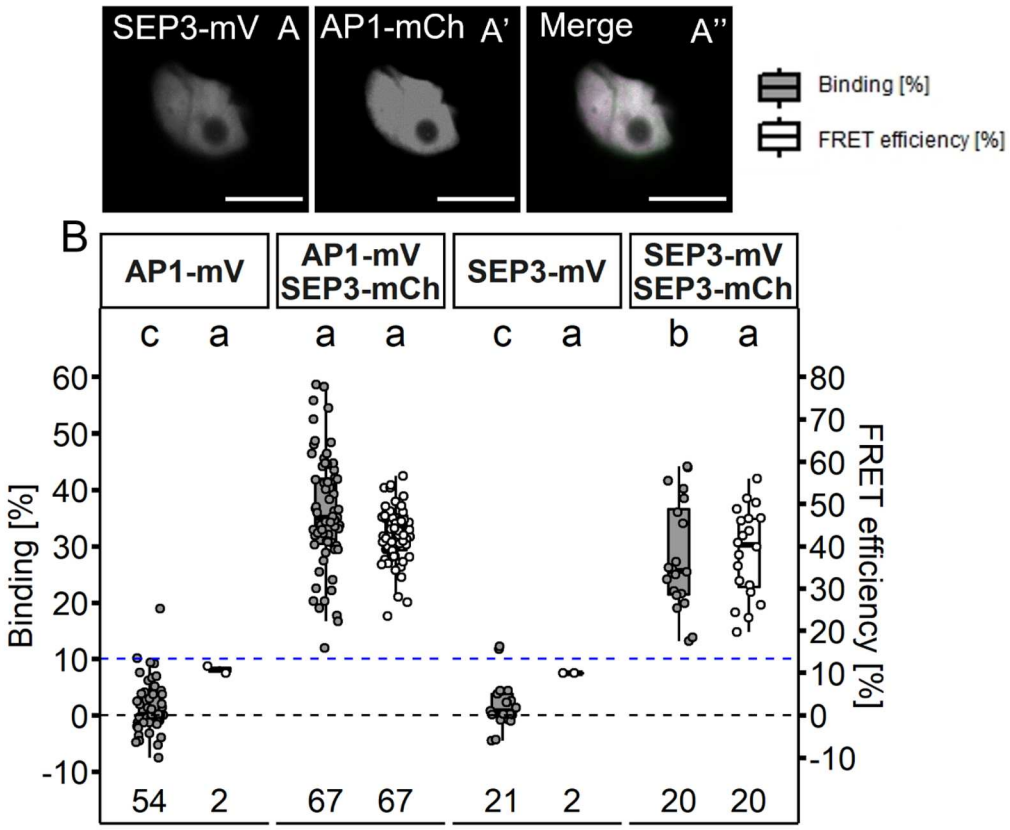

Fig. 6 Interaction between AP1 and SEP3 proteins in *N. benthamiana* leaf cells. **A**–**A**'' Co-localisation of SEP3-mV an AP1-mCh in *N. benthamiana* leaf cells (**A** SEP3-mV signal. **A**' AP1-mV signal. **A**'' Merged signal). Co-expression did not lead to a change of localisation. (Scalebars: **A**–**A**'': 10 µm) **B** BINDING [%] (grey) and FRET efficiencies [%] (white) for AP1-mV, AP1-mV SEP3-mCh, SEP3-mV and SEP3-mV SEP3-mCh. Analysis was done as described in Fig. 5. Mean BINDING (28.15% ± 9.7) and FRET Efficiency (38.53% ± 10.53) measured for SEP3 homomers were comparable to the values obtained for AP1 homomers (compare to Fig. 5). Mean BINDING of the AP1/SEP3 heteromer (36.06% ± 10.01) was slightly increased compared to both individual homomers. Mean FRET Efficiency of the heteromers (42.64% ± 6.26) was not significantly different compared to the SEP3 homomers. Statistical groups were assigned after multiple comparison with Kruskal–Wallis and a Post hoc test using the criterium Fisher's least significant difference (alpha parameter is 0.05) (Dashed blue line marks the BINDING cut-off of 10%; Number of repetitions are indicated below BINDING values and number of images with BINDING above 10% are indicated below the FRET efficiency values in the bottom of the plot)

localization to the nucleolus upon co-expression of the two proteins (Fig. 7A–C) as described [18, 29].

For this dimer, we determined high BINDING values (Fig. 7D, 35.3% ± 11.7 for AP3/PI and 36.0% ± 9.0 for PI/AP3), independent of the direction of the tested interaction. Heterodimerization of AP3 and PI is thought to be the evolutionary ancestral state and is necessary for DNA binding [47]. However, also homomeric interactions between AP3 or PI proteins have been reported in previous FRET-FLIM experiments [18]. In agreement with this, we could detect the formation of AP3/AP3 and PI/PI homomers, however with much lower affinities compared to AP3/PI heteromers (Fig. 8; 23.6% ± 17.2 and 10.2% ± 8.6 BINDING, respectively).

The addition of competitive PI to AP3/AP3 or AP3 to PI/PI samples, respectively, led to reduced, but statistically not significant average BINDING between AP3/AP3 or PI/PI when compared to samples without competitor (Fig. 8; 15.7% ± 12.04 and 7.0% ± 4.1 respectively).

SEP3 is necessary for stable tetramer formation

To date, interactions of AP1 with AP3 or PI could not be measured *in planta*. We therefore co-expressed AP3-mV and PI-mV with AP1-mCh transiently in the epidermis of *N. benthamiana* leaves (Fig. 9A–F).

In this experiment, the cellular localization of the fusion proteins was identical when compared to those expressing the proteins individually but in contrast to the AP3/PI heteromer, there was no accumulation in the nucleolus of either AP1, AP3 or PI. Using FRET-FLIM, we determined BINDING value of ~ 16% for both AP1/

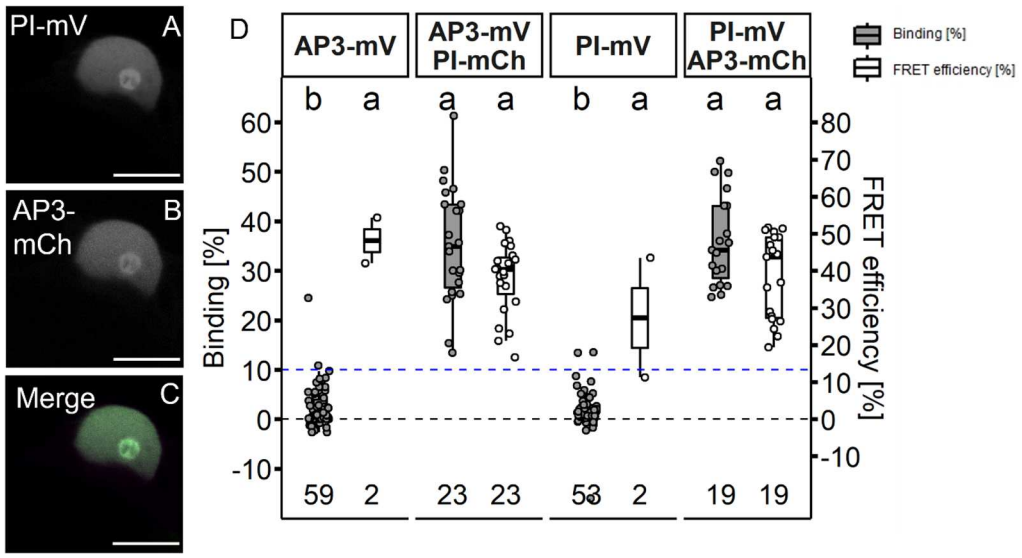

Fig. 7 AP3 and PI homomerization in *N. benthamiana* leaf cells. AP3 and PI fused to the indicated FPs were expressed via the *UBQ10* promoter and imaged three days after infiltration. **A**–**C** Co-localisation of PI-mV and AP3-mCh in *N. benthamiana* leaf cells (**A** PI-mV signal. **B** AP3-mV signal. **C** Merged signal). Co-expression of AP3 with PI lead to an accumulation of both AP3 and PI in the nucleolus (for individual expressed AP3 and PI compare Fig. 3; Scalebars: **A**–**C** 10 µm). **D** BINDING [%] (grey) and FRET efficiencies [%] (white) for AP3-mV, AP3-mV PI-mCh, PI-mV and PI-mV AP3-mCh. Analysis was done as described in Fig. 5. Average BINDING between AP3 and PI was high in both measured directions (35.25% ± 11.65 for AP3/PI and 35.97% ± 8.99 for PI/AP3) with mean FRET Efficiencies of ~ 38%. Statistical groups were assigned after multiple comparison with Kruskal–Wallis and a Post hoc test using the criterium Fisher's least significant difference (alpha parameter is 0.05) (Dashed blue line marks the BINDING cut-off of 10%; Number of repetitions are indicated below BINDING values and number of images with BINDING above 10% are indicated below the FRET efficiency values in the bottom of the plot)

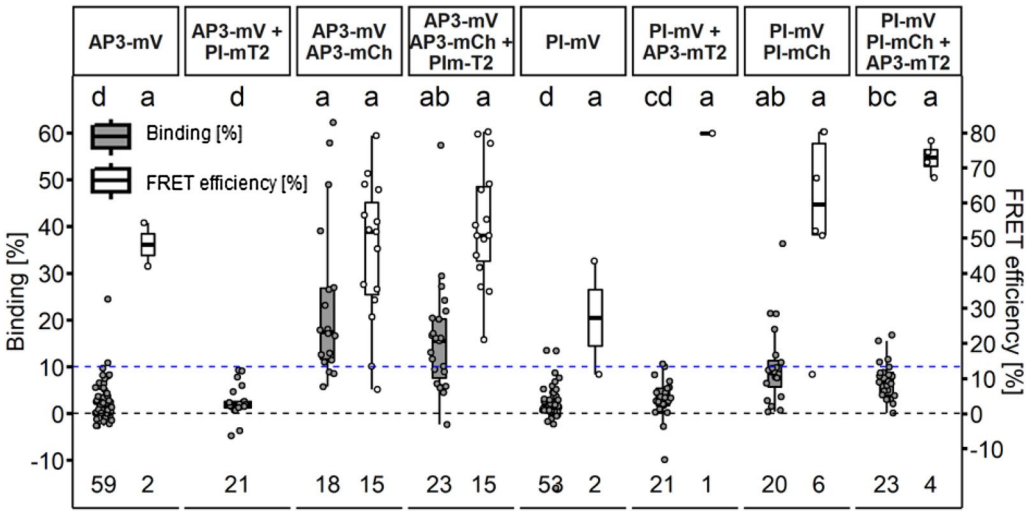

Fig. 8 AP3 and PI protein homomerization in *N. benthamiana* leaf cells. BINDING (grey) and FRET efficiencies (white) for AP3-mV, AP3-mV + PI-mT2, AP3-mV AP3-mCh, AP3-mV AP3-mV-mCh + PI-mT2, PI-mV, PI-mV + AP3-mT2, PI-mV PI-mCh, PI-mV PI-mV-mCh + AP3-mT2. For each analysed nucleus average BINDING and a corresponding average lifetime of mV were fitted. Nucleoli were excluded from FLIM analysis. mT2 did not have an influence on mV lifetime as FRET can only occur from mT2 towards mV but not vice versa. Nuclei with average BINDING below 10% were excluded from FRET efficiency calculation. Statistical groups were assigned after multiple comparison with Kruskal–Wallis and a Post hoc test using the criterium Fisher's least significant difference (alpha parameter is 0.05) (Dashed blue line marks the BINDING Cut-Off of 10%)

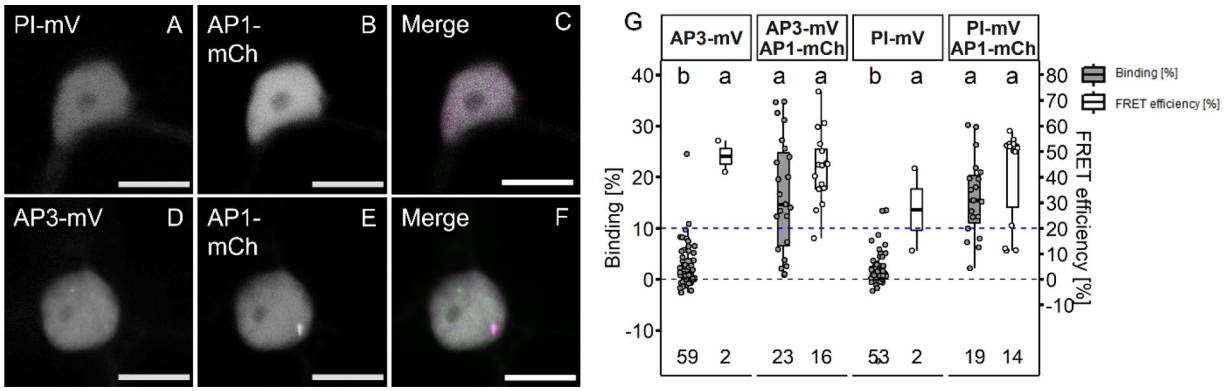

Fig. 9 Interaction analysis between AP1 and AP3 or PI proteins in *N. benthamiana* leaf cells. A-C: Co-localisation of PI-mV an AP1-mCh in *N. benthamiana* leaf cells (**A** PI-mV signal. **B** AP1-mV signal. **C** Merged signal). **D**–**F** Co-localisation of AP3-mV an AP1-mCh in *N. benthamiana* leaf cells (**D** AP3-mV signal. **E** AP1-mV signal. **F** Merged signal). MADS-domain proteins fused to the respective FP were expressed in *N. benthamiana* leaf cells via the*UBQ10 promoter* (AP3 and PI) or the *XVE* < < *oLexA-35S* estradiol inducible system (AP1). Nuclei were imaged 5–6 days after infiltration and expression of AP1 was induced one day prior to image acquisition. Co-expression of AP1 with AP3 or PI did not lead to a change of protein localisation. (Scalebars: **A**–**F** 10 µm) **G** BINDING [%] (grey) and FRET efficiencies [%] (white) for AP3-mV, AP3-mV AP1-mCh, PI-mV and PI-mV AP1-mCh. Analysis was done as described in Fig. 5. Both the AP1/AP3 and the AP1/PI heteromers displayed low average BINDING (16.46% ± 11.17 and 16.08% ± 7.77 respectively) and comparable FRET efficiencies of 43.61% ± 14.18 (AP1/AP3) and 41.54% ± 18.36. Statistical groups were assigned after multiple comparison with Kruskal–Wallis and a Post hoc test using the criterium Fisher's least significant difference (alpha parameter is 0.05) (Dashed blue line marks the BINDING cut-off of 10%; Number of repetitions are indicated below BINDING values and number of images with BINDING above 10% are indicated below the FRET efficiency values in the bottom of the plot).

AP3 and AP1/PI heteromers (Fig. 9G; 16.5% ± 11.2 and 16.1% ± 7.8 respectively), which, however, was lower than BINDING acquired for the AP3/PI or AP1/SEP3 heterodimers (Additional file 1: Table S1). Heteromeric complexes of AP1 and AP3 or PI therefore appear to be less stable perhaps the presence of an AP3/PI heterodimer or ability of tetramerization induced by other factors present are necessary to increase affinity. For example, the interaction of the AP3/PI heterodimer was enhanced by the addition of SEP3 in protoplast FRET-FLIM experiments [18]. Generic, two-fluorophore FRET-FLIM measurements only address the interaction between two partners. Hence, we combined FRET-FLIM with BiFC to analyse ternary or quaternary complex formation between the AP3/PI dimer and AP1 and SEP3 protein. One of the major downsides of BiFC is the high affinity of the two FP fragments for each other. As a result, the fragments may form stable fluorophores, although there may be no or only very weak interactions between the fused proteins of interest. As a proof of principle, AP3 and PI were tagged with the two FP fragments. Heteromerization of those two POIs is well characterized and appears to be essential for their stability, making them ideal partners for BiFC. mVenus was separated at amino acid residue 154. The N-terminal part (mVn) was tagged to AP3 and the C-terminal part (mVc) to PI. Fluorescence signal was detected in the nucleus of co-expressing epidermal cells and, as observed before, accumulated in the nucleolus, indicating no negative influence of the split mVenus on localization and complex formation (Fig. 10A).

Because altered localization for the AP3/PI heteromer in the presence of SEP3 was previously reported [18], the individual expression of AP3-mVn/PI-mVc, AP1-mCh and SEP3-mCh was monitored before co-expression. NLS-mCh served as a non-interacting control for both comparisons of localization and later as negative control for the FRET-FLIM experiments. AP1-mCh, SEP3-mCh and NLS-mCh were mainly found in the nucleus but were

(See figure on next page.)

Fig. 10 Localisation of co-expressed MADS-box proteins in *N. benthamiana* leaf cells. **A** Localisation of the AP3/PI heteromer visualized by BiFC. BiFC did not interfere with AP3/PI translocation to the nucleus or nucleolus. **B**–**D** Localisation of SEP3-mCh, NLS-mCh and AP1-mCh respectively. **E**–**E**″: Co-expression of AP3/PI and SEP3 (**E** Signal from AP3/PI, E′: Signal from SEP3, **E**″ Merged signal). SEP3 accumulated at the nucleolus and fully co-localized with AP3/PI. **F**–**F**″ Co-expression of AP3/PI and AP1 (**F** Signal from AP3/PI, **F**′ Signal from AP1, **F**″ Merged signal). AP1 weakly accumulated at in the presence of AP3/PI. **G**–**G**″ Co-expression of AP3/PI and NLS-mCh (**G** Signal from AP3/PI, **G**′ Signal from NLS-mCh, **G**″ Merged signal). NLS-mCh localisation did not change in the presence of AP3/PI. **H**–**H**‴ Co-expression of AP3/PI with SEP3 and AP1 (**E** Signal from AP3/PI, **E**′ Signal from SEP3, **E**″ Signal from AP1 **E**‴ Merged signal). Expression of SEP3 with AP3/P and AP1 lead to strong re-localisation of AP1 to the nucleolus and full co-localisation of all four MADS-domain proteins. (Scale bars: 10 µm)

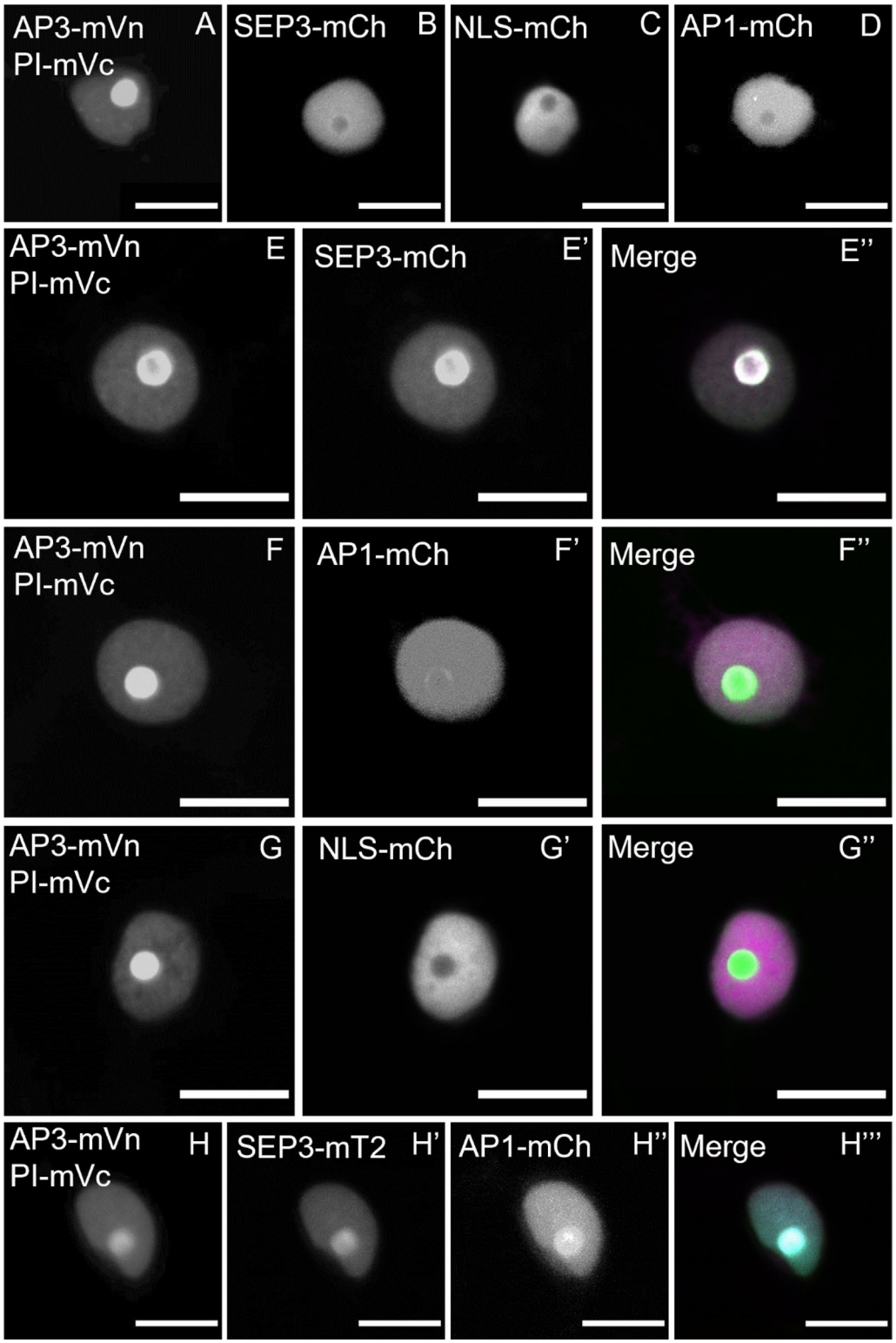

Fig. 10 (See legend on previous page.)

absent from the nucleolus (Fig. 10B–D). Co-expression of SEP3 with AP3/PI had no effect on AP3/PI localization, contrary to the confocal laser scanning microscopy data from *Arabidopsis* protoplasts previously published [18]. Interestingly, we found the opposite effect: AP3/PI seems to promote accumulation of the other MADS-domain factors in the nucleolus. The previously only weakly nucleolus-associated SEP3 fully co-localized with AP3/PI and showed strong nucleolar accumulation (Fig. 10E–E"). Although to a much weaker extend, this phenomenon could also be observed for AP1 (Fig. 10F–F"). NLS-mCh had no influence on AP3/PI localisation and vice versa (Fig. 10G–G"). Direct interactions between AP3-mVn/PI-mVc and AP1-mCh or SEP3-mCh were then analysed with FRET-FLIM. For the SEP3/AP3/PI combination, we measured increased BINDING values (Fig. 11; 23.2% ± 7.6), indicating ternary complexes or possible interaction between AP3/PI and SEP3/SEP3 dimers. In contrast, the combination of AP1/AP3/PI did not show high average BINDING values (Fig. 11; 8.4% ± 5.7), which were even lower compared to what we acquired before from the AP1/AP3 or AP1/PI combinations. We then tested whether co-expression of SEP3 could increase the affinity between AP1 and AP3/PI.

Indeed, additional SEP3 led to a stronger accumulation of AP1 in the nucleolus (Fig. 10H–H"') and strongly increased BINDING between AP1 and AP3/PI (Fig. 11; 28.8% ± 12.4).

To demonstrate the advantages OPA brings by separating BINDING from FRET efficiency, we included traditionally used average lifetimes, derived from bi-exponential fitting models, for the BiFC FRET-FLIM data (Additional file 1: Fig. S5). By using average lifetime analysis to evaluate the occurrence of FRET, we detected a significant influence of NLS-mCh on the AP3-mVn/PI-mVc donor lifetime, while we could not detect a significant difference between the NLS-mCh and AP1-mCh sample (Additional file 1: Fig. S5). In this case, average tau analysis suggests the occurrence of FRET in the negative control sample, while it could not detect FRET between AP3-mVn/PI-mVc and AP1-mCh. In contrast, OPA helps to better distinguish between interacting and non-interacting samples, as it shows no elevated BINDING between donor only and NLS-mCh, but significantly

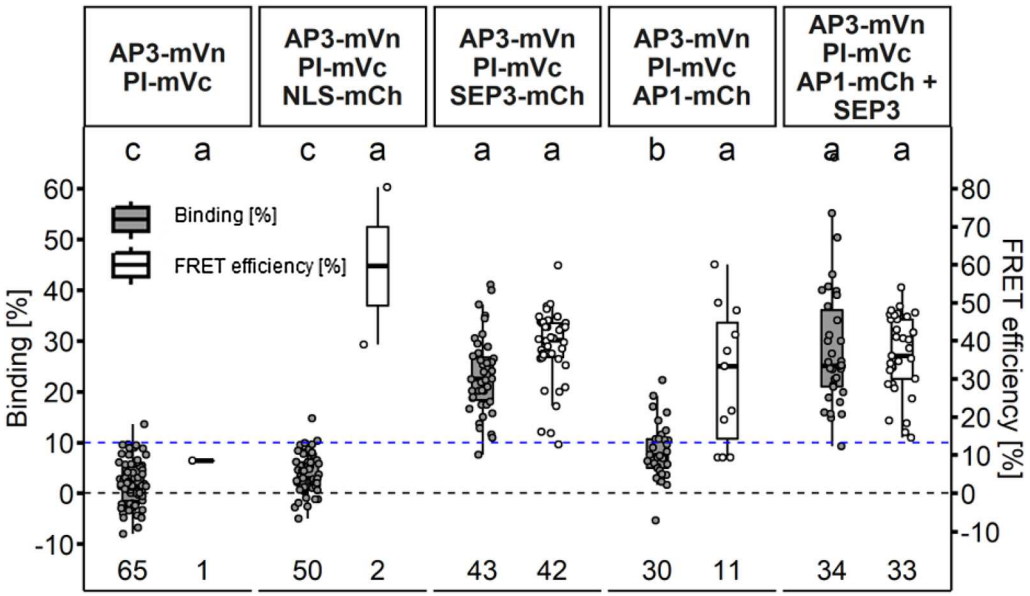

Fig. 11 Larger complex formation between AP1, AP3, PI and SEP3 proteins in *N. benthamiana*. Higher order complex formation of MADS-box proteins was analysed by a combination of BiFC with FRET-FLIM. Complemented mV by the n-terminal and c-terminal part of mV tagged to AP3 and PI respectively served as the donor in FRET-FLIM experiments. All MADS-domain protein fused to FP were expressed via the UBQ10 promoter. Untagged SEP3 was expressed from the same T-DNA as AP1-mCh using the *XVE* < < *oLexA-35S* estradiol inducible system. Images were acquired three days after infiltration and SEP3 was induced one day before imaging. BINDING [%] (grey) and FRET efficiencies [%] (white) for AP3-mVn PI-mVc, AP3-mVn PI-mVc NLS-mCh, AP3-mVn PI-mVc SEP3-mCh, AP3-mVn PI-mVc AP1-mCh and AP3-mVn PI-mVc AP1-mCh + SEP3. Analysis was done as described in Fig. 5. SEP3 together with AP3/PI displayed increased BINDING (23.21% ± 7.56) with a FRET efficiency of 38.57% ± 9.50. Affinity of AP1 for AP3/PI was low (8.40% ± 5.66 BINDING), but strongly increased in presence of SEP3 (28.80% ± 12.36 BINDING). Statistical groups were assigned after multiple comparison with Kruskal–Wallis and a Post hoc test using the criterium Fisher's least significant difference (alpha parameter is 0.05) (Dashed blue line marks the BINDING cut-off of 10%; number of repetitions are indicated below BINDING values and number of images with BINDING above 10% are indicated below the FRET efficiency values in the bottom of the plot)

increased BINDING between AP3-mVn/PI-mVc and AP1-mCh.

Thus, by using OPA we were able to show that the predicted complex for petal specification in the FQM can form *in planta*. Furthermore, assembly of AP1 with AP3/PI proteins in higher order complexes is dependent on SEP3. Thus, we argue that the equilibria between dimer and tetramerization of AP1, AP3 and PI could indeed be controlled by the concentration of SEP proteins.

FRET-FLIM could not detect MADS-domain protein interactions in young floral buds

Different MADS-domain protein di- and tetramers are thought to form in a whorl- specific manner in the developing tissue, however, *ex-situ* experiments reach their limits in the spatial and temporal resolution of complex formation. Therefore, it is of special interest to study such complexes predicted directly in developing floral meristems (FM). In 2012, Smaczniak and colleagues isolated MADS-domain protein complexes by immunoprecipitation and characterised them using LC–MS/MS [38]. While their data suggest that the proposed MADS-domain protein complexes form in developing flowers, these experiments lacked tissue-specific and cellular resolution. Additionally, in the same report, BiFC experiments were used to detect interaction between AG/SEP3, AP1/SEP3 and AP3/PI. Compared to BiFC, FRET assays have the advantage of having higher spatial resolution and, more importantly, are more specific, as complementing FP fragments show a tendency for self-assembly resulting in false positive interactions [13, 37]. FLIM in contrast to intensity- or spectral-based FRET methods, is more gentle on cells and tissues due to lower required laser intensity and is generally considered the more accurate method to detect FRET [10, 26, 27, 35, 40, 41].

Therefore, we here investigated interactions of AP1, SEP3, PI and AP3 in early-stage flowers using FRET-FLIM. Previously, GFP reporter of these MADS-domain proteins were generated and characterised [6, 48] and we aimed to use these as donor lines in FRET-FLIM experiments. To ensure high saturation of donor proteins with acceptor, we chose AP1 as acceptor, because it displayed the highest fluorescence signal among the MADS-box proteins we aimed to analyse. A ~ 3 kb promoter region upstream of the AP1 start codon was used to drive expression of AP1-mT2, AP1-mV or AP1-mCh fusion proteins. Constructs were transformed in *ap1-1* mutant plants using the floral dip method [51]. To analyse interactions between AP3 and PI we also generated a PI-mCh reporter with ~ 2 kb gPI fragment as promoter. The proPI::PI-mCh construct was transformed into wild-type plants and then crossed into the *pi-1* mutant background for complementation assays. All FP fusion constructs were able to rescue the respective stamen and/or petal deficiency of the *pi-1* or *ap1-1* mutant (Additional file 1: Fig. S9). The expression pattern of the GFP reporter as well as the here established AP1-FP and PI-mCh lines, analysis by confocal laser scanning microscopy, were in agreement with the expression pattern previously described [6, 32, 46, 48] for AP1, SEP3, AP3 and PI (Additional file 1: Fig. S7, S9). For co-localisation analysis of AP1 with SEP3, AP3 or PI we crossed an AP1-mT2 reporter with the SEP3, AP3 or PI GFP reporter and imaged the F1 progeny. We observed overlapping expression of SEP3 and AP1 in few cells of stage 2 floral buds and in the FM of stage 3, 4 and 5 flowers (Fig. 12A–A').

AP3 and PI co-localised in stage 3, 4 and 5 flowers (Fig. 12B–B', C–C'). In stage 3 and 4 buds, overlap between AP1 and AP3/PI proteins was detected in the ring formed expression pattern, characteristic for AP3 and PI, while in stage 5 flowers overlap was restricted to petal initiation sites (Fig. 12B' and C'; green arrows). For FRET-FLIM experiments, SEP3, AP3 and PI GFP reporter were crossed with a AP1-mCh or PI-mCh reporter line and lifetime images were acquired in the F1 progeny. Because of low signal from SEP3-, AP3- and PI-GFP we slightly increased the laser power of the 485 nm laser (from 1 to 1.4 µW at the objective). In deeper tissues of stage 5 flowers and petal initiation sites signal intensity was strongly reduced and we could not acquire suitable amounts of photons. We therefore restricted FRET-FLIM experiments to stage 3 and 4 flowers. To avoid autofluorescence, ROIs were used to select several nuclei per image and plastids with low lifetimes were excluded. Surprisingly, we could not detect any increase in BINDING above background in AP1/AP3, AP1/SEP3 PI/SEP3 or AP3/PI expressing plants (Fig. 13; Additional file 1: Table S2).

(See figure on next page.)

Fig. 12 Co-expression of AP1-mT2 with GFP reporeter of SEP3, AP3 and PI. **A**–**C** Z-stacks of AP1-mT2 (red) SEP3-GFP (green), AP1-mT2 (red) APP3-GFP (green) and AP1-mT2 (red) PI-GFP (green). **A'**–**C'** signal overlap was calculated in FIJI [19] using the Image calculator tool and were displayed with the "fire" color scale (low signal: purple; high signal: yellow). AP1 and SEP3 expression overlaps in few cells of late stage 2 floral buds and most cells of the dome shaped floral meristem in stage 3, stage 4 and stage 5 flowers. Overlaped expression of AP1 with AP3 or PI is first visibale in stage 3 floral buds. In stage 4 flowers AP1 and AP3 or PI proteins show an overlapping expression in a ringformed pattern while in stage 5 flowers, overlapping expression was restricted to petal initiation sites. Numbers indicate floral stage as previously defined (Smyth, Bowman, and Meyerowitz 1990). Scale bars: 50 µm

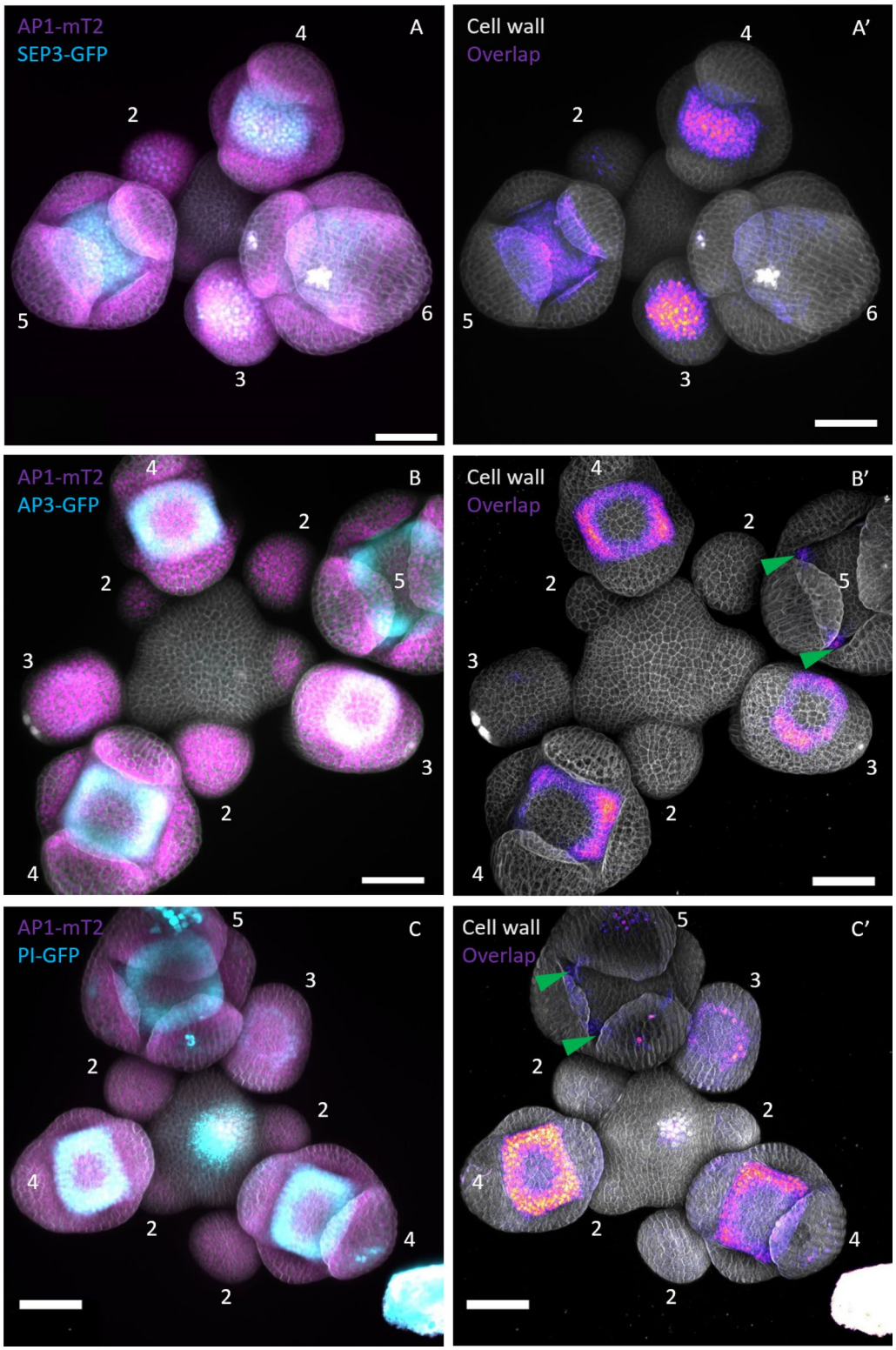

Fig. 12 (See legend on previous page.)

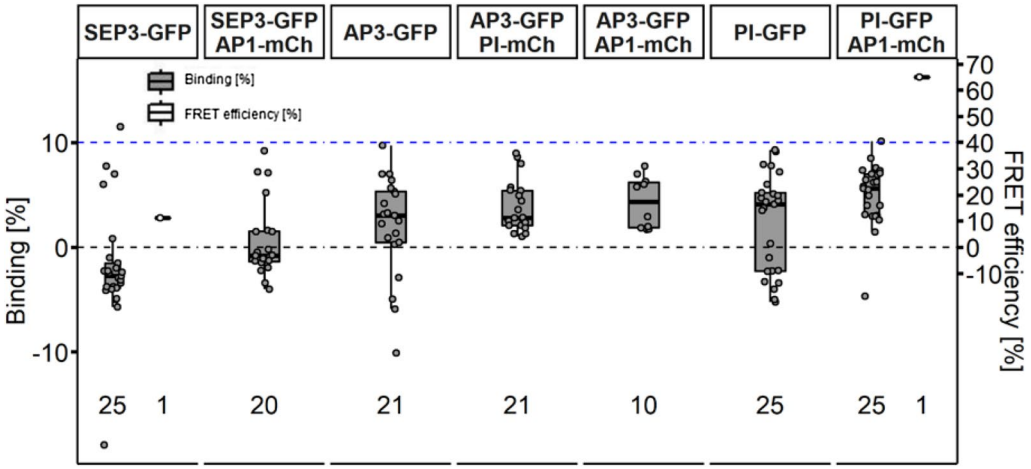

Fig. 13 No detectable interaction between MADS-domain proteins with FRET-FLIM in Arabidopsis GFP/mCh reporter. FLIM experiments were performed in stable *A. thaliana* lines. MADS-box proteins fused with the indicated FP were expressed by their endogenous promoter. Donor only images were acquired in homozygous GFP reporter lines. For the FRET samples, GFP lines were crossed with the respective mCherry reporter and FLIM images were acquired in resulting F1 plants. Each data point was calculated from a respective FLIM image containing several nuclei. Only nuclei containing both donor and acceptor were considered in FLIM image analysis of FRET samples. BINDING [%] (grey) and FRET efficiencies [%] (white) for SEP3-GFP, SEP3-GFP AP1-mCh, AP3-GFP, AP3-GFP PI-mCh, AP3-GFP AP1-mCh, PI-GFP and PI-GFP AP1-mCh. No increased BINDING above the 10% cut-off in FRET samples was detectable for any of the tested combinations. Statistical groups were assigned after multiple comparison with Kruskal–Wallis and a Post hoc test using the criterium Fisher's least significant difference (alpha parameter is 0.05) (Dashed blue line marks the BINDING Cut-Off of 10%; Number of repetitions are indicated below BINDING values and number of images with BINDING above 10% are indicated below the FRET efficiency values in the bottom of the plot)

BINDING values of nuclei containing both donor and acceptor molecules did no increase and were comparable to donor only nuclei in our analysis.

AP1 forms homomers in young floral organs

Since photon counts in the *Arabidopsis* experiments were lower compared to experiments in *N. benthamiana* (Additional file 1: Fig. S8), we wondered whether photon counts in *Arabidopsis* were just too low to detect FRET with our fitting model. Because AP1 expression is stronger compared to AP3, PI and SEP3 we tried AP1-mV as the donor, crossed it with our AP1-mCh or PI-mCh reporter line (Additional file 1: Fig. S9) and acquired lifetime images in the F1 progeny. Nuclei expressing PI-mCh as acceptor did no display decreased average donor lifetime and we could not detect significantly increased BINDING values (Additional file 1: Table S2; Fig. 14C–C'; D), comparable to the data we measured for PI-GFP AP1-mCh. In AP1-mV AP1-mCh expressing plants we detected nuclei with significantly increased BINDING slightly above 10% (Fig. 14; Additional file 1: Table S2), indicating homomer formation in these cells. Interestingly, we observed these interactions only in few cells with high protein concentration in young sepals (Fig. 14A–A'; B–B').

Discussion

FRET is a commonly used tool to investigate PPI in vivo. A frequently used technique to measure FRET is time domain FLIM. FLIM generates quantitative data providing information on protein affinities and spatial arrangement of the protein complexes under investigation. However, in the field of plant science, commonly lifetime or average amplitude weighted lifetime has been used to evaluate interactions, leading to the loss of valuable information [7, 10, 17, 18, 45].

Additionally, when evaluating our negative control and donor only samples, we found that for most samples, we could reliably fit an additional lifetime, but with a low relative amplitude. Lifetimes without context of their relative amplitudes should therefore be avoided to evaluate FRET. Instead, the possibility of resolving for BINDING and FRET efficiency from a complex decay behaviour as demonstrated here not only provides more information about complex formation, but also acts as a better measure of the presence of FRET and as an intrinsic control for FRET efficiencies.

Based on the results outlined above, we propose to use BINDING, which is derived from the amplitudes of the decay fractions and FRET efficiency, as a measure for protein affinity and proximity within the forming complexes respectively. This differentiation between BINDING and FRET efficiency to describe

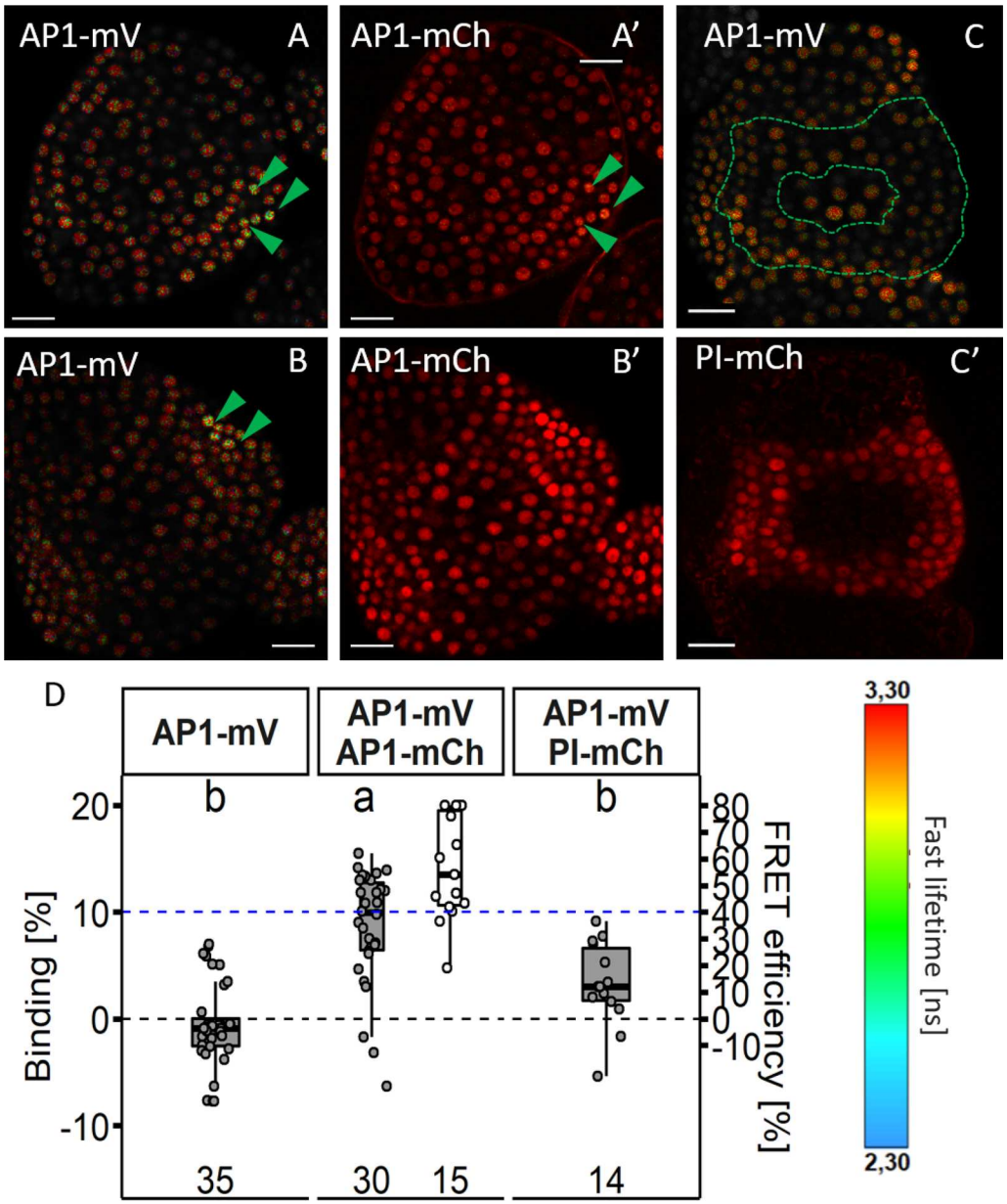

Fig. 14 AP1 homomer formation and no interaction between AP1 and PI. **A**, **B** Fast Lifetime images of AP1-mV in presence of AP1-mCh (depicted in **A**'–**B**', Zoom2). Green arrows highlight nuclei with decreased lifetime. **C** Lifetime images of AP1-mV in presence of PI-mCh (depicted in **C**–**C**', Zoom2). Dashed green line highlights region where AP1 and PI co-localise. No difference in lifetime between nuclei with or without acceptor could be observed. **D** BINDING [%] (grey) and FRET efficiencies [%] (white) for AP1-mV, AP1-mV AP1-mCh and AP1-mV PI-mCh. (Dashed blue line marks the BINDING cut-off of 10%; number of repetitions are indicated in the bottom of the plot). Data points were calculated from a respective FLIM image containing several nuclei (Zoom8 or Zoom2), but only nuclei containing both donor and acceptor were considered in FLIM image analysis of FRET samples. In half the images of AP1-mV AP1-mCh samples increased BINDING above the 10% Cut-off was measured (mean BINDING of 8.59% ± 5.37and mean FRET efficiency of 56.67% ± 19.52), while in the AP1-mV PI-mCh samples no BINDING above the 10% Cut-off could be detected (3.28% ± 3.91). Statistical groups were assigned after multiple comparison with Kruskal–Wallis and a post-hoc test using the criterium Fisher's least significant difference (alpha parameter is 0.01). Scale bars: 40 µm

FRET usually requires donor-only decays with a mono-exponentially decaying behaviour. The OPA method described here is specifically tailored for bi-exponentially decaying donors. It comes as a special script, which can be implemented into SymPhoTime 64 software and can be obtained by PicoQuant on request. Additionally, the underlying model is described in more detail in the methods section, allowing the integration

of OPA in other publicly available FLIM analysis scripts.

By investigating MADS-domain protein interactions as a proof of principle, we showed that OPA can serve to acquire BINDING and FRET efficiencies for bi-exponentially decaying donors. Additionally, OPA was able to determine BINDING to judge the occurrence of FRETin developing flowers, where protein expression levels from the native promoters are low.

In vivo interactions of MADS-domain proteins were previously mainly characterised by BiFC, intensity-based FRET or FLIM-FRET [14, 17, 18, 28, 38, 45]. BiFC and intensity-based methods come with the disadvantage of being prone to false positives. In addition, intensity-based FRET analyses are rather unsuitable for measuring interactions in living meristems or flowers due to the high laser radiation required and the associated photodamage of living tissues and fluorophores. In the FLIM-FRET experiments previously conducted, only lifetimes were used to assess FRET [18, 45]. While average lifetime analysis is a suitable tool to display PPI, it has difficulties to evaluate information of differences in causality for these interactions, as both increased affinity or conformational changes within the forming complexes can result in the reduction of average lifetime. In contrast, OPA can dissolve differences in affinity and protein proximity by separating BINDING and FRET efficiency.

Therefore, we repeated previously reported heterodimeric interactions of AP1 with SEP3 and AP3 with PI *in planta* [18], by also involving corresponding amplitudes of lifetimes, not only giving us additional information about the affinity of the proteins to each other, but also more confident data (Figs. 6, 7). We observed stable homomeric complexes formed by AP1 or SEP3 and stable interaction between AP3/PI (Figs. 5, 6). In line with the idea that homomer formation of AP3 or PI proteins is an ancestral state and the fact that DNA binding of either AP3 or PI requires AP3/PI heteromerization [47], we did not observe stable interaction between AP3/AP3 nor PI/PI (Fig. 8). Interaction of AP1 with AP3 or PI proteins is one of the major interactions proposed by the FQM model but was not yet precisely analysed *in planta.* While average lifetime analysis failed to detect significant FRET between AP3/PI and AP1, OPA revealed low affinity between AP1 and AP3, PI or both (Figs. 9, 11; Additional file 1: Fig. S5). Addition of SEP3 boosted the binding between AP3/PI and AP1 while proximity did not significantly change (Fig. 11, Additional file 1: Fig. S5), suggesting that quaternary complex formation with high affinity between AP1, AP3 and PI relied on the presence of SEP3 protein (Figs. 10, 11), This heavily supports the role of SEP proteins as a "glue" between MADS-domain proteins [18]. Similar to observations made with MADS-domain proteins from lily (*Lilium longiflorum*) [28], mean FRET-efficiencies of stable complexes were usually within the same range (Additional file 1: Table S1, Fig. S6), suggesting comparable proximity between the respective C-termini in the individual complexes.

Because tetramer composition is supposed to be of particular importance for the activity for MADS-domain proteins involved in floral organ specification, approaches which only look at two proteins at a time come to their limit for studying tetramer stoichiometry. The combination of BiFC with FRET-FLIM employed in the present study, is a first step towards reliably analysing binding specifications of the MADS-domain proteins and their tetrameric organization in vivo.

While informative, the characterization of PPIs in heterologous systems or in in vitro assays cannot fully replace an analysis in the cells or tissues in which the proteins under study are normally expressed. We therefore also attempted to assess different floral MADS-domain protein complexes in early-stage *Arabidopsis* flowers. In these experiments, we could not observe heteromeric interactions between AP1, SEP3, AP3 and PI, even though they have been detected by FRET in heterologous systems, or by BiFC and pull-down assays in *Arabidopsis* [18, 38]. It is possible that low endogenous expression levels and/or the presence of competing interaction partners, which are lacking in heterologous systems, could lead to a strong reduction of the FRET fraction, making it more difficult to detect interactions in FLIM assays. Future optimization of FRET set ups, and/or the use of improved spectroscopic methods, will likely be necessary to detect and quantify multimeric MADS-domain protein complex formation in vivo.

Conclusion

By re-assessing MADS-domain protein interactions, we here demonstrate that OPA can be used to extract both protein affinities and spatial information from FRET samples with bi-exponential donor decays in transient expression models like *N. benthamiana* but also in developing flowers of *Arabidopsis*.

While in the past mostly in vitro approaches for the analysis of MADS-domain protein interactions dominated the field, *in planta* approaches will be needed for a better characterization of putative interactions and to distinguish relevant complexes in a developmental context. Although experiments in *Arabidopsis* ultimately display the natural mechanisms of organ specification most accurately, experiments in transient plant systems such as *Arabidopsis* protoplasts or *N. benthamiana* leaf cells, already allow the observation of proteins in a more native environment than in vitro studies.

Transient expression reflects only a small part of the reality in which MADS-domain protein complexes can form. Of greater interest, though, is complex formation in the native environment during flowering. We tried to address this problem, but low expression levels or high donor–acceptor ratios made it difficult to observe any interaction. As FRET-FLIM is considered as a precise technique to quantify protein–protein interaction, our results raise the question whether previous data from BiFC experiments, which are more susceptible to false negative results and ignore transient interactions, can reliably be trusted. With our novel FLIM FRET analysis method we can more precisely dissect interactions to give important insights about protein affinity and complex formation in living tissues.

Supplementary Information

The online version contains supplementary material available at https://doi.org/10.1186/s13007-023-01049-3.

Additional file 1: Fig. S1. FLIM analysis of AP1-mV NLS-mCh and AP1-mV Ap1-mCh in *N. benthamiana* leaf cells. FLIM experiments were performed in *N. benthamiana* leaf epidermis cells. Fusion proteins were expressed from the *UBQ10* promoter and imaged 3–4 days after infiltration. BINDING [%] (grey) and FRET efficiencies [%] (white) for AP1-mV, AP1-mV NLS-mCh and AP1-mV AP1-mCh. Depicted are the same data as in Fig. 1, but FRET efficiencies with BINDING below 10% were not excluded. FRET efficiencies of AP1-mV and AP1mV AP1-mV-NLS-mCh samples have a higher variance compared to the AP1-mV AP1-mCh sample. When the value for BINDING was below 10%, FRET efficiencies showed a higher tendency for values close to the limits of the fitting model (10% and 80% FRET efficiencies). (Dashed blue line marks the BINDING Cut-Off of 10%; Number of repetitions are indicated below BINDING values and number of images with BINDING above 10% are indicated below the FRET efficiency values in the bottom of the plot). **Fig. S2.** Comparison of the One pattern analysis and a mono exponential Donor decay model. BINDING values for AP1-mV samples, fitted with the One pattern analysis or an analysis which assumes a mono exponentially decaying donor model. For the One pattern analysis, three lifetime components were fitted (see methods for details), and for the analysis which assumes a mono exponential decaying donor, two lifetime components were fitted. Due to the influence of the secondary shorter mV lifetime, the analysis assuming a monoexponentially decaying donor results in increased BINDING of more than 10% in almost one third of the images indicating false positive FRET. In contrast, using the One pattern analysis, most acquired BINDING values are below the 10% limit and are less variable. **Fig. S3.** Change in BINDING and FRET efficiency acquired in the same cell before and after acceptor bleaching. FLIM experiments were performed in *N. benthamiana* leaf cells. Fusion proteins were expressed via te *UBQ10* promoter and images were acquired 3 days after infiltration. After the first time series, photobleaching of mCherry was performed with a 561nm laser at 100 % for ninety frames, followed b a second time series. Analysis was done as described in Fig. 2. Binding between AP1-mV and AP1-mCh was not detectable anymore after acceptor bleaching. (Dashed blue line marks the BINDING cut-off of 10%; Number of repetitions are indicated below BINDING values and number of images with BINDING above 10% are indicated below the FRET efficiency values in the bottom of the plot). **Fig. S4.** Dependence of BINDING on acceptor concentration. **B** BINDING values calculated for AP1-mV AP1-mCh, and corresponding photons detected in the acceptor channel. BINDING correlates with the Acceptor concentration. **Fig. S5**. Standard fluorescence lifetime analysis of AP3-mVn PI-mVc samples. Donor only decays were fitted using a monoexponential decay model while decays from donor + acceptor samples were fitted using a biexponential decay model. The non-FRET sample, containing NLS-mCh, shows a significant reduction in fluorescence lifetime compared to the donor only sample (AP3-mVn PI-mVc). In contrast with the OPA, standard lifetime analysis does not reveal interaction between the NLS-mCh containing sample and the AP1-mCh containing sample. Only for the SEP3-mCh and AP1-mCh + SEP3 containing samples a significant reduction in fluorescence lifetime compared to the NLS-mCh containing sample was detectable. Statistical groups were assigned after multiple comparison with Kruskal-Wallis and a Post hoc test using the criterium Fisher's least significant difference (alpha parameter is 0.05) (Number of repetitions are indicated in the bottom of the plot). **Fig. S6.** Average BINDING and FRET efficiencies of all FRET and negative control samples. Interacting samples are labelled in green and non-interacting samples are labelled in magenta. Occurrence of interaction was judged by a significant increase in BINDING based on Kruskal-Wallis and a Post hoc test using the criterium Fisher's least significant difference (alpha parameter is 0.05). Error bars indicate the standard error. **Fig. S7**. MADS-domain protein reporters. Expression pattern of AP1-mT2 in *ap1-1* (**A**), SEP3-GFP (**B**), PI-GFP in *pi-1* (**C**) and AP3-GFP in *ap3-3* (**D**). Expression of AP1 starts in stage 2 floral buds. In stage 3 and stage 4 buds AP1 is braoldy expressed. Expression starts to become restricted to sepals and petal initiation sites stating in stage 5 flowers. Weak expressionin of SEP3 starts in late stage 2 buds. In lates stage buds SEP3 is is mexpressed in cells of the third and fourth whorl. AP3 and PI became visible in early stage 3 florla buds and are expressed in circular pattern in the second and third whorl of stage 4 and stage 5 flowers. In stage 6 flowers expression of AP3 or PI proteins is restricted to developing stamen and peatl initiation sites. Numbers indicate floral stage as previously defined (Smyth, Bowman, and Meyerowitz 1990). (Z-stacks, Scale Bars: 50 µm). **Fig. S8**. Photons in donor channel in different donor only samples. Number of photons was measured in ROIs marking several nuclei in Arabidopsis samples or one nucleus in *N. benthamiana* samples. Nucleoli of *N. benthamiana* nuclei were excluded from analysis. Counts in Arabidopsis GFP reporter lines of AP3, PI and SEP3 were lower compared to counts in the AP1-mV reporter or in *N. benthamiana* samples. **Fig. S9**. Co-expression of AP1 with PI and mutant complementation of *ap1-1* and *pi-1* and. **A**–**A**": Z-stack of AP1-mV signal, AP1-mCh signal and Merged signals respectivly. **B**–**B**": Z-stack of AP1-mV signal, PI-mCh signal and Merged signals respectivly. (Scale Bars: 50 µm). **C**–**F** Inflocrescences of *ap1-1* (**C**–**E**) or *pi-1* (**F**) mutants complemented with AP1-mCh (**C**), AP1-mV (**D**), AP1-mT2 (**E**) and PI-mCh (**F**). Indicated MADS-domain proteins, tagged with FPs, were expressed via their endogenous promoter. All fusion proteins rescued the organ deficient phenotype of the mutants in 4 (*ap1-1*) or 2 (*pi-1*) independent lines. **Table S1.** Summary of the FRET-FLIM measurements for the investigation of MADS-domain protein interactions in *N. benthamiana*. Mean, standard deviation (SD) and standard error (SE) of FRET efficiencies were calculated after removing values with BINDING < 10%. **Table S2.** Summary of the FRET-FLIM measurements for the investigation of MADS-domain protein interactions in *Arabidopsis*. Mean, standard deviation (SD) and standard error (SE) of FRET efficiencies were calculated after removing values with BINDING < 10%. **Table S3.** Plasmids used, but not constructed during this study. **Table S4.** Plasmids used from the GreenGate kit. **Table S5.** "Entry" plasmids generated in this study. The list contains all "entry" plasmids which were used for the construction of plant expression plasmids. Plasmids were cloned by restriction ligation using *BsaI*. Inserts were amplified with the respective primers from the according templates and cloned in the appropriate backbone. **Table S6.** Plant expression plasmids constructed in this study. Plasmids were used for stable *A. thaliana* transformation or transient transformation of *N. benthamiana*. Construction of the plasmids was achieved by the GreenGate method using the appropriate Inserts and assemble them in the respective Backbone. **Table S7.** Oligonucleotides used in this study.

Acknowledgements
We thank Cornelia Gieseler, Silke Winters, and Carin Theres for technical support. We also thank the Center for Advanced imaging (CAi) at HHU, Jenia Schlegel, Patrick Blümke, Grégoire Denay and Elmehdi Bahafid for microscopy support and fruitful discussions.

Author contributions
JEM, FW, SWP, YS and RS designed and planned the experiments. JEM per-formed all experiments. Data analysis was performed by JM, BK, YS, SWP and VIS, FW provided material. JEM, BK and RS wrote the manuscript with input from all authors.

Funding
Open Access funding enabled and organized by Projekt DEAL. RS and SWP were funded by the DFG through CRC1208. JEM and VIS received funding from the DFG.

Availability of data and materials
The datasets used and/or analysed during the current study are available from the corresponding author upon request.

Declarations

Ethics approval and consent to participate
This declaration is not applicable.

Competing interests
Parts of this method described in this manuscript is covered by a German patent application DE10 2021 107 759.1.

Author details
[1]Institute for Developmental Genetics and Cluster of Excellence on Plant Sciences, Heinrich Heine University, Universitätsstraße 1, 40225 Düsseldorf, Germany. [2]PicoQuant GmbH, Rudower Chaussee 29 (IGZ), 12489 Berlin, Germany. [3]Smurfit Institute of Genetics, Trinity College Dublin, Dublin, Ireland. [4]Centre for Advanced Imaging, Heinrich Heine University, Universitätsstraße 1, 40225 Düsseldorf, Germany.

Received: 13 December 2022 Accepted: 4 July 2023
Published online: 28 July 2023

References

1. Borst JW, Hink MA, van Hoek A, Visser AJ. Effects of refractive index and viscosity on fluorescence and anisotropy decays of enhanced cyan and yellow fluorescent proteins. J Fluoresc. 2005;15:153–60.
2. Bucherl CA, Bader A, Westphal AH, Laptenok SP, Borst JW. FRET-FLIM applications in plant systems. Protoplasma. 2014;251:383–94.
3. Clayton AH, Chattopadhyay A. Taking care of bystander FRET in a crowded cell membrane environment. Biophys J. 2014;106:1227–8.
4. Clegg RM, Murchie AIH, Zechel A, Carlberg C, Diekmann S, Lilley DMJ. Fluorescence resonance energy transfer analysis of the structure of the four-way DNA junction. Biochemistry. 1992;31:4846–56.
5. Datta R, Heaster TM, Sharick JT, Gillette AA, Skala MC. Fluorescence lifetime imaging microscopy: fundamentals and advances in instrumentation, analysis, and applications. J Biomed Opt. 2020;25:1–43.
6. de Folter S, Urbanus SL, van Zuijlen LG, Kaufmann K, Angenent GC. Tagging of MADS domain proteins for chromatin immunoprecipitation. BMC Plant Biol. 2007;7:47.
7. Denay G, Schultz P, Hansch S, Weidtkamp-Peters S, Simon R. Over the rainbow: a practical guide for fluorescent protein selection in plant FRET experiments. Plant Direct. 2019;3:e00189. https://www.mdpi.com/about/announcements/784
8. Favaro R, Pinyopich A, Battaglia R, Kooiker M, Borghi L, Ditta G, Yanofsky MF, Kater MM, Colombo L. MADS-box protein complexes control carpel and ovule development in *Arabidopsis*. Plant Cell. 2003;15:2603–11.
9. Förster Th. Zwischenmolekulare energiewanderung und fluoreszenz. Ann Phys. 1948;437:55–75.
10. Glockner N, Zur Oven-Krockhaus S, Rohr L, Wackenhut F, Burmeister M, Wanke F, Holzwart E, Meixner AJ, Wolf S, Harter K. Three-fluorophore FRET enables the analysis of ternary protein association in living plant cells. Plants. 2022;11:2630. https://authorservices.wiley.com/asset/photos/eLocators_text_for_author_site.pdf
11. Godet J, Mely Y. Exploring protein-protein interactions with large differences in protein expression levels using FLIM-FRET. Methods Appl Fluoresc. 2019;8:014007.
12. Honma T, Goto K. Complexes of MADS-box proteins are sufficient to convert leaves into floral organs. Nature. 2001;409:525–9.
13. Horstman A, Tonaco IA, Boutilier K, Immink RG. A cautionary note on the use of split-YFP/BiFC in plant protein-protein interaction studies. Int J Mol Sci. 2014;15:9628–43.
14. Hsu WH, Yeh TJ, Huang KY, Li JY, Chen HY, Yang CH. AGAMOUS-LIKE13, a putative ancestor for the E functional genes, specifies male and female gametophyte morphogenesis. Plant J. 2014;77:1–15.
15. Hu CD, Chinenov Y, Kerppola TK. Visualization of interactions among bZIP and Rel family proteins in living cells using bimolecular fluorescence complementation. Mol Cell. 2002;9:789–98.
16. Hugouvieux V, Silva CS, Jourdain A, Stigliani A, Charras Q, Conn V, Conn SJ, Carles CC, Parcy F, Zubieta C. Tetramerization of MADS family transcription factors SEPALLATA3 and AGAMOUS is required for floral meristem determinacy in *Arabidopsis*. Nucleic Acids Res. 2018;46:4966–77.
17. Immink RG, Gadella TW Jr, Ferrario S, Busscher M, Angenent GC. Analysis of MADS box protein-protein interactions in living plant cells. Proc Natl Acad Sci USA. 2002;99:2416–21.
18. Immink RG, Tonaco IA, de Folter S, Shchennikova A, van Dijk AD, Busscher-Lange J, Borst JW, Angenent GC. SEPALLATA3: the 'glue' for MADS box transcription factor complex formation. Genome Biol. 2009;10:R24.
19. Johannes SI, Erwin A-C, Verena F, Mark K, Tobias L, Stephan P, Curtis P, Stephan R, Benjamin S, Jean-Yves S, James TD, Volker W, Kevin H, Pavel E, Tomancak Albert C. Fiji: an open-source platform for biological-image analysis. Nature Methods 2012;9(7):676–82. https://doi.org/10.1038/nmeth.2019
20. Kaufmann K, Anfang N, Saedler H, Theissen G. Mutant analysis, protein-protein interactions and subcellular localization of the *Arabidopsis* B sister (ABS) protein. Mol Genet Genom. 2005;274:103–18.
21. Kaufmann K, Muino JM, Jauregui R, Airoldi CA, Smaczniak C, Krajewski P, Angenent GC. Target genes of the MADS transcription factor SEPALLATA3: integration of developmental and hormonal pathways in the *Arabidopsis* flower. PLoS Biol. 2009;7:e1000090.
22. Kaufmann K, Pajoro A, Angenent GC. Regulation of transcription in plants: mechanisms controlling developmental switches. Nat Rev Genet. 2010;11:830–42.
23. Kaufmann K, Wellmer F, Muino JM, Ferrier T, Wuest SE, Kumar V, Serrano-Mislata A, Madueno F, Krajewski P, Meyerowitz EM, Angenent GC, Riechmann JL. Orchestration of floral initiation by APETALA1. Science. 2010;328:85–9.
24. King C, Sarabipour S, Byrne P, Leahy DJ, Hristova K. The FRET signatures of noninteracting proteins in membranes: simulations and experiments. Biophys J. 2014;106:1309–17.
25. Lampropoulos A, Sutikovic Z, Wenzl C, Maegele I, Lohmann JU, Forner J. GreenGate—a novel, versatile, and efficient cloning system for plant transgenesis. PLoS ONE. 2013;8:e83043.
26. Long Y, Stahl Y, Weidtkamp-Peters S, Postma M, Zhou W, Goedhart J, Sanchez-Perez MI, Gadella TWJ, Simon R, Scheres B, Blilou I. In vivo FRET-FLIM reveals cell-type-specific protein interactions in *Arabidopsis* roots. Nature. 2017;548:97–102.
27. Long Y, Stahl Y, Weidtkamp-Peters S, Smet W, Du Y, Gadella TWJ Jr, Goedhart J, Scheres B, Blilou I. Optimizing FRET-FLIM Labeling conditions to detect nuclear protein interactions at native expression levels in living *Arabidopsis* roots. Front Plant Sci. 2018;9:639.
28. Mao WT, Hsu WH, Li JY, Yang CH. Distance-based measurement determines the coexistence of B protein hetero- and homodimers in lily tepal and stamen tetrameric complexes. Plant J. 2021;105:1357–73.
29. McGonigle B, Bouhidel K, Irish VF. Nuclear localization of the *Arabidopsis* APETALA3 and PISTILLATA homeotic gene products depends on their simultaneous expression. Genes Dev. 1996;10:1812–21.
30. Orthaus S, Buschmann V, Bülter A, Fore S, König M, Erdmann R. Quantitative in vivo imaging of molecular distances using FLIM-FRET. 2009. https://www.picoquant.com/scientific/technical-and-application notes/category/technical_notes_techniques_and_methods/P8, https://www.picoquant.com/images/uploads/page/files/7267/appnote_flim_fret.pdf

31. Piston DW, Kremers GJ. Fluorescent protein FRET: the good, the bad and the ugly. Trends Biochem Sci. 2007;32:407–14.
32. Prunet N, Yang W, Das P, Meyerowitz EM, Jack TP. SUPERMAN prevents class B gene expression and promotes stem cell termination in the fourth whorl of *Arabidopsis thaliana* flowers. Proc Natl Acad Sci USA. 2017;114:7166–71.
33. Puranik S, Acajjaoui S, Conn S, Costa L, Conn V, Vial A, Marcellin R, Melzer R, Brown E, Hart D, Theissen G, Silva CS, Parcy F, Dumas R, Nanao M, Zubieta C. Structural basis for the oligomerization of the MADS domain transcription factor SEPALLATA3 in *Arabidopsis*. Plant Cell. 2014;26:3603–15.
34. Riechmann JL, Wang M, Meyerowitz EM. 'DNA-binding properties of Arabidopsis MADS domain homeotic proteins APETALA1, APETALA3, PISTILLATA and AGAMOUS. Nucl Acids Res. 1996;24:3134–41.
35. Russinova E, Borst JW, Kwaaitaal M, Cano-Delgado A, Yin Y, Chory J, de Vries SC. Heterodimerization and endocytosis of Arabidopsis brassinosteroid receptors BRI1 and AtSERK3 (BAK1). Plant Cell. 2004;16:3216–29.
36. Sarkar P, Koushik SV, Vogel SS, Gryczynski I, Gryczynski Z. Photophysical properties of Cerulean and Venus fluorescent proteins. J Biomed Opt. 2009;14:034047.
37. Shyu YJ, Hu CD. Fluorescence complementation: an emerging tool for biological research. Trends Biotechnol. 2008;26:622–30.
38. Smaczniak C, Immink RGH, Muino JM, Blanvillain R, Busscher M, Busscher-Lange J, Dinh QD, Liu SJ, Westphal AH, Boeren S, Parcy F, Xu L, Carles CC, Angenent GC, Kaufmann K. Characterization of MADS-domain transcription factor complexes in *Arabidopsis* flower development. Proc Natl Acad Sci USA. 2012;109:1560–5.
39. Spatola Rossi T, Pain C, Botchway SW, Kriechbaumer V. FRET-FLIM to determine protein interactions and membrane topology of enzyme complexes. Curr Protoc. 2022;2:e598.
40. Stahl Y, Grabowski S, Bleckmann A, Kuhnemuth R, Weidtkamp-Peters S, Pinto KG, Kirschner GK, Schmid JB, Wink RH, Hulsewede A, Felekyan S, Seidel CA, Simon R. Moderation of Arabidopsis root stemness by CLAVATA1 and ARABIDOPSIS CRINKLY4 receptor kinase complexes. Curr Biol. 2013;23:362–71.
41. Strotmann VI, Stahl Y. Visualisation of in vivo protein-protein interactions. J Exp Bot. 2022. https://doi.org/10.1093/jxb/erac139.
42. Suhling K, Siegel J, Phillips D, French PM, Leveque-Fort S, Webb SE, Davis DM. Imaging the environment of green fluorescent protein. Biophys J. 2002;83:3589–95.
43. Theissen G, Melzer R, Rumpler F. MADS-domain transcription factors and the floral quartet model of flower development: linking plant development and evolution. Development. 2016;143:3259–71.
44. Theissen G, Saedler H. Plant biology —floral quartets. Nature. 2001;409:469–71.
45. Tonaco IA, Borst JW, de Vries SC, Angenent GC, Immink RG. In vivo imaging of MADS-box transcription factor interactions. J Exp Bot. 2006;57:33–42.
46. Urbanus SL, Martinelli AP, Dinh QD, Aizza LC, Dornelas MC, Angenent GC, Immink RG. Intercellular transport of epidermis-expressed MADS domain transcription factors and their effect on plant morphology and floral transition. Plant J. 2010;63:60–72.
47. Winter KU, Weiser C, Kaufmann K, Bohne A, Kirchner C, Kanno A, Saedler H, Theissen G. Evolution of class B floral homeotic proteins: obligate heterodimerization originated from homodimerization. Mol Biol Evol. 2002;19:587–96.
48. Wuest SE, O'Maoileidigh DS, Rae L, Kwasniewska K, Raganelli A, Hanczaryk K, Lohan AJ, Loftus B, Graciet E, Wellmer F. Molecular basis for the specification of floral organs by APETALA3 and PISTILLATA. Proc Natl Acad Sci USA. 2012;109:13452–7.
49. Yang Y, Jack T. Defining subdomains of the K domain important for protein-protein interactions of plant MADS proteins. Plant Mol Biol. 2004;55:45–59.
50. Zeug A, Woehler A, Neher E, Ponimaskin EG. Quantitative intensity-based FRET approaches—a comparative snapshot. Biophys J. 2012;103:1821–7.
51. Zhang X, Henriques R, Lin SS, Niu QW, Chua NH. Agrobacterium-mediated transformation of *Arabidopsis thaliana* using the floral dip method. Nat Protoc. 2006;1:641–6.

Publisher's Note

Chapter 5

PLETHORA-WOX5 interaction and subcellular localization control Arabidopsis root stem cell maintenance

This manuscript was published in *EMBO reports* in March 2022.

https://doi.org/10.15252/embr.202154105

Authors

Rebecca C. Burkart[1], Vivien I. Strotmann[1], Gwendolyn K. Kirschner[1,†], Abdullah Akinci[1], Laura Cempik[1,‡], Anika Dolata[1], Alexis Maizel[2], Stefanie Weidtkamp-Peters[3] and Yvonne Stahl[1]*

Affiliation

[1]Institute for Developmental Genetics, Heinrich-Heine-University, Düsseldorf, Germany

[2]Center for Organismal Studies (COS), University of Heidelberg, Heidelberg, Germany

[3]Center for Advanced Imaging, Heinrich-Heine-University, Düsseldorf, Germany

†Present address: Biological and Environmental Sciences and Engineering (BESE), King Abdullah University of Science and Technology (KAUST), Thuwal, Saudi Arabia

‡Present address: Molecular Plant Science/Plant Biochemistry, University Wuppertal, Wuppertal, Germany

*corresponding author

Author contribution

I contributed to this publication by performing qPCR and the imaging *PLT3* expression upon WOX5 induction *in planta*, supporting their mutual regulation in the root stem cell niche. Furthermore, I conducted replicates of other experiments shown in this publication and generated plasmids as well as transgenic *Arabidopsis* lines.

Article

SOURCE DATA | TRANSPARENT PROCESS | OPEN ACCESS

EMBO reports

PLETHORA-WOX5 interaction and subnuclear localization control *Arabidopsis* root stem cell maintenance

Rebecca C Burkart[1], Vivien I Strotmann[1], Gwendolyn K Kirschner[1,†], Abdullah Akinci[1], Laura Czempik[1,‡], Anika Dolata[1], Alexis Maizel[2], Stefanie Weidtkamp-Peters[3] & Yvonne Stahl[1,*]

Abstract

Maintenance and homeostasis of the stem cell niche (SCN) in the *Arabidopsis* root is essential for growth and development of all root cell types. The SCN is organized around a quiescent center (QC) maintaining the stemness of cells in direct contact. The key transcription factors (TFs) WUSCHEL-RELATED HOMEOBOX 5 (WOX5) and PLETHORAs (PLTs) are expressed in the SCN where they maintain the QC and regulate distal columella stem cell (CSC) fate. Here, we describe the concerted mutual regulation of the key TFs WOX5 and PLTs on a transcriptional and protein interaction level. Additionally, by applying a novel SCN staining method, we demonstrate that both WOX5 and PLTs regulate root SCN homeostasis as they control QC quiescence and CSC fate interdependently. Moreover, we uncover that some PLTs, especially PLT3, contain intrinsically disordered prion-like domains (PrDs) that are necessary for complex formation with WOX5 and its recruitment to subnuclear microdomains/nuclear bodies (NBs) in the CSCs. We propose that this partitioning of PLT-WOX5 complexes to NBs, possibly by phase separation, is important for CSC fate determination.

Keywords differentiation; nuclear bodies; prion-like domains; root stem cells; transcription factor complexes

Subject Categories Chromatin, Transcription & Genomics; Plant Biology; Stem Cells & Regenerative Medicine

DOI 10.15252/embr.202154105 | Received 5 October 2021 | Revised 17 March 2022 | Accepted 18 March 2022

EMBO Reports (2022) e54105

Introduction

The root system of higher plants is essential for plant life, as it provides anchorage in the soil and access to nutrients and water. It arises from a population of long-lasting stem cells residing in a structure called root apical meristem (RAM) at the tip of the root. Within the *Arabidopsis thaliana* RAM, the stem cell niche (SCN) consists of on average four to eight slowly dividing cells, the QC cells, which act as a long-term reservoir and signaling center by maintaining the surrounding shorter-lived, proliferating stem cells (also called initials) in a non-cell autonomous manner (van den Berg *et al*, 1997; Lu *et al*, 2021). These stem cells continuously divide asymmetrically, thereby generating new stem cells that are still in contact with the QC. The hereby-produced daughter cells frequently undergo cell divisions and are shifted further away from the QC to finally differentiate into distinct cell fates. By this mechanism, the position of the stem cells in the root remains the same throughout development and their precise orientation of division leads to the formation of concentrically organized clonal cell lineages representing a spatio-temporal developmental gradient (Dolan *et al*, 1993; van den Berg *et al*, 1997; Benfey & Scheres, 2000). From the inside to the outside, the following root cell tissues develop: vasculature, pericycle, endodermis, cortex, and epidermis plus columella and lateral root cap at the distal root tip (Fig 1A).

The necessary longevity and continuous activity of the RAM can only be achieved if its stem cell pool is constantly replenished, since cells are frequently leaving the meristematic region due to continuous cell divisions. Therefore, complex regulatory mechanisms involving phytohormones and key TFs regulate stem cell maintenance and the necessary supply of differentiating descendants (Drisch & Stahl, 2015). Here, the APETALA2-type PLT TF family and the homeodomain TF WOX5 play important roles (Aida *et al*, 2004; Sarkar *et al*, 2007). WOX5 is expressed mainly in the QC, but maintains the surrounding stem cells non-cell-autonomously by repressing their differentiation (Sarkar *et al*, 2007; Pi *et al*, 2015). Loss of WOX5 causes the differentiation of the CSCs, also called distal stem cells, into starch-accumulating columella cells (CCs), while increased WOX5 expression causes CSC over-proliferation. Hence, WOX5 abundance is critical and necessary to suppress premature CSC differentiation (Sarkar *et al*, 2007; Pi *et al*, 2015). WOX5 also represses QC divisions, maintaining the quiescence of the QC by repressing CYCLIN D (CYCD) activity within the QC (Forzani *et al*, 2014).

1 Institute for Developmental Genetics, Heinrich-Heine University, Düsseldorf, Germany
2 Center for Organismal Studies (COS), University of Heidelberg, Heidelberg, Germany
3 Center for Advanced Imaging, Heinrich-Heine University, Düsseldorf, Germany
*Corresponding author. Tel: +49 211 81 15809; E-mail: yvonne.stahl@hhu.de
†Present address: Biological and Environmental Sciences and Engineering (BESE), King Abdullah University of Science and Technology (KAUST), Thuwal, Saudi Arabia
‡Present address: Molecular Plant Science/Plant Biochemistry, University of Wuppertal, Wuppertal, Germany

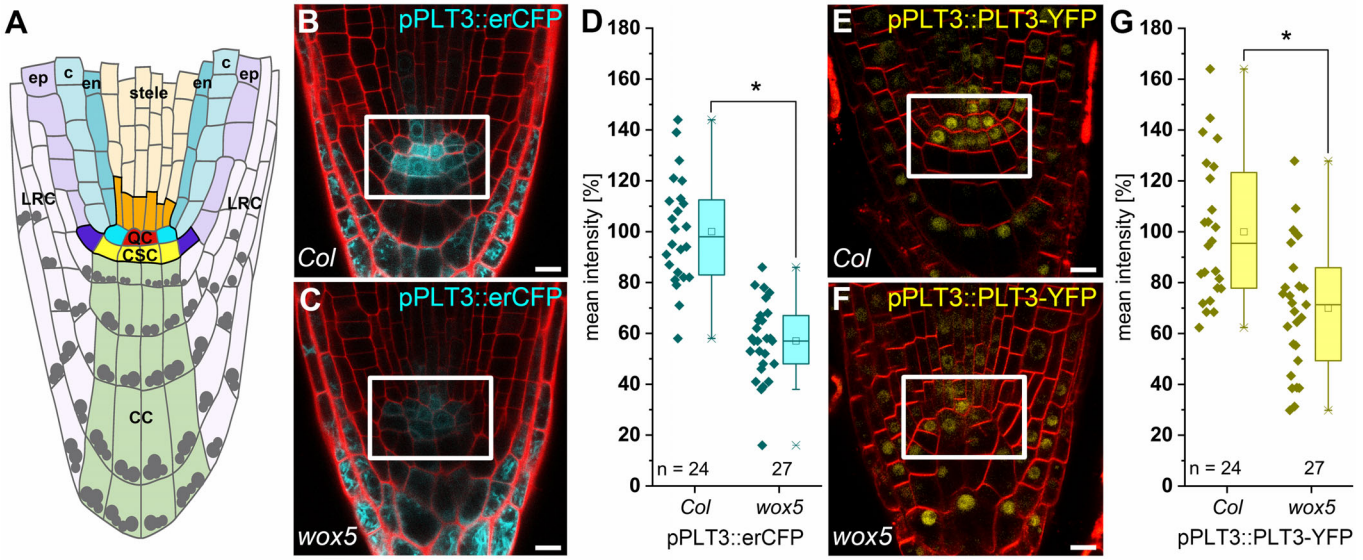

Figure 1. WOX5 positively regulates *PLT3* expression.

A Schematic representation of the *Arabidopsis* root meristem. The QC cells (red) maintain the surrounding stem cells (initials) outlined in black together building the root stem cell niche (SCN). The different cell types are color coded. QC = quiescent center (red); CSC = columella stem cells (yellow); CC = columella cells (green); LRC = lateral root cap (light purple); ep = epidermis (purple); c = cortex (light turquoise); en = endodermis (dark turquoise); bright turquoise = cortex/endodermis initials; dark purple = epidermis/lateral root cap initials; dark orange = stele initials; stele = light orange; grey dots = starch granules.

B, C Representative images of pPLT3::erCFP (cyan) expressing and PI-stained (red) *Arabidopsis* roots in *Col* or *wox5* background, respectively.

D Mean fluorescence intensities of the pPLT3::erCFP roots summarized in box and scatter plots. The mean fluorescence intensity of the CFP signal in *Col* roots was to set to 100%.

E, F Representative images of pPLT3::PLT3-YFP (yellow) expressing and FM4-64-stained (red) *Arabidopsis* roots in *Col* or *wox5* mutant background, respectively.

G Mean fluorescence intensities of the pPLT3::PLT3-YFP expressing roots summarized in box and scatter plots. The mean fluorescence intensity of the YFP signal in *Col* roots was to set to 100%.

Data information: (D, G) Box = 25–75% of percentile, whisker = 1.5 interquartile range, — = median, □ = mean value, X = minimum/maximum. The data were statistically analyzed by one-way ANOVA and Holm–Sidak *post-hoc* multiple comparisons test. Asterisks indicate statistically significant differences ($\alpha = 0.01$). Number of analyzed roots (*n*) (biological replicates) is indicated for each genotype and results from two technical replicates. (B, C, E, F) Scale bars represent 10 μm. SCN = stem cell niche; PI = propidium iodide; YFP = yellow fluorescent protein; CFP = cyan fluorescent protein.

The auxin-induced PLTs form a clade of six TFs and act as master regulators of root development, as multiple *plt* mutants fail to develop functional RAMs (Aida *et al*, 2004; Galinha *et al*, 2007; Mähönen *et al*, 2014). PLT1, 2, 3, and 4 are expressed mainly in and around the QC and form an instructive gradient, which is required for maintaining the balance of stem cell fate and differentiation. This PLT gradient is also necessary for separating auxin responses in the SCN, for the correct positioning of the QC, and the expression of QC markers (Aida *et al*, 2004; Galinha *et al*, 2007; Mähönen *et al*, 2014). Genetically, WOX5 and PLT1 were shown to play an interconnected role in auxin-regulated CSC fate, whereas PLT1 and PLT3 were found to directly positively regulate WOX5 expression (Ding & Friml, 2010; Shimotohno *et al*, 2018).

Although PLTs and WOX5 are known for controlling stem cell regulation and maintenance in the *Arabidopsis* RAM and genetic evidence for cross regulation exists, the underlying molecular mechanisms are until now largely elusive. Here, we show for the first time that the mutual regulation of expression, but importantly also the ability of PLTs to directly interact with and recruit WOX5 to NBs in CSCs controls stem cell homeostasis in the *Arabidopsis* RAM. NBs are membrane-less, self-assembling protein/RNA containing compartments thought to regulate a variety of physiological responses to differential environmental cues like light, temperature, or osmotic changes (Mao *et al*, 2011; Jung *et al*, 2020; Meyer, 2020). Therefore, we propose a model in which differential PLT/WOX5 complexes depending on their subnuclear localization in NBs or in the nucleoplasm regulate stem cell fate in the RAM, possibly by phase separation.

Results

WOX and PLTs regulate each other's expression in the root SCN

WOX5 and PLTs are essential players in distal stem cell maintenance (Aida *et al*, 2004; Galinha *et al*, 2007; Sarkar *et al*, 2007; Pi *et al*, 2015). This, as well as their overlapping expression and protein localization domains in the root SCN raised the question if they could act together in distal stem cell regulation, where, in comparison to all the other PLTs, particularly PLT3 is highly expressed (Fig 1B) (Galinha *et al*, 2007). Furthermore, PLT3 was recently predicted as one of the central nodes regulating other QC-enriched TFs in the underlying gene regulatory network (GRN) within the *Arabidopsis* root SCN. In contrast, PLT1 and PLT2 were predicted as minor nodes only and PLT4 (BBM) was not predicted as a node (de Luis Balaguer *et al*, 2017).

First, we tested if WOX5 influences *PLT3* expression. Both a transcriptional and translational PLT3 fluorescent reporter line showed a reduced expression in the QC and CSC in a *wox5* mutant background to around 57–70% compared to the *Col-0* (*Col*) wild-type roots (Fig 1B–G, Appendix Table S3). Next, we addressed, if *PLT3* expression is regulated directly or indirectly upon WOX5 induction by using the published *Arabidopsis* lines 35S::WOX5-GR (Sarkar *et al*, 2007) and 35S::WOX5-GFP-GR (Berckmans *et al*, 2020) in quantitative PCR experiments (qPCR) (Appendix Fig S1A, Appendix Table S1) and crosses with pPLT3::erCFP (Galinha *et al*, 2007) (Appendix Fig S1B–E, Appendix Table S2), respectively. In both independent experiments, we found no change of *PLT3* expression 4 h after WOX5 induction. After 21 h of WOX5 induction, we found *PLT3* expression significantly upregulated up to two-fold and therefore, we conclude that *PLT3* expression is not directly regulated by WOX5 (Appendix Fig S1B–E, Appendix Table S2). This extends the previously reported regulation of *PLT1* expression by WOX5 (Ding & Friml, 2010) and shows that WOX5 positively regulates expression of several *PLTs*, albeit in an indirect manner. To test if *WOX5* expression also depends on PLTs, we produced a transcriptional reporter, which expresses a nuclear-localized mVenus under control of the *WOX5* promoter. In agreement with previous reports, expression of *WOX5* in our transcriptional reporter line is confined to the QC and is only weakly expressed in the stele initials (Sarkar *et al*, 2007; Pi *et al*, 2015) (Fig 2A).

PLTs are known for their redundant function in SCN maintenance, that can be very strong especially when PLT1 is mutated in combination with other PLTs (Aida *et al*, 2004; Galinha *et al*, 2007). Because we aimed to look at the rather subtle QC and distal SCN phenotypes, we therefore included only *plt2* mutants for our analyses. In *plt2* and *plt3* single mutants, we observed additional mVenus-expressing cells in the QC region, which may derive from aberrant periclinal cell divisions of the QC (Fig 2B and C, Appendix Table S4). This effect is even stronger in the *plt2, plt3* double mutant roots, where extra cells are found in all observed roots and often even form an additional cell layer of *WOX5* expressing cells (Fig 2D).

Previously, it was reported that the *Arabidopsis* wild-type QC is composed of four to eight cells with a low division rate (Truernit *et al*, 2008; Cruz-Ramírez *et al*, 2013; Stahl *et al*, 2013; Lu *et al*, 2021). We quantified the number of *WOX5* expressing cells and the area of *WOX5* expression per root by acquiring transverse optical sections through the roots. We observed four to ten *WOX5* expressing cells in the *Col* wild type (Fig 2E and G, Appendix Table S4), whereas we found eight to 14 *WOX5* expressing cells and a laterally expanded *WOX5* expression domain in the *plt2, plt3* double mutants (Fig 2F–H, Appendix Table S4). Taken together, our data show that WOX5 positively regulates *PLT* expression, here shown for PLT3, whereas PLT2 and PLT3 redundantly restrict *WOX5* expression to a limited number of cells at QC position, possibly by negative feedback regulation. These observations are in agreement with a previous report, where a role for PLT1 and PLT2 in confining *WOX5* expression was reported (Sarkar *et al*, 2007).

A novel SCN staining method for simultaneous QC division and CSC differentiation analyses

QC cells rarely divide as they provide a long-term reservoir to maintain the surrounding stem cells (Cruz-Ramírez *et al*, 2013; Vilarrasa-Blasi *et al*, 2014). As WOX5 and PLTs control QC cell divisions and CSC maintenance (Aida *et al*, 2004; Galinha *et al*, 2007; Sarkar *et al*, 2007; Forzani *et al*, 2014; Mähönen *et al*, 2014; Pi *et al*, 2015), we asked if these two aspects are interdependent. Therefore, we analyzed the cell division rates in the QC and the CSC phenotypes in wild-type and mutant roots. To assess these two phenotypes and to probe for their interdependency, we needed to measure the number of dividing QC cells and CSC layers within the same root simultaneously. To enable this, we established a novel staining method, named SCN staining, by combining the 5-ethynyl-2′-deoxyuridine (EdU) and modified pseudo Schiff base propidium iodide (mPS-PI) stainings to simultaneously visualize cell divisions, starch granule distribution as well as cell walls within the same root (Truernit *et al*, 2008; Cruz-Ramírez *et al*, 2013). Applying this new staining combination, potential correlations between QC-divisions and CSC cell fates can be uncovered. The EdU-staining is used to analyze QC-divisions by staining nuclei that have gone through the S-phase, detecting cells directly before, during, and after cell division (Cruz-Ramírez *et al*, 2013). However, cell layers and different cell types are hard to distinguish using only EdU staining due to the lack of cell wall staining. Therefore, we additionally applied the mPS-PI-method to stain cell walls and starch which is commonly used for CC and CSC cell fate determination (Truernit *et al*, 2008; Stahl *et al*, 2009, 2013). CCs are differentiated, starch granule-containing cells in the distal part of the root mediating gravity perception. They derive from the CSCs that form one or, directly after cell division, two cell layers distal to the QC. The CSCs lack big starch granules and can thereby easily be distinguished from the differentiated CCs by mPS-PI staining (Truernit *et al*, 2008; Stahl *et al*, 2009, 2013) (see Fig 3A, B and I, Appendix Table S5).

QC division rate and CSC differentiation correlate in the root SCN

WOX5 was shown to be necessary for CSC maintenance, as loss of WOX5 causes their differentiation, while inducible overexpression of WOX5 leads to enhanced proliferation (Sarkar *et al*, 2007; Pi *et al*, 2015; Berckmans *et al*, 2020; Savina *et al*, 2020). In agreement with this, we found that the *wox5* mutants lack a starch-free cell layer in 78% of analyzed roots, indicating differentiation of the CSCs, compared to 17% in *Col* (Fig 3A, B, F and I, Appendix Table S5). In the *plt2* and *plt3* single mutants, the frequency of roots lacking a CSC layer increases to above 30% (36 and 32%, respectively), and in the *plt2, plt3* double mutant to 41% (see Fig 3C–E and I, Appendix Table S5). After overexpression of PLT3-mV by estradiol induction in wild-type *Col-0* background, we observed the opposite effect, an increase from 29 to 50% of two CSC layers (see Appendix Fig S2A–F). Therefore, we argue, that the observed CSC phenotypes are due to PLT3 function and are not caused by potential early embryonic defects described previously for multiple *plt* mutants (Aida *et al*, 2004).

Interestingly, the *wox5, plt3* double mutant as well as the *wox5, plt2, plt3* triple mutant show a frequency of differentiated CSCs comparable to the *wox5* single mutant (71 and 77%, respectively) (Fig 3G–I, Appendix Table S5). This data suggests that PLTs and WOX5 may act together in the same pathway to maintain CSC homeostasis, as there is no additive effect observable in the multiple mutant roots.

To analyze QC division phenotypes in detail, we quantified the number of EdU-stained cells in QC position in transversal optical

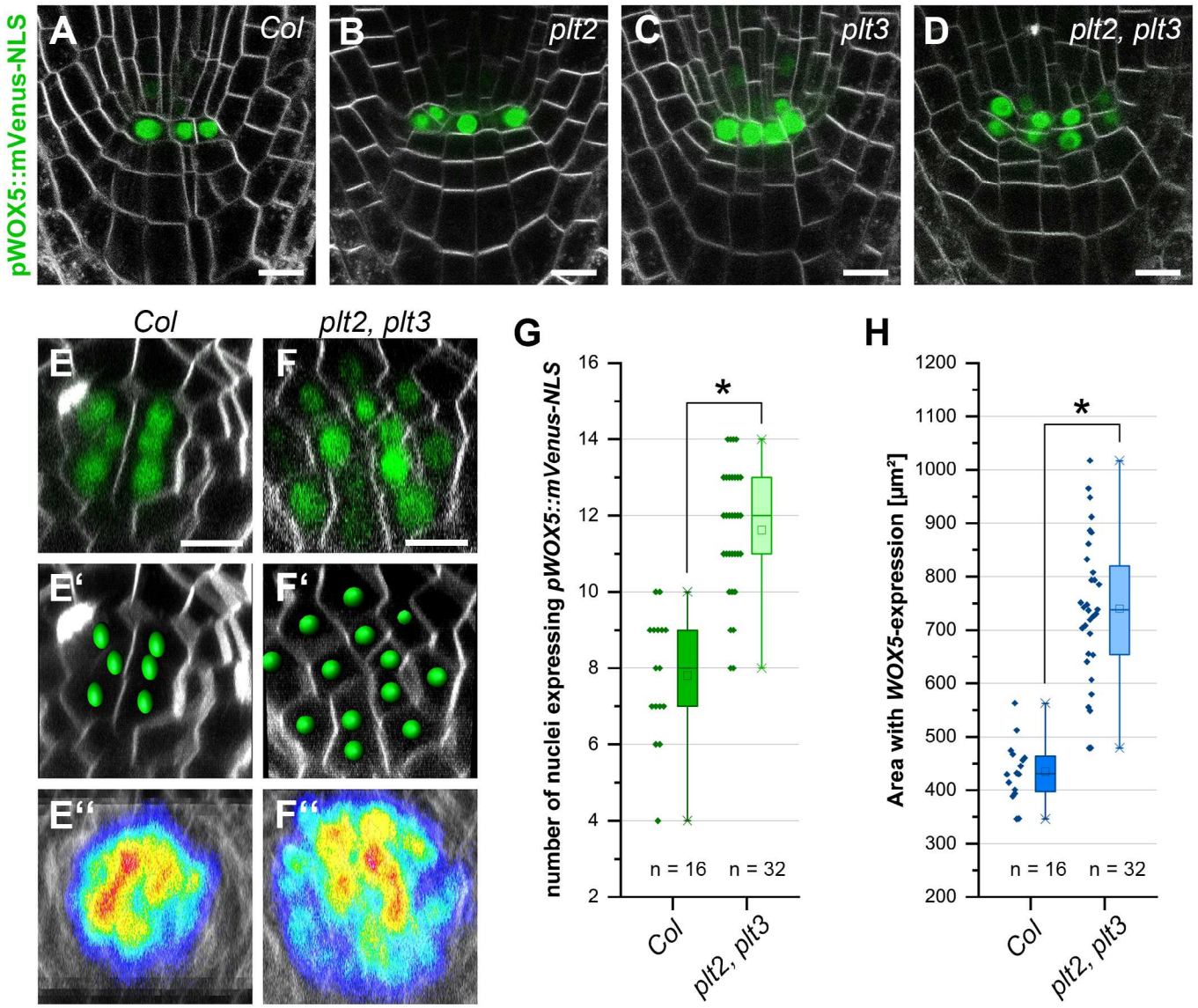

Figure 2. PLTs constrain the *WOX5* expression domain.

A–F Representative FM4-64-stained *Arabidopsis* roots (grey) expressing pWOX5::mVenus-NLS (green) in *Col*, *plt2*, *plt3*, and *plt2, plt3* double mutant background in longitudinal (A-D), or transversal (E-F) optical sections. (E′, F′) Analysis of representative images in (E) and (F) in Imaris to detect and count individual expressing nuclei. (E″, F″) Overlay of 10 roots (biological replicates) showing the area of detected fluorescence (high levels in red, low levels in blue) in *Col* and *plt2, plt3* double mutant roots.

G Number of nuclei (biological replicates) expressing pWOX5::mVenus-NLS in *Col* and *plt2, plt3* double mutant roots summarized in box and scatter plots.

H Area of WOX5 expression in μm^2 in *Col* and *plt2, plt3* double mutant roots summarized in box and scatter plots.

Data information: (G, H) Box = 25-75% of percentile, whisker = 1.5 interquartile range, – = median, □ = mean value, X = minimum/maximum. (G, H) Kruskal–Wallis ANOVA with subsequent Dunn's test (G) or one-way ANOVA and *post-hoc* Holm–Sidak multiple comparisons test was used to test for statistical significance (H). Asterisks indicate statistically significant differences ($\alpha = 0.01$). Number of analyzed roots (*n*) (biological replicates) is indicated for each genotype and results from three technical replicates per genotype. Scale bars represent 10 µm; NLS = nuclear localization signal.

sections. QC cells were identified by their position within the root SCN, as they are located directly distal to the stele initials and surrounded by the CEIs in a circular arrangement (Fig 3A and J). In *Col*, 27% of the analyzed roots show at least one cell division in the QC within the 24 h staining window (Fig 3J, K and R, Appendix Table S5), which is consistent with already published frequencies (Cruz-Ramírez *et al*, 2013). This frequency almost doubles to 45–50% in the *plt2* and *plt3* single mutants and is even higher in the *plt2, plt3* double mutant (57%) (Fig 3L–N and R, Appendix Table S5). Additionally, the *plt* double mutant roots often show disordered QC regions with a disruption of the circular arrangement of cells surrounding the QC (Fig 3N) which could be a result of uncontrolled divisions. *wox5* mutants show a disordered SCN accompanied by a high overall QC cell division frequency of at least one

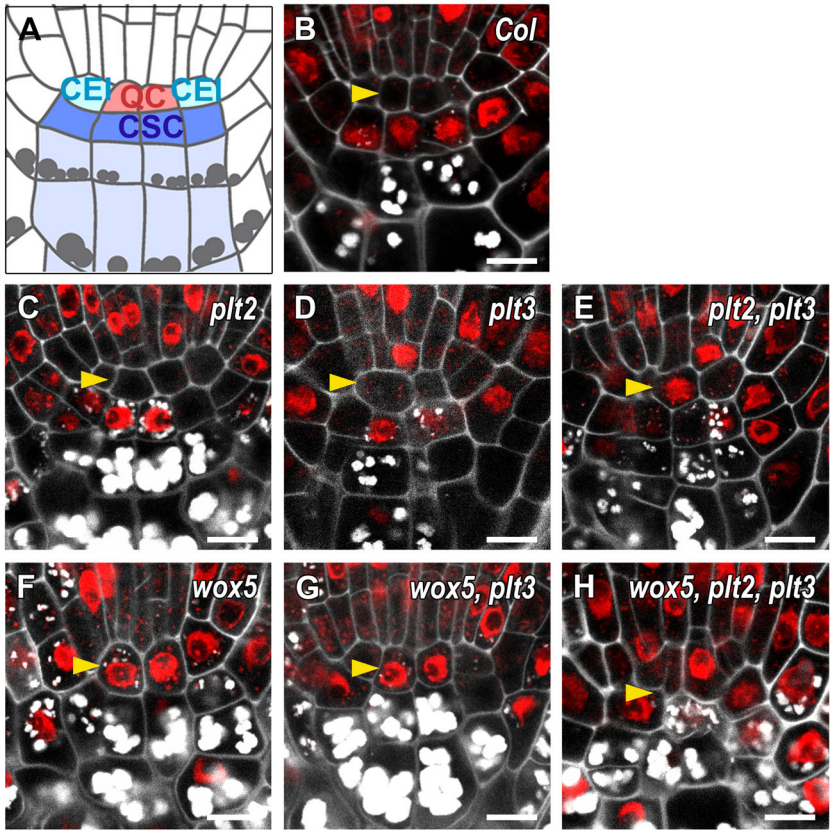

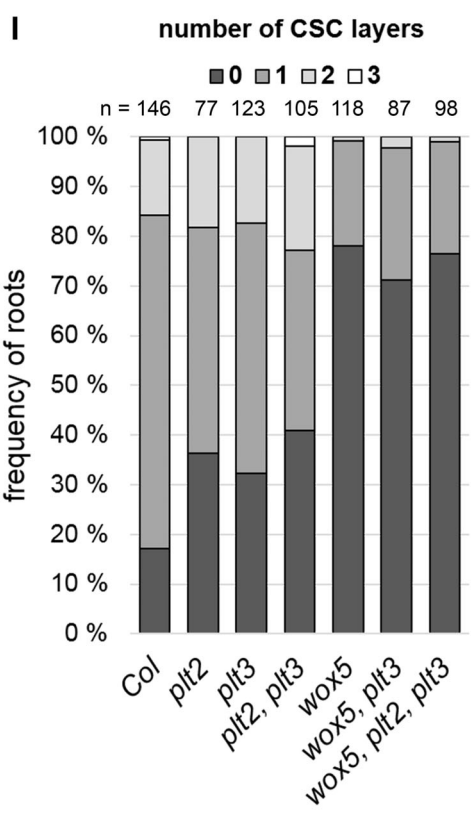

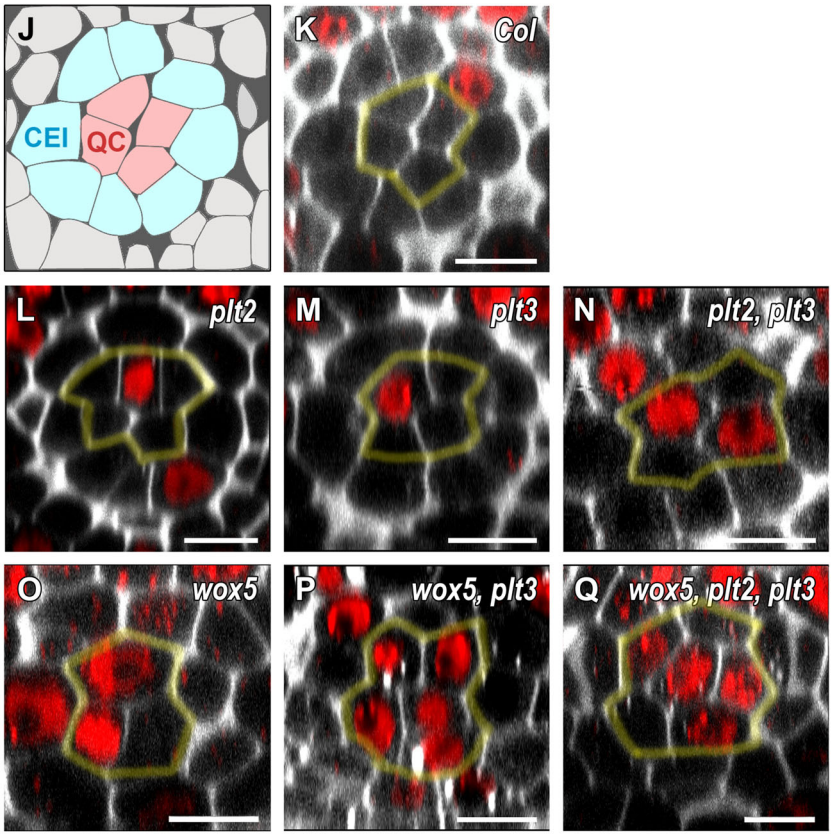

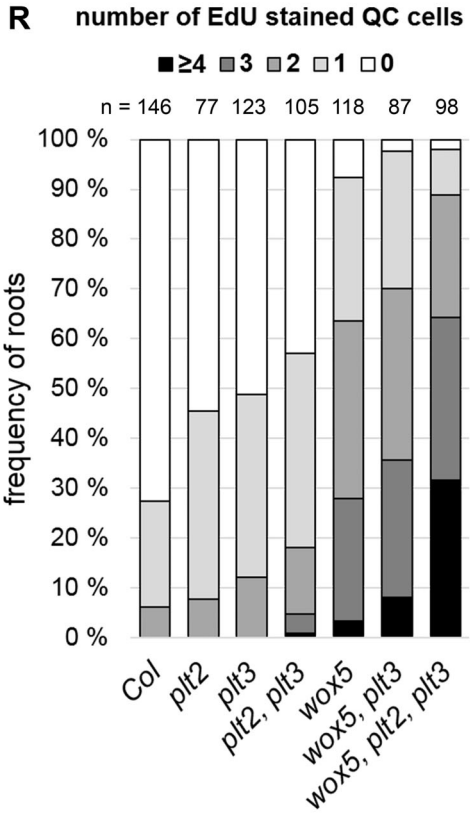

Figure 3.

Figure 3. *plt* and *wox5* mutants show more CSC differentiation and QC divisions.

A Schematic representation of a longitudinal section of an *Arabidopsis* RM. QC cells are marked in red, CSCs are marked in dark blue, CCs in light blue. Combined mPSPI (grey) and EdU (red) staining for 24 h (SCN staining) to analyze the CSC (A-I) and QC division phenotype (J-R) within the same roots are shown.

B–H Representative images of the SCN staining in *Col*, and the indicated single, double, and triple mutant roots. QC positions are marked by yellow arrowheads.

I Analyses of the SCN staining for CSC phenotypes. Frequencies of roots showing 0, 1, 2, or 3 CSC layers are plotted as bar graphs.

J Schematic representation of a transversal section of an *Arabidopsis* RM. QC cells are marked in red, CEI initials are marked in turquoise.

K–Q Representative images of transversal sections with QC cells outlined in yellow.

R Analyses of the SCN staining for QC division phenotypes. Frequencies of roots showing 0, 1, 2, 3 or $\geq$ 4 dividing QC cells are plotted as bar graphs.

Data information: Number of analyzed roots (*n*) (biological replicates) is indicated for each genotype and results from 2-5 technical replicates per genotype.
QC = quiescent center, CSC = columella stem cell, CEI = cortex endodermis initial, SCN = stem cell niche, mPSPI = modified pseudo-Schiff propidium iodide, EdU = 5-ethynyl-2′-deoxyuridine, scale bars represent 5 μm.
Source data are available online for this figure.

dividing QC cell in 92% of roots (Fig 3O and R) and on average more dividing QC cells per root (Appendix Table S5). The number of dividing QC cells per root increases further in the *wox5*, *plt3* double mutant and is even higher in the *wox5*, *plt2*, *plt3* triple mutant; here, in one third of the roots all QC cells undergo cell division (Fig 3P–R, Appendix Table S5). Taken together, this data implies an additive effect of PLT2, PLT3, and WOX5 regarding the QC-division phenotype, suggesting that WOX5 and PLTs act in parallel pathways to maintain the quiescence of the QC.

Additionally, we quantified roots showing at least one aberrant periclinal cell division in the QC in longitudinal optical sections (Fig EV1). Whereas the occurrence of these aberrant periclinal divisions in *Col* wild-type roots is very rare (3%) (Fig EV1A), it increases in the *plt*-single mutants to 21% and in *wox5* and *wox5, plt3* mutants to around 40% (Fig EV1B and C). We found the most severe phenotypes in the *plt2, plt3* double and *wox5, plt2, plt3* triple mutants with an occurrence of periclinal QC-cell divisions in 53% of the observed roots, indicating a synergistic regulatory role of PLTs in periclinal QC cell divisions (Fig EV1B and C, Appendix Table S6).

2D plots of SCN staining facilitate assessment of root phenotypes

To visualize correlations of QC division and CSC differentiation, we combined the acquired data in 2D-plots in which the frequencies of the two phenotypes are color-coded (Fig 4). This visualization reveals a regular pattern for *Col* wild-type roots, which peaks at one CSC layer and no QC divisions (Fig 4A). The pattern of the *plt* single mutants is more irregular with a shift to less CSC layers (indicating more differentiation) and more EdU-stained QC cells (indicating more QC divisions) compared to the wild-type *Col* roots (Fig 4B and C). The *plt2, plt3* double mutants have an additional maximum at a position showing no CSC layer and one divided QC cell, resulting in two phenotypic populations, one at a wild-type-like position, the other showing a strong mutant phenotype (Fig 4D). The 2D-pattern for the *wox5* mutant shifts to less CSC-layers and more QC-divisions with a maximum at no CSC-layers and two QC-divisions (Fig 4E). The QC phenotype is more severe in the *wox5, plt3* double mutant towards more cell divisions and is even stronger in the *wox5, plt2, plt3* triple mutant which peaks at zero CSC layers and three QC-divisions (Fig 4F and G). In summary, our data acquired by applying the novel SCN staining demonstrates that higher CSC differentiation correlates with a higher division rate in the QC, possibly to replenish missing stem cells by increased QC divisions.

PLT3, but not WOX5, localizes to nuclear bodies (NBs)

WOX5 and PLT3 are expressed and localize to overlapping domains in the SCN of the *Arabidopsis* root and based on our results regulate SCN maintenance together. To test for functionality of our generated reporter lines, we used the mVenus (mV) tagged WOX5 and PLT3 versions driven by their own endogenous promoters for rescue experiments in the respective mutant phenotypes in *Arabidopsis*. We observed a rescue of the *wox5* mutant expressing pWOX5::WOX5-mV (Fig EV2A–C, J and K, Appendix Table S7) and a rescue of the *plt3* mutant expressing pPLT3::PLT3-mV to almost wild-type *Col* phenotypes (Fig EV2E, G, J and K, Appendix Table S7), indicating that the labelling with mVenus did not or only very little influence WOX5 or PLT3 functionality. To our surprise, we observed PLT3 localization in bright subnuclear structures, hereafter called NBs, in the PLT3-mV reporter line. Most frequently, we found PLT3 NBs in young, developing lateral root primordia (LRP) (Fig 5A, Movie EV1) already at stages where PLT1 and PLT2 are not yet expressed (Du & Scheres, 2017). Importantly, we also observed PLT3 NBs in CSCs of some established primary roots, but never in QC cells (Fig 5B and C′). To further examine the PLT3 NBs in a context, where no other PLTs are expressed, we used an estradiol-inducible system to control expression of FP-tagged PLT3 and WOX5 transiently in *Nicotiana benthamiana* (*N. benthamiana*) leaf epidermal cells (Stahl *et al*, 2013). In agreement with our observations in *Arabidopsis*, we found that PLT3 mainly localizes to NBs and to a lesser extend to the nucleoplasm (Fig 6B). We quantified NB formation of PLTs in this transient system using estradiol inducible versions of PLT1-4 tagged with mVenus by acquiring z-stacks through the expressing nuclei exactly 5 h after induction. Here, we found that PLT3 forms at least three times more NBs compared to PLT1, PLT2 and PLT4 (see Appendix Fig S3A–E, Appendix Table S8).

In co-expression experiments in *N. benthamiana*, we found that PLT3 recruits WOX5 to the same NBs, whereas on its own WOX5 remains homogenously localized within the nucleoplasm (Fig 6G–G″, Fig EV3A).

Prion-like domains (PrDs) are responsible for NB localization of PLT3

Next, we examined the protein domains putatively responsible for the localization of PLT3 to NBs and found that the PLT3 amino acid (aa) sequence contains two glutamine (Q)-rich regions in the C-terminal part of the protein (see Figs 6A and EV3K and L). Proteins containing polyQ stretches form aggregates or inclusions, a

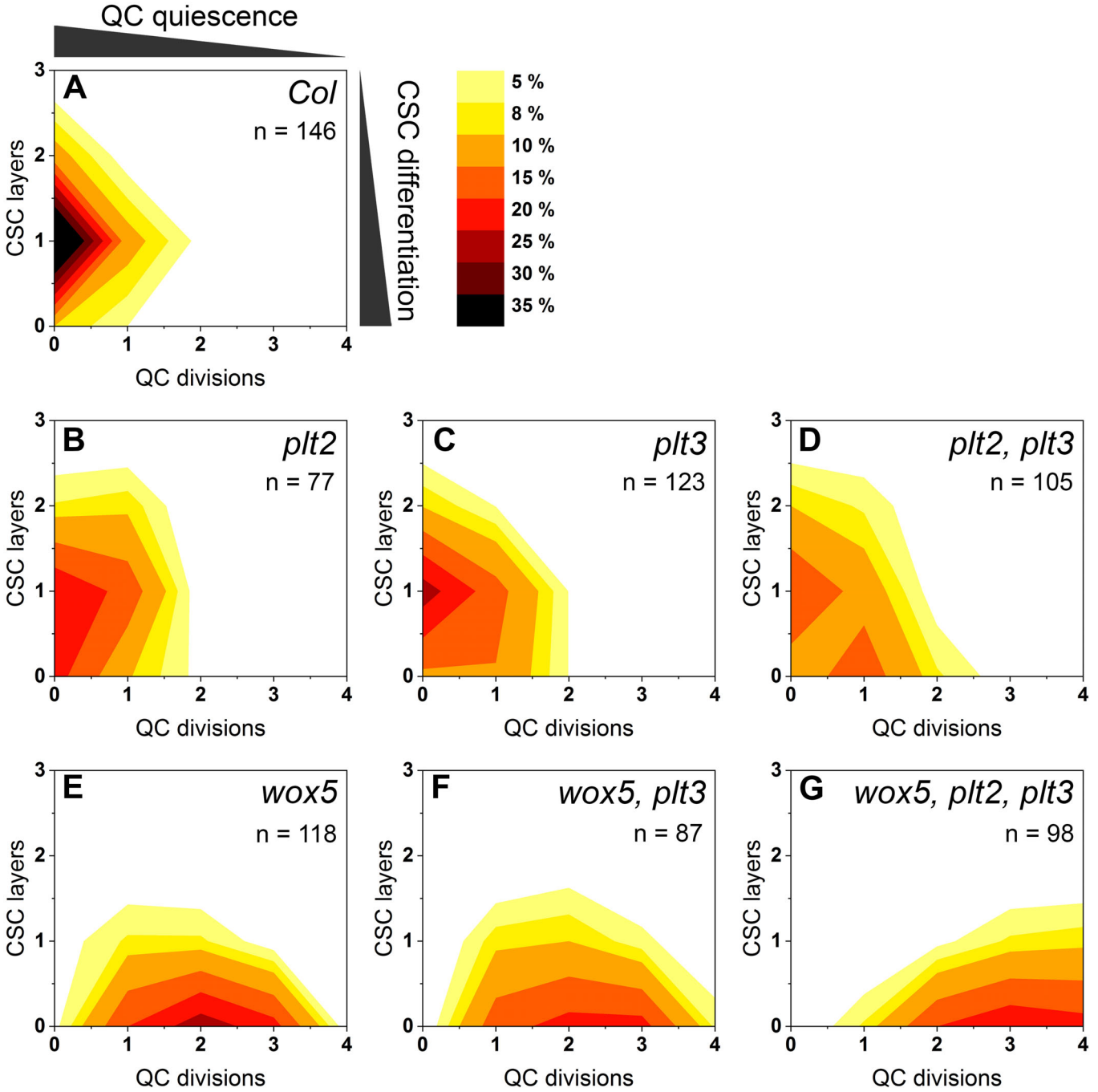

Figure 4. QC divisions correlate negatively with the number of CSC layers.

A–G The combined results of the SCN staining in Fig 3 are shown as 2D plots to visualize the correlation of the CSC layer and QC division phenotypes. Number of CSC layers are shown on the y axis and the QC division phenotype is shown on the x-axis. The darker the color, the more roots show the respective phenotype (see color gradient top right indicating the frequencies in percent). *Col* wild-type roots show one layer of CSCs and no EdU stained cells (no QC division) after 24 h EdU staining. Number of analyzed roots (*n*) (biological replicates) is indicated for each genotype and results from 2 to 5 technical replicates per genotype.

Source data are available online for this figure.

process often linked to pathological conditions in humans, such as Huntington's disease (Scarafone *et al*, 2012). However, polyQ proteins can also convey diverse cellular functions like promotion of nuclear assemblies (e.g., the transcription initiation complex), formation of protein-protein complexes, recruitment of other polyQ-containing proteins (Mikecz, 2009; Atanesyan *et al*, 2012), and enhancement of the transcriptional activation potential of TFs (Gerber *et al*, 1994; Schwechheimer *et al*, 1998; Atanesyan *et al*,

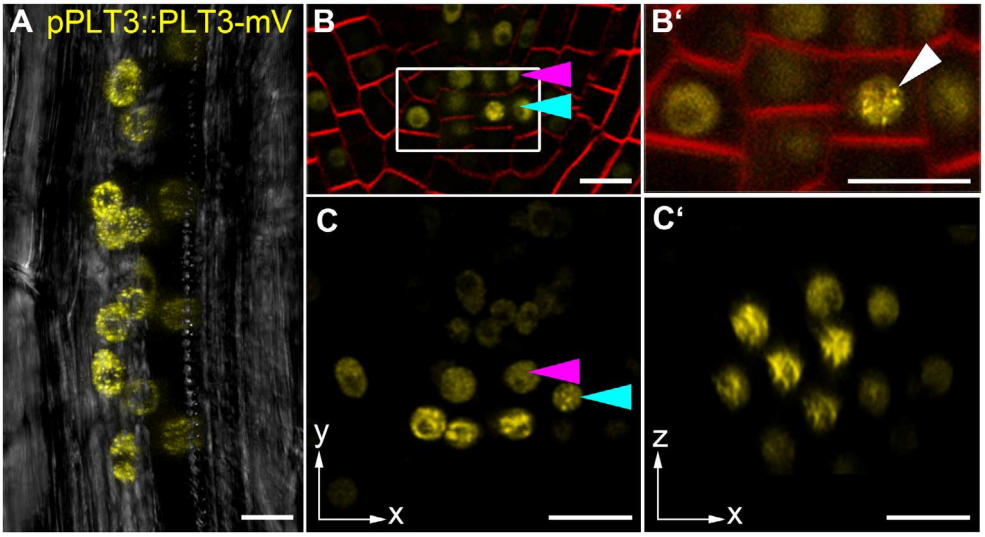

Figure 5. PLT3 localizes to NBs in *Arabidopsis thaliana* LRPs and CSCs.

A–C′ PLT3-mV expression driven by the PLT3 endogenous promoter in LRP (A) and primary root SCN (B-C′) in *plt3* mutant *Arabidopsis* roots. (A) Representative image of PLT3-mV expression (yellow) in an LRP showing the subnuclear localization to NBs. Transmitted light image in grey. (B, B′) SCN of an PLT3-mV expressing FM4-64-stained (red) *Arabidopsis* primary root. The magnification of the CSC layer (B′) shows the subnuclear localization of PLT3 to NBs in a CSC. White arrowhead points at a NB. (C, C′) SCN of an PLT3-mV expressing *Arabidopsis* primary root. NBs are visible in the CSC layer in (C, also in the transversal view of the CSC layer C′). Arrowheads in B and C point at the QC (magenta) and CSC (cyan) positions. mV = mVenus; LRP = lateral root primordium; SCN = stem cell niche; NBs = nuclear bodies; CSC = columella stem cell. Scale bars represent 10 μm.

2012). PolyQ domains were also found to be enriched in plant TFs (Kottenhagen *et al*, 2012).

Next, we tested if the polyQ-stretches in PLT3 are responsible for the subnuclear localization and the recruitment of WOX5 to NBs. To this end, we deleted the polyQ domains of PLT3 and expressed the resulting PLT3ΔQ fused to mVenus transiently in *N. benthamiana*. We found that the subnuclear localization and the recruitment of WOX5 did not change compared to the full-length PLT3 (see Fig 6B, C and H–H″). Therefore, we conclude that the polyQ domains in PLT3 are not, or at least not alone, responsible for the subnuclear localization and translocation to NBs.

Apart from proteins with polyQ domains, many proteins that form concentration-dependent aggregates contain larger, intrinsically disordered regions (IDRs) with a low complexity similar to yeast prions (Cuevas-Velazquez & Dinneny, 2018). Prion-like proteins in *Arabidopsis* were first discovered by analyzing protein sequences of 31 different organisms, identifying Q- and N-rich regions in the proteins to be sufficient to cause protein aggregation (Michelitsch & Weissman, 2000). Recently, the existence of more than 500 proteins with prion-like behavior in *Arabidopsis* was reported (Chakrabortee *et al*, 2016) and the presence of prion-like domains (PrDs) in protein sequences is predictable with web-based tools (Lancaster *et al*, 2014). Therefore, we analyzed the PLTs and WOX5 sequences using the PLAAC PrD prediction tool and found that PLT3 has three predicted PrDs in its aa sequence, two of them located at the C terminus, containing the above described two polyQ-stretches (see Figs 6A and EV3K and L). PLT1, PLT2, and PLT4 also show predicted PrD domains, but PLT1 and PLT2 contain no and PLT4 shorter polyQ stretches within them (Fig EV3D–I and M–O). WOX5 does not show any predicted PrD domains, nor any polyQ stretches (Fig EV3A–C). To test the importance of the PrD domains in PLT3, we replaced the first PrD by a 27 aa linker (AAGAAGGAGGGAAAAAGGAGAAAAAGA) and deleted the C-terminally located PrDs. The resulting PLT3-version (PLT3ΔPrD) was fused to the mVenus FP and inducibly expressed in *N. benthamiana* epidermal cells. Here, we did not observe a localization of PLT3ΔPrD-mVenus to NBs, but in contrast a homogenous distribution within the nucleus (Fig 6D). In addition, upon co-expression of PLT3ΔPrD-mVenus with WOX5-mCherry, we observed that WOX5 was no longer recruited to NBs (Fig 6I–I″). In line with this, we observed PLT3 NBs in developing *Arabidopsis* LRP expressing pPLT3::PLT3-mVenus, but no more NBs were found in a pPLT3::PLT3ΔPrD-mVenus expressing line (Fig 6E and F). Based on these observations, we conclude that the PrD domains of PLT3 are responsible for its localization to NBs and the recruitment of WOX5 to NBs. This is further supported by our observation that PLT3, in contrast to PLT1, 2 and 4, is found most frequently in NBs in transiently expressing in *N. benthamiana* correlating with the presence of PrD domains containing long polyQ-stretches in its aa sequence (Fig EV3D–O, Appendix Fig S3A–E).

PLT NBs recruit RNA

Proteins containing polyQ-stretches or PrDs are often involved in RNA binding, RNA processing and/or RNA compartmentalization (Macknight *et al*, 1997; Schomburg *et al*, 2001; Alberti *et al*, 2009; Sonmez *et al*, 2011; Castilla-Llorente & Ramos, 2014; Fang *et al*, 2019). To test if PLT3 is involved in these processes, we performed an RNA-staining in *N. benthamiana* epidermal cells transiently expressing PLT3-mVenus with 5-ethynyl-2′-uridine (EU) (see Fig 6J–J‴). EU is incorporated into RNA during transcription, and we found that most of the stained RNA co-localizes with the PLT3-

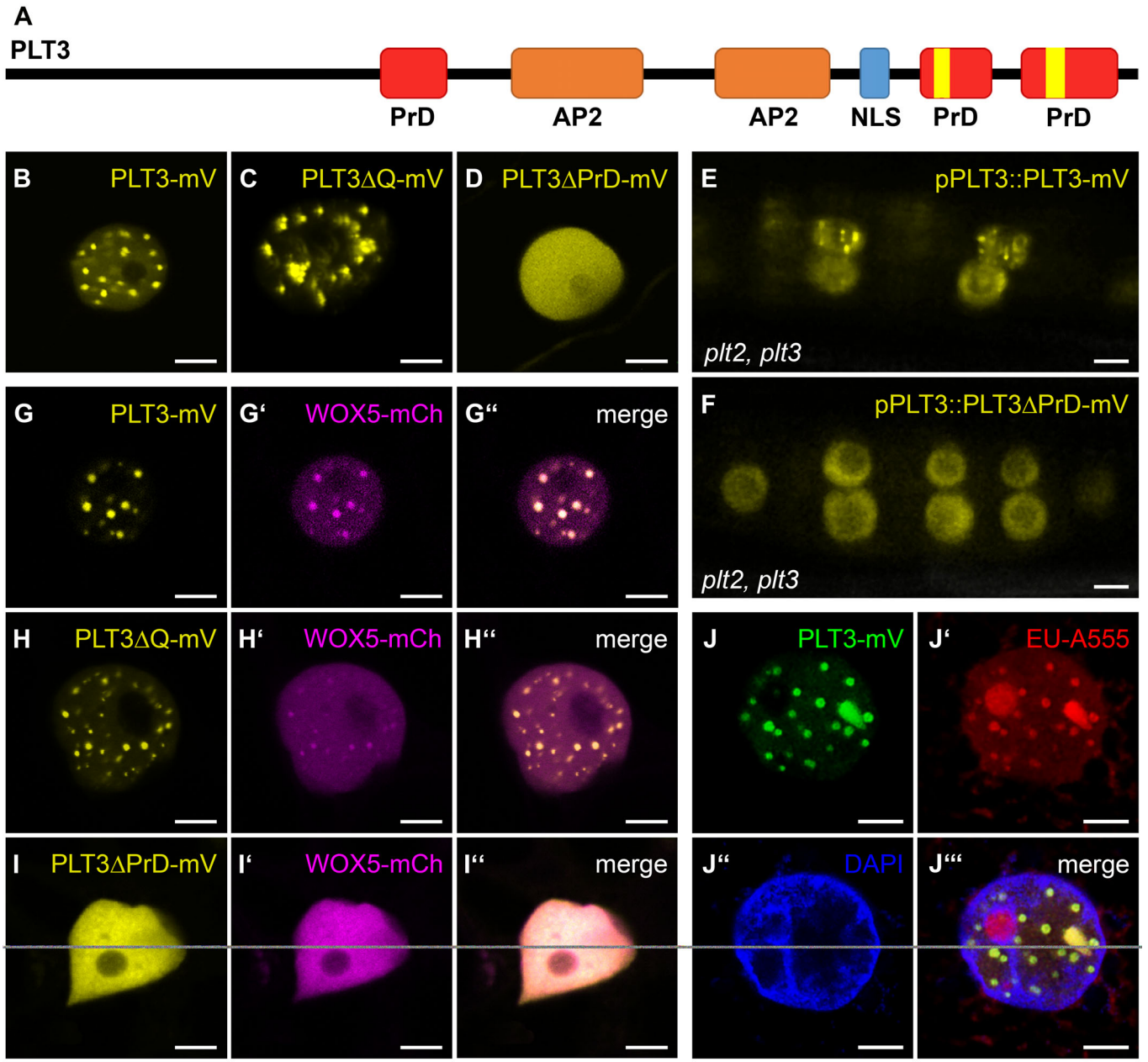

Figure 6. PLT3 PrD domains influence its subnuclear localization.

A Schematic representation of PLT3 protein domains. The areas in red are predicted prion-like domains (PrDs) and were deleted in PLT3ΔPrD-mV. The areas highlighted in yellow contain polyQ-stretches and were deleted in PLT3ΔQ-mV.

B–D Representative images of PLT3-mV (B), PLT3ΔQ-mV (C) and PLT3ΔPrD-mV (D) in transiently expressing *N. benthamiana* leaf epidermal cells.

E, F PLT3-mV (E) and PLT3ΔPrD-mV (F) expression driven by the PLT3 endogenous promoter in lateral root primordia of *plt2, plt3* double mutant *Arabidopsis* roots.

G-I″ Co-expression of PLT3-mV (G), PLTΔQ-mV (H) and PLT3ΔPrD-mV (I) with WOX5-mCh (G′, H′, I′) in transiently expressing *N. benthamiana* leaf epidermal cells.

J–J‴ Expression of PLT3-mV (J) in transiently expressing *N. benthamiana* leaf epidermal cells in combination with RNA staining with EU (18 h), visualized by click-reaction with Alexa Fluor® 555 (J′) and a DNA staining with DAPI (J″).

Data information: mV = mVenus; PrD = prion-like domain; AP2 = APETALA2 domain; NLS = nuclear localization signal; EU = 5-ethynyl-2′-uridine. Scale bars in (B–J‴) represent 5 μm.

mVenus NBs except for the EU-stained nucleolus (see Fig 6J–J‴). Based on these observations, we conclude that the PLT NBs act as important sites for the recruitment of RNA and other factors, including WOX5.

WOX5 and PLT proteins can interact with each other

Because the WOX5 and PLT protein expression domains overlap in the SCN and PLT1, PLT2, PLT3 and PLT4 contain PrD domains, we

asked whether PLTs and WOX5 can interact *in vivo*, especially considering the observed recruitment of WOX5 to PLT3 NBs. For this, we used fluorescence lifetime imaging microscopy (FLIM) to measure Förster resonance energy transfer (FRET) to analyze the potential protein-protein interaction of WOX5 and PLTs *in vivo*. To perform FLIM, we inducibly co-expressed WOX5-mVenus as donor together with individual PLTs-mCherry as acceptors for FRET in *N. benthamiana* leaf epidermal cells. The fluorescence lifetime of the donor fluorophore mVenus fused to WOX5 alone is 3.03 ± 0.07 ns. A reduction of fluorescence lifetime is due to Förster resonance energy transfer (FRET) of the two fluorophores in very close proximity (≤ 10 nm) caused by the direct interaction of the two observed proteins. When free mCherry is co-expressed as a negative control, the WOX5-mVenus mean fluorescence lifetime is not significantly decreased (3.00 ± 0.06 ns) (Fig 7A, B and I). When WOX5-mVenus is co-expressed with PLT1-mCherry the fluorescence lifetime significantly decreases to 2.79 ± 0.11 ns, with PLT2-mCherry to 2.73 ± 0.12 ns, with PLT3-mCherry to 2.75 ± 0.17 ns and with PLT4-mCherry to 2.75 ± 0.24 ns, indicating FRET and hence direct protein-protein interactions (Fig 7C–F and H). The observed interaction of WOX5 with PLT1-4 lead us to propose that they regulate SCN maintenance by the formation of complexes, either all together or in diverse compositions depending on the cell identity or their function. Interestingly, we observed a stronger lifetime decrease of WOX5-mVenus in the PLT3 NBs than in the nucleoplasm, indicating that the NBs function as main interaction sites of WOX5 with PLT3 (Fig 7J and K, Appendix Table S9).

To address this, we measured the interaction between WOX5 and PLT3 in *Arabidopsis* roots via FLIM experiments in a translational line expressing WOX5-mVenus and PLT3-mCherry under control of their respective endogenous promoters. This resulted in the inevitable low protein concentration in comparison to the inducible system used in *N. benthamiana*. Probably due to this, we could not observe NBs in established root meristems of our *Arabidopsis* FLIM line (Fig EV4A–A″) and we could only measure a very small, albeit statistically significant, decrease in fluorescence lifetime from 2.97 ± 0.07 ns in the pWOX5::WOX5-mVenus (donor only FRET control) expressing roots to 2.94 ± 0.08 ns when pPLT3:PLT3-mCherry is co-expressed in the SCN of LRP in *Col-0* background (Fig EV4B).

Formation of PLT3 NBs is concentration-dependent

In *Arabidopsis* seedlings, we only sometimes observed PLT3 NBs in the CSC layer of the root tip, but more frequently in young, developing LRP (Fig 5A), whereas in *N. benthamiana* we observed NBs in almost all cells. Therefore, we argue that the formation of the NBs is flexible because it is concentration-dependent. In a transient *N. benthamiana* experiment, we could observe a correlation between the fluorescence intensity of nuclear PLT3-mVenus and the size and number of the NBs (Fig EV5). NBs start to form after a certain intensity-threshold (Fig EV5A–C and F), and their number decreases while their volume increases with overall rising fluorescence intensity (Fig EV5D, E and G). A similar concentration-dependency has been previously described for proteins that undergo phase separation, in particular for liquid-liquid phase separation (LLPS) (McSwiggen *et al*, 2019). This mechanism separates membrane-free microdomains from the surrounding liquid and could potentially represent the underlying NB-forming process of PLTs. This process is possibly PrD-dependent as we observed less NB formation in the PrD-deletion variant of PLT3 (Fig 6D and F).

PrD-domains in PLT3 are required for interaction with WOX5 and are necessary for root SCN maintenance

Moreover, we asked if the PrD and polyQ domains in PLT3 are required for protein-protein interaction with WOX5. To test this, we performed FLIM experiments with mCherry-tagged full-length PLT3, PLT3ΔQ, and PLT3ΔPrD as acceptors and WOX5-mVenus as donor in *N. benthamiana*. Here, we observed that co-expression of the PLT3ΔQ and PLT3ΔPrD deletion variants did not lead to a significantly reduced fluorescence lifetime, and therefore, no protein-protein interaction takes place in comparison to the full-length version (see Fig 7E and G–I). This implies that PrD domains, containing the polyQ domains in PLT3, are necessary for the NB localization, but also, notably, for protein complex-formation with WOX5. Still, the exact effect of the polyQ domains on PLT-WOX5 interaction remains to be determined as PLT1, PLT2 and PLT4 still show protein-protein interaction with WOX5, even though they do not contain extended polyQ domains like in PLT3. We therefore cannot rule out that the deletion of the polyQ domain in PLT3 (PLT3ΔQ) could lead to a disturbed PrD domain resulting in a loss of interaction with WOX5.

Next, we asked if the PrD domains of PLT3 are also required for root SCN homeostasis. Therefore, we tested if the *plt2, plt3* double mutant phenotypes can be rescued by expressing full-length PLT3 or PLT3ΔPrD under control of the endogenous PLT3 promoter. We observed that full-length PLT3 expression can rescue the *plt2, plt3* double mutant phenotype of more QC divisions and less CSC layers to the expected levels of *plt2* or *plt3* single mutant phenotypes (Fig EV2D–F, H, J and K, Appendix Table S7). Importantly, PLT3ΔPrD could not rescue the *plt2, plt3* double mutant phenotype, suggesting that the PrD domains in PLT3 are indeed functionally relevant for SCN regulation and maintenance (Fig EV2I–K, Appendix Table S7).

In summary, our findings show that QC quiescence and CSC maintenance are interdependently regulated by WOX5 and PLTs. We could show that mutual transcriptional regulation of PLTs and WOX5, but also their direct protein-protein interaction is required for QC division and CSC fate regulation. Here, especially the observed subnuclear partitioning of PLT3 to NBs in the CSCs of mature RAMs which is dependent on the presence of PrDs is important as it could provide another layer of regulation to the complex and intertwined SCN maintenance of the *Arabidopsis* root.

Discussion

In summary, we found that in agreement with a previous report (Sarkar *et al*, 2007), high *PLT* expression in the QC-region is promoted by WOX5, albeit in an indirect manner, possibly by other factors, such as the described WOX5-induced TAA1-mediated auxin biosynthesis (Savina *et al*, 2020; Pardal & Heidstra, 2021). This *PLT* expression confines WOX5 to a defined and restricted number of cells within the QC region. In line with this, loss of PLTs leads to an expanded expression domain of *WOX5* and a reduced QC quiescence reflected in more QC divisions. Therefore, we could confirm

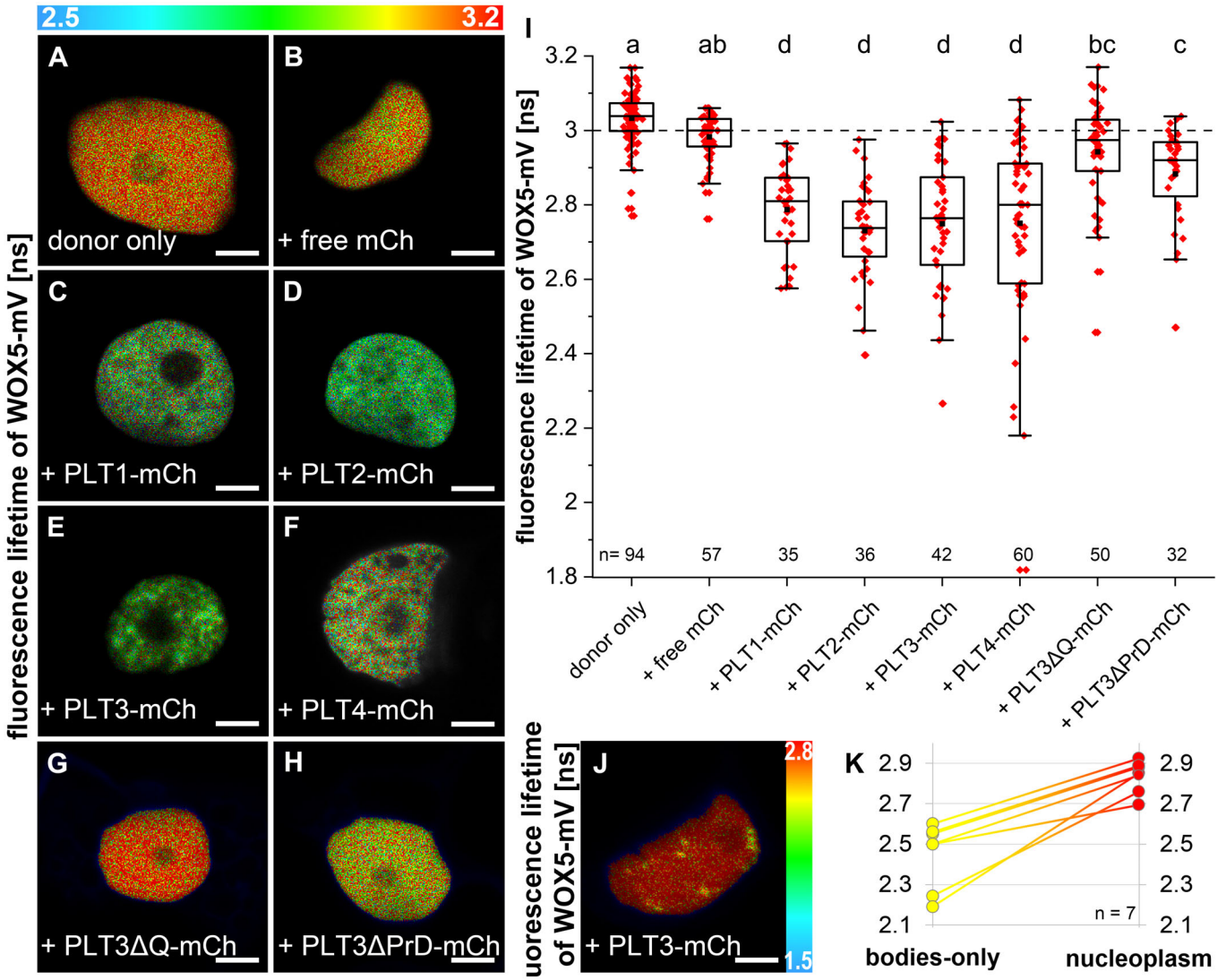

Figure 7. WOX5 can interact with PLTs.

A–H Fluorescence Lifetime Imaging (FLIM) results of transiently expressing *N. benthamiana* leaf epidermal cells. Representative FLIM images of WOX5-mVenus (donor only) plus the indicated acceptors after a pixel-wise mono-exponential fit of the mVenus fluorescence signal. The fluorescence lifetime of WOX5-mVenus in ns is color-coded. Low lifetimes (blue) due to FRET indicate strong interaction of the two proteins and high lifetimes (red) indicate weaker or no interaction. Scale bars represent 5 μm.

I Fluorescence lifetimes in ns are summarized in combined jitter and box plots. The dashed line represents the fluorescence lifetime mean value of the WOX5-mV co-expressed with free mCh as negative control. The one-way ANOVA and Holm–Sidak *post-hoc* multiple comparisons test was used to test for statistical significance. Samples with identical letters do not show significant differences ($\alpha = 0.01$). Number of nuclei analyzed (n) (biological replicates) is indicated and results from 2 to 9 technical replicates. Box = 25–75% of percentile, whisker = 1.5 interquartile range, – = median, ■ = mean value.

J Representative FLIM image of WOX5-mVenus plus the indicated acceptor after a pixel-wise mono-exponential fit of the mVenus fluorescence signal. The fluorescence lifetime of WOX5-mVenus in ns is color-coded. Low lifetimes (blue) due to FRET indicate strong interaction of the two proteins and high lifetimes (red) indicate weaker or no interaction. Scale bars represent 5 μm.

K Individual nuclei showing nuclear bodies during co-expression of WOX5-mV and PLT3-mCh were analyzed for WOX5-mV lifetime in the nuclear bodies or nucleoplasm separately ($n = 7$ (biological replicates), from four technical replicates. mCh = mCherry. mV = mVenus.

Source data are available online for this figure.

that the control of QC quiescence and CSC maintenance is mediated by mutual transcriptional regulation of PLTs and WOX5 possibly by negative feedback loop regulation. As *WOX5* expression is normally limited to the QC, the question arises if, in absence of PLTs, either the *WOX5* expression domain expands to regions surrounding the QC or the QC region itself expands and therefore also the expression domain of *WOX5*. Interestingly, a previous report demonstrated that the expression of several QC markers is missing or highly reduced in *plt* mutants, suggesting that they fail to maintain an intact QC (Aida *et al*, 2004). Therefore, the expansion of the *WOX5* expression

domain in the *plt* mutants is likely uncorrelated to the QC identity of these cells.

The observed higher frequency of cell divisions in the QC region of *wox5* mutants could be explained by the reduced expression of *PLTs,* which consequently negatively impacts QC quiescence but also by a PLT-independent pathway where WOX5 itself may have a positive effect on QC quiescence. Previous findings also suggest that WOX5 maintains QC quiescence through the repression of CYCD activity (Forzani *et al*, 2014). Considering our observation that PLT2, PLT3, and WOX5 show additive effects regarding the QC division phenotype, we propose a model in which WOX5 and PLTs could act in parallel pathways to maintain QC quiescence. The noted correlation of reduced QC quiescence and higher CSC differentiation that we could now show for individual roots by our newly introduced SCN staining could be necessary to replenish missing stem cells by QC divisions. This possible explanation is in agreement with the proposed function of the QC as a long-term stem cell reservoir, especially in case of stress or damage (Vilarrasa-Blasi *et al*, 2014).

For CSC homeostasis, PLTs and WOX5 may act together in the same pathway, possibly by complex formation, as there is no observable additive effect in the multiple mutant roots which is in agreement with previous findings (Ding & Friml, 2010). We show that WOX5 can directly interact with PLT1, PLT2, PLT3 and PLT4, which indicates that they regulate CSC maintenance by the formation of complexes, either all together or in diverse homo- or heteromeric compositions depending on cell identity or function.

In transient *N. benthamiana* experiments, PLT3 forms NBs and recruits WOX5 into them. The stronger decrease of fluorescence lifetime in NBs compared to the nucleoplasm measured by FLIM implies that the PLT3 NBs function as major sites of protein-protein interaction with WOX5, which could be due to a favored complex-formation within the NBs or due to transport of preformed WOX5/PLT3 complexes from the cytosol to NBs. We could observe PLT3 NBs in cells of the CSC layer of some *Arabidopsis* primary root tips, but never in the QC region. Nevertheless, PLT3 NBs were found more frequently in several cells of developing LRPs. LRPs are in a younger and less-determined stage than the primary root and the observed subnuclear localization to NBs could represent a marker for the occurring determination and future cell differentiation. This agrees with the observed localization of PLT3 to NBs in the CSCs in some of the primary roots. Here, PLT3 NBs could represent compartments for the recruitment of and interaction with WOX5 and possibly other factors involved in CSC fate determination and maintenance.

Furthermore, we found that the aa sequence of PLT3 comprises PrDs (including polyQs) that are necessary for the localization to NBs, complex formation with WOX5, and for SCN maintenance in the primary root meristem. Proteins containing polyQ-stretches or PrDs are often involved in RNA binding, RNA processing, and/or RNA compartmentalization (Macknight *et al*, 1997; Schomburg *et al*, 2001; Alberti *et al*, 2009; Sonmez *et al*, 2011; Castilla-Llorente & Ramos, 2014; Fang *et al*, 2019) and we could show that the PLT3 NBs indeed co-localize with RNA. Just as PLT3, FLOWERING CONTROL LOCUS A (FCA) is a PrD-containing protein (Chakrabortee *et al*, 2016) that localizes to subnuclear structures (Fang *et al*, 2019). The FCA bodies separate from the cytosol by LLPS to provide compartments for RNA 3′-end processing factors (Fang *et al*, 2019). Similarly, PLT3 NBs could represent compartments for the recruitment of interacting factors and RNA for further processing, sequestration, or transportation. As PLT3 is a TF, the co-localizing RNA could also represent newly transcribed RNA at the transcription

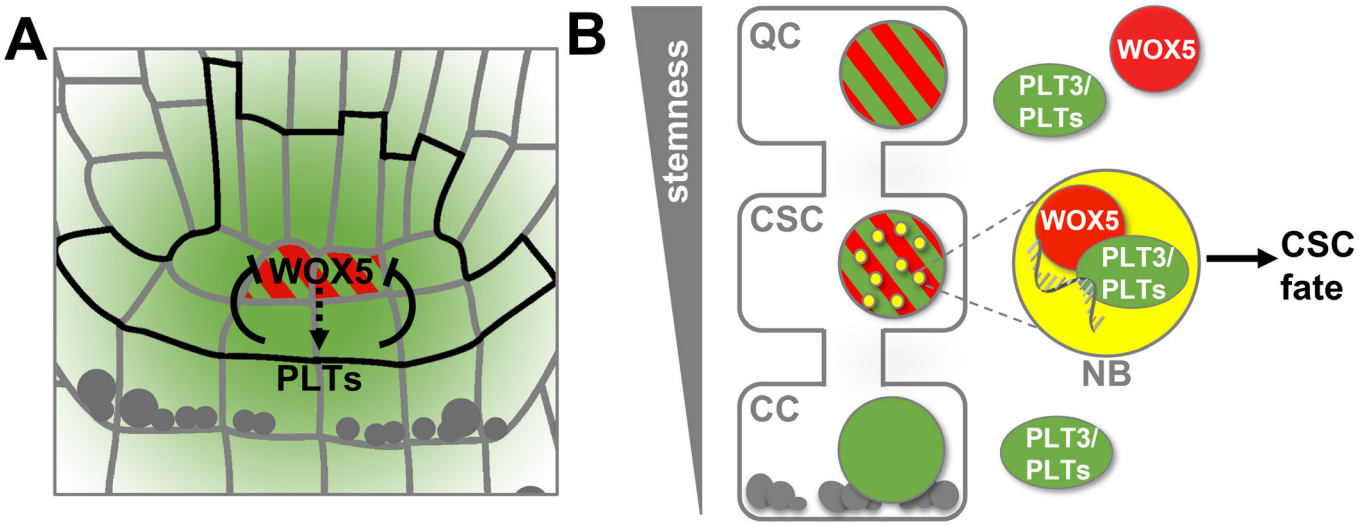

Figure 8. Model of PLT and WOX5 transcriptional regulation, interaction and subnuclear localization during distal root stem cell maintenance.

A Transcriptional regulation of *WOX5* (red) and *PLT* (green) expression by negative feedback regulation in the *Arabidopsis* RAM. *WOX5* is expressed in the QC and indirectly promotes *PLT* expression (dashed arrow), whereas *PLT* expression is directly regulating *WOX5* expression confining it to the QC position (solid barred lines).

B Both WOX5 (red) and PLT3 (green) are present homogenously within the nuclei of the QC cells. WOX5 can move to the CSCs and is recruited there by PLT3 to NBs (yellow), where interaction takes place and RNA is present (grey in magnification). This maintains the stem cell character of the CSCs (arrow) but already leads to a determination to subsequent CC fate. Gray dots represent starch granules.

sites where PLT3 binds to DNA, for example, to the WOX5 promoter region (Shimotohno *et al*, 2018). Another recently described PrD- and polyQ-containing protein, EARLY FLOWERING3 (ELF3), forms NBs by LLPS in response to temperature thereby regulating flowering time in *Arabidopsis* (Jung *et al*, 2020).

The possible liquid-like nature of the PLT3 NBs will be an interesting subject for further studies investigating its putative phase separation properties in response to external cues. In this study, we showed that the PLT3 NB formation is concentration-dependent, which is indicative for LLPS. This concentration-dependency of PLT3 NB formation could also explain the rare occurrence of PLT3 NBs at endogenous protein levels in the CSCs of the *Arabidopsis* RAM. Here, NB formation is possibly triggered only above a certain protein concentration threshold serving as a read-out for future cell fate. In the established distal root meristem, this is not continuously needed and therefore the protein concentration is mainly maintained below this threshold, so that often no NBs are formed. Consequently, the observed PLT3-FP fluorescence intensity in the CSCs can vary and is lower or higher at a given time (Figs 1E and 5B and C).

Therefore, we propose that the regulation of QC quiescence and CSC maintenance are not only mediated by the mutual transcriptional regulation of PLT and WOX5 (see Fig 8A), but also, importantly, by building protein complexes that are differentially localized to distinct nuclei within the SCN (see Fig 8B). The observed subnuclear localization of PLT3 to NBs could represent a marker for the determination to future cell differentiation in the CSC layer. Furthermore, the PrD domains in PLT3 may act as an initial starting point to compartmentalize and partition WOX5 that has moved from the QC towards the CSC layer into NBs, possibly by a concentration-dependent LLPS process. The observed sites could represent transcriptionally active sites for the regulation of target genes involved in CSC fate determination or repress WOX5 expression.

The dynamic compartmentalization to subcellular or subnuclear microdomains of proteins with intrinsically disordered, PrD and/or polyQ domains was shown to have severe effects, for example, in human pathological disorders like Huntington's disease (Scarafone *et al*, 2012). But also beneficial functions of prions that are responsible for some neurodegenerative diseases in mammals (Aguzzi *et al*, 2013; Kim *et al*, 2013) as a protein-based memory is highly discussed, as their self-replicating conformations could act as molecular memories to transmit heritable information (Bailey *et al*, 2004; Shorter & Lindquist, 2005). If this is also the case in plants remains to be determined. In general, the dynamic formation of subcellular structures could be necessary for a changing composition of assemblies in dependence of their functional status (Mikecz, 2009). The transition of these proteins between condensed and soluble forms requires high flexibility in their protein structure, which can be provided by flexible intrinsically disordered domains, such as polyQ-stretches which are predominantly positioned at the surface of a protein, supporting the idea of their involvement in protein-protein interactions (Totzeck *et al*, 2017).

In *Arabidopsis*, PrD and polyQ dependent compartmentalization could present a fast and reversible concentration-dependent regulatory mechanism (Cuevas-Velazquez & Dinneny, 2018), for example, in case of PLT3 and WOX5 to determine CSC cell fate but probably also in other developmental contexts such as lateral root development. It remains to be determined if LLPS is the underlying mechanism of the observed subnuclear compartmentalization of these key TFs involved in *Arabidopsis* root stem cell homeostasis and if also other processes necessary for determination of cell fates and stemness in *Arabidopsis* are regulated by this or similar dynamic processes.

Materials and Methods

Cloning

pWOX5::mVenus-NLS, pWOX5::WOX5-mVenus, pPLT3::PLT3-mVenus, pPLT3::PLT3-mCherry, pPLT3::PLT3ΔPrD-mVenus, β-estradiol inducible PLT3ΔPrD-mVenus, and β-estradiol inducible PLT3ΔPrD-mCherry were created by using the GreenGate cloning method (Lampropoulos *et al*, 2013). The internal *BsaI* restriction sites in the WOX5 promoter and WOX5 CDS were removed by PCR amplification of the sequences upstream and downstream of the *BsaI* sites with primer pairs whereof one primer has an altered nucleotide sequence at this site (Appendix Table S10), followed by an overlap extension PCR to reconnect the gene fragments. The sequences upstream of the ATG start codon of WOX5 (4,654 bp) and PLT3 (4,494 bp) were used as promoter regions and were amplified by PCR and primers to add flanking *BsaI* restriction sites and matching overlaps for the GreenGate cloning system. Afterward, they were cloned into the GreenGate entry vector pGGA000 via *BsaI* restriction and ligation. The GreenGate promoter module carrying the β-estradiol inducible cassette was provided by (Denninger *et al*, 2019). The CDS of WOX5, PLT2, PLT3, PLT3ΔPrD and PLT4 as well as the FPs mVenus and mCherry were amplified by PCR using adequate primer pairs to add flanking *BsaI* restriction sites and matching overlaps for cloning into the GreenGate entry vectors pGGC000 (for CDS) and pGGD000 (for FPs) via *BsaI* restriction and ligation. All created entry vectors were confirmed by sequencing. The expression cassettes were created with a GreenGate reaction using pGGZ001 as destination vector. The correct assembly of the modules was controlled by sequencing. All module combinations used to construct the expression vectors can be found in Appendix Table S11.

All other β-estradiol inducible constructs for *N. benthamiana* expression (free mCherry, WOX5-mVenus, WOX5-mCherry, PLT1-mVenus, PLT1-mCherry, PLT2-mCherry, PLT3-mVenus, PLT3-mCherry, PLT3ΔQ-mVenus, PLT3ΔQ-mCherry were created by Gateway cloning (Invitrogen™, Thermo Fisher Scientific Inc.). The CDS of WOX5, PLT1, PLT2, PLT3, PLT3ΔQ were amplified and cloned into pENTR/D-TOPO®. The Entry-vectors were confirmed by sequencing. The destination vector carrying the mVenus (pRD04) is based on pMDC7 (Curtis & Grossniklaus, 2003) which contains a β-estradiol inducible system for expression *in planta*. The mVenus was introduced via restriction/ligation C-terminally to the Gateway cloning site. The destination vector carrying the mCherry (pABindmCherry) was described before (Bleckmann *et al*, 2010). The expression vectors were created by LR-reaction of destination and entry vectors. Gateway expression vectors were verified by test digestion.

For the creation of the domain-deletion variants of PLT3 (PLT3ΔQ and PLT3ΔPrD), the CDS parts upstream and downstream of the desired sequence deletions were amplified with PCR and afterward reconnected with overlap-PCR. The 27 aa linker (AAGAAGGAGGGAAAAAGGAGAAAAAGA) to replace the first PrD

in PLT3ΔPrD was also introduced by overlap-PCR. All primers used for cloning can be found in Appendix Table S10. For a list of the constructs produced in this study see Appendix Table S11.

Plant work

All *Arabidopsis* lines used in this study were in the Columbia (*Col-0*) background. The single mutants *wox5-1* and *plt3-1* have been described before (Galinha *et al*, 2007) (Appendix Table S4). The *plt2* (SALK_128164) and *wox5-1* (SALK038262) single mutants were provided by the *Arabidopsis* Biological Resource Center (ABRC, USA). The homozygous double and triple mutants were created by crossings (Appendix Table S12) and homozygous F3 es were confirmed by PCR with appropriate primer pairs (Appendix Table S13). The transgenic lines were created by floral dip as described before (Zhang *et al*, 2006) except for the published, transgenic *Col-0* lines with pPLT3::erCFP and pPLT3::PLT3-YFP (Galinha *et al*, 2007) constructs. They were crossed into the *wox5-1* mutant background. Homozygous lines were confirmed by genotyping and hygromycin selection. All plants for crossing, floral dips, genotyping, and seed amplification were grown on soil in phytochambers under long day (16 h light/8 h dark) conditions at 21°C. For microscopy *Arabidopsis* seeds were fume-sterilized (50 ml 13% sodiumhypochlorite (v/v) + 1 ml hydrochloric acid), imbedded in 0.2% (w/v) agarose, stratified at 4°C for 2 days and plated on GM agar plates (1/2 strength Murashige Skoog medium including Gamborg B5 vitamins, 1.2% (w/v) plant agar, 1% (w/v) sucrose, supplemented with 0.05% (w/v) MES hydrate). *Arabidopsis* seedlings were grown for 5 days under continuous light at 21°C and directly imaged afterward.

Cell wall and plasma membrane staining

For root imaging, the cell walls in *Arabidopsis* seedlings were stained by incubation in aqueous solutions of either 10 μM propidium iodide (PI) or 2.5 μM FM4-64 dye (Invitrogen™, Thermo Fisher Scientific Inc.). The staining solution was used as mounting medium for microscopy.

Nicotiana benthamiana infiltration

For transient gene expression in *N. benthamiana*, the *Agrobacterium* strain GV3101::pMP50 was used as vector, carrying plasmids with the desired constructs and additionally either the helper plasmid p19 as silencing suppressor or the helper plasmid pSOUP that harbours a replicase needed for GreenGate vectors. Cultures were grown over night in 5 ml dYT-medium at 28 C on a shaker. The cultures were centrifuged for 10 min at 3,345 *g*, the pellet was resuspended in infiltration medium (5% (w/v) sucrose, 0.01% (v/v) Silwet, 0.01% (w/v) MgSO4, 0.01% (w/v) glucose, 450 μM acetosyringone) to an optical density OD_{600} of 0.4 and cultures were incubated for 1 h at 4°C. The infiltration was done either with one single or with a combination of two different *Agrobacteria* cultures for co-expression of two constructs. A syringe without needle was used for the infiltration on the adaxial side of the leaves of well-watered *N. benthamiana* plants. For the expression of GreenGate constructs, an *Agrobacterium* strain carrying the p19 plasmid was co-infiltrated. The expression was induced 2–5 days after infiltration by applying an aqueous β-estradiol solution (20 μM β-estradiol, 0.1% (v/v) Tween®-20) to the adaxial leaf surface. Imaging or FLIM experiments were done 3–16 h after induction, depending on the expression level.

Quantification of nuclear bodies

NBs were quantified by expression of translational fusions of PLTs to mVenus in *N. benthamiana* after induction with β-estradiol for exactly 5 h. All image acquisition settings (e.g., laser power, gain, filter, pixel size, averaging, scan speed) were kept the same for the analyses of the different PLTs for comparability. Optical z-stacks containing the whole nuclei were acquired and the number of NBs per nucleus and the nuclear volumes quantified using Imaris (version 9.1.2, Bitplane, Oxford Instruments plc).

SCN staining

Arabidopsis seedlings were grown under continuous light for 5 days on GM agar plates without sucrose and then transferred on fresh plates containing additionally 7 μg/ml EdU to continue growing for 24 h. Afterward, we performed an mPS-PI staining like described before (Truernit *et al*, 2008). Preliminary to the clearing step, the EdU-staining was performed. The permeabilization of the cells and the subsequent staining of EdU-containing DNA with Alexa Fluor® 488 was done as described in the Click-it® EdU Imaging Kits from Invitrogen™ (Thermo Fisher Scientific Inc.) with adapted incubation times for *Arabidopsis* seedlings (permeabilization for 1–2 h and click-reaction for 1 h). The click-reaction cocktail was prepared freshly with self-made solutions (Tris buffer with 50 mM Tris and 150 mM NaCl at pH 7.2–7.5; 4 mM CuSO4; 1.5 μM Alexa Fluor® 488 picolyl azide; 50 mM ascorbic acid). The Alexa Fluor® 488 picolyl azide (Thermo Fisher Scientific Inc.) was added from a 500 μM stock in DMSO. The ascorbic acid was added last from a freshly prepared aqueous 500 mM stock solution. After staining was done, the clearing step with chloralhydrate was performed like described before (Truernit *et al*, 2008). Images were acquired with a ZEISS LSM880 confocal microscope with imaging acquisition settings as stated below. z-stacks through the QC-region were recorded to obtain transversal views. To calculate the CSC phenotype, the number of CSC layers was counted in xy-images of each root. For this, we defined an intact CSC layer as a stem-cell layer below QC position without any differentiated cells (visible by no starch-accumulation). Cells in the layer below QC position containing starch granules were scored as differentiated, and we therefore score the whole layer as differentiated, even if only some of these cells contain starch.

The QC-division phenotype is the number of EdU-Alexa Fluor® 488-stained cells in the QC, which was counted in the cross-sectional images up to a maximal number of 4 stained QC cells. In case of duplicated QC cells as in *plt2, plt3* double mutants only one layer of QC cells, the one with the most QC divisions, was counted (usually the bottom layer).

The phenotype frequencies of CSC differentiation and QC divisions (Fig 3) where visualized in bar graphs with Excel (Microsoft Office 365 ProPlus, Microsoft Corporation). In order to correlate the two investigated phenotypes, we combined the CSC data and the QC-division data in 2D-plots. The combined QC/CSC-phenotype of every root was entered in a matrix with QC-divisions on the x- and CSC layers on the y-axis. 2D plots were created with Origin 2018b and 2020b (OriginLab Corporation).

RNA staining

RNA-staining in *N. benthamiana* epidermal cells was done on *N. benthamiana* leaves harboring a construct for a β-Estradiol inducible *PLT3-mVenus* expression. 5-ethynyl-2′-uridine (EU) was infiltrated in *N. benthamiana* leaves the day before staining. The expression of PLT3-mVenus was induced the next morning, 3 h before fixation of the plant tissue. For fixation and permeabilization of cells, pieces of the leaves were cut and treated with 4% (w/v) paraformaldehyde and 0.5% (v/v) TritonX-100 in PBS under vacuum for 1 h. The click-reaction of EU with Alexa Fluor® 555 picolyl azide was performed similarly to the EdU-Alexa Fluor® 488-staining described for the SCN staining in this article. A DAPI- counterstaining was carried out afterward by incubating the leaf pieces in 0.1 μg/ml DAPI for 30 min. PBS was used as mounting medium for imaging.

Microscopy

Imaging of *Arabidopsis thaliana* roots and *Nicotiana benthamiana* leaves was carried out with a ZEISS LSM780 or LSM880. Excitation and detection of fluorescent emission of fluorescent dyes was done as follows: DAPI was exited at 405 nm and emission was detected at 408–486 nm, Cerulean was excited at 458 nm and emission was detected at 460–510 nm; CFP was excited at 458 nm and emission was detected at 463–547 nm. mVenus was excited at 514 nm and emission was detected at 517–560 nm, or for co-expression with red dyes excited at 488 nm and detected at 500–560 nm. YFP was excited at 514 nm and emission was detected at 518–548 nm. Alexa Fluor® 488 was excited at 488 nm and emission was detected at 490–560 nm. Alexa Fluor® 555 was excited at 561 nm and emission was detected at 565–640 nm. PI was excited at 561 nm and emission was detected at 590–710 nm. FM4-64 was excited at 514 or 561 nm and emission was detected at 670-760 nm. mCherry was excited at 561 nm and emission was detected at 590–640 nm. Imaging of more than one fluorophore was done in sequential mode to avoid cross talk. The movie of pPLT3::PLT3-mVenus in a lateral root primordium was acquired with a MuViSPIM (Luxendo, Bruker) light sheet microscope equipped with a 40×/0.8 Nikon objective with a 1.5× tube lens on the detection axis to provide a 60× magnification.

Image deconvolution

The microscope images in Fig 5A and C–C′ were deconvolved with Huygens 16.10.0p3 64b (Scientific Volume Imaging B.V.).

Analyses of expression patterns and levels in *Arabidopsis*

For the comparison of relative fluorescence levels in the SCN of 5-day-old *Arabidopsis* seedlings expressing either transcriptionally FP tagged PLT3 (pPLT3::erCFP) or translationally FP tagged *PLT3* (pPLT3::PLT3-YFP) driven by the endogenous PLT3 promoter in either the *Col* wild type or the *wox5-1* mutant, images were acquired with constant settings per FP. A ZEISS LSM880 confocal microscope was used. The mean fluorescence levels were measured with Fiji (Schindelin *et al*, 2012) in equally sized rectangular ROIs including the QC and CSC positions in the SCN. The thereby generated values were normalized to the *Col* mean fluorescence intensity and visualized in box and scatter plots created with Origin 2018b (OriginLab Corporation).

Images of the root tips of 5 day old *Arabidopsis* seedlings expressing *mVenus-NLS* driven by the endogenous WOX5 promoter in *Col* and *plt2* or *plt3-1* single mutants and the *plt2,plt3* double mutant were acquired. Additionally, z-stacks through the QC region of the roots were recorded to get a transversal view of the QC. The visualization and counting of nuclei with *WOX5* expression (Fig 2) was done with Imaris (version 9.1.2, Bitplane, Oxford Instruments plc). Box and scatter plots showing the number of expressing nuclei were created with Origin 2018b and 2020b (OriginLab Corporation). For the heat-map images, 10 acquired images were overlaid with Fiji (Schindelin *et al*, 2012) and the resulting fluorescence distribution was displayed with a 16-colors lookup table. To calculate the area of lateral *WOX5* expression in the QC region, a freehand-ROI surrounding the expressing cells was created in every image with Fiji (Schindelin *et al*, 2012). The ROI-areas were visualized in box and scatter plots, and all statistical analyses were carried by using Origin 2018b and 2020b (OriginLab Corporation).

Measurement of *PLT3* expression upon WOX5 induction

For qPCR analyses of *PLT3* expression after WOX5 induction, *Arabidopsis thaliana* p35S:WOX5-GR seeds were sterilized, stratified, and sown on GM plates without sucrose as described above onto a 20 μm nylon mesh for easy and fast transfer. The seedlings were grown under continuous light conditions at 21°C and 60% humidity for 5 days. For cycloheximide (CHX) and CHX + dexamethasone (DEX) treatments, the seedlings were transferred to GM plates without sucrose containing 10 μM CHX (Sigma) for 15 min and then transferred to GM plates without sucrose containing 10 μM CHX or 10 μM CHX and 20 μM DEX (Sigma), respectively. For DEX induction tests, seedlings were transferred to GM plates without sucrose containing 20 μM DEX. As a control, seedlings were transferred to GM plates without sucrose containing 10 μM DMSO. To ensure uptake of CHX and/or DEX, seedlings were additionally sprayed with a solution containing 0.1% Tween-20 and 10 μM CHX or 20 μM DEX or both. Isolation of RNA from roots was performed with the "RNeasy Plant Mini Kit" (Qiagen). For cDNA synthesis, 1 μg total root RNA per sample was reverse-transcribed using SuperScript III first strand synthesis kit (Invitrogen) according to the manufacturer's protocol. Quantitative real-time PCR (qPCR) was performed using Luna® Universal qPCR Master Mix (NEB) according to manufacturer's instructions on a Stratagene Mx3005P (Agilent technologies). Data normalization was performed as described before and *ACTIN* used as reference gene (Livak & Schmittgen, 2001). qPCR primers are listed in Appendix Table S13.

F1 generation seeds of a crossing of *Arabidopsis* lines carrying 35S::WOX5-GFP-GR or pPLT3::erCFP in *Col-0* background were grown as described above at 21°C and continuous light for 5 days. For DEX induction, seedlings were treated with 20 μM DEX. Images were taken 4 or 21 h after treatment, respectively. To visualize the cell walls, seedlings were mounted in 25 μM propidium iodide staining solution prior to imaging. Imaging was carried out with a ZEISS LSM780, with two different tracks: Track 1 was used for simultaneous detection of GFP and PI with a 488/561 nm beam splitter, track 2 was used for CFP detection with a 458 nm beam splitter. GFP was excited at 488 nm and was detected at 500–535 nm and PI was

excited at 561 nm and was detected at 597–663 nm. CFP was excited at 458 nm and was detected at 464–509 nm and tracks were acquired framewise to avoid crosstalk. Laser power and detector gain were kept the same during the experiment and the same acquisition settings were used for all images. For quantification of fluorescence intensities, three different ROIs were chosen with a size of 200 × 150 or 70 × 180 pixels, respectively, and were arranged at the same location within the root during the experiment. For each ROI, the ratio of CFP to GFP fluorescence intensity was calculated and normalized to the control group of the same ROI.

FLIM measurements

FLIM was performed either in *N. benthamiana* leaf epidermal cells expressing the desired gene combinations or in roots of 6-10 dag old *Col-0 Arabidopsis* seedlings expressing WOX5-mVenus and PLT3-mCherry with their endogenous promoters. The FLIM measurements of the SCNs in *Arabidopsis* were performed in LRPs due to higher fluorescence levels and less movement during measurements compared to the main RAM. mVenus-tagged proteins were always used as donor and mCherry-tagged proteins as acceptor for FRET. A ZEISS LSM 780 was used for the experiments equipped with a time correlated single-photon counting device (Hydra Harp 400, PicoQuant GmbH). The mVenus donor was excited with a linearly polarized diode laser (LDH-D-C-485) at 485 nm and a pulse frequency of 32 MHz. The excitation power was adjusted to 0.1–0.5 μW at the objective (C-Apochromat 40×/1.2 W Corr M27, ZEISS) for experiments in *N. benthamiana* and 1.5–2 μW for experiments in *Arabidopsis*. The higher laser power in *Arabidopsis* was needed due to lower fluorescence levels. τ-SPAD single photon counting modules with 2 channel detection units (PicoQuant GmbH) and a bandpass filter (534/30) were used to detect parallel and perpendicular polarized emission of the mVenus fluorescence. Images were acquired with a frame size of 256 × 256 pixel, a pixel dwell time of 12.6 μs and a zoom factor of 8. 40–60 frames were recorded in the *N. benthamiana* experiments, 80 frames in the experiments performed in *Arabidopsis*.

Fluorescent lifetimes were obtained by further analyses of the acquired data with SymPhoTime64 (PicoQuant GmbH). The instrument response function (IRF) of the microscope hardware is needed for fluorescence lifetime calculation to correct the system-specific internal time lag between laser pulse and data acquisition. The IRF was recorded preliminary to each experiment by time-correlated single photon counting (TCSPC) of an aqueous solution of erythrosine B in saturated potassium iodide. For data analysis of *N. benthamiana* experiments, an intensity threshold of 100–200 photons per pixel was applied to remove background fluorescence and a monoexponential fit was used. Due to low fluorescence intensities in *Arabidopsis* experiments, no threshold was applied to obtain the maximal possible photon number. In this case, a two-exponential fit was used to separate the mVenus fluorescence signal from the background fluorescence created by the plant tissue. This results in two lifetimes whereof one matches with the mVenus fluorescence lifetime of about 3 ns and the other representing the very short background lifetime of < 0.4 ns. All data were obtained in at least two independent experiments. For visualization of the lifetimes, box and scatter plots were created with Origin 2020b (OriginLab Corporation). Lifetime images of representative measurements were created with a pixel wise FLIM-fit in SymPhoTime64 (PicoQuant GmbH). The line graph showing the lifetime difference between the bodies and the nucleoplasm of WOX5-mVenus co-expressed with PLT3-mCherry was created using Excel (Microsoft Office 365 ProPlus, Microsoft Corporation).

Statistical testing

Data were tested for normal distribution by Kolmogorov-Smirnov testing. In case of normal distribution below 0.05 niveau, the data were subsequently analyzed by one-way ANOVA and *post-hoc* Holm–Sidak multiple comparisons test with a = 0.01 to identify statistically significant differences. In case of non-normal distribution of the data, the non-parametric Kruskal–Wallis ANOVA with subsequent Dunn's test was used to test for statistical significance (a = 0.01). Statistical tests were carried out in Origin 2020b (OriginLab Corporation) or in R.

Prediction of protein domains

The PrDs in the WOX5, PLT1, PLT2, and PLT3 aa sequences were predicted using the PLAAC application (Lancaster *et al*, 2014). The nuclear localization signals (NLSs) of WOX5 and the studied PLT proteins were predicted using the cNLS Mapper (Kosugi *et al*, 2009) for WOX5 and PLT3 and SeqNLS (Lin & Hu, 2013) for PLT1 and PLT2.

Figure assembly

All figures in this study were assembled using Adobe Photoshop (Adobe Inc.).

Data availability

No primary datasets have been generated and deposited.

Expanded View for this article is available online.

Acknowledgements
We would like to acknowledge funding of R.C.B. by the Deutsche Forschungsgemeinschaft (DFG) through grant Sta1212/1-1 to Y.S. We thank Andrea Bleckmann for sharing the Greengate Cerulean construct, Renze Heidstra, and Ben Scheres for sharing published *Arabidopsis* lines (PLT::PLT-YFP, PLT::CFP, PLT4 cDNA and *plt* mutants). We thank Rüdiger Simon and Thomas Laux for providing seeds of the published 35S::WOX5-GFP-GR and 35S::WOX5-GR *Arabiodpsis thaliana* lines, respectively. We thank Meik H. Thiele for help with statistical analyses. We also thank the Center for Advanced Imaging (CAi) for technical assistance, and Rüdiger Simon and Peter Welters for critical discussion of the manuscript. Open Access funding enabled and organized by Projekt DEAL.

Author contributions
Rebecca C Burkart: Conceptualization; Data curation; Validation; Investigation; Visualization; Methodology; Writing – original draft. **Vivien I Strotmann:** Data curation; Investigation; Writing – review & editing. **Gwendolyn K Kirschner:** Investigation. **Abdullah Akinci:** Investigation. **Laura Czempik:** Investigation. **Anika Dolata:** Investigation; Visualization. **Alexis Maizel:** Investigation; Visualization. **Stefanie Weidtkamp-Peters:** Validation. **Yvonne**

Stahl: Conceptualization; Data curation; Formal analysis; Supervision; Funding acquisition; Validation; Investigation; Methodology; Writing – original draft; Project administration; Writing – review & editing.

In addition to the CRediT author contributions listed above, the contributions in detail are:

YS conceived the project. YS, RCB and VIS designed the experiments, analyzed and interpreted the data. RCB, VIS, AA, AD, LC, and GKK carried out experiments. SW-P contributed to FLIM data analyses. AM carried out light sheet imaging. YS and RCB wrote the manuscript. All authors commented on the manuscript.

Disclosure and competing interests statement

The authors declare that they have no conflict of interest.

References

Aguzzi A, Nuvolone M, Zhu C (2013) The immunobiology of prion diseases. *Nat Rev Immunol* 13: 888 – 902

Aida M, Beis D, Heidstra R, Willemsen V, Blilou I, Galinha C, Nussaume L, Noh Y-S, Amasino R, Scheres B (2004) The PLETHORA genes mediate patterning of the Arabidopsis root stem cell niche. *Cell* 119: 109 – 120

Alberti S, Halfmann R, King O, Kapila A, Lindquist S (2009) A systematic survey identifies prions and illuminates sequence features of prionogenic proteins. *Cell* 137: 146 – 158

Atanesyan L, Günther V, Dichtl B, Georgiev O, Schaffner W (2012) Polyglutamine tracts as modulators of transcriptional activation from yeast to mammals. *Biol Chem* 393: 63 – 70

Bailey CH, Kandel ER, Si K (2004) The persistence of long-term memory: a molecular approach to self-sustaining changes in learning-induced synaptic growth. *Neuron* 44: 49 – 57

Benfey PN, Scheres B (2000) Root development. *Curr Biol* 10: 13

Berckmans B, Kirschner G, Gerlitz N, Stadler R, Simon R (2020) CLE40 signaling regulates root stem cell fate. *Plant Physiol* 182: 1776 – 1792

van den Berg C, Willemsen V, Henriks G, Weisbeek P, Scheres B (1997) Short-range control of cell differentiation in the *Arabidopsis* root meristem. *Nature* 390: 287 – 289

Bleckmann A, Weidtkamp-Peters S, Seidel CAM, Simon R (2010) Stem cell signaling in *Arabidopsis* requires CRN to localize CLV2 to the plasma membrane. *Plant Physiol* 152: 166 – 176

Castilla-Llorente V, Ramos A (2014) PolyQ-mediated regulation of mRNA granules assembly. *Biochem Soc Trans* 42: 1246 – 1250

Chakrabortee S, Kayatekin C, Newby GA, Mendillo ML, Lancaster A, Lindquist S (2016) Luminidependens (LD) is an *Arabidopsis* protein with prion behavior. *Proc Natl Acad Sci USA* 113: 6065 – 6070

Cruz-Ramírez A, Díaz-Triviño S, Wachsman G, Du Y, Arteága-Vázquez M, Zhang H, Benjamins R, Blilou I, Neef AB, Chandler V *et al* (2013) A SCARECROW-RETINOBLASTOMA protein network controls protective quiescence in the *Arabidopsis* root stem cell organizer. *PLoS Biol* 11: e1001724

Cuevas-Velazquez CL, Dinneny JR (2018) Organization out of disorder: liquid-liquid phase separation in plants. *COPB* 45: 68 – 74

Curtis MD, Grossniklaus U (2003) A gateway cloning vector set for high-throughput functional analysis of genes in planta. *Plant Physiol* 133: 462 – 469

Denninger P, Reichelt A, Schmidt VAF, Mehlhorn DG, Asseck LY, Stanley CE, Keinath NF, Evers J-F, Grefen C, Grossmann G (2019) Distinct RopGEFs successively drive polarization and outgrowth of root hairs. *Curr Biol* 29: 1854 – 1865.e5

Ding Z, Friml J (2010) Auxin regulates distal stem cell differentiation in *Arabidopsis* roots. *Proc Natl Acad Sci USA* 107: 12046 – 12051

Dolan L, Janmaat K, Willemsen V, Linstead P, Poethig S, Roberts K, Scheres B (1993) Cellular organisation of the *Arabidopsis thaliana* root. *Development* 119: 71 – 84

Drisch RC, Stahl Y (2015) Function and regulation of transcription factors involved in root apical meristem and stem cell maintenance. *Front Plant Sci* 6: 505

Du Y, Scheres B (2017) PLETHORA transcription factors orchestrate de novo organ patterning during *Arabidopsis* lateral root outgrowth. *Proc Natl Acad Sci USA* 114: 11709 – 11714

Fang X, Wang L, Ishikawa R, Li Y, Fiedler M, Liu F, Calder G, Rowan B, Weigel D, Li P *et al* (2019) *Arabidopsis* FLL2 promotes liquid-liquid phase separation of polyadenylation complexes. *Nature* 569: 265 – 269

Forzani C, Aichinger E, Sornay E, Willemsen V, Laux T, Dewitte W, Murray JAH (2014) WOX5 suppresses CYCLIN D activity to establish quiescence at the center of the root stem cell niche. *Curr Biol* 24: 1939 – 1944

Galinha C, Hofhuis H, Luijten M, Willemsen V, Blilou I, Heidstra R, Scheres B (2007) PLETHORA proteins as dose-dependent master regulators of *Arabidopsis* root development. *Nature* 449: 1053 – 1057

Gerber H, Seipel K, Georgiev O, Hofferer M, Hug M, Rusconi S, Schaffner W (1994) Transcriptional activation modulated by homopolymeric glutamine and proline stretches. *Science* 263: 808 – 811

Jung J-H, Barbosa AD, Hutin S, Kumita JR, Gao M, Derwort D, Silva CS, Lai X, Pierre E, Geng F *et al* (2020) A prion-like domain in ELF3 functions as a thermosensor in *Arabidopsis*. *Nature* 585: 256 – 260

Kim HJ, Kim NC, Wang Y-D, Scarborough EA, Moore J, Diaz Z, MacLea KS, Freibaum B, Li S, Molliex A *et al* (2013) Mutations in prion-like domains in hnRNPA2B1 and hnRNPA1 cause multisystem proteinopathy and ALS. *Nature* 495: 467 – 473

Kosugi S, Hasebe M, Tomita M, Yanagawa H (2009) Systematic identification of cell cycle-dependent yeast nucleocytoplasmic shuttling proteins by prediction of composite motifs. *Proc Natl Acad Sci USA* 106: 10171 – 10176

Kottenhagen N, Gramzow L, Horn F, Pohl M, Theißen G (2012) Polyglutamine and polyalanine tracts are enriched in transcription factors of plants. *German conference on Bioinformatics*

Lampropoulos A, Sutikovic Z, Wenzl C, Maegele I, Lohmann JU, Forner J (2013) GreenGate - a novel, versatile, and efficient cloning system for plant transgenesis. *PLoS One* 8: e83043

Lancaster AK, Nutter-Upham A, Lindquist S, King OD (2014) PLAAC: a web and command-line application to identify proteins with prion-like amino acid composition. *Bioinformatics* 30: 2501 – 2502

Lin J-R, Hu J (2013) SeqNLS: nuclear localization signal prediction based on frequent pattern mining and linear motif scoring. *PLoS One* 8: e76864

Livak KJ, Schmittgen TD (2001) Analysis of relative gene expression data using real-time quantitative PCR and the 2(-Delta Delta C(T)) Method. *Methods* 25: 402 – 408

Lu R, Canher B, Bisht A, Heyman J, de Veylder L (2021) Three-dimensional quantitative analysis of the *Arabidopsis* quiescent center. *J Exp Bot* 72: 6789 – 6800

de Luis Balaguer MA, Fisher AP, Clark NM, Fernandez-Espinosa MG, Möller BK, Weijers D, Lohmann JU, Williams C, Lorenzo O, Sozzani R (2017) Predicting gene regulatory networks by combining spatial and temporal gene expression data in *Arabidopsis* root stem cells. *Proc Natl Acad Sci USA* 114: E7632 – E7640

Macknight R, Bancroft I, Page T, Lister C, Schmidt R, Love K, Westphal L, Murphy G, Sherson S, Cobbett C *et al* (1997) FCA, a gene controlling flowering time in *Arabidopsis*, encodes a protein containing RNA-binding domains. *Cell* 89: 737 – 745

Mähönen AP, ten Tusscher K, Siligato R, Smetana O, Díaz-Triviño S, Salojärvi J, Wachsman G, Prasad K, Heidstra R, Scheres B (2014) PLETHORA gradient formation mechanism separates auxin responses. *Nature* 515: 125 – 129

Mao YS, Zhang B, Spector DL (2011) Biogenesis and function of nuclear bodies. *Trends Genet* 27: 295 – 306

McSwiggen DT, Mir M, Darzacq X, Tjian R (2019) Evaluating phase separation in live cells: diagnosis, caveats, and functional consequences. *Genes Dev* 33: 1619 – 1634

Meyer HM (2020) In search of function: nuclear bodies and their possible roles as plant environmental sensors. *COPB* 58: 33 – 40

Michelitsch MD, Weissman JS (2000) A census of glutamine/asparagine-rich regions: implications for their conserved function and the prediction of novel prions. *Proc Natl Acad Sci USA* 97: 11910 – 11915

von Mikecz A (2009) PolyQ fibrillation in the cell nucleus: who's bad? *Trends Cell Biol* 19: 685 – 691

Pardal R, Heidstra R (2021) Root stem cell niche networks: it's complexed! Insights from *Arabidopsis*. *J Exp Bot* 72: 6727 – 6738

Pi L, Aichinger E, van der Graaff E, Llavata-Peris CI, Weijers D, Hennig L, Groot E, Laux T (2015) Organizer-derived WOX5 signal maintains root columella stem cells through chromatin-mediated repression of CDF4 expression. *Dev Cell* 33: 576 – 588

Sarkar AK, Luijten M, Miyashima S, Lenhard M, Hashimoto T, Nakajima K, Scheres B, Heidstra R, Laux T (2007) Conserved factors regulate signalling in *Arabidopsis thaliana* shoot and root stem cell organizers. *Nature* 446: 811 – 814

Savina MS, Pasternak T, Omelyanchuk NA, Novikova DD, Palme K, Mironova VV, Lavrekha VV (2020) Cell dynamics in WOX5-overexpressing root tips: the impact of local auxin biosynthesis. *Front Plant Sci* 11: 560169

Scarafone N, Pain C, Fratamico A, Gaspard G, Yilmaz N, Filée P, Galleni M, Matagne A, Dumoulin M (2012) Amyloid-like fibril formation by polyQ proteins: a critical balance between the polyQ length and the constraints imposed by the host protein. *PLoS One* 7: e31253

Schindelin J, Arganda-Carreras I, Frise E, Kaynig V, Longair M, Pietzsch T, Preibisch S, Rueden C, Saalfeld S, Schmid B *et al* (2012) Fiji: an open-source platform for biological-image analysis. *Nat Methods* 9: 676 – 682

Schomburg FM, Patton DA, Meinke DW, Amasino RM (2001) FPA, a gene involved in floral induction in *Arabidopsis*, encodes a protein containing RNA-recognition motifs. *Plant Cell* 13: 1427 – 1436

Schwechheimer C, Smith C, Bevan MW (1998) The activities of acidic and glutamine-rich transcriptional activation domains in plant cells: design of modular transcription factors for high-level expression. *Plant Mol Biol* 36: 195 – 204

Shimotohno A, Heidstra R, Blilou I, Scheres B (2018) Root stem cell niche organizer specification by molecular convergence of PLETHORA and SCARECROW transcription factor modules. *Genes Dev* 32: 1085 – 1100

Shorter J, Lindquist S (2005) Prions as adaptive conduits of memory and inheritance. *Nat Rev Genet* 6: 435 – 450

Sonmez C, Bäurle I, Magusin A, Dreos R, Laubinger S, Weigel D, Dean C (2011) RNA 3′ processing functions of *Arabidopsis* FCA and FPA limit intergenic transcription. *Proc Natl Acad Sci USA* 108: 8508 – 8513

Stahl Y, Grabowski S, Bleckmann A, Kühnemuth R, Weidtkamp-Peters S, Pinto K, Kirschner G, Schmid J, Wink RH, Hülsewede A *et al* (2013) Moderation of *Arabidopsis* root stemness by CLAVATA1 and *Arabidopsis* CRINKLY4 receptor kinase complexes. *Curr Biol* 23: 362 – 371

Stahl Y, Wink RH, Ingram GC, Simon R (2009) A signaling module controlling the stem cell niche in *Arabidopsis* root meristems. *Curr Biol* 19: 909 – 914

Totzeck F, Andrade-Navarro MA, Mier P (2017) The protein structure context of PolyQ regions. *PLoS One* 12: e0170801

Truernit E, Bauby H, Dubreucq B, Grandjean O, Runions J, Barthélémy J, Palauqui J-C (2008) High-resolution whole-mount imaging of three-dimensional tissue organization and gene expression enables the study of Phloem development and structure in *Arabidopsis*. *Plant Cell* 20: 1494 – 1503

Vilarrasa-Blasi J, González-García M-P, Frigola D, Fàbregas N, Alexiou K, López-Bigas N, Rivas S, Jauneau A, Lohmann J, Benfey P *et al* (2014) Regulation of plant stem cell quiescence by a brassinosteroid signaling module. *Dev Cell* 30: 36 – 47

Zhang X, Henriques R, Lin S-S, Niu Q-W, Chua N-H (2006) Agrobacterium-mediated transformation of *Arabidopsis thaliana* using the floral dip method. *Nat Protoc* 1: 641 – 646

Chapter 6

Stem cell homeostasis in the root of *Arabidopsis* is regulated by cell type specific complex formation of key transcription factors

This manuscript was uploaded to the preprint server bioRxiv and submitted to Review Commons in April 2024.

https://doi.org/10.1101/2024.04.26.591257

Authors

Vivien I. Strotmann[1], Monica L. García-Gómez[3,4,5], Yvonne Stahl[1,2,‡*]

Affiliation

[1]Institute for Developmental Genetics, Heinrich-Heine University, Universitätsstraße 1, 40225 Düsseldorf, Germany

[2]Cluster of Excellence on Plant Sciences (CEPLAS), Heinrich-Heine University, Universitätsstraße 1, 40225 Düsseldorf, Germany

[3]Theoretical Biology and Bioinformatics (IBB), Utrecht University, Heidelberglaan 8, 3584 CS Utrecht, The Netherlands

[4]Experimental and Computational Plant Development (IEB), Utrecht University, Heidelberglaan 8, 3584 CS Utrecht, The Netherlands

[5]CropXR Institute, The Netherlands

[‡]Present address: Institute for Molecular Biosciences, Goethe-Universität, Max-von-Laue Str. 9, 60438 Frankfurt am Main, Germany

*corresponding author

Author contribution

All experiments of this study were conducted by me except for the modelling. Additionally, the manuscript was mainly written by me.

Stem cell homeostasis in the root of *Arabidopsis* involves cell type specific complex formation of key transcription factors

Vivien I. Strotmann[1], Monica L. García-Gómez[3,4,5], Yvonne Stahl[1,2,‡*]

Affiliation

[1]Institute for Developmental Genetics, Heinrich-Heine University, Universitätsstraße 1, 40225 Düsseldorf, Germany

[2]Cluster of Excellence on Plant Sciences (CEPLAS), Heinrich-Heine University, Universitätsstraße 1, 40225 Düsseldorf, Germany

[3]Theoretical Biology and Bioinformatics (IBB), Utrecht University, Padualaan 8, 3584 CS Utrecht, The Netherlands

[4]Experimental and Computational Plant Development (IEB), Utrecht University, Padualaan 8, 3584 CS Utrecht, The Netherlands

[5]CropXR Institute, The Netherlands

*Correspondence should be addressed to Y.S. (email: y.stahl@bio.uni-frankfurt.de)

‡Present address: Institute for Molecular Biosciences, Goethe-Universität, Max-von-Laue Str. 9, 60438 Frankfurt am Main, Germany

Key words: mathematical modelling; root stem cell niche; FRET-FLIM; transcription factor complexes; PLTs; WOX5; BRAVO

Date of submission: 26/04/2024

Number of Figures: 8

Total word count: 7603

Abstract

In *Arabidopsis thaliana*, the stem cell niche (SCN) within the root apical meristem (RAM) is maintained by an intricate regulatory network that ensures optimal growth and high developmental plasticity. Yet, many aspects of this regulatory network of stem cell quiescence and replenishment are still not fully understood. Here, we investigate the interplay of the key transcription factors (TFs) BRASSINOSTEROID AT VASCULAR AND ORGANIZING CENTRE (BRAVO), PLETHORA 3 (PLT3) and WUSCHEL-RELATED HOMEOBOX 5 (WOX5) involved in SCN maintenance. Phenotypical analysis of mutants involving these TFs uncover their combinatorial regulation of cell fates and divisions in the SCN. Moreover, interaction studies employing Fluorescence resonance energy transfer fluorescence lifetime imaging microscopy (FRET-FLIM) in combination with novel analysis methods, allowed us to quantify protein-protein interaction (PPI) affinities as well as higher-order complex formation of these TFs. We integrated our experimental results into a computational model, suggesting that cell type specific profiles of protein complexes and characteristic complex formation, that is also dependent on prion-like domains in PLT3, contribute to the intricate regulation of the SCN. We propose that these unique protein complex ‘signatures’ could serve as a read-out for cell specificity thereby adding another layer to the sophisticated regulatory network that balances stem cell maintenance and replenishment in the *Arabidopsis* root.

Introduction

As sessile organisms, plants must cope with environmental challenges and adapt their growth and development accordingly, as they cannot escape adverse conditions. The root system of higher plants plays a pivotal role for the plant's fitness, as it provides anchorage to the soil and access to water and nutrients. To ensure high developmental plasticity, plants maintain a reservoir of stem cells that reside in the root apical meristem (RAM) at the tip of the root. In *Arabidopsis thaliana* (*A. thaliana*), the center of the RAM harbours a group of slowly dividing, pluripotent stem cells termed the quiescent centre (QC). The QC exerts two key functions: first it produces the surrounding tissue-specific stem cells, also referred to as initials, which by asymmetric cell divisions give rise to different cell types from the outside to the inside: epidermis/lateral root cap, cortex, endodermis, pericycle and stele, as well as the columella at the root tip (Fig. 1 G). Second, the QC serves as signalling hub to maintain the surrounding stem cells in a non-cell autonomous manner (Dolan *et al.*, 1993; van den Berg *et al.*, 1997; Benfey and Scheres, 2000). The balance between QC quiescence and stem cell replenishment has to be maintained throughout the entire life cycle of a plant and therefore requires fine-tuned regulation, necessitating phytohormones, receptors and their ligands as well as several key transcription factors (TFs) (García-Gómez *et al.*, 2021; Strotmann and Stahl, 2021).

The homeodomain TF WUSCHEL-RELATED HOMEOBOX 5 (WOX5) was shown to act as a key regulator for stem cell maintenance in the root (Sarkar *et al.*, 2007). By repressing *CYCLIN D3;3* (*CYCD3;3*) and *CYCLIN D1;1* (*CYCD1;1*), WOX5 inhibits periclinal cell divisions in the QC (Forzani *et al.*, 2014). Furthermore, WOX5 preserves the undifferentiated status of the columella stem cells (CSCs) by repressing *CYCLING DOF FACTOR 4* (*CDF4*), which involves the recruitment of TOPLESS (TPL) and HISTONE DEACETYLASE 19 (HDA19) (Pi *et al.*, 2015). Recent findings suggest that to control the balance between maintaining the stem cell fate of CSCs and their differentiation, WOX5 also interacts with the auxin-dependent APETALA2-type TF PLETHORA 3 (PLT3) (Burkart *et al.*, 2022). The *PLT* gene family comprises six members that are described as master regulators of root development (Aida *et al.*, 2004; Galinha *et al.*, 2007; Mähönen *et al.*, 2014). While PLT5 and 7 are mainly involved in lateral root development (Hofhuis *et al.*, 2013; Du and Scheres, 2017), PLT1-4 are expressed in the main root forming instructive

protein gradients that are necessary for correct QC positioning and cell fate decisions (Aida *et al.*, 2004; Galinha *et al.*, 2007; Mähönen *et al.*, 2014). Interestingly, loss of PLT3 or WOX5 function, as observed in *plt3-1* and *wox5-1* mutants, causes an increase of QC divisions (Sarkar *et al.*, 2007; Pi *et al.*, 2015; Burkart *et al.*, 2022). This phenotype is even more severe in the *plt3 wox5* double mutant indicating that PLT3 and WOX5 act in parallel pathways to control stem cell maintenance in the root (Burkart *et al.*, 2022).

In the past decade the brassinosteroids (BRs), a class of phytohormones, were described to play an important role in the regulation of the root stem cell niche (SCN) maintenance (González-García *et al.*, 2011). In the *Arabidopsis* RAM, BRs act via the R2R3-MYB TF BRASSINOSTEROIDS AT VASCULAR AND ORGANIZING CENTRE (BRAVO) which inhibits QC divisions and is negatively regulated by the BR-dependent repressor complex formed by BRI1-EMS-SUPPRESSOR 1 (BES1) and TPL on transcript and protein level (Vilarrasa-Blasi *et al.*, 2014; Espinosa-Ruiz *et al.*, 2017). Recently, the ability of BRAVO to control formative QC divisions was linked to WOX5 (Betegón-Putze *et al.*, 2021), as *bravo-2* mutants, like *wox5-1* mutants, show an increased frequency of QC divisions (Sarkar *et al.*, 2007; Pi *et al.*, 2015; Betegón-Putze *et al.*, 2021; Burkart *et al.*, 2022).

In addition to the described genetic interactions, one-on-one protein-protein interactions (PPIs) have been reported for WOX5 and PLT3 as well as for BRAVO and WOX5 (Betegón-Putze *et al.*, 2021; Burkart *et al.*, 2022). However, It is still unknown whether these TFs can also form higher order complexes. Additionally, it remains elusive how these genetic and physical interactions could possibly influence the regulation of stem cell maintenance. To unravel the underlying interplay of key TFs in the root SCN, we used an integrative experimental and computational approach to analyze the protein complex formation between WOX5, PLT3 and BRAVO in the cells of the root SCN. Here, we show that cell type specific profiles of protein complexes are formed and align their occurrence with phenotypical SCN defects of the respective mutants. Moreover, by the deletion of specific interaction sites, we could demonstrate that heterodimerization contributes to maintaining stem cells in the root. Altogether, our results suggest that these unique protein complex ‘signatures’ convey cell type specificity and could explain the different roles played by BRAVO, PLT3 and WOX5 in root SCN maintenance.

Results

BRAVO, PLT3 and WOX5 exhibit cell type specific differences in protein abundance in the root SCN

First, we analysed the absolute and relative abundance of BRAVO, PLT3 and WOX5 protein levels in the different cell types found in the SCN of the *Arabidopsis* root, focusing on the stele initials (SIs), QC, CSCs and columella cells (CCs) (Fig. 1 G), by measuring the fluorescence intensity of mVenus (mV) in nuclei of the previously described *pPLT3:PLT3-mV* and *pWOX5:WOX5-mV* translational reporters in *Col-0* WT background (Burkart *et al.*, 2022). Additionally, we generated a stable transgenic *Arabidopsis* line expressing *pBRAVO:BRAVO-mV* also in the *Col-0* WT background. We used the same microscopy settings for these quantifications to ensure that the detected protein levels are comparable. Consistent with previous findings, BRAVO protein levels are highest in the SIs and gradually decrease towards the CCs (Fig. 1 A, B) (Vilarrasa-Blasi *et al.*, 2014). PLT3 levels are similar in SIs, QC and CSCs, but notably lower in the CCs (Fig. 1 C, D). WOX5 protein levels peak in the QC, decrease in the adjacent SIs and CSCs and are almost completely absent in CCs (Fig. 1 E, F).

We summarized our findings in a protein abundance profile for each individual cell type displaying relative protein levels of BRAVO, PLT3 and WOX5. The protein levels are normalized to the overall maximum intensity, which was found for BRAVO in SIs (Fig. 1 H). Accordingly, We found that BRAVO is the most abundant protein in the SIs, followed by PLT3 and WOX5 in descending order. Conversely, in the QC, we observe a contrasting pattern, marked by WOX5 as the most abundant protein, followed by PLT3 and BRAVO. PLT3 emerges as the predominant protein in the adjacent CSCs, accompanied by low levels of WOX5 and BRAVO protein. In differentiated CCs, WOX5 and BRAVO are almost absent and only low levels of PLT3 can be found. Interestingly, while all of these regulators are expressed in several root SCN cells, our observations reveal quantitative differences in protein abundance that can be combined into a cell type specific ‘fingerprint’. This provides a comprehensive snapshot of the unique protein levels within each cellular context, which could act as an instructive output of cell type specification (Fig. 1 H).

BRAVO, PLT3 and WOX5 jointly control CSC fate and QC divisions

Several studies have highlighted the inhibitory effect of BRAVO, PLT3 and WOX5 on QC divisions and CSC differentiation in the *Arabidopsis* root (Aida *et al.*, 2004; Galinha *et al.*, 2007; Vilarrasa-Blasi *et al.*, 2014; Mähönen *et al.*, 2014; Forzani *et al.*, 2014; Pi *et al.*, 2015). While all three proteins have been demonstrated to be present in the QC and CSCs, a combinatory effect on QC division and CSC fate has only been demonstrated for WOX5 and PLT3 (Burkart *et al.*, 2022) as well as for WOX5 and BRAVO (Betegón-Putze *et al.*, 2021). Notably, such interplay has not been observed for BRAVO and PLT3, nor for the simultaneous involvement of all three proteins.

To address this, we have performed SCN stainings, that combines 5-ethynyl-2'-deoxyuridine (EdU) and modified pseudo Schiff base propidium iodide (mPS-PI) stainings (Burkart *et al.*, 2022), in several single and multiple mutants. This allowed us to analyse the differentiation status of the distal meristem, as well as the number of QC divisions that occurred within the last 24 h within the same root. To quantify CSC layers, the number of cell layers that lack starch granules distally to the QC were counted. In *Col-0* WT, 68 % of the roots show one CSC layer, whereas only 2 % of the roots lack the starch-free CSC layer and 30 % show two CSC layers, most likely because they have recently divided (Fig. 2 A, B, J, Fig. S1 A). In *bravo-2* and *plt3-1* single mutants, the number of roots showing no CSC layer increases to 11 % and 12 %, respectively (Fig. 2 C, D, J, Fig. S1 B, C). Interestingly, the number of roots displaying no starch-free CSC layer increased to 37 % in *bravo plt3* double mutants (Fig. 2 F, J, Fig. S1 F). This additive effect indicates that PLT3 and BRAVO act in parallel pathways to control CSC differentiation. In 53 % of the *wox5-1* mutant roots, the starch-free CSC layer is missing (Fig. 2 E, J, Fig. S1 D), further emphasizing the importance of WOX5 for CSC fate (Sarkar *et al.*, 2007; Pi *et al.*, 2015; Burkart *et al.*, 2022). Additionally, the *bravo wox5* and the *plt3 wox5* double mutants show an even higher percentage of roots lacking the starch-free CSC, 90 % and 74 % respectively, compared to the single mutants and the *bravo plt3* double mutants (Fig. 2 G, H, J, Fig. S1 E, G). On the other hand, the *bravo plt3 wox5* triple mutant, with 85 % of the roots having a differentiated CSC layer, resembles the *bravo wox5* and *plt3 wox5* double mutants (Fig. 2 I, J, Fig. S1 H). These results suggest that BRAVO, PLT3 and WOX5 jointly control CSC fate.

Additionally, the quantification of QC divisions was performed by counting the number of EdU-stained nuclei within an optical transversal section through the RAM as described in (Burkart *et al.*, 2022). QC cells were identified by their relative position within the RAM, directly below the vascular initials and surrounded by CEIs in a circular arrangement (Fig. 2 K). In the WT, 57 % of the roots do not show any QC cell divisions, and 35 % show one QC cell division (Fig. 2 L, T, Fig. S1 A). In 6 % and 2 % of the analysed roots, two and three QC divisions could be observed, respectively, so that in total 43 % of the analysed roots showed EdU-stained QC cells. In *bravo*-2 and *plt3-1* single mutants, the number of roots showing at least one EdU-stained QC cell increased to 78 % and 73 %, respectively (Fig. 2 M, N, T, Fig. S1 B, C). This phenotype is even more severe in *wox5-1* mutants, where at least one EdU-stained QC cell could be observed in 86 % of the roots (Fig. 2 O, T, Fig. S1 D). Like the above-described additive effects of CSC differentiation in the double and triple mutants, the number of roots showing at least one QC cell division increases to 100 % and 98 % in the *bravo wox5* and *plt3 wox5* double mutants, respectively (Fig. 2 P-R, T, Fig. S1 E-G). Additionally, the double mutants show a strongly increased frequency of four divided QC cells in comparison to the respective single mutants: 7 % in the *bravo plt3* double mutant, 36 % in the *bravo wox5* double mutant and 30 % in the *plt3 wox5* double mutant in comparison to 3 %, 0 % and 11 % in the *bravo-2*, *plt3-1* and *wox5-1* single mutants, respectively. A further increase in EdU-stained QC cells can be observed in the *bravo plt3 wox5* triple mutant where 44 % of the roots display a completely divided QC (Fig. 2 S, T, Fig. S1 H). These observations indicate that BRAVO, PLT3 and WOX5 jointly control QC divisions, which may also involve other factors, e. g. SHORT-ROOT (SHR) and SCARECROW (SCR) (Cruz-Ramírez *et al.*, 2013; Long *et al.*, 2017; Clark *et al.*, 2020).

Furthermore, we also examined if the QC exhibits extra periclinal cell divisions, which in *Col-0* WT occurs only in 4 % of the roots (Fig. S1 I, K). This phenotype manifests in 85 % of *bravo-2* mutants (Fig. S1 J, K). Additional periclinal cell divisions can also be observed in 43 % of *plt3-1* single mutants and in 62 % *wox5-1* single mutants (Fig. S1 K). In contrast to the number of EdU-stained QC cells, the frequency of periclinal cell divisions are relatively similar in the double or triple mutants, with 77 %, 84 %, 79 % and 85 % of the roots showing additional periclinal cell divisions of the QC cells in the *bravo plt3*, *bravo wox5*, *plt3 wox5* and *bravo plt3*

wox5 mutants, respectively (Fig. S1 K). This effect has already been described for *wox5-1* and *bravo-2* single mutants in comparison to the *bravo wox5* double mutant in earlier studies (Betegón-Putze *et al.*, 2021).
Taken together, our findings suggest a combinatory effect of BRAVO, PLT3, and WOX5 on QC division frequency and CSC fate decision.

BRAVO, PLT3 and WOX5 can form a trimeric complex

In addition to the observed overlapping yet cell type specific protein levels and the genetic interplay of BRAVO, PLT3 and WOX5, recent reports also provide evidence for one-on-one PPIs of BRAVO and WOX5, as well as for PLT3 and WOX5 (Betegón-Putze *et al.*, 2021; Burkart *et al.*, 2022). These findings raised the question if also BRAVO and PLT3 could interact. To address this, we first performed Fluorescence resonance energy transfer fluorescence lifetime imaging microscopy (FRET-FLIM) measurements in transiently expressing *Nicotiana benthamiana* (*N. benthamiana*) abaxial epidermal leaf cells using BRAVO-mV as donor molecule under control of a β-estradiol inducible promoter as described earlier (Burkart *et al.*, 2022). Results of FRET-FLIM measurements are often displayed as the average amplitude-weighted lifetime which is a mixture of differentially decaying components and is calculated by summing each component's lifetime weighted by its respective amplitude. In case of FRET, the fluorescence lifetime decreases and serves as a measure for PPI. This reduction of lifetime results either from a large number of molecules that undergo FRET indicating a high affinity of the two proteins of interest (POIs) or a highly efficient energy transfer which demonstrates high proximity of the POIs and/or favourable fluorophore dipole orientation (Fig. 3. A, B). The use of a novel analysis method allowed us to distinguish between these two scenarios, providing deeper insights into protein affinities, hereafter referred to as 'binding', between BRAVO, PLT3 and WOX5 (Maika *et al.*, 2023).
The reference sample BRAVO-mV (donor-only control) shows an average binding of 2.3 ± 7.4 % (Fig. 3 C) and the negative control composed of BRAVO-mV co-expressed with mCherry-NLS shows a binding of 8.8 ± 4.3 % (Fig. 3 C). A binding of below 10 % is interpreted as no interaction (Maika *et al.*, 2023), cohering with the reference and negative control samples. Upon co-expression of BRAVO-mV with PLT3-mCh, the binding increases to 28.0 ± 11.7 % (Fig. 3 C). To compare this observation with already confirmed interactions of BRAVO with WOX5 (Betegón-

Putze *et al.*, 2021), as well as with BES1 or TPL (Vilarrasa-Blasi *et al.*, 2014), we co-expressed BRAVO-mV with WOX5-mCh or TPL-mCh, which results in binding values of 22.4 ± 14.1 % and 26.7 ± 9.8 %, respectively (Fig. 3 C). Interaction of BRAVO with BES1 was tested by co-expression of BRAVO-mV with BES1D-mCh, which was shown to mimic the dephosphorylated and thereby active form of BES1 and yielded an average binding of 27.4 ± 11.9 %. This suggests similar affinities of BRAVO towards PLT3, BES1 and TPL, but a lower affinity towards WOX5 (Fig. 3 C).

These findings together with previously described interactions of WOX5 with PLT3, TPL or BES1, as well as BES1 and TPL, prompted us to investigate, whether these TFs can also form higher-order complexes (Vilarrasa-Blasi *et al.*, 2014; Espinosa-Ruiz *et al.*, 2017; Betegón-Putze *et al.*, 2021; Burkart *et al.*, 2022). To address this, we used a combination of bimolecular fluorescence complementation (BiFC) and FRET (Fig. 4 A, B) (Kwaaitaal *et al.*, 2010; Maika *et al.*, 2023). Here, the donor fluorophore is split into two fragments: the N-terminal part of mVenus (mV(N)) and the C-terminal part (mV(C)). The interaction of WOX5 and PLT3, which has been described earlier (Burkart *et al.*, 2022), has been shown to have a high affinity (Supplemental table S13). This is why we have chosen to tag WOX5 and PLT3 with mV(N) and mV(C), respectively. In this scenario, the interaction of WOX5 and PLT3 leads to the reconstruction of mV and restores its fluorescence, enabling us to perform FRET-FLIM when co-expressing another acceptor-labelled protein. The ‘donor only’ reference sample WOX5-mV(N) PLT3-mV(C) yields an average binding of 1.6 ± 14.1 %, and the negative control WOX5-mV(N) PLT3-mV(C) with mCherry-NLS shows an average binding of 2.9 ± 5.0 % (Fig. 4 C). Upon co-expression of BES1D-mCh or TPL-mCh, the binding significantly increases to 18.7 ± 8.0 % and 23.3 ± 8.3 %, respectively (Fig. 4 C). Notably, in the presence of BRAVO-mCh, the average binding strongly increases to 36.3 ± 10.7 % (Fig. 4 C). Thus, the heterodimer of WOX5 and PLT3 shows higher affinity to BRAVO, which could suggest an increased probability and stability of the trimeric complex composed of WOX5, PLT3 and BRAVO compared to WOX5, PLT3 and BES1D, or TPL.

To gain further insights into the potential of trimeric complex formation, we conducted additional FRET-FLIM measurements in *N. benthamiana* with rearranged fluorescent tags. Here, the donor fluorophore is shared between BRAVO and PLT3, namely BRAVO-mV(N) and PLT3-mV(C), which also showed high affinity (Fig. 3).

The ‘donor only’ reference sample BRAVO-mV(N) PLT3-mV(C) exhibits an average binding of 2.2 ± 3.6 % (Fig. S2). The negative control composed of BRAVO-mV(N) PLT3-mV(C) and mCherry-NLS shows a similar average binding of 3.2 ± 3.1 % (Fig. S2). Surprisingly, co-expression of BES1D-mCh yields an average binding of only 10.2 ± 5.9 % (Fig. S2), indicating that a trimeric complex composed of BRAVO, PLT3 and BES1D is unlikely to form. Contrary, the co-expression of TPL-mCh or WOX5-mCh leads to a significantly increased average binding of 21.1 ± 8.3 % and 29.8 ± 10.6 %, respectively (Fig. S2). This again suggests that a trimeric complex formed by BRAVO, PLT3 and WOX5 is more stable and occurs with a higher probability. Taken together, these findings reveal the formation of several combinations of protein multimers with different probabilities of occurrence as judged by their binding capacities. Here, the complex composed of BRAVO, PLT3 and WOX5 seems to be the most frequent and stable.

Modelling reveals cell type specific TF complex compositions

Our results reveal distinct, cell type specific patterns of protein abundance for BRAVO, PLT3 and WOX5 in the root SCN (Fig. 1) along with the formation of diverse heterodimers with varying binding affinities as well as higher-order complexes in *N. benthamiana* (Fig. 3, Fig. 4, Fig. S2). The protein complexes formed in the cells of the root SCN are ultimately a result of the cell type specific protein levels and the binding affinities between the proteins. This raises the question whether dimerization and complex formation in the context of the root apex also display cell type specificity, and how this is influenced by the protein levels in each cell of the SCN (Fig. 1). For example, BRAVO protein levels in the QC are notably lower compared to PLT3 or WOX5 (Fig. 1 H), yet its consequence on protein complex formation remains undetermined. While the FRET-FLIM approach could in theory be used to investigate the formation of dimer- and oligomerization in *Arabidopsis* root cells, previous efforts to assess the interaction of PLT3 and WOX5 under the control of their endogenous promoter in roots have been challenging due to limited protein abundance and, consequently, low photon counts (Burkart *et al.*, 2022). This is a limitation difficult to overcome without altering the endogenous protein levels. Therefore, as an alternative to identify potential TF specificity and cell type specific complexes in the root SCN, we use a two-step mathematical modelling approach that combines the endogenous protein abundances (Fig.1) with the binding

probabilities for one-on-one PPIs and trimeric protein complexes (Fig. 3, Fig. 4, Fig. S2).

First, we performed a parameter analysis to predict the relative association and dissociation rates to form the WOX5-PLT3, BRAVO-PLT3, BRAVO-WOX5 heterodimers, and the WOX5-PLT3-BRAVO trimeric complex. For the trimeric complex, we evaluate its formation via WOX5-PLT3 and BRAVO-PLT3 as donors (Fig. 4, Fig. S2). We start our simulations with equal levels of both donor and acceptor as initial condition, to mimic the conditions in the *N. benthamiana* experiments. Then, we simulate the protein complex formation using association and dissociation rates from a wide range of possible parameter values, until a steady state is reached. For each parameter combination tested, we evaluated if the proportion of protein in complex in steady state corresponds to the value from the respective relative binding affinity determined with our experiments. Repeating this parameter estimation for each of the protein complexes under study, allows us to identify several parameter combinations capable of producing protein complexes in line with FRET-FLIM experimental data (Fig. S3, Fig. S4). The predicted parameter combination for protein complexes with a high binding affinity (i.e. WOX5-PLT3) fall in the space where association rates are higher than the dissociation rates (Fig. S3), in contrast to lower binding affinity complexes (i.e. BRAVO-WOX5). These determined parameters allow us to describe our binding experimental data in a computational model.

Next, we simulated the protein complexes formed by BRAVO, WOX5 and PLT3 in each of the cells of the root SCN. For this, we use as initial condition the values from the relative fluorescence intensities we quantified for BRAVO, PLT3 and WOX5 in the SI, QC, CSC, and CC (Fig. 1 H), and the association/dissociation rates per complex from our parameter analysis. Therefore, the cell type specific profiles of protein complexes predicted by modelling are the emergent result of how much protein is available in each cell type and the binding affinities between specific protein pairs and complexes (Fig. 5). We summarized these results in a radar chart where the level of each protein complex is arranged in a different radial axis and displayed free protein levels that remain after complex formation separately as bar plots (Fig. 5 A, B). Furthermore, we combined these results in a heat map (Fig. 5 C). Additionally, we performed several controls that assume different combinations of experimental data, both binding affinities and cell type specific protein

abundances, and varying ratios of association and dissociation (Fig. S5, Material and Methods). Interestingly, results comparable to our model were only observed in control 2, assuming higher association and dissociation rates, which indicates higher association also in our experimental data.

Our simulation reveals that SIs are characterized by high levels of BRAVO-PLT3 protein complex (Fig. 5 A, C). The QC cells are predicted to be enriched in the WOX5-PLT3 complexes, followed closely by the CSC. Such enrichment could be related to the previously described function of the WOX5-PLT3 complex in QC divisions and CSC maintenance (Burkart *et al.*, 2022). However, predictions of the trimeric complex WOX5-PLT3-BRAVO displays only intermediate levels in both the SI and the QC. Finally, the CCs are predicted to have negligible levels of all protein complexes studied, consistent with the very low BRAVO, PLT3, and WOX5 protein levels present in these cells according to our quantification (Fig. 1). Notably, these protein complex 'signatures' are strikingly different in each of the simulated cells and the resulting polygons are unique for each cell type (Fig. 5 A), which might be related to their specific function.

Curiously, the levels of free protein also show cell type specific patterns, that allow to further distinguish between SIs, QC and CSCs (Fig. 5 B, C). SIs are enriched in free BRAVO, while the QC shows high levels of free WOX5. Both, CSCs and CCs, exhibit high levels of PLT3. It is interesting to consider that these free proteins could participate in both, binding other proteins not considered here, and/or intercellular movement, assuming an increased mobility if the protein is not in complexes (Fig. 5 B, C). For instance, the levels of free WOX5 in the QC cells could constitute a pool of free protein available for intercellular mobility towards the neighbouring CSCs as previously described (Pi *et al.*, 2015). In summary, these results support the hypothesis that complex formation, especially heterodimerization, occurs in a cell type specific context.

Prion-like domains of PLT3 serve as conserved interaction hub

After we have found evidence for the formation of TF complexes with cell type dependent variations, we asked whether these complexes are important for root SCN maintenance. To address this, we aimed to destabilize the interaction of these TFs by mutating their specific interaction sites and observe if this altered protein can still rescue the phenotypical defects in the SCN. First, we explored the literature to

identify potential interaction sites of BRAVO, PLT3 and WOX5. Previous studies have shown that prion-like domains (PrDs) in PLT3 mediate the interaction with WOX5 (Burkart *et al.*, 2022). PrDs are intrinsically disordered regions (IDRs) and serve not only as mediators of multivalent interactions, but have also been demonstrated to be involved in chromatin opening (Levy *et al.*, 2002) and phase separation (Jung *et al.*, 2020). Given the presence of PrDs also in PLT1, PLT2 and PLT4, albeit in lower numbers (Burkart *et al.*, 2022), we hypothesized that these regions function as conserved interaction sites. Thus, we performed FRET-FLIM measurements to investigate how the deletion of PLT3 PrDs, termed PLT3ΔPrD, affects its interaction with BRAVO. The 'donor only' reference control BRAVO-mV yields an average binding of 1.7 ± 4.6 %, which increases to 3.9 ± 2.4 % in the presence of mCherry-NLS serving as negative control (Fig. 6). Upon co-expression of BRAVO-mV with PLT3-mCh the binding significantly increases to 22.8 ± 10.5 % (Fig. 6). However, BRAVO-mV co-expressed with PLT3ΔPrD-mCh yields an average binding of only 11.7 ± 9.6 %, suggesting that the deletion of the PrDs significantly reduces the interaction of PLT3 with BRAVO.

To further support our hypothesis that the PrDs in PLTs act as conserved interaction site, we investigated whether PLT3 also interacts with BES1 and TPL, which were shown before for to interact with BRAVO and WOX5 (Vilarrasa-Blasi *et al.*, 2014; Pi *et al.*, 2015; Betegón-Putze *et al.*, 2021) and if this interaction can also be altered by the deletion of PLT3 PrDs. To address this, we conducted FRET-FLIM in the presence of an acceptor-labelled PLT3 or PLT3ΔPrD. For the donor only reference control measurements BES1D-mV, an average binding of 0.0 ± 6.3 % could be observed which increases to 16.9 ± 8.1 % in the presence of PLT3-mCh indicating PPI (Fig. S6 A). However, co-expression of BES1D-mV with PLT3ΔPrD-mCh shows a reduced binding of 8.4 ± 4.8 % which is not significantly different from the negative control BES1D-mV with mCherry-NLS exhibiting an average binding of 4.9 ± 6.5 % (Fig. S6 A). The reference control TPL-mV exhibits an average binding of 0.6 ± 5.5 %, increasing to 6.4 ± 2.4 % when co-expressed with the negative control mCherry-NLS (Fig. S6 B). Upon co-expression of TPL-mV with PLT3-mCh, the average binding significantly increases to 13.5 ± 4.3 %, suggesting a moderate interaction of TPL with PLT3 (Fig. S6 B). Similar to BES1, the interaction of TPL and PLT3 is also abolished by the deletion of PrDs, demonstrated by a significantly decreased average binding of 8.99 ± 5.26 % for TPL-mV with PLT3ΔPrD-mCh (Fig. S6). In

summary, these findings support the idea that the PrDs of PLT3 serve as a conserved interaction site for numerous TFs present in the root SCN.

Redistribution of TF complexes alters regulation of QC divisions

Next, we aimed to analyse the functional relevance of the eliminated or reduced interaction of PLT3 with other TFs present in the *Arabidopsis* root by deleting its PrDs. To address this, we created two transgenic *Arabidopsis* lines, using either full-length PLT3 or PLT3ΔPrD C-terminally tagged with mTurquoise2 (mT2) in combination with the dexamethasone (DEX) inducible glucocorticoid receptor (GR) in the *plt3-1* mutant background. Using the *WOX5* promoter allowed us to specifically investigate how the loss of PLT3 PrD influences QC maintenance. These lines were named *pWOX5:GR-PLT3-mT2* (*pWOX5:iPLT3)* and *pWOX5:GR-PLT3ΔPrD-mT2* (*pWOX5:iPLT3ΔPrD)*. Finally, we performed a SCN staining and investigated if the QC exhibits additional periclinal cell divisions after inducing the plants by DEX treatment or in the presence of dimethyl sulfoxide (DMSO), which serves as a control (Fig. 7 A-I).

Under control conditions, only 27 % of *Col-0* WT roots show additional periclinal cell divisions in the QC, which does not change significantly in the presence of DEX (Fig. 7 A, E, I). In agreement with previous observations (Burkart *et al.*, 2022), *plt3-1* single mutant roots show additional periclinal cell divisions in the QC of 73 % under control conditions and 87 % after induction with DEX (Fig. 7 B, F, I). In *pWOX5:iPLT3* and *pWOX5:iPLT3ΔPrD* transgenic lines, 83 % and 94 % of the roots exhibit a periclinal cell division in the QC under control conditions, respectively, which is even higher than the *plt3-1* single mutant (Fig. 7 C, D, I). However, in the presence of DEX, only 67 % of the roots expressing *pWOX5:iPLT3* show this phenotype, indicating that full-length PLT3 in the QC partially restores the *plt3-1* periclinal cell division phenotype (Fig. 7 G, I). Contrary, the observed overproliferated phenotype that we see under control conditions in *pWOX5:iPLT3ΔPrD* mutant roots, is unaffected in the presence of DEX, indicating that the PrDs of PLT3 are necessary to inhibit additional periclinal QC divisions and thereby contribute to PLT3 function in root SCN maintenance (Fig. 7 H, I).

After observing the reduced affinity of PLT3ΔPrD for BRAVO and WOX5, and that it was unable to rescue SCN defects in *plt3-1* single mutants, we decided to use our computational model to predict immediate changes in the protein complex

'signatures' in the root SCN that may have contributed to this failed rescue. Thus, we simulated the protein complex formation in the SI, QC, CSC, and CC as described before but set the association rate of PLT3ΔPrD-WOX5 to zero (Burkart *et al.*, 2022) and use the binding affinity we have determined experimentally for PLT3ΔPrD-BRAVO (Fig. 6 and S6). This leads to a dramatic shift in the protein complex ‘signatures’ of the root SCN cells (Fig. 7 J-L). The elimination of WOX5-PLT3 dimer formation causes a redistribution of PLT3 and WOX5 to the other protein complexes and an increase of free PLT3 and WOX5 protein levels in the SI and the QC cells, as well as higher levels of free PLT3 in the CSC (Fig. 7 J, K). While the BRAVO-PLT3 complex can still be formed, it is noticeably reduced in the SI, QC and CSC cells. Furthermore, the BRAVO-WOX5 complex levels increase in the SI and QC cells. Surprisingly, the profile of the trimeric complex shows only minor disruptions in the modelled cells. Therefore, even if the WOX5-PLT3 protein complex cannot be formed due to the removal of PLT3 PrDs, the trimeric complex can still be formed by the association of WOX5 with the BRAVO-PLT3 protein complex. Altogether, our PLT3ΔPrD simulation provides insights into the alterations on cell type specific protein levels that could be causative for defects observed experimentally in the root SCN.

Discussion

In the past decades, our understanding of stem cell function and maintenance in the root of *Arabidopsis* has witnessed significant advances. Various aspects, including hormonal, developmental, as well as stress-related mechanisms have been discovered (Nolan *et al.*, 2020; García-Gómez *et al.*, 2021; Ubogoeva *et al.*, 2021; Strotmann and Stahl, 2021). However, the underlying intricate network of molecular factors, still remains largely enigmatic. In this study, we aimed to unravel a new aspect of the regulatory network that controls root SCN maintenance, related to protein complex formation.

By utilizing a distinct SCN staining technique (Burkart *et al.*, 2022), we assessed phenotypical defects in the architecture of the *Arabidopsis* root SCN of several single and multiple mutants (Fig. 2). We observed an increased CSC differentiation and an elevated periclinal QC division frequency in the SCN of *plt3-1* mutants (Burkart *et al.*, 2022). The observed phenotypes agree with previous observations, and their relatively moderate phenotypic manifestation can be attributed to the substantial redundancy within the PLT TF family (Galinha *et al.*, 2007; Burkart *et al.*, 2022). Moreover, these observations are consistent with a uniform PLT3 protein abundance in SIs, QC and CSCs (Fig. 1). Compared to *plt3-1* single mutants, we could observe a stronger effect for QC division frequency in *bravo-2* single mutants but a similar mild phenotype for CSC differentiation. Again, these results are supported by the observed protein levels: Although BRAVO is most abundant in SIs, it can also be found in the QC, whereas it is notably reduced in CSCs. *wox5-1* single mutants show a severely defective root SCN, as demonstrated by the loss of CSCs and greatly increased periclinal QC divisions, as described before (Sarkar *et al.*, 2007; Cruz-Ramírez *et al.*, 2013; Pi *et al.*, 2015; Betegón-Putze *et al.*, 2021; Burkart *et al.*, 2022). Similar to PLT3 and BRAVO, these phenotypes correlate with high WOX5 protein levels in the QC and less protein in the CSC where WOX5 was shown to move to (Pi *et al.*, 2015; Berckmans *et al.*, 2020).

In the *bravo plt3*, *bravo wox5*, and *plt3 wox5* double mutants, we observed an increase in both QC division frequency and CSC differentiation, that were consistently higher than the respective single mutants. For PLT3 and WOX5 such additive effects have been described before and were hypothesized to show that they act in parallel pathways to maintain the integrity of the root SCN (Burkart *et al.*, 2022). However, previous findings suggest that BRAVO and WOX5 act in the same

pathway to control CSC fate and QC divisions based on quantifications of additional periclinal cell divisions (Betegón-Putze *et al.*, 2021). We could observe similar effects when analysing periclinal cell divisions in the QC but using a novel SCN staining technique, we observed additive effects for QC division alterations in the *bravo wox5* double mutant compared to the respective single mutants (Fig. 2, Fig. S1). Our findings suggest the presence of an additional pathway that involves BRAVO and PLT3. Moreover, this indicates that these TFs could act in three independent constellations to regulate SCN maintenance. However, in the *bravo plt3 wox5* triple mutant, an additional additive effect could only be observed for QC divisions but not for CSC differentiation. A potential interpretation of these results is that none of these TFs is involved in an additional pathway to control CSC differentiation. However, they may partially contribute to other pathways that inhibit QC divisions. Additional functions in other independent pathways have already been described for WOX5 in the SHR-SCR regulatory network (Cruz-Ramírez *et al.*, 2013; Zhai *et al.*, 2020; Clark *et al.*, 2020). Additionally, TEOSINTE-BRANCHED/CYCLOIDEA/PCNA 20 (TCP20) was found to mediate the interaction of PLT3 and SCR, to specify the QC and establish the root SCN (Shimotohno *et al.*, 2018). If and to what extent these molecular factors genetically interact with other TFs in the SCN, will be an interesting perspective for future investigations.

In addition to the identified genetic interplay of BRAVO, PLT3 and WOX5 regarding root SCN maintenance, we were able to evaluate their physical interaction (Fig. 3, Supplementary Table S13). While interactions of PLT3 and WOX5 as well as BRAVO and WOX5, have been described before (Betegón-Putze *et al.*, 2021; Burkart *et al.*, 2022), evidence for an interaction of PLT3 and BRAVO was still missing. Our results reveal for the first time PPI between BRAVO and PLT3 as well as between PLT3 and BES1 and TPL (Fig. 3, Fig. S6). Together with previously described, independent one-on-one interactions, these findings support the hypothesis of three parallel pathways that control CSC differentiation and QC divisions in parallel. Furthermore, the observed variations of stability and probability of occurrence as indicated by a special analysis tool (Orthaus *et al.*, 2009; Maika *et al.*, 2023), could indicate a specific mechanism that facilitates the interaction of two POIs in a highly dynamic microenvironment, where the number of proteins is generally high, such as in the QC. (Fig. 1).

Next, the combination of BiFC and FRET allowed us to investigate the formation of higher-order complexes (Fig. 4, Fig. S2). Like in the one-on-one interaction studies, we found differences in protein affinities of the complexes under investigation. Here, the trimeric complex formed by WOX5-PLT3-BRAVO appeared to be the most abundant and stable. The heterodimerization of transcriptional regulators increases binding specificity and affinity and allows the combination of different internal as well as external signal inputs into gene regulation (Strader *et al.*, 2022). This idea is reinforced when considering that both the auxin-regulated WOX5 and BR-dependent BRAVO have been demonstrated to control the same cell cycle-related genes (*CYCD1;1, CYCD3;3*) (Forzani *et al.*, 2014; Vilarrasa-Blasi *et al.*, 2014). So far, cell cycle-related downstream targets of PLT3 remain unknown. Further investigations are necessary to uncover potentially common downstream targets of BRAVO, PLT3 and WOX5.

To elaborate on differences in protein abundance and complex formation in cells of the root SCN, we used a computational modelling approach. This strategy allowed us to describe cell type specific protein complex profiles in WT roots (Fig. 5). Here, the combination of high levels of the BRAVO-PLT3 heterodimer and high levels of free BRAVO appears to be characteristic for stele initials. Interestingly, BRAVO protein abundance not only decreased when moving distally from the SIs, but also in proximal direction (Fig. 1). However, alterations of SCN defects in *bravo-2* single mutants had only been evaluated for CSC differentiation and QC division. New phenotypical analyses are necessary to determine whether SIs and their descendants are also affected upon loss of BRAVO function.

Our simulations of protein 'signatures' revealed that both, QC as well as CSC, are enriched in the WOX5-PLT3 heterodimer, which aligns with their previously described impact on QC divisions and CSC differentiation (Burkart *et al.*, 2022). However, the protein 'signatures' of QC and CSC could be distinguished when free protein levels were considered. In the QC, our model predicted high protein levels of free WOX5, while CSCs were predicted to possess higher levels of PLT3. Several studies highlighted the elevated abundance of WOX5 in the QC, which could be either linked to interactions with other proteins not analysed here or its non-cell autonomous function in the adjacent initials, although its necessity as mobile stemness factor is still under debate (Pi *et al.*, 2015; Berckmans *et al.*, 2020). The predicted high levels of PLT3 protein in CSCs might be linked to nuclear body (NB)

formation of PLT3, which was linked to its PrDs and is concentration dependent and may involve PLT3 homomerization. This mechanism could facilitate the recruitment of the WOX5-PLT3 heterodimer into these pre-formed NBs, as demonstrated previously (Burkart *et al.*, 2022).

In CCs, the absence of BRAVO and WOX5 hinders complex formation, resulting in high levels of free PLT3. However, compared to CSC PLT3 levels are notably lower accompanied with loss of NBs formation. This implies that a specific protein concentration is required to initially trigger NB formation highlighting the difference between differentiated CCs and the stem cell fate determination process in CSCs.

Based on our results, we created a final model that summarizes the described protein 'signatures' (Fig. 8). Here, SIs are characterized by high levels of free BRAVO protein and the heterodimer BRAVO-PLT3. QC cells and CSCs possess elevated levels of the WOX5-PLT3 heterodimer, which is accompanied by high levels of free WOX5 in the QC and high levels of free PLT3 in CSC. In CCs, complex formation is hindered by negligible levels of BRAVO and WOX5, resulting in elevated levels of free PLT3. All together our findings imply the formation of dimers that together with differences of free protein levels convey cell type specificity in the root.

In the future, it should be addressed how the predicted protein complex 'signatures' drive changes in gene expression, including *BRAVO*, *PLT3*, and *WOX5*, but also other target genes, and how this relates to QC division and CSC number alterations in single and multiple mutants. As a next step, the model could also consider the complex gene regulatory networks in the root SCN (Cruz-Ramírez *et al.*, 2012; García-Gómez *et al.*, 2017; Pardal and Heidstra, 2021), the role of cell-cell mobility of free protein (Mähönen *et al.*, 2014; Pi *et al.*, 2015; García-Gómez *et al.*, 2020; Betegón-Putze *et al.*, 2021), the presence of membrane-less compartments to account for the localization of WOX5-PLT3 in nuclear bodies in the CSC (Burkart *et al.*, 2022) and other key regulatory processes involved. The integration of experimental and computational approaches holds promise to uncover these complex mechanisms underlying root SCN maintenance.

To investigate the impact of heterodimer- and oligomerization on root SCN maintenance, we aimed to identify potential interaction sites in the BRAVO, PLT3 or WOX5 amino acid sequence. Previous studies revealed that PrDs found in PLT3 act as mediator of its interaction with WOX5 (Burkart *et al.*, 2022). PrDs are also present in PLT1,2 and 4 which is also accompanied by NB formation. However, PLT3

harbours the highest number of PrDs, which correlates with stronger NB formation compared to PLT1, 2 and 4. Here, we demonstrated that loss of PrDs also negatively influences PLT3 interaction with BRAVO, BES1 and TPL (Fig. 6, Fig. S6). These findings suggest that PrDs act as a multivalent interaction hub, which could also indicate a conserved function among other PLTs.

In a rescue experiment, we could demonstrate that the PrDs of PLT3 affect its ability to inhibit periclinal QC divisions by demonstrating that PLT3ΔPrD, expressed in the QC, is unable to rescue the *plt3-1* periclinal QC division phenotype (Fig. 7). This indicates that correct dimer- and oligomerization is necessary for proper QC maintenance. We integrated our findings of diminished interactions of PLT3ΔPrD with BRAVO and WOX5 to our model and found a severe shift of protein complex 'signatures', especially for the WOX5-PLT3 dimer in the QC and CSCs. This further strengthens our hypothesis that the protein complexes form instructive protein signatures important for cell fate decisions in the *Arabidopsis* root SCN.

Interestingly, full-length PLT3 under control of the *WOX5* promoter only partially rescues the *plt3-1* periclinal QC division phenotype. This emphasizes that functional PLT3 is also necessary to locally maintain CSC fate and repress differentiation as the QC divides to replenish lost CSCs (Cruz-Ramírez *et al.*, 2013). Furthermore, this could indicate a specific function for PLT3 in the CSC fate, as the presence of other PLTs was not able to fully compensate for the loss of PLT3. Previous findings in yeast suggest that differences in IDRs mediate specificity of transcription factors that share the same DNA-binding motif (Brodsky *et al.*, 2020). This is often observed among TFs that belong to the same family. If a similar mechanism also exists in plants, this could suggest that PLT3 function in CSC fate is specifically linked to its PrDs and that, due to their differentially structured PrDs, the other PLTs cannot compensate for this specific function. Additionally, this could indicate that mobile PLT3 which might move from the QC to CSC is not enough to maintain CSC stem cell character.

IDRs or PrDs also play a role in a recently described alternative mechanism of how TF find and locate to their specific DNA target (Staller, 2022). Indeed, the majority of TF found in eukaryotes is mainly composed of IDRs and only a small fraction of the protein sequence is well-characterized (Ward *et al.*, 2004; Wang *et al.*, 2016). According to this theory, IDRs of TFs scan the genome for matching protein clouds which mediate binding of the DNA-binding domain to its specific genomic target site

(Staller, 2022). TFs possess two main functions: bind other TFs and bind to their specific DNA target to alter gene expression (Strader *et al.*, 2022). Some TFs possess an additional important role; pioneer transcription factors, like LEAFY (Lai *et al.*, 2021; Jin *et al.*, 2021), bind to nucleosome bound DNA, open the target locus, e.g. by displacing H1 linker histones and/or recruiting chromatin remodellers, and make it accessible for other TFs. In plants, the concept of pioneer transcription factors is a newly emerging research field, but studies in animals suggest, that 'master regulators' appear to be promising candidates for pioneer transcription factors (as reviewed in Yamaguchi, 2021). The identification of IDRs and/or PrDs, that possess the ability to facilitate multivalent interaction and have been shown to act in chromatin opening (Levy *et al.*, 2002), together with high redundancy within the PLT TF family, their role as master regulators of root formation and the stable protein abundance in the SCN, especially in cells that possess stem cell character, could indicate that also PLTs act as pioneer transcription factors in the root SCN. Interestingly, DNA affinity purification-sequencing (DAP-seq) results found PLT3, as well as PLT7, to be highly enriched in mCG-methylated DNA, providing yet another hint for this theory (O'Malley *et al.*, 2016). Nevertheless, more evidence is necessary to further support the potential function of PLTs as pioneer transcription factor in root SCN maintenance.

Overall, our results suggest that BRAVO, PLT3 and WOX5 form cell type specific profiles of protein complexes and that proper complex formation contributes to optimal stem cell maintenance. Furthermore, we propose that these unique protein complex signatures serve as a read-out for cell specificity and could explain the different roles played by BRAVO, PLT3 and WOX5 in the regulation of stem cell homeostasis in the root.

Material and Methods

Plant work

All *Arabidopsis thaliana* lines used in this study were in *Col-0* background and can be found in Appendix Table S5. The *wox5-1* and *plt3-1* single mutants (Galinha *et al.*, 2007) as well as the *bravo-2* single mutant (Vilarrasa-Blasi *et al.*, 2014) and *bravo-2 wox5-1* double mutant (Betegón-Putze *et al.*, 2021) were described before. The *bravo-2 plt3-1* double and *bravo-2 plt3-1 wox5-1* triple mutants were created by crossings. Homozygous F3 plants were verified by PCR using appropriate primers (Appendix Table S2). Transgenic lines were created by the floral dip method (Zhang *et al.*, 2006). The *pPLT3:PLT3-mV* and *pWOX5:WOX5-mV* translational reporters in *Col-0* WT background were described earlier (Burkart *et al.*, 2022). For *pBRAVO:BRAVO-mVenus*, *pWOX5:GR-PLT3-mTurquoise2,* and *pWOX5:GR-PLT3ΔPrD-mTurquoise2* transgenic plants, lines were selected, that possess a single T-DNA insertion, which was tested by observing the segregation on selection marker containing plates. Plants for crossing, genotyping, transformation, floral dip and amplification were grown under long-day conditions (8 h dark, 16 h light) at 21 °C and 60 % humidity. For microscopy, seeds were sterilized with chlorine gas (50 ml 13 % sodium hypochlorite (v/v), 1 ml hydrochloric acid) in a desiccator, mounted in 0.15 % (w/v) agarose and stratified in the dark at 4 °C for minimum two days before sowing on GM agar plates without sucrose (1/2 MS including Gamborg B5 vitamins, 1.2 % plant agar (w/v) and 0.05 % MES hydrate (w/v)). Seedlings for imaging were grown for five to six days under continuous light at 80 µmol m^{-2} s^{-1}, 21 °C and 60 % humidity.

Cloning

Plasmids for the transgenic lines *pBRAVO:BRAVO-mVenus*, *pWOX5:GR-PLT3-mTurquoise2* and *pWOX5:GR-PLT3ΔPrD-mTurquoise2* as well as for transient expression in *N. benthamiana* were generated using the GreenGate cloning method in the pGGZ001 destination vector (Lampropoulos *et al.*, 2013). The region of the *WOX5* promoter, the CDS of WOX5, PLT3 and PLT3ΔPrD CDS as well as WOX5, PLT3 and PLT3ΔPrD constructs for transient expression in *N. benthamiana* were described before (Burkart *et al.*, 2022). The region upstream of the transcriptional start of BRAVO (2,925 bp) (Lee *et al.*, 2006) was assigned as promoter and

amplified by PCR with appropriate primers containing flanking *Bsa*I restriction sites and matching overlaps for GreenGate cloning. The internal *Bsa*I recognition site in the *BRAVO* promoter region was not removed, but incubation times for restriction digestion and GreenGate reaction were adapted accordingly. After PCR, the promoter sequence was cloned into the GreenGate entry vector pGGA000 using *Bsa*I restriction and ligation. The CDS of BRAVO and TPL were amplified from cDNA derived from extracted RNA by PCR using primers carrying the *Bsa*I recognition site and matching GreenGate overhangs. Next, they were cloned into the GreenGate entry vector pGGC000 via restriction digest and ligation. All entry vectors were confirmed by sequencing. The GreenGate entry vector carrying the β-estradiol inducible promoter cassette was provided by (Denninger *et al.*, 2019). For bimolecular fluorescence complementation, the GreenGate M and N intermediate vectors, each of which carried one expression cassette, were used. The correct assembly of the modules was confirmed by sequencing. All module combinations, constructs as well as primers used for cloning are listed in Appendix Tables S4, S3, and S1, respectively.

SCN staining

SCN staining was performed according to (Burkart *et al.*, 2022). For CSC layer quantification, optical longitudinal sections of the *Arabidopsis* root were acquired. The cell layer below the QC was scored as differentiated if three or more cells in this layer accumulated starch granules. QC cell divisions were quantified using an optical cross-section of the RAM on a scale of zero to four or more cells. If the QC was duplicated and showed two layers, as often seen for *bravo-2* mutants, only QC divisions in the upper layer were counted.

The CSC layer and QC cell division phenotypes were visualized separately in bar plots using Microsoft Excel (Microsoft Office 365, Microsoft Corporation). To assess potential correlations between CSC layers and QC divisions, data were combined into 2D-plots showing QC division on the x-axis and CSC layer on the y-axis using Origin 2021b (OriginLab Corporation).

Transient expression in *Nicotiana benthamiana*

For transient expression in *N. benthamiana*, the *Agrobacterium* strain GV3101::pMP50 was used that in addition to the plasmid harbouring the desired

construct, carried the helper plasmid pSOUP needed for GreenGate vectors. *Agrobacteria* were grown overnight in 5 ml dYT medium at 28 °C with shaking. After centrifugation for 10 min at 4,000 rpm and 4 °C, the pellet was resuspended in infiltration medium (5 % sucrose (w/v), 0.01 % $MgSO_4$ (w/v), 0.01 % glucose (w/v) and 450 µM acetosyringone) to an optical density OD_{600} of 0.6 and mixed with an *Agrobacterium* strain carrying the p19 silencing repressor and eventually with a second *Agrobacterium* strain carrying a different construct for co-expression. Subsequently, the cultures were incubated for 1 h at 4 °C. To trigger stomatal opening and thereby allow easy infiltration, *N. benthamiana* plants were sprayed with water and kept under high humidity prior to infiltration. The abaxial side of the leaf was infiltrated using a syringe without a needle. Expression was induced 2-4 days after infiltration by spraying a 20 µM β-estradiol solution containing 0.1 % Tween®-20 (v/v) to the abaxial side of the leaf. Depending on the expression level, FLIM measurements were performed 2-16 h after induction.

Microscopy

Imaging of *Arabidopsis thaliana* roots was performed using an inverted ZEISS LSM780 or LSM880. For cell wall staining, Arabidopsis seedlings were mounted in an aqueous solution of propidium iodide (PI) (10 µM). Fluorophores and fluorescent dyes were excited and detected as follows: PI was excited with 561 nm and detected at 590-670 nm; Alexa Fluor® 488 was excited at 488 and detected at 500-580 nm; mVenus was excited at 514 nm and detected at 520-570 nm and mCherry was excited at 561 nm and detected at 580-680 nm. When mVenus was co-expressed with mCherry, it was excited at 488 nm and detected at 505-555 nm.

Intensity measurements of protein levels in *A. thaliana*

For analysis of expression levels of different reporters in 6 DAG *Arabidopsis* roots of different genotypes, an inverted LSM880 microscope with constant settings for all reporters was used. The mean fluorescence levels were measured in ImageJ using an oval region of interest (ROI) of the size of one nucleus. One to three nuclei were measured per cell type and root of which the mean was calculated. Data were normalized to mean value of the combination cell type and reporter that yielded the highest intensity. Data result from three technical replicates.

Induction of GR inducible Arabidopsis lines

For the *plt3-1* rescue experiments, seeds were sown on GM agar plates without sucrose (1/2 MS including Gamborg B5 vitamins, 1.2 % plant agar (w/v) and 0.05 % MES hydrate (w/v)) containing either 0.1 % DMSO (v/v) for control condition or 20 µM DEX (diluted in DMSO) for GR induction. After 5 days, seedlings were transferred to GM agar plates without sucrose containing 7 µg/ml 5-ethynyl-2'-deoxyuridine (EdU) and either 0.1 % DMSO (v/v) or 20 µM DEX (diluted in DMSO) and grown for 24 h. SCN staining, imaging and scoring of QC divisions and CSC layers were performed as described above.

FRET-FLIM measurements

FRET-FLIM measurements were performed in transiently expressing epidermal leaf cells of 3 to 4 weeks old *N. benthamiana* using an inverted ZEISS LSM 780 equipped with additional time-correlated single-photon counting devices (Hydra Harp 400, PicoQuant GmbH) and a pulsed laser diode. mVenus was chosen as donor and excited at 485 nm with 1 µW laser power at the objective (40 x C-Apochromat/1.2 Corr W27, ZEISS) and a frequency of 32 MHz and detected using two τ-SPAD single photon counting detectors in perpendicular and parallel orientation. Photons were collected over 40 frames at 256x256 pixels per frame, a pixel dwell time of 12.6 µs and a digital zoom of 8. Prior to image acquisition, a calibration routine was performed. To test system functionality, fluorescence correlation spectroscopy (FCS) measurements of deionized water and Rhodamine110 were acquired. Additionally, monitoring the decay of erythrosine B in saturated potassium iodide served as instrument response function (IRF) to correct the fitting for system specific time shift between laser pulse and data acquisition.

First, fluorescence decays of the donor-only control were analysed using the ‘Grouped FLIM’ analysis tool to determine the average fluorescence lifetime using a mono- or biexponential fitting model (SymPhoTime, PicoQuant GmbH). Next, to extract information about protein affinities and proximities, the ‘Grouped LT FRET Image’ tool was utilized for a monoexponentially decaying donor and the ‘One Pattern Analysis (OPA)’ tool was used for samples with a biexponentially decaying donor (SymPhoTime, PicoQuant GmbH). These tools allow separate analyses of the amplitude and fluorescence lifetime of the FRET fraction of each sample. Consequently, the amplitude of the FRET component serves as a measure for the

number of molecules undergoing FRET, termed binding or protein affinity, whereas the difference of the fluorescence lifetime of the FRET component compared to the lifetime of the donor-only fraction is used to calculate the FRET efficiency which serves as a measure for protein proximity and orientation (Maika *et al.*, 2023). For samples where molecules do not undergo FRET e.g., the donor-only and negative control, binding values mostly varied between - 10 and 10 % and corresponding FRET efficiencies mostly accumulated at 10 or 80 %, which was defined during the fitting process (Maika *et al.*, 2023).

Statistical tests

Data were tested for normal distribution by Shapiro test (α = 0.05) followed by a Levene's test for equality of variances (α = 0.05). Since some data did not show normal distribution or equality of variances or both, all data sets were tested with a non-parametric Kruskal-Wallis ANOVA with *post-hoc* Dunn's test (α = 0.05). Statistical testing was performed using R.

Protein complex modelling

To estimate the relative association and dissociation rates for each of the dimeric and trimeric complexes studied here, we used the following ordinary differential equations:

(1)
$$\frac{dDA}{dt} = a \cdot A \cdot D - d \cdot DA$$

(2)
$$\frac{dA}{dt} = d \cdot DA - a \cdot A \cdot D$$

(3)
$$\frac{dD}{dt} = d \cdot DA - a \cdot A \cdot D$$

where *DA* is the protein complex formed by donor protein *D* and acceptor protein *A*. Using these equations, we simulated that the amount of protein complex, *DA*, is determined by the product of the association rate (*a*), the concentrations of donor, *D*, and acceptor, *A*, proteins, and how much it dissociates given a certain

dissociation rate (*d*). To explain the relative binding affinity values determined experimentally for each dimeric and trimeric protein complex, we assessed association and dissociation rates involved in the protein complex formation from a wide range (0 – 0.5 arbitrary units, step 0.001), and simulated the protein complex *AB* formation until a steady state was reached. We deemed a particular combination of association and dissociation rates successful if they produce a value of *AB* at steady state in line with the relative binding affinity rates. In this way, we were able to predict relative binding rates for the dimeric and trimeric protein complexes studied here.

Next, we simulated the protein complex formation in the cells of the root SCN using the following ordinary differential equations to describe the formation of each dimeric and trimeric complex:

(4)

$$\frac{dWOX5}{dt} = d_{BRAVOWOX5} \cdot BRAVOWOX5 + d_{WOX5PLT3} \cdot WOX5PLT3 + d_{WOX5PLT3BRAVO2} \cdot WOX5PLT3BRAVO - WOX5 \cdot (a_{BRAVOWOX5} \cdot BRAVO + a_{WOX5PLT3} \cdot PLT3 + a_{WOX5PLT3BRAVO2} \cdot BRAVOPLT3)$$

(5)

$$\frac{dBRAVO}{dt} = d_{BRAVOWOX5} \cdot BRAVOWOX5 + d_{BRAVOPLT3} \cdot BRAVOPLT3 + d_{WOX5PLT3BRAVO1} \cdot WOX5PLT3BRAVO - BRAVO \cdot (a_{BRAVOWOX5} \cdot WOX5 + a_{BRAVOPLT3} \cdot PLT3 + a_{WOX5PLT3BRAVO1} \cdot WOX5PLT3)$$

(6)

$$\frac{dPLT3}{dt} = d_{BRAVOPLT3} \cdot BRAVOPLT3 + d_{WOX5PLT3} \cdot WOX5PLT3 - PLT3 \cdot (a_{BRAVOPLT3} \cdot BRAVO + a_{WOX5PLT3} \cdot WOX5)$$

(7)

$$\frac{dWOX5PLT3}{dt} = a_{WOX5PLT3} \cdot WOX5 \cdot PLT3 - d_{WOX5PLT3} \cdot WOX5PLT3 - a_{WOX5PLT3BRAVO1} \cdot WOX5PLT3 \cdot BRAVO + d_{WOX5PLT3BRAVO1} \cdot WOX5PLT3BRAVO$$

(8)

$$\frac{dBRAVOPLT3}{dt} = a_{BRAVOPLT3} \cdot BRAVO \cdot PLT3 - d_{BRAVOPLT3} \cdot BRAVOPLT3 - a_{WOX5PLT3BRAVO2} \cdot WOX5PLT3 \cdot BRAVO + d_{WOX5PLT3BRAVO2} \cdot WOX5PLT3BRAVO$$

(9)

$$\frac{dBRAVOWOX5}{dt} = a_{BRAVOWOX5} \cdot BRAVO \cdot WOX5 - d_{BRAVOWOX5} \cdot BRAVOWOX5$$

(10)

$$\frac{dWOX5PLT3BRAVO}{dt} = a_{WOX5PLT3BRAVO1} \cdot WOX5PLT3 \cdot BRAVO + a_{WOX5PLT3BRAVO2} \cdot BRAVOPLT3 \cdot WOX5 - WOX5PLT3BRAVO \cdot (d_{WOX5PLT3BRAVO1} + d_{WOX5PLT3BRAVO2})$$

Notice the trimeric complex can be formed either by the binding of BRAVO to WOX5-PLT3, or WOX5 to BRAVO-PLT3. Then, we modelled the protein complexes formed in the cells of the root SCN using equations 4-10 and the relative protein levels of WOX5, BRAVO and PLT3 determined for SI, QC, CSC, and CC cells as initial condition. As several sets of binding rates were predicted per complex, for these simulations we used one selected at random. Notably, the specific parameters used for the results we present here do not change the protein complex signatures predicted by the model (Fig. S4).

To evaluate the effect in our model of both, the cell type specific protein levels as well as differential binding affinities are necessary for our model, we performed different control simulations. On the one hand, we tested the effect of equal association/dissociation rates ($a = d = 0.1$), higher association than dissociation rate ($a = 0.1, d = 0.05$), and lower association than dissociation ($a = 0.05, d = 0.1$) for all protein complexes using our experimental protein level quantification in the SI, QC, CSC and CC displayed as Control 1-3, respectively (Fig. S5). On the other hand, we consider an alternative scenario where all proteins have the same abundance levels, while the association/dissociation rates are based on our binding data (Control 4, Fig. S5). Finally, we consider the scenarios where the control conditions meet pairwise: Control 5 is a combination of equal association/dissociation rate together with the assumption of equal protein

abundances among cell types and proteins. In Control 6, the equality of protein levels is combined with higher association than dissociation rates. Finally, Control 7 combines lower association that dissociation rates with equal protein abundances (Fig. S5). Notably only control 2, which uses experimentally determined protein abundances together with a higher association than dissociation rate, produced results comparable to our model. Thus, leading to the conclusion that also in our experimental data, association rates must be higher than dissociations rates. Moreover, this indicates a key role of the protein levels in each cell in the resulting protein complex and free protein signatures. In all other cases, we could observe strikingly different protein complex 'signatures' to those we described with the model that uses our experimental data, indicating that our findings result from the combination of experimentally determined specific protein levels and binding affinities.

The code for the computational model generated in this study was implemented in R, and will be available at the Garcia Group webpage in the server of the Theoretical Biology and Bioinformatics Group (https://bioinformatics.bio.uu.nl/monica/Cell type-specific-complex-formation-of-key-transcription-factors-in-the-root-SCN) and in GitHub (https://github.com/moneralee/Cell type-specific-complex-formation-of-key-transcription-factors-in-the-root-SCN) upon publication.

Acknowledgements

We would like to acknowledge funding of V.I.S. by the Deutsche Forschungsgesellschaft (DFG) through grant STA1212/4-1 to Y.S. M.L.G.G. is supported by the long-term program PlantXR: A new generation of breeding tools for extra-resilient crops (KICH3.LTP.20.005) which is financed by the Dutch Research Council (NWO), the Foundation for Food & Agriculture Research (FFAR), companies in the plant breeding and processing industry, and Dutch universities. These parties collaborate in the CropXR Institute (www.cropxr.org) that is funded through the National Growth Fund (NGF) of the Netherlands. We thank Rebecca C. Burkart for sharing PLT3, PLT3ΔPrD and WOX5 constructs and stable Arabidopsis lines. We thank Ana Caño-Delgado for sharing seeds of *bravo-2* single and *bravo-2 wox5-1* double mutants. We thank Kirsten ten Tusscher for insightful discussions on

the modelling and Jan Kees van Amerongen for management of computational facilities of the Theoretical Biology group (Utrecht University). We thank Cornelia Gieseler, Carin Theres and Silke Winters for technical assistance. We thank Meik H. Thiele for help with statistical analyses and data visualisation with R. We also thank Jan E. Maika for help with fitting FRET-FLIM data. We would like to acknowledge the Center for Advanced Imaging (CAi) at Heinrich-Heine-University Düsseldorf for providing access to the Zeiss LSM780 and LSM880 and especially Dr. Sebastian Hänsch and Prof. Dr. Stefanie Weidtkamp-Peters for general support during imaging and analysis. Funding for instrumentation: Zeiss LSM 780: DFG-INST 208/551-1 FUGG and Zeiss LSM 880: DFG- INST 208/746-1 FUGG.

Author contributions

Y.S. conceived the project. Y.S. and V.I.S. designed, analyzed and interpreted the data. V.I.S. carried out all experiments. M.L.G.G. formulated and performed mathematical modelling. The manuscript was written by V.S. and M.L.G.G. and was revised by Y.S. All authors commented and approved the manuscript.

Declaration of competing interests

The authors declare no competing interests.

This manuscript has not been accepted or published elsewhere.

References

Aida M, Beis D, Heidstra R *et al.* 2004. The PLETHORA genes mediate patterning of the Arabidopsis root stem cell niche. *Cell* **119,** 109–120.

Benfey PN, Scheres B. 2000. Root development. *Current biology CB* **10,** R813-5.

Berckmans B, Kirschner G, Gerlitz N, Stadler R, Simon R. 2020. CLE40 Signaling Regulates Root Stem Cell Fate. *Plant physiology* **182,** 1776–1792.

Betegón-Putze I, Mercadal J, Bosch N *et al.* 2021. Precise transcriptional control of cellular quiescence by BRAVO/WOX5 complex in Arabidopsis roots. *Molecular systems biology* **17,** e9864.

Brodsky S, Jana T, Mittelman K *et al.* 2020. Intrinsically Disordered Regions Direct Transcription Factor In Vivo Binding Specificity. *Molecular cell* **79,** 459-471.e4.

Burkart RC, Strotmann VI, Kirschner GK *et al.* 2022. PLETHORA-WOX5 interaction and subnuclear localization control Arabidopsis root stem cell maintenance. *EMBO reports* **23,** e54105.

Clark NM, Fisher AP, Berckmans B *et al.* 2020. Protein complex stoichiometry and expression dynamics of transcription factors modulate stem cell division. *Proceedings of the National Academy of Sciences of the United States of America* **117,** 15332–15342.

Cruz-Ramírez A, Díaz-Triviño S, Blilou I *et al.* 2012. A bistable circuit involving SCARECROW-RETINOBLASTOMA integrates cues to inform asymmetric stem cell division. *Cell* **150,** 1002–1015.

Cruz-Ramírez A, Díaz-Triviño S, Wachsman G *et al.* 2013. A SCARECROW-RETINOBLASTOMA protein network controls protective quiescence in the Arabidopsis root stem cell organizer. *PLoS biology* **11,** e1001724.

Denninger P, Reichelt A, Schmidt VAF *et al.* 2019. Distinct RopGEFs Successively Drive Polarization and Outgrowth of Root Hairs. *Current biology CB* **29,** 1854-1865.e5.

Dolan L, Janmaat K, Willemsen V *et al.* 1993. Cellular organisation of the Arabidopsis thaliana root. *Development (Cambridge, England)* **119,** 71–84.

Du Y, Scheres B. 2017. PLETHORA transcription factors orchestrate de novo organ patterning during Arabidopsis lateral root outgrowth. *Proceedings of the National Academy of Sciences of the United States of America* **114,** 11709–11714.

Espinosa-Ruiz A, Martínez C, Lucas M de ***et al.*** 2017. TOPLESS mediates brassinosteroid control of shoot boundaries and root meristem development in Arabidopsis thaliana. *Development (Cambridge, England)* **144,** 1619–1628.

Forzani C, Aichinger E, Sornay E *et al.* 2014. WOX5 suppresses CYCLIN D activity to establish quiescence at the center of the root stem cell niche. *Current biology CB* **24,** 1939–1944.

Galinha C, Hofhuis H, Luijten M *et al.* 2007. PLETHORA proteins as dose-dependent master regulators of Arabidopsis root development. *Nature* **449,** 1053–1057.

García-Gómez ML, Azpeitia E, Álvarez-Buylla ER. 2017. A dynamic genetic-hormonal regulatory network model explains multiple cellular behaviors of the root apical meristem of Arabidopsis thaliana. *PLoS computational biology* **13,** e1005488.

García-Gómez ML, Garay-Arroyo A, García-Ponce B, La Sánchez MdP, Álvarez-Buylla ER. 2021. Hormonal Regulation of Stem Cell Proliferation at the Arabidopsis thaliana Root Stem Cell Niche. *Frontiers in plant science* **12,** 628491.

García-Gómez ML, Ornelas-Ayala D, Garay-Arroyo A, García-Ponce B, La Sánchez MdP, Álvarez-Buylla ER. 2020. A system-level mechanistic explanation for asymmetric stem cell fates: Arabidopsis thaliana root niche as a study system. *Scientific reports* **10,** 3525.

González-García M-P, Vilarrasa-Blasi J, Zhiponova M *et al.* 2011. Brassinosteroids control meristem size by promoting cell cycle progression in Arabidopsis roots. *Development (Cambridge, England)* **138,** 849–859.

Hofhuis H, Laskowski M, Du Y *et al.* 2013. Phyllotaxis and rhizotaxis in Arabidopsis are modified by three PLETHORA transcription factors. *Current biology CB* **23,** 956–962.

Jin R, Klasfeld S, Zhu Y *et al.* 2021. LEAFY is a pioneer transcription factor and licenses cell reprogramming to floral fate. *Nature communications* **12,** 626.

Jung J-H, Barbosa AD, Hutin S *et al.* 2020. A prion-like domain in ELF3 functions as a thermosensor in Arabidopsis. *Nature* **585,** 256–260.

Kwaaitaal M, Keinath NF, Pajonk S, Biskup C, Panstruga R. 2010. Combined bimolecular fluorescence complementation and Forster resonance energy

transfer reveals ternary SNARE complex formation in living plant cells. *Plant physiology* **152,** 1135–1147.

Lai X, Blanc-Mathieu R, GrandVuillemin L *et al.* 2021. The LEAFY floral regulator displays pioneer transcription factor properties. *Molecular plant* **14,** 829–837.

Lampropoulos A, Sutikovic Z, Wenzl C, Maegele I, Lohmann JU, Forner J. 2013. GreenGate---a novel, versatile, and efficient cloning system for plant transgenesis. *PloS one* **8,** e83043.

Lee J-Y, Colinas J, Wang JY, Mace D, Ohler U, Benfey PN. 2006. Transcriptional and posttranscriptional regulation of transcription factor expression in Arabidopsis roots. *Proceedings of the National Academy of Sciences of the United States of America* **103,** 6055–6060.

Levy YY, Mesnage S, Mylne JS, Gendall AR, Dean C. 2002. Multiple roles of Arabidopsis VRN1 in vernalization and flowering time control. *Science (New York, N.Y.)* **297,** 243–246.

Long Y, Stahl Y, Weidtkamp-Peters S *et al.* 2017. In vivo FRET-FLIM reveals cell type-specific protein interactions in Arabidopsis roots. *Nature* **548,** 97–102.

Mähönen AP, Tusscher K ten, **Siligato R *et al.*** 2014. PLETHORA gradient formation mechanism separates auxin responses. *Nature* **515,** 125–129.

Maika JE, Krämer B, Strotmann VI *et al.* 2023. One pattern analysis (OPA) for the quantitative determination of protein interactions in plant cells. *Plant methods* **19,** 73.

Nolan TM, Vukašinović N, Liu D, Russinova E, Yin Y. 2020. Brassinosteroids: Multidimensional Regulators of Plant Growth, Development, and Stress Responses. *The Plant cell* **32,** 295–318.

O'Malley RC, Huang S-SC, Song L *et al.* 2016. Cistrome and Epicistrome Features Shape the Regulatory DNA Landscape. *Cell* **165,** 1280–1292.

Orthaus S, Buschmann V, Bäter A, Fore S, König M, Erdmann R. 2009. Quantitative in vivo imaging of molecular distances using FLIM-FRET.

Pardal R, Heidstra R. 2021. Root stem cell niche networks: it's complexed! Insights from Arabidopsis. *Journal of experimental botany* **72,** 6727–6738.

Pi L, Aichinger E, van der Graaff E *et al.* 2015. Organizer-Derived WOX5 Signal Maintains Root Columella Stem Cells through Chromatin-Mediated Repression of CDF4 Expression. *Developmental cell* **33,** 576–588.

Sarkar AK, Luijten M, Miyashima S *et al.* 2007. Conserved factors regulate signalling in Arabidopsis thaliana shoot and root stem cell organizers. *Nature* **446,** 811–814.

Shimotohno A, Heidstra R, Blilou I, Scheres B. 2018. Root stem cell niche organizer specification by molecular convergence of PLETHORA and SCARECROW transcription factor modules. *Genes & development* **32,** 1085–1100.

Staller MV. 2022. Transcription factors perform a 2-step search of the nucleus. *Genetics* **222**.

Strader L, Weijers D, Wagner D. 2022. Plant transcription factors - being in the right place with the right company. *Current opinion in plant biology* **65,** 102136.

Strotmann VI, Stahl Y. 2021. At the root of quiescence: function and regulation of the quiescent center. *Journal of experimental botany* **72,** 6716–6726.

Strotmann VI, Stahl Y. 2022. Visualization of in vivo protein-protein interactions in plants. *Journal of experimental botany* **73,** 3866–3880.

Ubogoeva EV, Zemlyanskaya EV, Xu J, Mironova V. 2021. Mechanisms of stress response in the root stem cell niche. *Journal of experimental botany* **72,** 6746–6754.

van den Berg C, Willemsen V, Hendriks G, Weisbeek P, Scheres B. 1997. Short-range control of cell differentiation in the Arabidopsis root meristem. *Nature* **390,** 287–289.

Vilarrasa-Blasi J, González-García M-P, Frigola D *et al.* 2014. Regulation of plant stem cell quiescence by a brassinosteroid signaling module. *Developmental cell* **30,** 36–47.

Wang C, Uversky VN, Kurgan L. 2016. Disordered nucleiome: Abundance of intrinsic disorder in the DNA- and RNA-binding proteins in 1121 species from Eukaryota, Bacteria and Archaea. *Proteomics* **16,** 1486–1498.

Ward JJ, Sodhi JS, McGuffin LJ, Buxton BF, Jones DT. 2004. Prediction and functional analysis of native disorder in proteins from the three kingdoms of life. *Journal of molecular biology* **337,** 635–645.

Yamaguchi N. 2021. LEAFY, a Pioneer Transcription Factor in Plants: A Mini-Review. *Frontiers in plant science* **12,** 701406.

Zhai H, Zhang X, You Y, Lin L, Zhou W, Li C. 2020. SEUSS integrates transcriptional and epigenetic control of root stem cell organizer specification. *The EMBO journal* **39,** e105047.

Zhang X, Henriques R, Lin S-S, Niu Q-W, Chua N-H. 2006. Agrobacterium-mediated transformation of Arabidopsis thaliana using the floral dip method. *Nature protocols* **1,** 641–646.

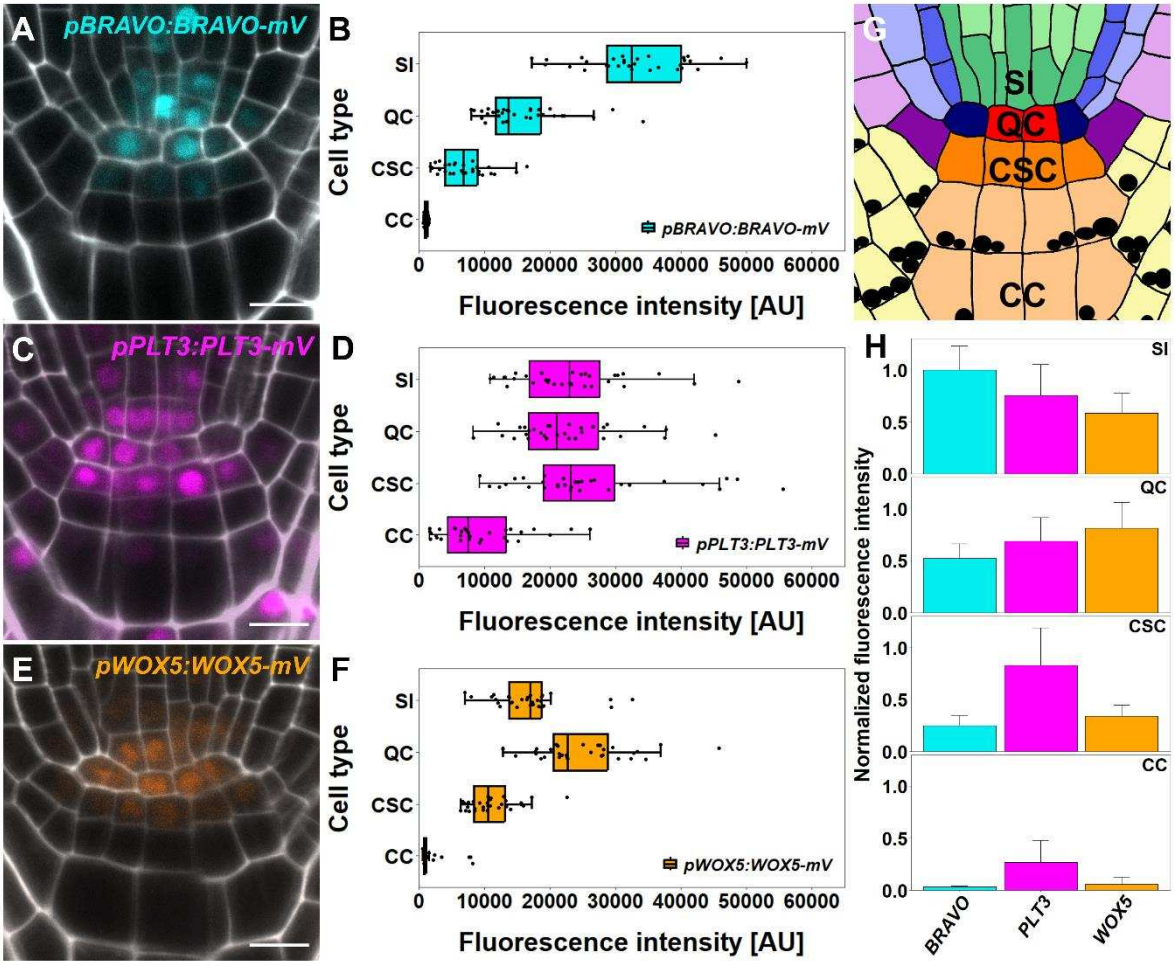

Figure 1: Abundance of BRAVO, PLT3 and WOX5 in the Arabidopsis RAM. Representative images of translational reporter of **A)** BRAVO, **C)** PLT3 and **E)** WOX5 in wildtype *Col-0* background in the RAM as well as the cell type specific quantification of mVenus (mV) fluorescence intensity in **B)** for BRAVO, **D)** for PLT3 and **F)** for WOX5. **G)** Schematic overview of the organisation of the Arabidopsis RAM. The different cell types are represented by different colours. QC: red, cortex endodermis initial: dark blue, endodermis: mid blue, cortex: light blue, stele initials (SI): green, stele: light green, lateral root cap/epidermis initial: purple, epidermis: light purple, lateral root cap: light yellow, columella stem cell (CSC): orange and columella cell (CC): light orange. Starch granules are visualised as black dots. **H)** Bar plot representing the mean fluorescence intensities of mV in BRAVO, PLT3 or WOX5 translational reporters in SIs, QCs, CSCs and CCs normalized to the maximum intensity found for BRAVO in SIs. Error bars display standard deviation. Cell walls were stained using PI and are shown in white, expression of TF is visualized by mVenus in cyan (BRAVO), pink (PLT3) or orange (WOX5). Scalebars represent 10 µm.

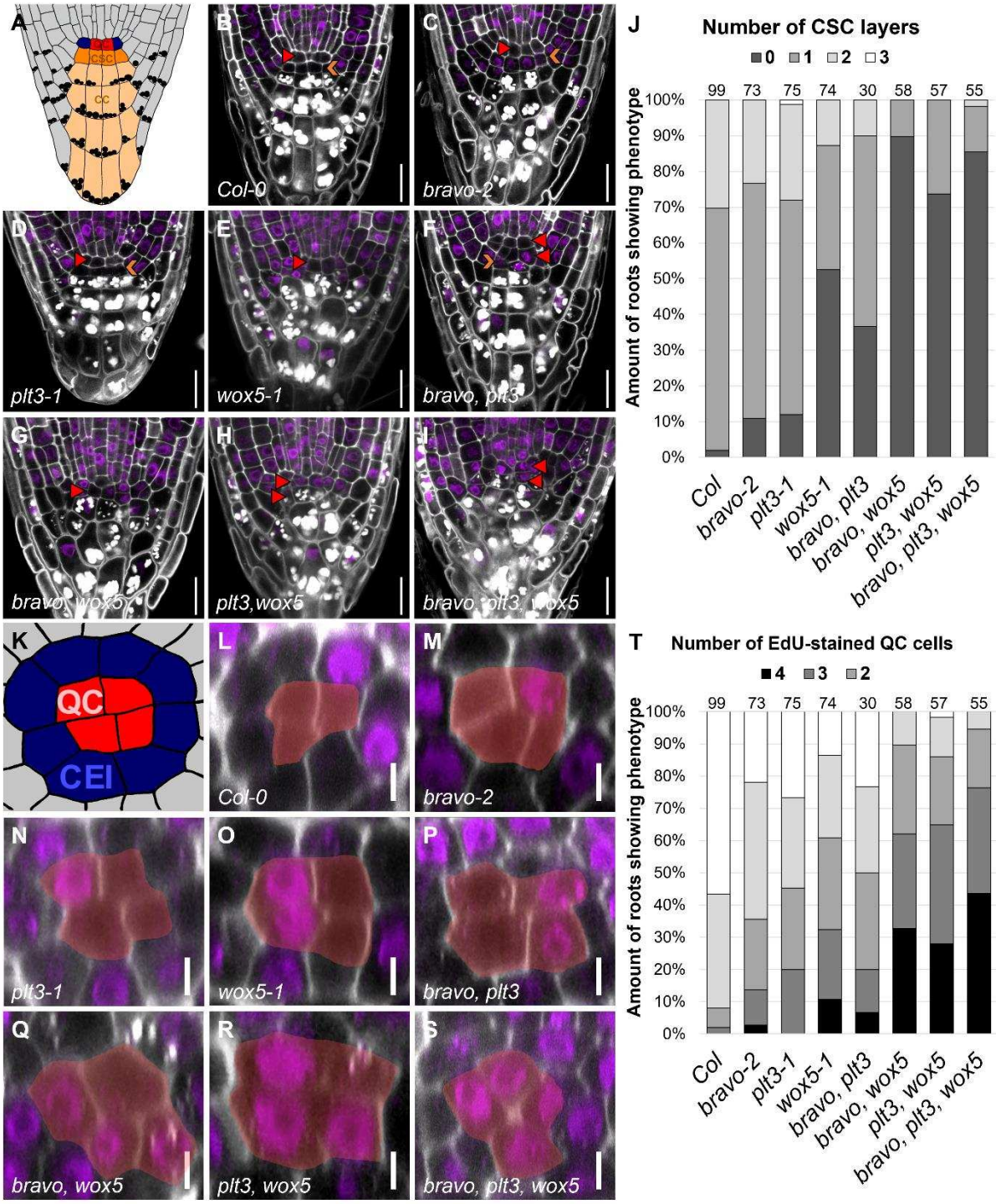

Figure 2: BRAVO, PLT3 and WOX5 jointly regulate CSC differentiation and QC quiescence. A) Schematic representation of a longitudinal section of the Arabidopsis RAM. Red: QC, blue: CEI, dark orange: CSC, light orange: CC. **B-I)** Representative images of the mutant CSC phenotype in the indicated mutant background after combined mPSPI (white) EdU (purple) staining. The position of the QC is indicated by a red arrowhead and the CSC layer is marked with an orange arrowhead. Scale bars represent 20 µm. **J)** Quantification of SCN staining displaying 0, 1, 2 or 3 layers of CSC. The number of analyzed roots for each genotype is

indicated above each bar and results from to 3-5 technical replicates. **K)** Schematic representation of a transversal section of the Arabidopsis RAM. QC cells are highlighted in red and CEIs are displayed in blue. **L-S)** Representative images of optical cross sections of the Arabidopsis RAM in the indicated mutant background. The combined mPSPI/EdU staining reveals the cells that have divided within 24 h. QC is highlighted in yellow. Scale bars represent 5 µm **T)** Quantification of SCN staining displaying 0, 1, 2, 3 or 4 or more QC divisions. The number of analyzed roots for each genotype is indicated above each bar and result from to 3-5 technical replicates.

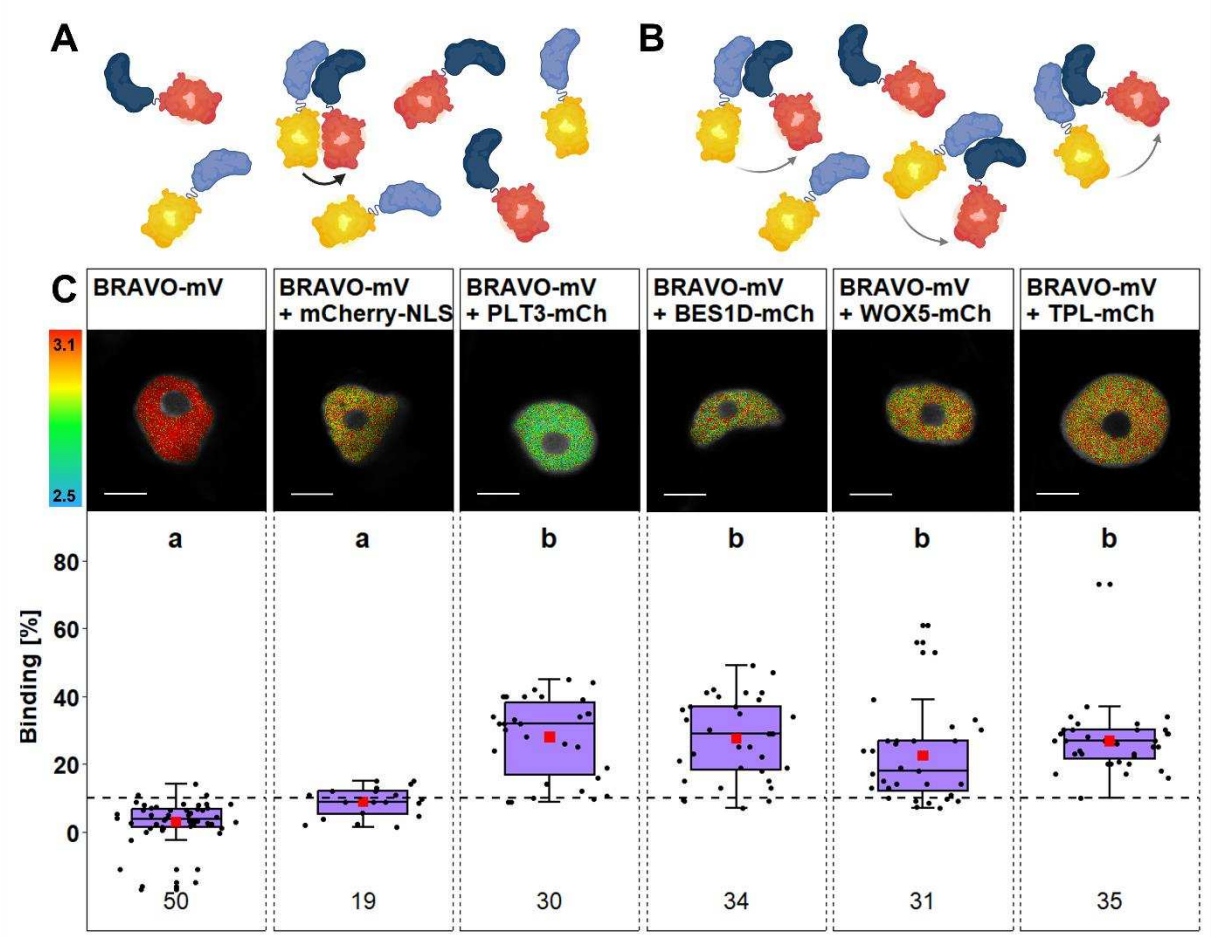

Figure 3: BRAVO interacts with PLT3, WOX5, BES1D and TPL. A) A reduction of fluorescence lifetime as a consequence of FRET can either be a result of a highly efficient energy transfer indicating close proximity or **B)** a high affinity of the two proteins. Figure created with BioRender.com and modified from (Maika *et al.*, 2023). **C) Upper panel:** Representative images of fluorescence lifetime imaging microscopy (FLIM) measurements of nuclei in *N. benthamiana* epidermal leaf cells after pixel-wise mono- or biexponential fitting. The fluorescence lifetime of the donor BRAVO-mV in absence or presence of the indicated acceptor (of mCherry-NLS, PLT3-mCh, BES1D-mCh, WOX5-mCh or TPL-mCh) is color-coded: blue (2.5) refers to low fluorescence lifetime [in ns], red (3.1) indicates high fluorescence lifetime [in ns]. Scale bars represent 6 µm. **Lower panel:** Binding values [%] are represented as purple box plots of the same samples as in the upper panel. Statistical groups were assigned after a non-parametric Kruskal-Wallis ANOVA with *post-hoc* Dunn's test ($\alpha = 0.05$). Mean values are visualised as red squares. Black dotted line indicates the Binding cut-off of 10 %. Number of analysed nuclei is indicated below each sample and results from 3-5 technical replicates. Partially created with BioRender.com.

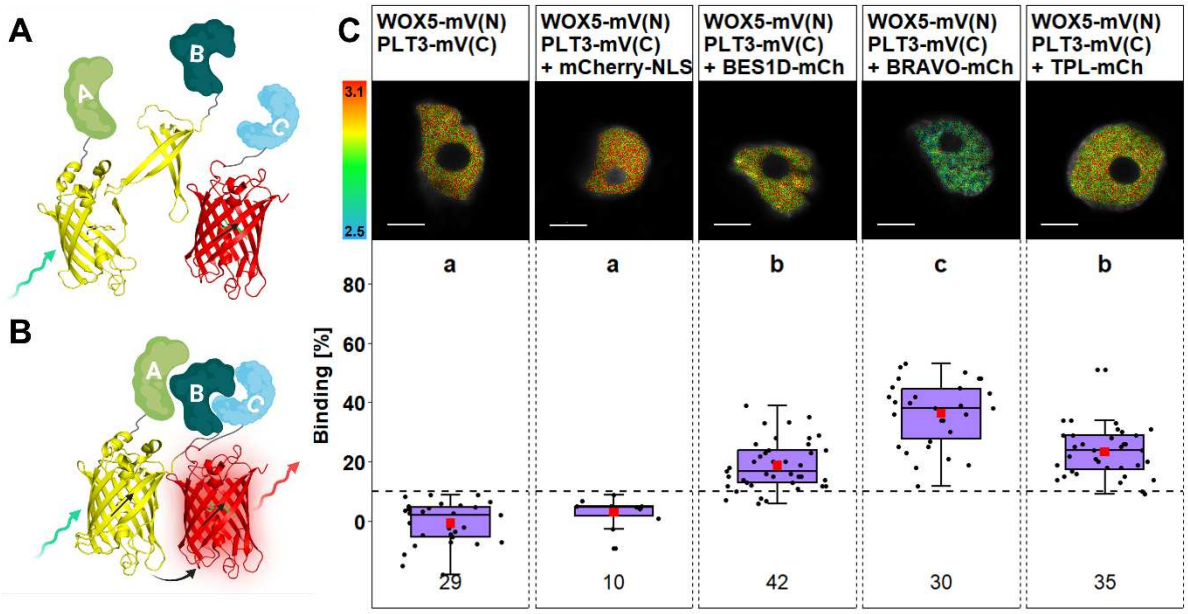

Figure 4: Trimeric complex formation of WOX5 and PLT3 with BRAVO, BES1D and TPL. A) The combination of BiFC-FRET allows the detection of higher-order complexes. Here, the two fragments of a split donor fluorophore are fused to two proteins of interest (POI), while a third POI is fused to the acceptor. **B)** In case of trimeric complex formation, the donor molecule is reconstructed and transfer energy to the acceptor molecule by FRET after excitation. Created with BioRender.com and modified from (Strotmann and Stahl, 2022). **C) Upper panel:** Representative images of fluorescence lifetime imaging microscopy (FLIM) measurements of nuclei *N. benthamiana* epidermal leaf cells after pixel-wise mono- or biexponential fitting. The fluorescence lifetime of the donor WOX5-mV(N)/PLT3-mV(C) in absence or presence of the indicated acceptor (mCherry-NLS, BES1D-mCh, BRAVO-mCh or TPL-mCh) is color-coded: blue (2.5) refers to low fluorescence lifetime [in ns], red (3.1) indicates high fluorescence lifetime. Scale bars represent 6 µm. **Lower panel:** Binding values [%] are represented as purple boxplots of the same samples as in the upper panel. Statistical groups were assigned after non-parametric Kruskal Wallis ANOVA with *post-hoc* Dunn's test (α = 0.05). Mean values are visualised as red squares. Black dotted line indicates the Binding cut-off of 10 %. Number of analysed nuclei is indicated below each sample and results from 2-3 technical replicates. Partially created with BioRender.com.

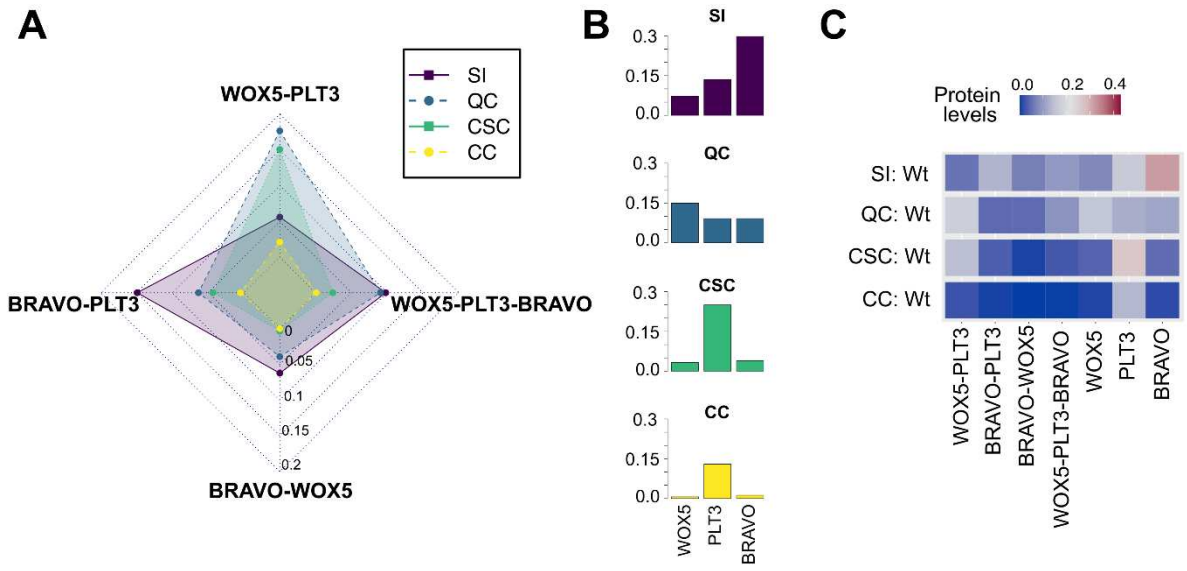

Figure 5. *In silico* prediction of protein complex signatures in the WT root SCN. **A)** Radar plot showing the levels of heterodimers and trimeric complex of WOX5, PLT3 and BRAVO formed in the SI (purple), QC (blue), CSC (green) and CC (yellow). The radial axis shows the protein levels (in arbitrary units). **B)** Free WOX5, PLT3 and BRAVO protein in each of the simulated root SCN cells. **C)** Heatmap showing the protein complexes and free protein in the cells of WT simulation. High concentrations are displayed in red, low concentration are displayed in blue. SI: stele initals; QC: quiescent center; CSC: columella stem cells; CC: columella cells.

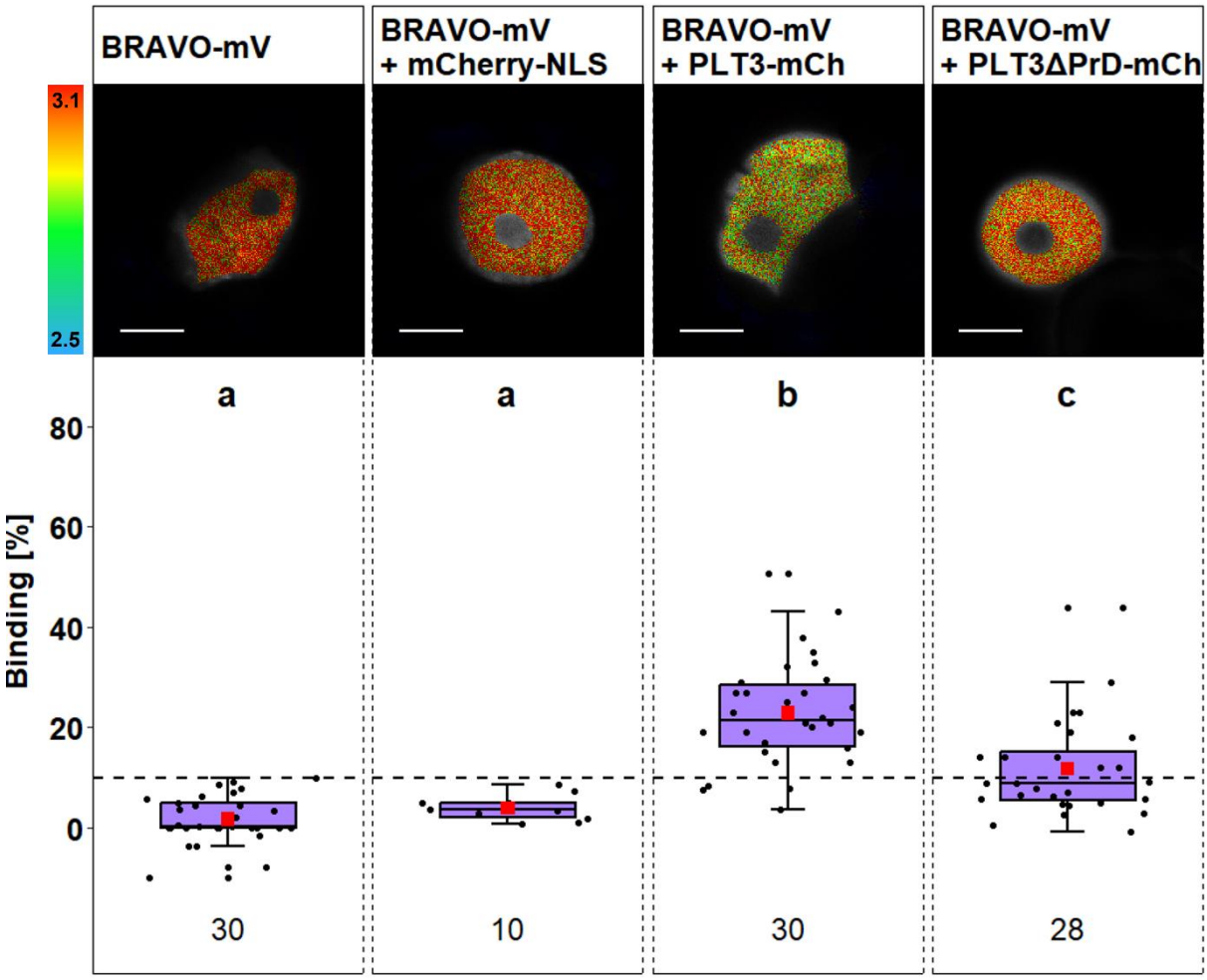

Figure 6: PrDs of PLT3 stabilize interaction with BRAVO. Upper panel: Representative images of fluorescence lifetime imaging microscopy (FLIM) measurements of nuclei in *N. benthamiana* epidermal leaf cells after pixel-wise mono- or biexponential fitting. The fluorescence lifetime of the donor BRAVO-mV in absence or presence of the indicated acceptor (mCherry-NLS, PLT3-mCh or PLT3dPrD-mCh) is color-coded: blue (2.5) refers to low fluorescence lifetime [in ns], red (3.1) indicates high fluorescence lifetime. Scale bars represent 6 µm. **Lower panel:** Binding values [%] are displayed as purple box plots of the same samples as the upper panel. Statistical groups were assigned after non-parametric Kruskal Wallis ANOVA with *post-hoc* Dunn's test (α = 0.05). Mean values are visualised as red squares. Black dotted line indicates the Binding cut-off of 10 %. Number of analysed nuclei is indicated below each sample and results from 2-3 technical replicates.

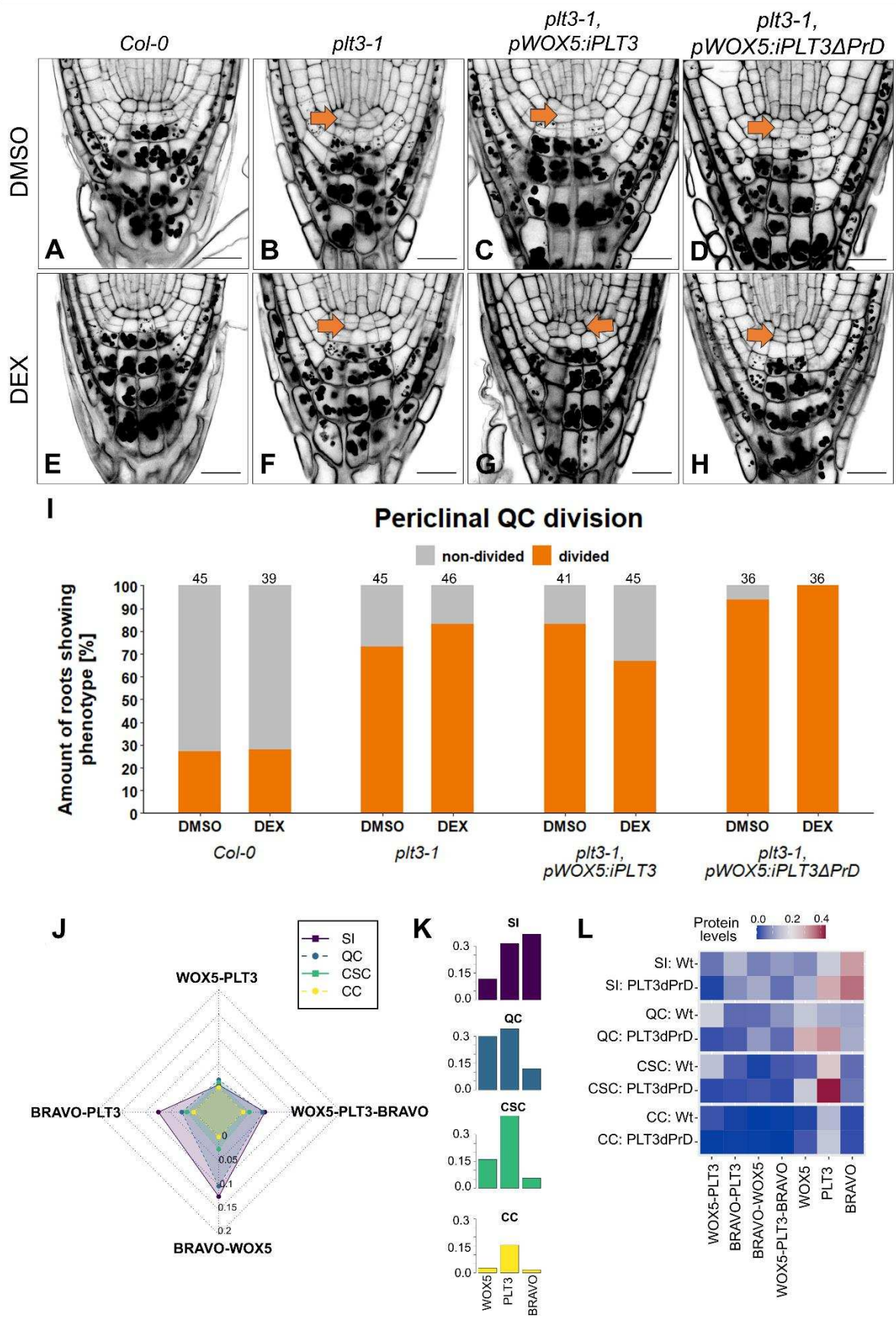

Figure 7. PLT3 PrDs inhibit periclinal QC divisions and *in silico* predicted protein complex signatures in the root SCN. Representative images of the

Arabidopsis root meristem showing additional periclinal cell divisions in the QC in the absence **A-D)** or presence **E-H)** of DEX in the indicated genetic background. Divided QCs are highlighted with orange arrows. Scalebars represent 20 μm. **I)** Quantification of periclinal cell divisions when roots are treated with DMSO or DEX. Number of analysed roots is indicated above each bar and results from three replicates. **J)** Radar plot showing the levels of heterodimers and trimeric complex between WOX5, PLT3 and BRAVO formed in the stele initials (purple), QC (blue), CSC (green) and CC (yellow). **K)** Free WOX5, PLT3 and BRAVO protein in each of the simulated root SCN cells. **L)** Heatmap showing the protein complexes and free protein in the cells of WT and PLT3ΔPrD simulations, the profiles are visibly different with a marked increase in free PLT3 in the CSC. High concentrations are displayed in red, low concentration are displayed in blue. SI: stele initials; QC: quiescent center; CSC: columella stem cells; CC: columella cells.

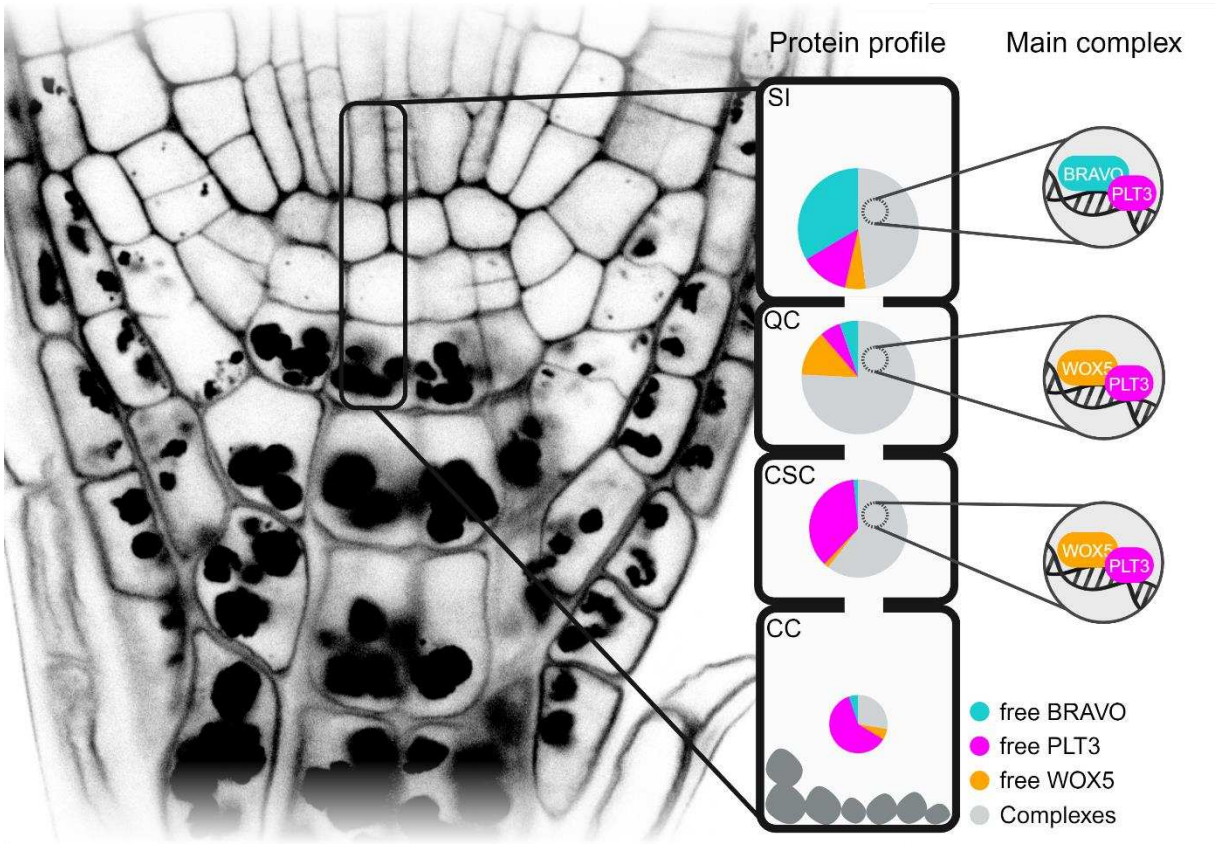

Figure 8: Model of protein signatures and complexes in the root SCN. The nuclei of different cell types (SI, QC, CSC, CC) show distinct protein profile of free BRAVO (turquoise), PLT3 (magenta), and WOX5 (orange) protein levels and main complexes (gray and insets). The size of the pie chart reflects the overall protein concentration in the nuclei of the specific cell type from high concentration (big) to low concentration (small). Created with BioRender.com.

Appendix

Table of Contents

List of figures

List of tables

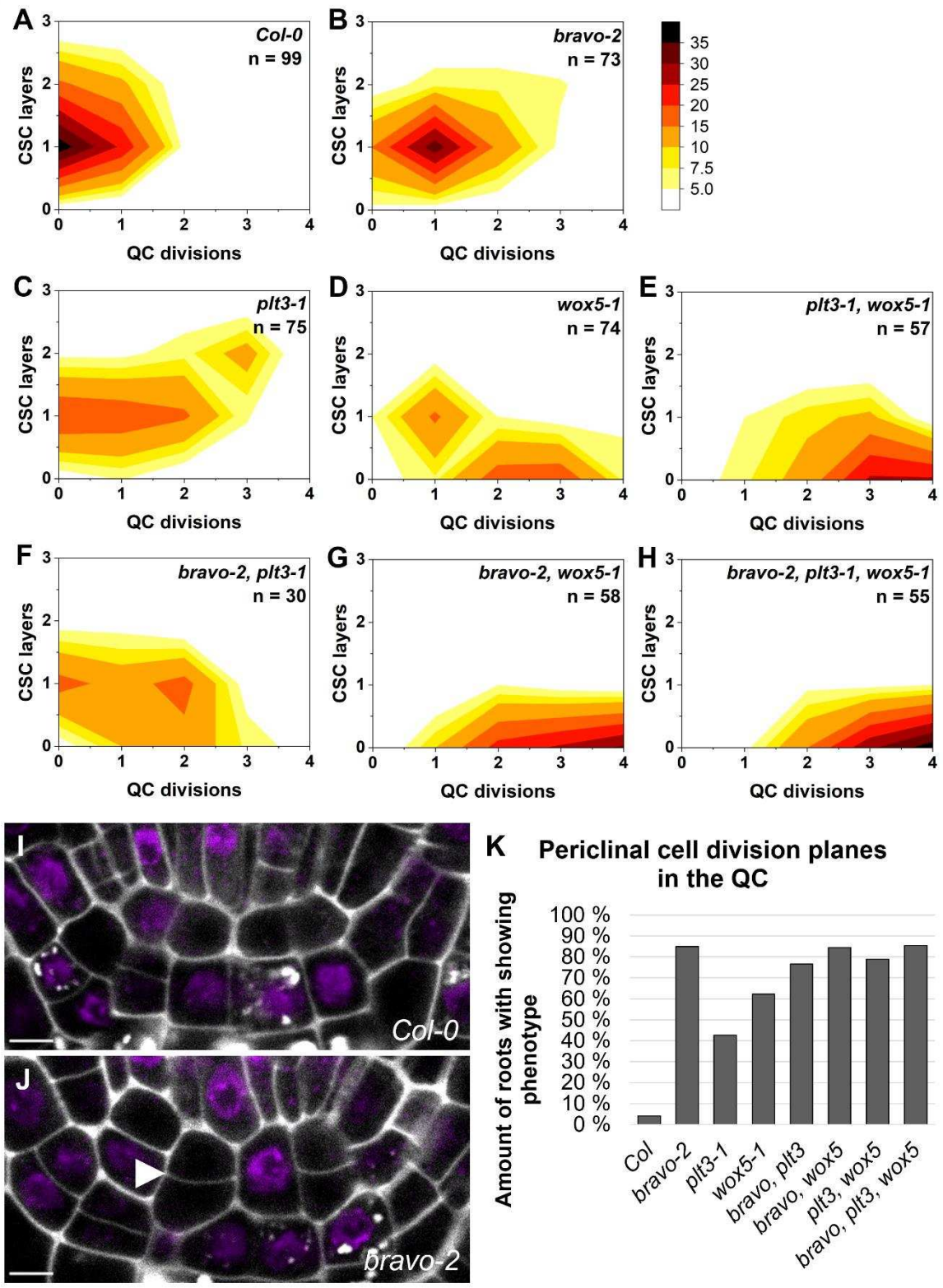

Figure S1: Elevated QC division frequencies negatively correlate to the number of CSC layers. A-H. 2D histograms visualizing the combined results of the SCN staining in the respective genotype showing the number of CSC layers on the y-axis and QC divisions on the x-axis. Darker colours correspond to a higher number of roots showing the phenotype. Number of analysed roots per genotype (biological

replicate) is indicated in each graph and results from 3-5 technical replicates. **I.** Close-up of the QC in the Col-0 WT and **J.** in the *bravo-2* mutant showing an additional periclinal cell division plane (white arrowhead). **K.** Quantification of periclinal cell division planes in the different mutants.

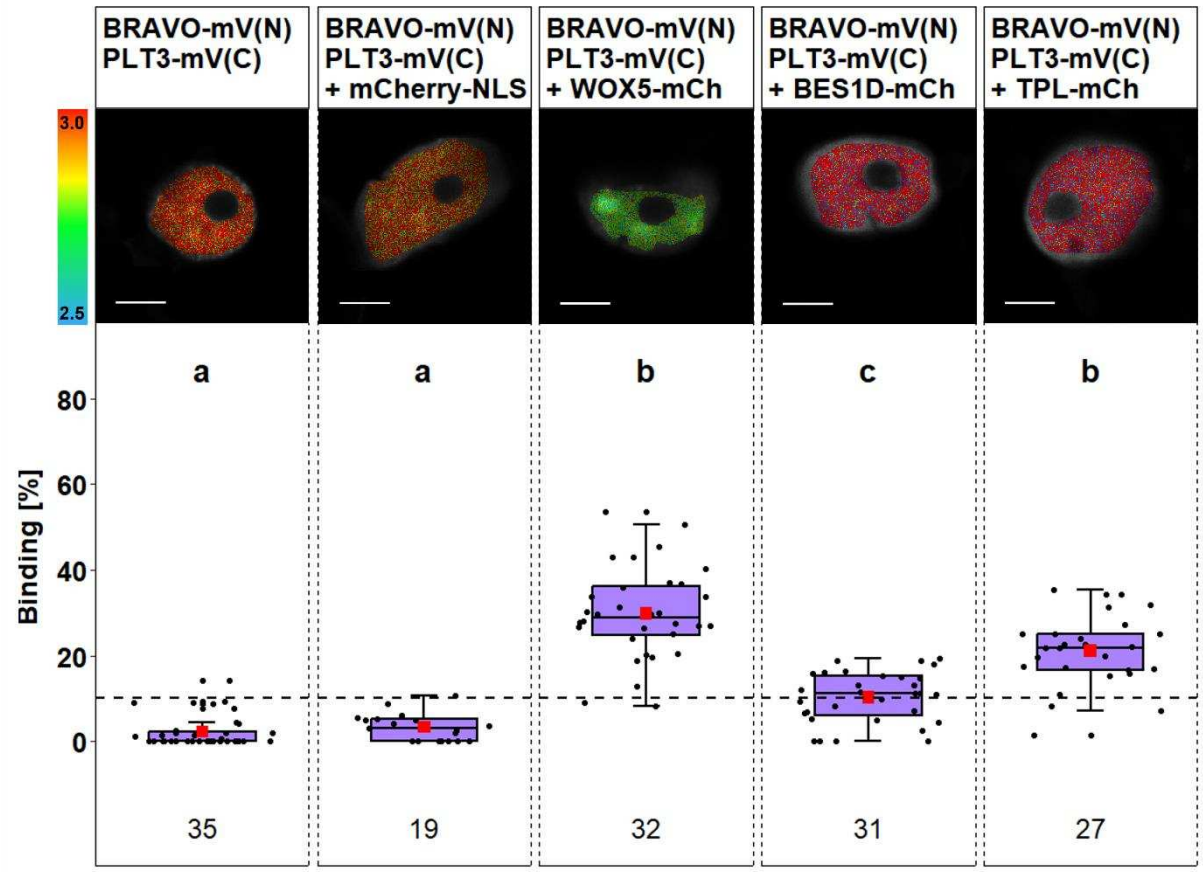

Figure S2: Trimeric complex formation of BRAVO and PLT3 with WOX5, BES1D and TPL. Upper panel: Representative images of fluorescence lifetime imaging microscopy (FLIM) measurements in *N. benthamiana* epidermal leaf cells after a pixel-wise mono- or biexponential fit. The fluorescence lifetime of the donor BRAVO-mV(N) PLT3-mV(C) in presence or absence of the indicated acceptor is color-coded: blue (2.5) refers to low fluorescence lifetime [in ns], red (3.0) indicates high fluorescence lifetime. Scale bar represents 6 µm. **Lower panel:** Binding [%] (magenta) for BRAVO-mV(N) PLT3-mV(C) with or without co-expression of mCherry-NLS, WOX5-mCh, BES1D-mCh or TPL-mCh. Statistical groups were assigned after a non-parametric Kruskal Wallis ANOVA with *post-hoc* Dunn's test ($\alpha = 0.05$). Black dotted line indicates the Binding cut-off of 10 %. Number of analysed nuclei is indicated below each sample and results from 3-4 technical replicates.

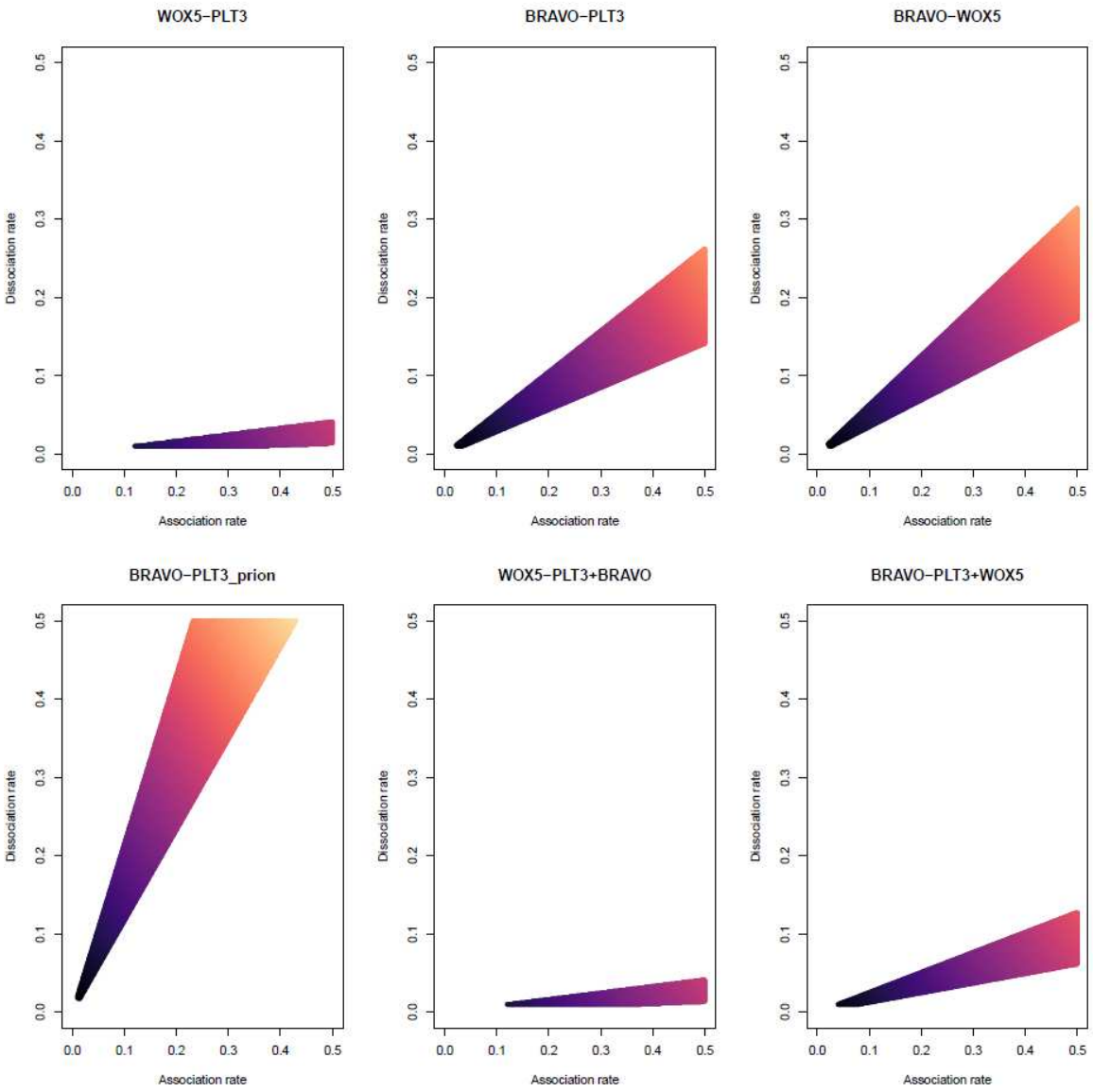

Figure S3: Association and dissociation parameters predicted for the heterodimers and trimeric complex modelled. For each protein complex studied we show the combination of association and dissociation parameters (colored area) that can produce the protein complex formation in agreement with the binding affinities described experimentally.

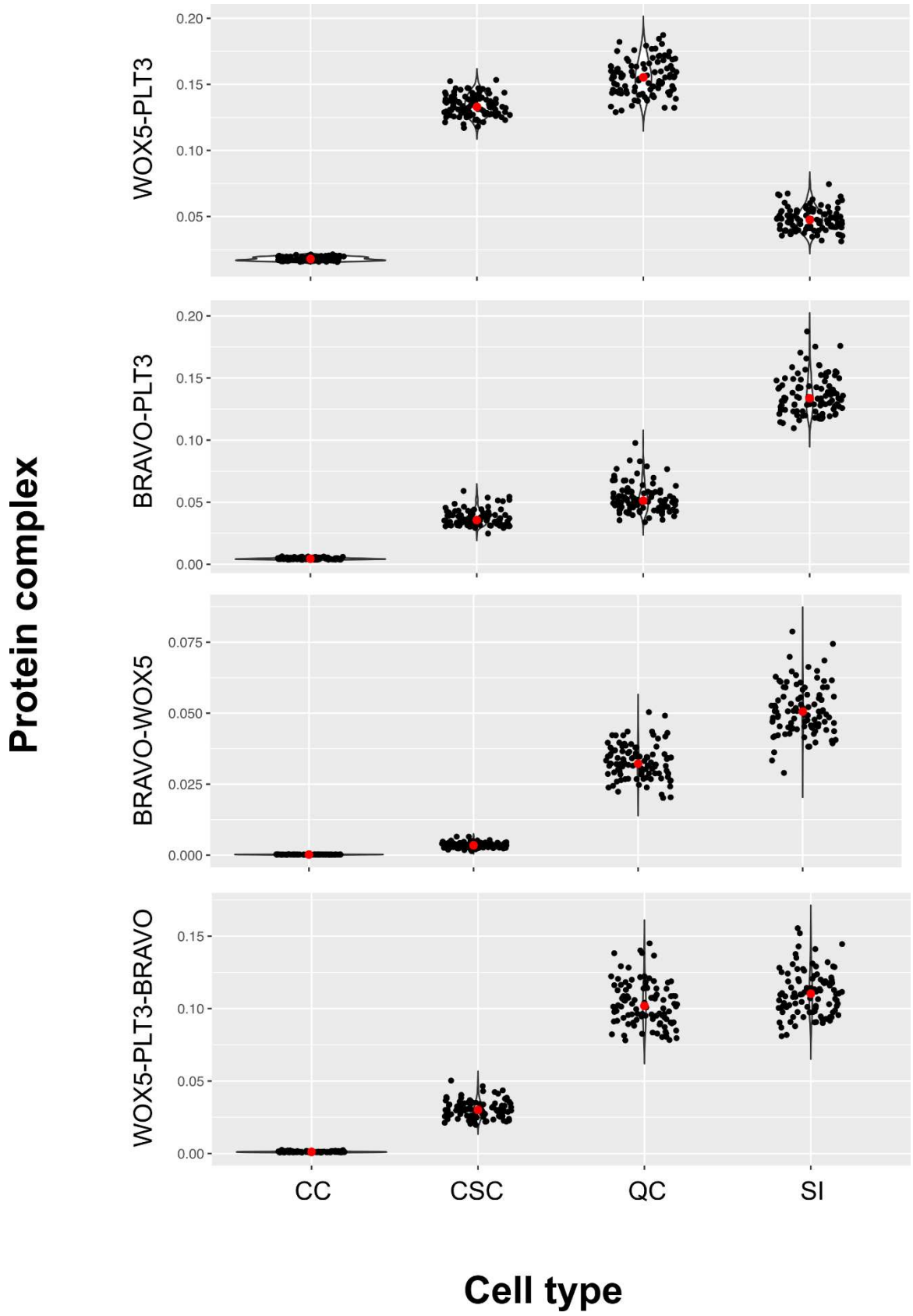

Figure S4: Robustness of the protein complex cell signatures. Simulations of the formation of protein complexes in the cells of the root stem cell niche using 100 different association and dissociation parameter sets. The resulting levels of each

simulation for WOX5-PLT3, BRAVO-PLT3, BRAVO-WOX5 and WOX5-PLT3-BRAVO in each cell type are shown, indicating they are robust to the specific parameters used in the simulations. Mean values shown in red.

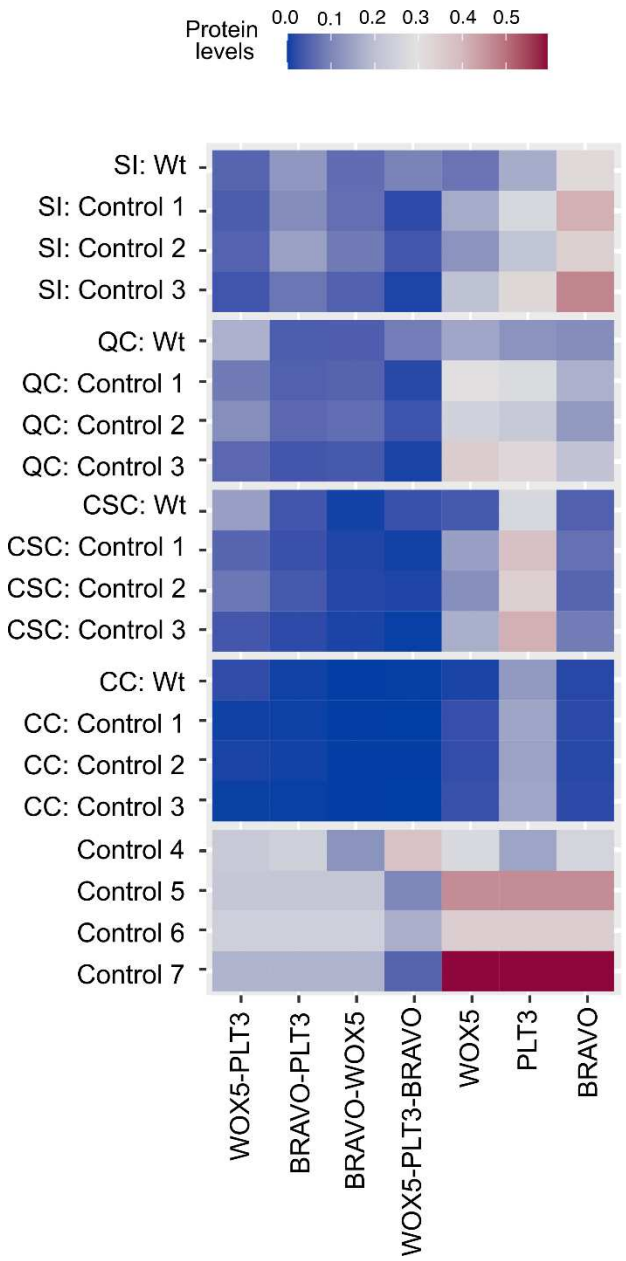

Figure S5:Controls for *in silico* prediction of protein complex signatures in the WT root SCN. For Control 1-3, the experimentally determined protein abundances were used, combined with the assumptions that association and dissociation rates are equal, a higher association and a higher dissociation rate, respectively. For Control 4, experimentally determined association and dissociation rates were used in combination with equal protein abundances among all cell-types and TFs. Controls 5-7 combine equal protein levels with assumed association/dissociation rates from Control 1-3, respectively. Heatmap showing the protein complexes and free protein in the cells of WT simulation. High concentrations are displayed in red, low concentration are displayed in blue. SI: stele initals; QC: quiescent center; CSC: columella stem cells; CC: columella cells.

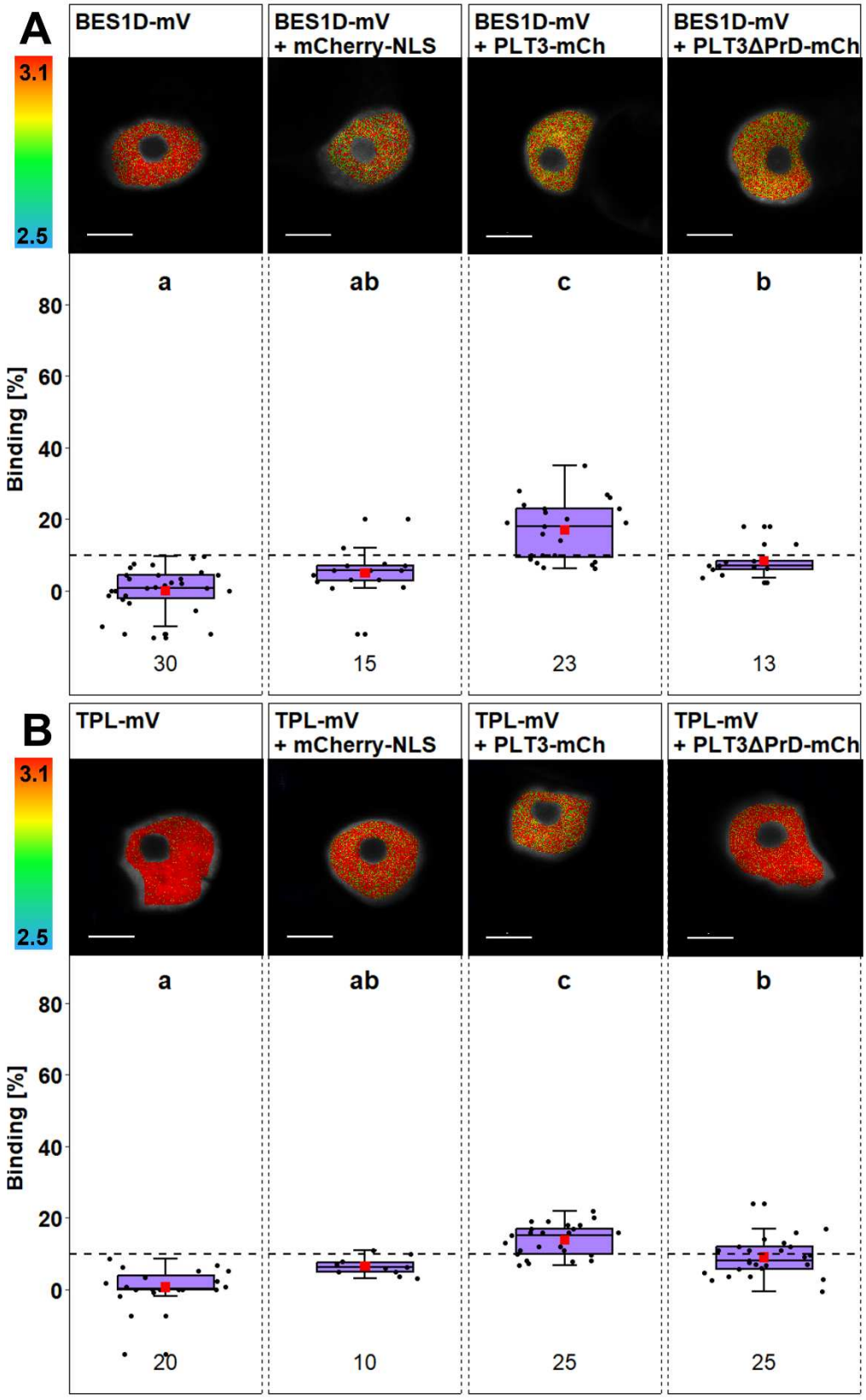

Figure S6: Interaction of PLT3 with BES1D and TPL depends on PrDs found in PLT3. Upper panels: Representative images of fluorescence lifetime imaging microscopy (FLIM) measurements in *N. benthamiana* epidermal leaf cells after a pixel-wise mono- or biexponential fit. The fluorescence lifetime of the donor BES1D-

mV (A) or TPL-mV (B) in presence or absence of the indicated acceptor is color-coded: blue (2.5) refers to low fluorescence lifetime [in ns], red (3.1) indicates high fluorescence lifetime. Scale bar represents 6 µm. Lower panels: Binding [%] (magenta) for BES1D-mV (A) or TPL-mV (B) with or without co-expression of mCherry-NLS, PLT3-mCh or PLT3dPrD-mCh. Statistical groups were assigned separately for experiments with BES1D-mV and TPL-mV after a non-parametric Kruskal Wallis ANOVA with *post-hoc* Dunn's test ($\alpha = 0.05$). Black dotted line indicates the Binding cut-off of 10 %. Number of analysed nuclei is indicated below each sample and results from 2-3 technical replicates.

Table S1: List of primers used for cloning. Italic bases represent overhangs and *Bsa*I recognition sites necessary for GreenGate cloning.

Gene identifier	alias	Primer name	Orientation	Sequence 5'-3' orientation
Promoter modules				
AT5G17800	BRAVO	VS_GG_pBRAVO_F	F	*AAAGGTCTCAACCT*CCACTAACCATTTCGTAA
		VS_GG_pBRAVO_R	R	*AAAGGTCTCATGTT*GTTTCTGGTTTAGGGATTA
CDS in C modules				
AT1G19350	BES1	VS_GG_BES1D_CDS_F	F	*AAAGGTCTCAGGCTTA*ATGACGTCTGACGGAGCAA C
		VS_GG_BES1D_CDS_R	R	*AAAGGTCTCACTGA*ACTATGAGCTTTACCATTTCC
AT5G17800	BRAVO	RD_GG_BRAVO F	F	*AAAGGTCTCAGGCTTA*ATGAATCCAAATC
		RD_GG_BRAVO R	R	*AAAGGTCTCACTGA*GGAAGCTCCAAC
AT1G15750	TPL	VS_GG_TPL_CDS_F	F	*AAAGGTCTCAGGCTTA*ATGTCTTCTCTTAG
		VS_GG_TPL_CDS_R	F	*AAAGGTCTCACTGA*TCTCTGAGGCTG

Table S2: List of primers used for genotyping.

Gene ID	SALK ID	alias	Primer		
			Orientation	Name	Sequence 5'-3'
AT5G17800	SALK_062413	*bravo-2*	F	VS_bravo-2_F	TCCCTTAATCCCTAAACCCAGC
			R	VS_bravo-2_R	CCTGATGCAAGGGTACTATCG
AT3G11260	SALK_038262	*wox5-1*	F	GK_WOX5 F	AAACAGTTGAGGACTTTACATCTGA
			R	WOX5 R	CGGATAATATGTCATAATTCAAAAT
AT5G10510	SALK_127417	*plt3-1*	F	GK_PLT3L	TTGTGATTTGCCATTGACTAAAGGT
			R	GK_PLT3R	GAAAACAGTCCAATGGTCTCACATC

Table S3: List of entry vectors used for GreenGate cloning.

Name	Module (Backbone)	Insert	Reference
pGGB002	B	Omega element	(Lampropoulos et al. 2013)
pGGD007	D	Linker-NLS	
pGGE009	E	UBIQUITIN 10 terminator	
pGGF002	F	BASTA resistance	
pGGG001	G	Adapter	
pGGG002	G	Adapter	
pGGM000	M	Empty intermediate vector	
pGGN000	N	Empty intermediate vector	
pGGZ001	Z	Empty destination vector	
pRD42	C	mVenus	(Burkart et al. 2022)
pRD43	D	mVenus	
pRD53	D	mCherry	
pRD45	A	*WOX5* promoter	
pRD40	C	WOX5 CDS	
pRD41	C	PLT3 CDS	
pRD65	B	Glucocorticoid receptor	
pRD101	C	PLT3dPrD	
pPD161	A	Ubi-XVE oLexA-35S	(Denninger et al. 2019)
pVS125	A	*BRAVO* promoter	This study
pRD135	C	BRAVO CDS	
pVS191	C	BES1D	
pVS84	C	TPL	
pJM81	D	mVenus(N)	(Maika et al. 2023)
pJM82	D	mVenus(C)	
pBLAD011	D	mTurquoise2	

Table S4: List of expression vectors for stable transformation of *A. thaliana* or transient transformation of *N. benthamiana* generated in this study.

Plasmid ID	Construct	GreenGate module							Resistance
		A	B	C	D	E	F	Z	
pVS133	pBRAVO:BRAVO-mV	*BRAVO* promoter	Ω element (pGGB002)	BRAVO	mVenus	UBQ10 terminator (pGGE009)	BASTA R (pGGF002)	pGGZ001	Spec
pVS139	Inducible BES1D-mVenus	Ubi-XVE oLexA-35S	Ω element (pGGB002)	BES1D	mVenus	UBQ10 terminator (pGGE009)	BASTA R (pGGF002)	pGGZ001	Spec
pVS140	Inducible BES1D-mCherry	Ubi-XVE oLexA-35S	Ω element (pGGB002)	BES1D	mCherry	UBQ10 terminator (pGGE009)	BASTA R (pGGF002)	pGGZ001	Spec
pVS141	Inducible BRAVO-mVenus	Ubi-XVE oLexA-35S	Ω element (pGGB002)	BRAVO	mVenus	UBQ10 terminator (pGGE009)	BASTA R (pGGF002)	pGGZ001	Spec
pVS142	Inducible BRAVO-mCherry	Ubi-XVE oLexA-35S	Ω element (pGGB002)	BRAVO	mCherry	UBQ10 terminator (pGGE009)	BASTA R (pGGF002)	pGGZ001	Spec
pVS143	Inducible TPL-mCherry	Ubi-XVE oLexA-35S	Ω element (pGGB002)	TPL	mCherry	UBQ10 terminator (pGGE009)	BASTA R (pGGF002)	pGGZ001	Spec
pVS85	Inducible TPL-mVenus	Ubi-XVE oLexA-35S	Ω element (pGGB002)	TPL	mVenus	UBQ10 terminator (pGGE009)	BASTA R (pGGF002)	pGGZ001	Spec
pVS154	Inducible WOX5-mVenus(N)	Ubi-XVE oLexA-35S	Ω element (pGGB002)	WOX5	mVenus(N)	UBQ10 terminator (pGGE009)	-	pGGM000	Kan
pVS156	Inducible PLT3-mVenus(C)	Ubi-XVE oLexA-35S	Ω element (pGGB002)	PLT3	mVenus(C)	UBQ10 terminator (pGGE009)	BASTA R (pGGF002)	pGGN000	Kan
pVS163	Inducible WOX5-mVenus(N)/ Inducible PLT3-mVenus(C)	pVS154 + pVS156						pGGZ001	Spec
pVS167	Inducible nuclear localized mCherry	Ubi-XVE oLexA-35S	Ω element (pGGB002)	mCherry (pGGC015)	linker-NLS (pGGD007)	UBQ10 terminator (pGGE009)	BASTA R (pGGF002)	pGGZ001	Spec
pVS180	Inducible BRAVO-mVenus(N)	Ubi-XVE oLexA-35S	Ω element (pGGB002)	BRAVO	mVenus(N)	UBQ10 terminator (pGGE009)	-	pGGM000	Kan

pVS233	Inducible BRAVO-mVenus(N)/ Inducible PLT3-mVenus(C)	pVS180 + pVS156						pGGZ001	Kan
pVS288	pWOX5:GR-PLT3-mTurquoise2	*WOX5* promoter	GR	PLT3	mT2	UBQ10 terminator (pGGE009)	BASTA R (pGGF002)	pGGZ001	Spec
pVS289	pWOX5:GR-PLT3ΔPrD-mTurquoise2	*WOX5* promoter	GR	PLT3ΔPrD	mT2	UBQ10 terminator (pGGE009)	BASTA R (pGGF002)	pGGZ001	Spec

Table S5: List of Arabidopsis mutants and transgenic lines used in this study.

Gene ID	Alias	Reference
AT5G17800	*bravo-2*	(Vilarrasa-Blasi et al. 2014)
	Col-0, pBRAVO:BRAVO-mVenus	This study by dipping
AT5G10510	*plt3-1*	(Galinha et al. 2007)
	Col-0, pPLT3:PLT3-mVenus	(Burkart et al. 2022)
AT5G17800, AT5G10510	*bravo-2, plt3-1*	This study by crossing of *bravo-2* and *plt3-1*
AT3G11260	*wox5-1*	(Burkart et al. 2022)
	Col-0, pWOX5:WOX5-mVenus	
AT5G10510, AT3G11260	*plt3-1, wox5-1*	(Burkart et al. 2022)
	plt3-1, pWOX5:GR-PLT3-mTurquoise2	This study by dipping
	plt3-1, pWOX5:GR-PLT3ΔPrD-mTurquoise2	This study by dipping
AT5G17800, AT3G11260	*bravo-2, wox5-1*	(Betegón-Putze et al. 2021)
AT5G17800, AT5G10510, AT3G11260	*bravo-2, plt3-1, wox5-1*	This study by crossing of *bravo-2* and *plt3-1, wox5-1*

Table S6: Fluorescence intensities of *pPLT3:PLT3-mV, pBRAVO:BRAVO-mV* and *pWOX5:WOX5-mV* translational reporter in different cell types corresponding to Fig. 1, 5 and 7.

Fluorescence intensity	Date	Cell type			
		SI	QC	CSC	CC
pPLT3:PLT3-mV	28.11.23	30360.17	37523.45	48567.14	17482.71
		19709.9	18540.11	22274.4	15590.86
		19782.11	16327.93	26233.66	6335.124
		24665.88	22914.56	22039.49	13233.82
		16336.64	14473.61	16777.05	7263.823
		20659.51	17532.76	19131.18	9199.955
		48822.24	37769.87	55574.26	5490.301
		42071.03	23881.81	28888.19	6474.87
		31306.43	28682.1	43367.48	26115.04
		26035.98	24754.96	37376.88	5407.617
	AV	27974.99	24240.11	32022.97	11259.41
	SD	9945.883	7853.973	12737.42	6457.178
	08.12.23	13458.53	12022.34	10693.72	3079.556
		11382.8	19661.37	23237.77	2543.246
		31222.01	28196.38	24778.53	1576.29
		28921.69	24819.56	21161.82	6278.363
		25231.6	12692.34	9225.459	9485.656
		14733.96	15308.52	30900.44	19996.52
		13009.25	19128.18	18887.84	1805.671
		17399.32	20006.95	19149.94	6983.197
		10872.27	8227.07	12223.45	1741.223
		21828.1	21030.97	24277.79	2664.413
	AV	18805.95	18109.37	19453.67	5615.413
	SD	7111.341	5781.51	6587.363	5426.973
	28.12.23	36705.69	30759.92	32179.98	13431.11
		23201.13	22910.14	26746.3	12992.69
		14505.16	16790.7	14650.75	10778.34
		25326.28	16618.53	15902.32	7739.259
		22976.1	22252.79	13183.53	15139.32
		26289.13	34416.08	46981.29	13944.07
		23456.61	45225.47	45902.98	7467.853
		19359.14	19409.83	23114.97	23172.93
	AV	23977.41	26047.93	27332.76	13083.19
	SD	5938.235	9373.698	12570.98	4640.888
	Overall AV	23267.05	22671.05	25904.29	9224.714
	Overall SD	8745.45	8164.877	11578.14	6400.249
pWOX5:WOX5-mV	28.11.23	29201.12	45834.2	10795.79	896.549
		13869.69	21386.9	8486.974	1496.997
		19027.65	28070.95	7576.267	779.7283
		14906.16	27262.89	9271.191	685.0723
		15691.41	27641.05	6953.646	687.679
		17316.21	20991.05	10378.01	705.1347

		11098.75	30414.8	9765.741	766.4405
		29355.06	22623.3	7448.115	882.8665
		18739.97	22616.32	9814.987	1002.133
		13616.57	17752.29	12525.81	7864.905
	AV	18282.26	26459.37	9301.653	1576.75
	SD	5953.816	7460.556	1638.761	2108.523
	08.12.23	11408.16	12757.81	7483.419	532.5793
		14144.85	17938.5	8482.929	958.597
		18676.1	20097.02	12921.63	838.317
		18215.11	22406.33	10450.67	730.0777
		12329.53	17780.14	8244.796	3459.093
		32552.77	32325.28	15897.64	8156.247
		18057.62	34627.05	17197.87	833.5587
		20081.02	33351.82	12183.4	2112.58
		16962.96	27887.07	13940.99	854.592
		11985.38	14764.86	6683.364	731.142
	AV	17441.35	23393.59	11348.67	1920.678
	SD	5841.4	7655.123	3466.346	2246.346
	28.12.23	18809.39	21126.97	13228.5	969.778
		18091.15	21354.1	13364.58	661.5485
		13782.29	25015.66	7060.959	837.938
		11749.74	32733.76	10815.74	2313.319
		16980.22	19147.65	10490.34	719.408
		16397.84	28137.24	15536.71	1107.079
		17359.42	26238.14	10937.61	680.671
		16533.92	36878.85	15549.16	7561.397
	AV	16213	26329.05	12122.95	1856.392
	SD	2183.395	5708.609	2682.338	2214.819
	Overall AV	16790.78	25132.08	11061.31	1684.39
	Overall SD	5507.95	7039.065	3596.461	2105.804
pBRAVO:BRAVO-mV	**28.11.23**	33296	16940.47	4615.491	852.569
		32465.25	12767.84	8112.653	989.9733
		36508.05	19942.11	14826.77	1133.772
		31225.91	18182.72	8115.524	919.5017
		40549.32	20651.28	8776.193	1081.686
		40143.53	29515.55	8153.343	1102.827
		19431.36	10567.79	3988.657	695.031
		29660.65	12654.5	4704.077	1479.854
		28870.52	16931.86	3053.96	872.8765
		31988.38	16361	8163.813	1257.115
	AV	32413.9	17451.51	7251.048	1038.52
	SD	5777.106	5065.289	3233.365	213.1088
	08.12.23	17139.23	12128.37	3986.173	845.2763
		35034.8	21779.82	10615.84	1246.433
		32923.36	12882.26	6763.008	946.799
		19276.64	14514.07	9689.346	906.56
		25266.62	12037.34	6404.131	734.922

		41025.65	18926.21	7023.33	1303.169
		24780.18	10123.88	3126.593	844.1405
		39899.04	18246.41	10925.48	1296.336
		22975.67	13452.88	11498.59	1244.351
		31024.35	13617	9103.976	1312.867
	AV	28934.55	14770.82	7913.646	1068.085
	SD	7890.066	3481.702	2766.423	219.4884
	28.12.23	46147.85	26669.37	16433.59	1442.835
		49948.21	7967.577	2823.43	770.814
		39406.01	34224.94	6801.504	1497.628
		41437.48	16972.48	5323.483	1414.79
		25584.47	9576.138	2069.954	805.6805
		40467.97	9512.593	5478.113	1207.251
		42555.79	10385.78	5205.178	1349.889
		30363.89	13326.26	9106.051	1152.85
	AV	39488.96	16079.39	6655.162	1205.217
	SD	7454.075	8898.174	4222.165	264.0782
	Overall AV	33047.28	15892.74	6833.518	1058.715
	Overall SD	7897.687	6132.839	3588.269	257.7053

AV: average, STD: standard deviation.

Table S7: Average number of QC divisions and CSC layers per root related to Fig. 2 and S1.

Genotype	Average number of QC divisions per root	Average number of CSC layers per root	Number of analysed roots
Col-0	0.535354	1.282828	99
bravo-2	1.30137	1.123288	73
plt3-1	1.386667	1.293333	75
wox5-1	1.90541	0.594595	74
bravo, plt3	1.5333333	0.73333333	30
bravo, wox5	2.844827586	0.103448276	58
plt3, wox5	2.7719298	0.2631579	57
bravo, plt3, wox5	3.145454545	0.163636364	55

Table S8: Ratio of periclinal cell division planes in the QC related to Fig. S1.

Genotype	Periclinal cell division planes in the QC [%]	Number of analysed roots
Col-0	4	99
bravo-2	85	73
plt3-1	43	75
wox5-1	62	78
bravo, plt3	77	30
bravo, wox5	84	59
plt3, wox5	79	57
bravo, plt3, wox5	85	55

Table S9: Measured FRET efficiency and Binding values related to Fig. 3, 5 and 7.

Sample	**BRAVO-mV**		**BRAVO-mV mCherry-NLS**		**BRAVO-mV PLT3-mCh**		**BRAVO-mV BES1D-mCh**		**BRAVO-mV WOX5-mCh**		**BRAVO-mV TPL-mCh**	
Date	**FRET E**	**Binding**	**FRET E**	**Binding**	**FRET E**	**Binding**	**FRET E**	**Binding**	**FRET E**	**Binding**	**FRET E**	**Binding**
20.12.19	80.00	3.00			54.00	34.00						
	80.00	1.70			51.00	33.00						
	80.00	2.40			56.00	35.00						
	80.00	7.10			54.00	30.00						
	80.00	5.30			60.00	40.00						
	80.00	2.50			53.00	45.00						
	80.00	8.00			57.00	35.00						
	80.00	8.90			53.00	40.00						
	80.00	5.10			58.00	32.00						
	78.00	8.00			59.00	34.00						
04.02.20	9.88	-11.00					80.00	9.20				
	9.88	-17.00					0.97	7.00				
	17.00	7.40					0.66	37.00				
	10.00	-0.30					0.90	13.00				
	71.00	6.30					0.49	34.00				
	80.00	6.90					0.93	15.00				
	80.00	8.20					1.10	22.00				
	9.88	-23.00					0.64	40.00				
	67.00	4.30					1.30	9.05				
	16.00	5.00										
17.02.20	80.00	2.50	45.00	11.00			48.00	29.00	58.00	9.60	43.00	24.00
	80.00	0.51	43.00	8.41			48.00	25.00	55.00	27.00	39.00	27.00
	41.00	8.20	63.00	8.90			46.00	35.00	64.00	14.00	37.00	30.00
	80.00	2.40	50.00	15.00			47.00	19.00	61.00	14.00	46.00	28.00
	10.10	-11.00	53.00	14.00			41.00	29.00	56.00	33.00	40.00	29.00
	75.00	2.20					42.00	30.00	58.00	19.00	43.00	30.00
	80.00	1.00					45.00	33.00	59.00	27.00	40.00	34.00
	80.00	4.10					45.00	47.00	51.00	7.30	42.00	32.00

	80.00	1.40					45.00	41.00	64.00	7.00	49.00	20.00
	80.00	6.70					48.00	49.00	65.00	11.00	38.00	29.00
							41.00	36.00	40.00	24.00	48.00	27.00
							45.00	41.00	49.00	27.00	44.00	32.00
							48.00	42.00	52.00	31.00	77.00	73.00
							45.00	37.00	50.00	39.00	43.00	37.00
							44.00	39.00	55.00	61.00	43.00	34.00
17.08.20	80.00	6.40	80.00	12.00	74.00	8.70			79.00	15.00	59.00	16.00
	80.00	8.20	66.00	9.60	61.00	28.00			66.00	10.00	57.00	18.00
	80.00	11.00	68.00	11.00	80.00	10.00			65.00	17.00	55.00	23.00
	80.00	11.00	80.00	8.90	80.00	8.70			56.00	24.00	56.00	22.00
	80.00	14.00	80.00	13.00	73.00	10.70			55.00	26.00	56.00	20.00
	80.00	5.50	77.00	8.70	77.00	12.00			63.00	14.00	50.00	26.00
	80.00	6.40	80.00	12.00	80.00	9.60					76.00	10.00
	80.00	3.50	78.00	15.00	62.00	16.00					48.00	25.00
	80.00	6.50			55.00	24.00					53.00	20.80
	80.00	3.20			52.00	25.00					52.00	23.00
27.06.22	35.00	1.10	63.00	1.40	49.00	14.00	47.00	13.00	44.00	13.00	44.00	17.00
	80.00	3.50	80.00	3.90	45.00	40.00	45.00	21.00	59.00	9.10	43.00	25.00
	78.00	5.00	63.00	2.40	43.00	26.00	44.00	19.00	43.00	18.00	38.00	29.00
	80.00	-0.15	54.00	2.10	48.00	19.00	39.00	18.00	48.00	53.00	45.00	20.00
	9.92	-2.40	61.00	5.70	47.00	32.00	43.00	29.00	45.00	27.00	40.00	30.00
	65.00	3.10	37.00	4.60	46.00	39.00	45.00	25.00	52.00	56.00	41.00	23.00
	79.00	3.80			43.00	32.00	45.00	23.00	55.00	9.10	37.00	27.00
	73.00	1.20			47.00	42.00	56.00	15.00	56.00	13.00	41.00	17.00
	9.92	-16.00			41.00	44.00	45.00	9.50	45.00	30.00	39.00	30.00
	9.92	-15.00			39.00	40.00	42.00	41.00	42.00	8.40	35.00	27.00
N	**50.00**	**50.00**	**19.00**	**19.00**	**30.00**	**30.00**	**34.00**	**34.00**	**31.00**	**31.00**	**35.00**	**35.00**
AV	**63.49**	**2.33**	**64.26**	**8.82**	**56.57**	**27.96**	**35.76**	**27.40**	**55.16**	**22.37**	**46.77**	**26.71**
STD	**27.50**	**7.43**	**13.81**	**4.26**	**11.94**	**11.69**	**20.41**	**11.85**	**8.45**	**14.08**	**9.66**	**9.82**

N: number of observations, AV: average, STD: standard deviation.

Table S10: FRET efficiencies and Binding related to Fig. 4 and 5.

Date	**WOX5-mV(N) PLT3-mV(N)**		**WOX5-mV(N) PLT3-mV(N) mCherry-NLS**		**WOX5-mV(N) PLT3-mV(N) BRAVO-mCh**		**WOX5-mV(N) PLT3-mV(N) BES1D-mCh**		**WOX5-mV(N) PLT3-mV(N) TPL-mCh**	
	FRET E	**Binding**	**FRET E**	**Binding**	**FRET E**	**Binding**	**FRET E**	**Binding**	**FRET E**	**Binding**
16.03.2020	80.00	4.90			55.00	23.00	59.00	11.00	39.00	33.00
	80.00	6.50			50.00	52.00	53.00	18.00	39.00	15.00
	80.00	68.00			51.00	42.00	43.00	29.00	44.00	25.00
	80.00	-2.30			47.00	34.00	46.00	19.00	34.00	34.00
	10.10	-7.00			48.00	48.00	55.00	15.00	38.00	30.00
	80.00	8.90			46.00	45.00	61.00	33.50	40.00	26.00
	80.00	6.00			45.00	38.00	42.00	20.00	49.00	25.00

	78.00	8.80			52.00	50.00	48.00	24.00	48.00	18.00
	79.00	4.50			49.00	39.00	45.00	26.00	43.00	22.00
	80.00	5.10			46.00	36.00	43.00	33.00	39.00	31.00
							51.00	35.00	43.00	34.00
							44.00	39.00	48.00	29.00
							44.00	23.00	44.00	51.00
							46.00	28.00	48.00	20.00
									41.00	29.00
18.12.2020	9.96	-18.00	65.00	4.70	53.00	43.00	57.00	7.20	33.00	16.00
	9.96	-11.00	63.00	7.00	51.00	45.00	43.00	15.00	34.00	26.00
	80.00	-4.20	61.00	5.20	51.00	19.00	41.00	15.00	32.00	24.00
	9.96	-4.70	51.00	8.80	43.00	21.00	49.00	12.00	37.00	26.00
	9.96	-7.60	48.00	5.00	45.00	30.00	41.00	28.00	41.00	13.00
	73.00	2.60			48.00	48.00	45.00	13.00	33.00	28.00
	80.00	4.20			48.00	38.00	46.00	7.80	39.00	21.00
	54.00	2.20			51.00	25.00	55.00	6.05	41.00	14.00
	71.00	3.20			49.00	27.00	44.00	15.00	27.00	10.00
	18.00	3.70			45.00	36.00	39.00	10.00	35.00	20.00
							42.00	14.00		
							50.00	14.00		
							37.00	24.00		
							50.00	12.00		
							39.00	12.00		
21.12.2020	9.95	-15.00	12.00	-2.70	53.00	42.00	42.00	18.00	39.00	17.00
	9.95	-5.20	9.95	-9.10	51.00	48.00	41.00	13.00	31.00	29.00
	10.00	-3.60	10.00	4.30	46.00	34.00	56.00	6.90	43.00	19.00
	48.00	-0.40	51.00	5.20	47.00	25.00	44.00	22.00	45.00	18.00
	69.00	2.60	63.00	1.00	51.00	12.00	42.00	17.00	55.00	9.30
	17.00	8.30			46.00	18.00	39.00	16.00	42.00	14.00
	57.00	5.50			51.00	53.00	36.00	12.00	36.00	31.00
	9.95	-2.00			46.00	40.00	45.00	20.00	37.00	24.00
	9.95	-8.30			47.00	40.00	40.00	20.00	41.00	15.00
	9.95	-7.00			50.00	38.00	37.00	23.00	36.00	19.00
							41.00	16.00		
							38.00	26.00		
AV	**46.46**	**1.62**	**43.40**	**2.94**	**48.70**	**36.30**	**45.34**	**18.74**	**39.83**	**23.29**
SD	**31.88**	**14.13**	**22.14**	**5.01**	**2.88**	**10.73**	**6.24**	**8.03**	**5.75**	**8.29**
N	**30.00**	**30.00**	**10.00**	**10.00**	**30.00**	**30.00**	**41.00**	**41.00**	**35.00**	**35.00**

N: number of observations, AV: average, STD: standard deviation.

Table S11: FRET efficiencies and Binding related to Fig. S2 and 5.

Date	BRAVO-mV(N) PLT3-mV(N)		BRAVO-mV(N) PLT3-mV(N) mCherry-NLS		BRAVO-mV(N) PLT3-mV(N) WOX5-mCh		BRAVO-mV(N) PLT3-mV(N) BES1D-mCh		BRAVO-mV(N) PLT3-mV(N) TPL-mCh	
	Binding	FRET E	Binding	FRET E	Binding	FRET E	Binding	FRET E	Binding	FRET E
03.07.23	0.00	10.17	0.00	8.47	31.40	44.41	7.10	10.17	11.00	49.15
	0.00	80.03	2.00	80.03	40.29	42.37	0.00	10.17	16.49	31.53
	2.35	80.03	0.00	8.47	35.98	42.81	0.00	10.17	1.46	80.03
	0.00	10.17	0.00	80.00	27.89	46.78	0.00	79.66	22.00	13.22
	0.00	80.03	0.00	10.17	30.09	38.98	0.00	10.17	25.10	14.58
	0.66	10.17					2.50	80.03	8.20	10.17
	1.33	10.17							7.02	10.17
05.07.23	0.00	80.00	2.51	79.97	26.61	46.67	6.72	43.33		
	0.00	10.00	0.00	10.00	26.49	40.67	11.10	26.67		
	0.00	10.00	10.60	15.67	8.29	51.00	16.37	31.67		
	0.00	79.97	4.10	60.00	23.92	33.33	18.80	38.33		
	0.00	10.00			36.81	46.53	13.05	35.67		
	14.20	10.00			43.11	43.00				
	1.80	10.33			8.91	63.33				
	0.00	10.00								
04.12.23	0.00	10.26	5.34	14.24	25.03	36.75	5.25	80.03	22.54	31.46
	1.85	30.46	5.97	25.17	50.54	48.01	13.14	35.43	19.53	36.09
	4.00	17.22	3.49	80.03	42.89	45.03	15.10	25.17	34.21	24.83
	9.00	10.26	2.99	10.26	27.60	42.72	4.95	40.40	35.26	26.16
	0.00	10.26	5.00	80.03	53.65	51.32	19.30	35.43	15.13	42.05
	1.06	27.15			45.49	45.43	17.91	28.81	21.90	32.45
	9.30	11.59			12.83	46.69	15.72	49.34	31.38	27.15
	0.00	80.13			19.65	45.36	14.77	45.36	25.12	31.79
	8.80	26.82			29.73	43.71	15.30	37.09	24.00	37.75
	1.87	80.03			36.98	44.70	11.88	37.75	34.16	29.80
16.12.23	0.00	79.93	5.30	10.03	33.80	48.16	11.34	39.80	17.02	56.52
	0.00	10.03	4.90	79.97	20.27	45.48	9.20	24.75	22.69	57.19
	0.00	10.03	8.70	79.97	29.88	43.48	11.19	42.14	16.94	49.16
	4.40	10.03	0.00	10.03	26.93	39.46	16.09	42.14	20.00	48.83
	0.00	10.03	0.00	10.03	28.11	45.15	18.74	39.80	15.68	61.20
	0.00	10.03			29.75	45.48	6.64	29.77	24.97	36.45
	8.86	10.03			33.79	50.84	4.34	29.77	31.80	29.10
	1.50	80.00			20.37	38.13	10.94	38.46	17.50	44.48
	0.00	10.03			26.92	46.82	8.10	43.14	27.25	28.76
	7.59	20.74			18.77	45.48	9.75	29.77	21.80	39.13
AV	2.24	30.18	3.21	39.61	29.77	44.94	10.17	37.11	21.12	36.27
SD	3.64	29.78	3.10	32.79	10.57	5.13	5.93	17.45	8.28	15.98
N	35.00	35.00	19.00	19.00	32.00	32.00	31.00	31.00	27.00	27.00

N: number of observations, AV: average, STD: standard deviation.

Table S12: Additional FRET efficiencies and Binding used for Fig. 5.

Sample	WOX5-mV PLT3-mCh	
Date	**FRET E**	**Binding**
20.12.2019	71	11
	53	44
	57	34
	56	40
	56	43
	62	27
	55	48
	54	41
	56	26
	52	36
AV	57.2	35
SD	5.268776	10.47855
N	10	10

N: number of observations, AV: average, STD: standard deviation.

Table S13: FRET efficiencies and Binding related to Fig. 6 and 7.

	BRAVO-mV		BRAVO-mV mCherry-NLS		BRAVO-mV PLT3-mCh		BRAVO-mV PLT3ΔPrD-mCh	
Date	FRET E	Binding	FRET E	Binding	FRET E	Binding	FRET E	Binding
23.03.2021	9.71	0.00			48	27	52	14
	9.71	0.00			51	19	49	23
	70.00	2.10			48	33	76	4.8
	76.00	3.40			58	8.2	79.9	5.6
	80.00	8.50			42	17	59	6.3
	10.00	0.00			43	7.7	79.9	4.7
	48.00	0.50			53	21	63	4.5
	9.71	0.00			45	35	43	7.9
	79.90	3.60			43	27	43	29
	9.71	0.00			56	22	43	44
06.04.2021	10.00	-10.00	56.00	0.81	61.00	7.50	54.00	7.10
	11.00	-3.70	46.00	1.90	78.00	3.70	65.00	2.90
	10.10	-8.00	80.00	1.00	43.00	27.00	42.00	23.00
	15.00	6.20	67.00	3.30	47.00	21	41.00	18.00
	14.00	10.00	71.00	3.70	42.00	25.00	80.00	0.50
	10.00	-1.50			48.00	24	9.70	-0.80
	33.00	4.30			48.00	19.00	64.00	2.60
	80.00	-3.60			51.00	19.00		
	80.00	0.18			54.00	20.00		
	14.00	5.00			46.00	38.00		
21.05.2021	80.00	7.80	62.00	2.80	50.00	29.00	46.00	12
	76.00	5.60	58.00	8.60	47.00	13.00	45.00	21.00
	45.00	0.29	35.00	7.30	52.00	32.00	45.00	9.10
	69.00	9.00	61.00	4.80	49.00	16.00	34.00	5.60
	54.00	4.30	56.00	4.90	47.00	23	35.00	8.80
	36.00	7.10			49.00	29.60	47.00	6.60
	9.93	0.00			33.00	13.00	39.00	12.00
	9.93	0.01			47.00	43.00	37.00	19.00
	9.93	0.01			47.00	50.60	40.00	14.00
	9.93	0.01			47.00	15.00	29.00	14.00
							37.00	8.90
AV	35.99	1.70	59.20	3.91	49.10	22.84	49.20	11.72
STD	29.38	4.59	11.94	2.43	7.50	10.53	16.38	9.58
n	30.00	30.00	10.00	10.00	30.00	30.00	28.00	28.00

N: number of observations, AV: average, STD: standard deviation.

Table S14: FRET efficiency and Binding values corresponding to Figure S4.

Date	TPL-mV		TPL-mV mCherry-NLS		TPL-mV PLT3-mCh		TPL-mV PLT3ΔPrD-mCh	
	FRET E	Binding	FRET E	Binding	FRET E	Binding	FRET E	Binding
12.04.2021	10.10	0.01	42.00	6.20	58.00	7.40	32.00	8.00
	10.10	0.00	53.00	3.50	40.00	16.00	35.00	7.00
	10.10	0.00	14.00	5.00	35.00	13.00	35.00	9
	10.00	0.01	47.00	6.90	36.00	8.00	41.00	7.60
	49.00	0.65	24.00	5.00	25.00	11.00	32.00	6.00
	55.00	2.20			41.00	16.00	46.00	12.00
	73.00	6.30			29.00	17.00	33.00	14.00
	10.10	0.01			30.00	9.50	50.00	9.7
	10.00	0.01			47.00	8.00	32.00	17.00
	30.00	5.10			35.00	12.00	43.00	11.00
					34.00	16.00	34.00	11.00
					25.00	19.00	36.00	16.00
					36.00	20.00	35.00	7.10
					34.00	18.00	27.00	6.80
					29.00	22.00	44.00	24.00
06.04.2021	10.00	-18.00	74.00	3.10	43.00	7.70	35.00	2.60
	10.00	-7.30	40.00	10.00	50.00	6.70	51.00	3.60
	10.00	5.10	47.00	7.70	42.00	12.00	64.00	2.90
	10.00	-0.80	39.00	6.00	46.00	9.80	43.00	11.00
	10.00	8.60	48.00	11.00	42.00	16.00	59.00	3.50
	11.00	3.40			46.00	11.00	26.00	4.60
	15.00	1.80			48.00	15.00	70.00	5.80
	10.00	-2.00			44.00	17.00	47.00	13.00
	27.00	0.86			47.00	19.00	47.00	12.00
	10.00	6.80			29.00	18.00	80.00	-0.48
AV	19.52	0.64	42.80	6.44	38.84	13.80	43.08	8.99
STD	17.91	5.51	15.32	2.44	8.31	4.42	13.19	5.26
n	20.00	20.00	10.00	10.00	25.00	25.00	25.00	25.00

N: number of observations, AV: average, STD: standard deviation.

Table S15: FRET efficiency and Binding values corresponding to Fig. S4.

Date	BES1-mV		BES1-mV mCherry-NLS		BES1-mV PLT3-mCh		BES1-mV PLT3ΔPrD-mCh	
	FRET E	Binding	FRET E	Binding	FRET E	Binding	FRET E	Binding
21.05.2021	9.91	-10.00	80.00	20.00	68.00	16.00	34.00	13.00
	10.00	-1.30	48.00	2.60	48.00	7.70	44.00	7.10
	80.00	0.95	46.00	5.70	45.00	9.90	54.00	8.00
	39.00	0.78	45.00	12.00				
	9.91	-2.40	50.00	7.60				
	54.00	3.40						
	18.00	4.40						
	9.91	-13.00						
	9.91	-12.00						
	9.91	-5.60						
27.04.2021	80.00	3.40	39.00	0.73	76.00	6.50	57.00	4.40
	80.00	0.00	60.00	5.70	59.00	8.90	54.00	6.30
	10.10	0.00	80.10	4.30	48.00	19.00	57.00	7.10
	10.10	0.00	80.00	1.00	43.00	23.00	45.00	18.00
	59.00	4.40	65.00	3.20	51.00	24.00	47.00	18.00
	67.00	4.40			45.00	35.00	13.00	2.20
	70.00	9.20			66.00	8.10	76.00	6.00
	55.00	9.70			55.00	6.10	56.00	3.50
	80.00	2.30			49.00	9.90	67.00	6.70
	80.00	2.00			46.00	22.00	51.00	8.3
28.05.2021	80.00	-3.50	10.00	-12.00	56.00	9.90		
	80.00	0.67	77.00	3.2	41.00	18.00		
	10.00	-12.00	63.00	7.00	45.00	20.00		
	80.00	7.50	49.00	7.00	47.00	26.00		
	80.00	-1.40	48.00	5.60	65.00	7.30		
	10.00	-12.00			42.00	23.00		
	80.00	1.40			42.00	27.00		
	80.00	6.60			45.00	28.00		
	57.00	7.20			48.00	19.00		
	64.00	5.10			46.00	14.00		
AV	48.76	0.01	56.01	4.91	51.13	16.88	50.38	8.35
STD	30.59	6.34	18.55	6.46	9.34	8.09	14.74	4.81
n	30.00	30.00	15.00	15.00	23.00	23.00	13.00	13.00

N: number of observations, AV: average, STD: standard deviation.

Table S16: Ratio of periclinal cell divisions in the QC related to Fig. 7.

Treatment	Genotype	Periclinal cell division planes in the QC [%]	Number of analysed roots
DMSO	*Col-0*	27	44
	plt3-1	73	45
	plt3-1, pWOX5:GR-PLT3-mT2	83	41
	plt3-1, pWOX5:GR-PLT3dPrD-mT2	94	36
DEX	*Col-0*	28	39
	plt3-1	87	46
	plt3-1, pWOX5:GR-PLT3-mT2	67	45
	plt3-1, pWOX5:GR-PLT3dPrD-mT2	100	36

References

Betegón-Putze, Isabel; Mercadal, Josep; Bosch, Nadja; Planas-Riverola, Ainoa; Marquès-Bueno, Mar; Vilarrasa-Blasi, Josep et al. (2021): Precise transcriptional control of cellular quiescence by BRAVO/WOX5 complex in Arabidopsis roots. In: *Molecular systems biology* 17 (6), e9864. DOI: 10.15252/msb.20209864.

Burkart, Rebecca C.; Strotmann, Vivien I.; Kirschner, Gwendolyn K.; Akinci, Abdullah; Czempik, Laura; Dolata, Anika et al. (2022): PLETHORA-WOX5 interaction and subnuclear localization control Arabidopsis root stem cell maintenance. In: *EMBO reports* 23 (6), e54105. DOI: 10.15252/embr.202154105.

Denninger, Philipp; Reichelt, Anna; Schmidt, Vanessa A. F.; Mehlhorn, Dietmar G.; Asseck, Lisa Y.; Stanley, Claire E. et al. (2019): Distinct RopGEFs Successively Drive Polarization and Outgrowth of Root Hairs. In: *Current biology : CB* 29 (11), 1854-1865.e5. DOI: 10.1016/j.cub.2019.04.059.

Galinha, Carla; Hofhuis, Hugo; Luijten, Marijn; Willemsen, Viola; Blilou, Ikram; Heidstra, Renze; Scheres, Ben (2007): PLETHORA proteins as dose-dependent master regulators of Arabidopsis root development. In: *Nature* 449 (7165), S. 1053–1057. DOI: 10.1038/nature06206.

Lampropoulos, Athanasios; Sutikovic, Zoran; Wenzl, Christian; Maegele, Ira; Lohmann, Jan U.; Forner, Joachim (2013): GreenGate---a novel, versatile, and efficient cloning system for plant transgenesis. In: *PloS one* 8 (12), e83043. DOI: 10.1371/journal.pone.0083043.

Maika, Jan Eric; Krämer, Benedikt; Strotmann, Vivien I.; Wellmer, Frank; Weidtkamp-Peters, Stefanie; Stahl, Yvonne; Simon, Rüdiger (2023): One pattern analysis (OPA) for the quantitative determination of protein interactions in plant cells. In: *Plant methods* 19 (1), S. 73. DOI: 10.1186/s13007-023-01049-3.

Vilarrasa-Blasi, Josep; González-García, Mary-Paz; Frigola, David; Fàbregas, Norma; Alexiou, Konstantinos G.; López-Bigas, Nuria et al. (2014): Regulation of plant stem cell quiescence by a brassinosteroid signaling module. In: *Developmental cell* 30 (1), S. 36–47. DOI: 10.1016/j.devcel.2014.05.020.

Summary

Stem cell homeostasis in the root apical meristem (RAM) of higher plants facilitates high developmental plasticity which allows the plant to adapt to biotic and abiotic stresses. In the center of the RAM, a pool of rarely dividing stem cells, termed the quiescent center (QC), is maintained and produces the surrounding tissue specific initials. The balance of stem cell quiescence and replenishment is regulated by a highly dynamic regulatory network, which, among other things, involves different phytohormones, peptides, receptors and transcription factors (TFs) e.g. BRASSINOSTEROID AT VASCULAR AND ORGANIZING CENTRE (BRAVO), PLETHORA 3 (PLT3) and WUSCHEL-RELATED HOMEOBOX 5 (WOX5). In this study new aspects of stem cell homeostasis in the root of the model plant *Arabidopsis thaliana* have been uncovered.

First, I contributed to the optimization and establishment of a novel fitting routine for Förster resonance energy transfer fluorescence lifetime imaging microscopy (FRET-FLIM) with multi-exponentially-decaying donor fluorophores that allowed us to distinguish between protein affinity and orientation/distance, which was tested using multiple MADS-box domain TFs that control flower development in *Arabidopsis*. This novel tool has the potential to improve our understanding of all biological processes that rely on protein-protein-interactions (PPI).

Next, I took part in investigations on the concerted mutual regulation of WOX5 and PLTs in the homeostasis of the stem cell niche in the *Arabidopsis* root. Here, we could demonstrate that both WOX5 and PLT3 control QC maintenance and columella stem cell (CSC) fate interdependently. Moreover, our data suggest that the regulation of CSC fate determination relies on the partitioning of WOX5-PLT3 heterodimers in so-called nuclear bodies (NBs). NB formation occurs only in CSCs and depends on intrinsically-disordered regions containing prion-like domains (PrDs) identified in the PLT3 aa sequence necessary for complex formation with WOX5. Furthermore, we hypothesized that NB formation is a result of liquid-liquid-phase-separation (LLPS).

Subsequently, the balance of stem cell quiescence and replenishment regulated by PLT3 and WOX5 was linked to the brassinosteroid-dependent TF BRAVO. Mutant analysis, and their overlapping expression pattern in specific cell types of the root, support the hypothesis that these TFs exhibit a combinatory triangle in regulating

stem cell maintenance. Additionally, FRET-FLIM studies were performed to obtain quantitative interaction data that together with the novel analysis routine allowed us to decipher variations in protein affinities for different heterodimer and oligomer compositions. The following computational modelling, which combined cell type specific protein abundances and variations in protein affinities, revealed unique cell type specific protein complex 'signatures' that contribute to stem cell homeostasis in the root.

In summary, the results of this study add another layer to the intricate regulatory network that balances stem cell maintenance and replenishment in the *Arabidopsis* root. Interdisciplinary approaches like the combination of experimental data and computational modelling offer a great potential for all fields of plant research.

Zusammenfassung

Die Stammzellenhomöostase im Wurzelapikalmeristem (engl. *root apical meristem*, RAM) höherer Pflanzen ermöglicht eine hohe Entwicklungsplastizität, die es der Pflanze erlaubt, sich an biotische und abiotische Stressfaktoren anzupassen. Im Zentrum des Wurzelapikalmeristems befindet sich ein Pool von sich kaum teilenden Stammzellen, das so genannte ruhende Zentrum (engl. *quiescent center*, QC), das die umliegenden gewebespezifischen Initialen produziert. Das Gleichgewicht von Stammzellruhe und -nachschub wird durch ein hochdynamisches Netzwerk reguliert, an dem unter anderem verschiedene Phytohormone, Peptide, Rezeptoren und Transkriptionsfaktoren (engl. *transcription factors*, TFs) beteiligt sind, z.B. BRASSINOSTEROID AT VASCULAR AND ORGANIZING CENTRE (BRAVO), PLETHORA 3 (PLT3) und WUSCHEL-RELATED HOMEOBOX 5 (WOX5). In dieser Studie wurden neue Aspekte der Stammzell-Homöostase in der Wurzel der Modellpflanze *Arabidopsis thaliana* aufgedeckt.

Zunächst trug ich zur Optimierung und Etablierung einer neuartigen Analyseroutine für die Förster-Resonanz-Energie-Transfer-Fluoreszenz-Lebenszeit-Imaging-Mikroskopie (FRET-FLIM) mit exponentiell zerfallenden Donor-Fluorophoren bei, die es uns ermöglichte, zwischen Proteinaffinität und Orientierung/Distanz zu unterscheiden, was anhand mehrerer MADS-Box-Domänen-TFs getestet wurde, die die Blütenentwicklung in *Arabidopsis* steuern. Dieses neue Instrument hat das Potenzial, unser Verständnis aller biologischen Prozesse zu verbessern, die auf Protein-Protein-Interaktionen (PPIs) beruhen.

Desweiteren beteiligte ich mich an Untersuchungen zur abgestimmten, gegenseitigen Regulierung von WOX5 und PLTs bei der Homöostase der Stammzellnische in der *Arabidopsis*-Wurzel. Hier konnten wir zeigen, dass sowohl WOX5 als auch PLT3 die Aufrechterhaltung des QCs und das Schicksal der Columella-Stammzellen (engl. *columella stem cells*, CSCs) in gegenseitiger Abhängigkeit steuern. Darüber hinaus deuten unsere Daten darauf hin, dass die Regulierung der Bestimmung des CSC-Schicksals von der Verteilung von WOX5-PLT3-Heterodimeren in sogenannten Kernkörperchen (engl. *nuclear bodies*, NBs) abhängt. Die Bildung von NBs erfolgt nur in CSCs und hängt von intrinsisch ungeordneten Regionen ab, die prion-ähnliche Domänen (engl. prion-like domains, PrDs) enthalten, die in der PLT3 Aminosäure-Sequenz identifiziert wurden und für

die Komplexbildung mit WOX5 notwendig sind. Darüber hinaus stellten wir die Hypothese auf, dass die Bildung von NB eine Folge von Flüssig-Flüssig-Phasen-Separation (engl. *liquid-liquid phase separation*, LLPS ist.

Anschließend wurde das von PLT3 und WOX5 regulierte Gleichgewicht zwischen Stammzellruhe und -erneuerung mit dem Brassinosteroid-abhängigen TF BRAVO in Verbindung gebracht. Eine Mutantenanalyse und ihr sich überschneidendes Expressionsmuster in bestimmten Zelltypen der Wurzel stützen die Hypothese, dass diese TFs ein kombinatorisches Dreieck bei der Regulierung der Stammzellerhaltung bilden. Zusätzlich wurden FRET-FLIM-Studien durchgeführt, um quantitative Interaktionsdaten zu erhalten, die es uns zusammen mit der neuartigen Analyseroutine ermöglichten, Variationen der Proteinaffinitäten für verschiedene Heterodimer- und Oligomerzusammensetzungen zu entschlüsseln.

Die anschließende computergestützte Modellierung, bei der zelltypspezifische Proteinhäufigkeiten und Variationen der Proteinaffinitäten kombiniert wurden, ergab einzigartige, zelltypspezifische Proteinkomplex-„Signaturen“, die zur Stammzell-Homöostase in der Wurzel beitragen.

Zusammenfassend lässt sich sagen, dass die Ergebnisse dieser Studie das komplizierte regulatorische Netzwerk, das die Erhaltung und Erneuerung der Stammzellen in der *Arabidopsis*-Wurzel ausbalanciert, um eine Ebene erweitern. Interdisziplinäre Ansätze wie die Kombination von experimentellen Daten und mathematischer Modellierung bieten ein großes Potenzial für alle Bereiche der Pflanzenforschung.

Appendix

1. List of Abbreviations

~	Around
°C	Degree Celsius
µ	Micro
2D	2-dimensional
35S	Promoter of the *Cauliflower Mosaic Virus*
3D	3-dimensional
Å	Ångström
A. thaliana	*Arabidopsis thaliana*
A1	First acceptor
A2	Second acceptor
ABA	Abscisic acid
ACR4	ARABIDOPSIS CRINKLY 4
AG	AGAMOUS
ALOG	Arabidopsis LSH1 and Oryza G1
AMP	Adenosine monophosphate
AN	ANANTHA
AP1	APETALA1
AP2	APETALA2
AP3	APETALA3
APB	Acceptor photobleaching
ARF	AUXIN RESPONSE FACTOR
ATP	Adenosine triphosphate
BBM	BABYBOOM; PLETHORA 4
BES1	BRI1-EMS-SUPRRESSOR 1
BiFC	Bimolecular fluorescence complementation
Binding	Relative amplitude of the FRET fraction
bp	Base pairs
BR	Brassinosteroids

BRAVO	BRASSINOSTEROIDS AT VASCULAR AND ORGANIZING CENTER
c	Cortex
CC	Columella cell
CDF4	CYCLIN DOF FACTOR 4
CEI	Cortex endodermis initial
CLE40	CLAVATA3/EMBRYOSURROUNDING REGION 40
CLV3	CLAVATA3
Co-IP	Co-immunoprecipitation
Col	*Arabidopsis thaliana* ecotype Columbia
Col-0	*Arabidopsis thaliana* ecotype Columbia
CRN	CORYNE
CSC	Columella stem cell
CYCD1;1	CYCLIND1;1
CYCD3;3	CYCLIND3;3
CYCD6;1	CYCLIND6;1
D	Donor fluorophore
Da	Dalton
DAG	Days after germination
DEX	Dexamethasone
DMSO	Dimethylsulfoxide
DNA	Desoxy ribonucleic acid
EAR	ERF-associated amphiphilic repression
eCFP	Enhanced cyan fluorescent protein
EdU	5-ethynyl-2’-deoxyuridine
E_{FRET}	FRET efficiency
eGFP	Enhanced green fluorescent protein
ELF3	EARLY FLOWERING 3
EMSA	Electrophoretic mobility shift essay
en	Endodermis
ep	Epidermis

erCFP	Endoplasmatic reticulum targeted cyan fluorescent protein
ERF115	ETHYLENE RESPONSE FACTOR 115
ESP	EXTRA SPINDLE POLES
EU	5-ethynyl-2'-uridine
eYFP	Enhanced yellow fluorescent protein
FCA	FLOWERING CONTROL LOCUS A
FCCS	Fluorescence cross-correlation spectroscopy
FCS	Fluorescence correlation spectroscopy
FLC	FLOWERING LOCUS C
FLIM	Fluorescence Lifetime Imaging
FM	Floral meristem
FP	Fluorescent protein
FQM	Floral quartet model
FRAP	Fluorescence recovery after photobleaching
FRET E	FRET efficiency
FRET	Förster Resonance Energy Transfer
FRI	FRIGIDA
g	gram
GFP	Green fluorescent protein
GR	Glucocorticoid receptor
GRN	Gene regulatory network
h	hour
HDA19	HISTONE DEACETYLASE 19
HPLC	High performance liquid chromatography
i	Components
$I_{\|\|}$	Intensity of the emitted light parallel to polarized excitation light
$I_{\perp}$	Intensity of the emitted light perpendicular to polarized excitation light
$I_{D\ after}$	Intensity of donor fluorescence after bleaching
$I_{D\ before}$	Intensity of donor fluorescence before bleaching
I_D	Intensity of donor fluorescence

IDR	Intrinsically disordered region
J(λ)	Integral of donor emission and acceptor absorption spectra
JA	Jasmonate
JKD	JACKDAW
k	kilo
kb	Kilo base pairs
KIN7	Kinesin 7
KISC	Kinesin-separase complex
KSP	Knocksideways in plants
l	litre
LCD	Low-complexity domain
LC-MS	Liquid chromatography-mass spectrometry
LLPS	Liquid-liquid phase separation
LRC	Lateral root cap
LRP	Lateral root primordia
LRR	Leucine-rich repeat
m	milli
M	Molar
mCh	mCherry
min	minute
MP	MONOPTEROS
mPS-PI	Modified pseudo Schiff base propidium iodide
MR	Middle region
mRFP	Mono red fluorescent protein
MS	Mass-spectrometry
mT2	mTurquoise2
mV	mVenus
mV(C)	C-terminal part of mVenus
mV(N)	N-terminal part of mVenus
mVc	C-terminal part of mVenus
mVn	N-terminal part of mVenus

N	Newton
n	Number of observations
N. benthamiana	*Nicotiana benthamiana*
NB	Nuclear body
NLS	Nuclear localization sequence
Nluc	Nano luciferase
nm	Nanometer
ns	Nanosecond
OPA	One pattern analysis
PB1	Phox and Bem1p
pBRAVO	Promoter of *BRAVO*
PHB3	PROHIBITIN 3
PI	PISTILLATA
PIF	PHYTOCHROME INTERACTING FACTOR
PIN	PINFORMED
PLT3	PLETHORA 3
PM	Plasma membrane
POI	Protein of interest
polyQ	Poly-glutamine
PPI	Protein-protein interaction
pPLT3	Promoter of *PLT3*
PrD	Prion-like domain
PSK5	PHYTOSULFOKINES 5
pWOX5	Promoter of *WOX5*
Q	Glutamine
QC	Quiescent center
QHB	QUIESCENT-CENTER-SPECIFIC HOMEOBOX
r	Anisotropy
R	Arginine
R_0	Förster radius
RAM	Root apical meristem

RBOH	Respiratory burst oxidase homolog
RBR	RETINOBLASTOMA-RELATED
R_{DA}	Distance between donor and acceptor fluorophores
RICS	Raster image correlation spectroscopy
RLK	Receptor-like kinase
RM	Repression motif
RNA	Ribonucleic acid
ROS	Reactive oxygen species
ROW1	REPRESSOR OF WUSCHEL 1
rpm	rounds per minute
s	second
SA	Salicylic acid
SAM	Shoot apical meristem
SCN	Stem cell niche
SCR	SCARECROW
SD	Standard deviation
SEP3	SEPALLATA3
SEU	SEUSS
SFH8	SEC FOURTEEN-HOMOLOG8
SHR	SHORTROOT
SI	Stele initials
TCP	Plant-specific teosinte-branched cycloidea PCNA
TCSPC	Time correlated single photon counting
T-DNA	Transfer-DNA
TEM	Transmission electron microscopy
TF	Transcription factor
TFAM	TMF FAMILY MEMBERS
TMF	TERMINATING FLOWER
TPL	TOPLESS
TRP	TOPLESS-RELATED proteins
v/v	volume per volume

VA-TIRF	Variable angle total internal reflection microscopy
VRN1	VERNALIZATION 1
W	Watt
w/v	weight per volume
WOX5	WUSCHEL-RELATED HOMEOBOX 5
WT	Wildtype
WUS	WUSCHEL
Y2H	Yeast two-hybrid
YFP	Yellow fluorescent protein
*Zm*WOX5	*Zea mays* WOX5
α	Pre-exponential factor (amplitude)
α_i	Sum of each component's amplitude
κ^2	Dipole orientation
τ	Fluorescence lifetime
τ_D	Donor fluorescence lifetime in the absence of the acceptor
τ_{DA}	Donor fluorescence lifetime in the presence of the acceptor
τ_i	Sum of each component's lifetime
τ_m	Amplitude-weighted lifetime

2. Exemplary plasmid maps

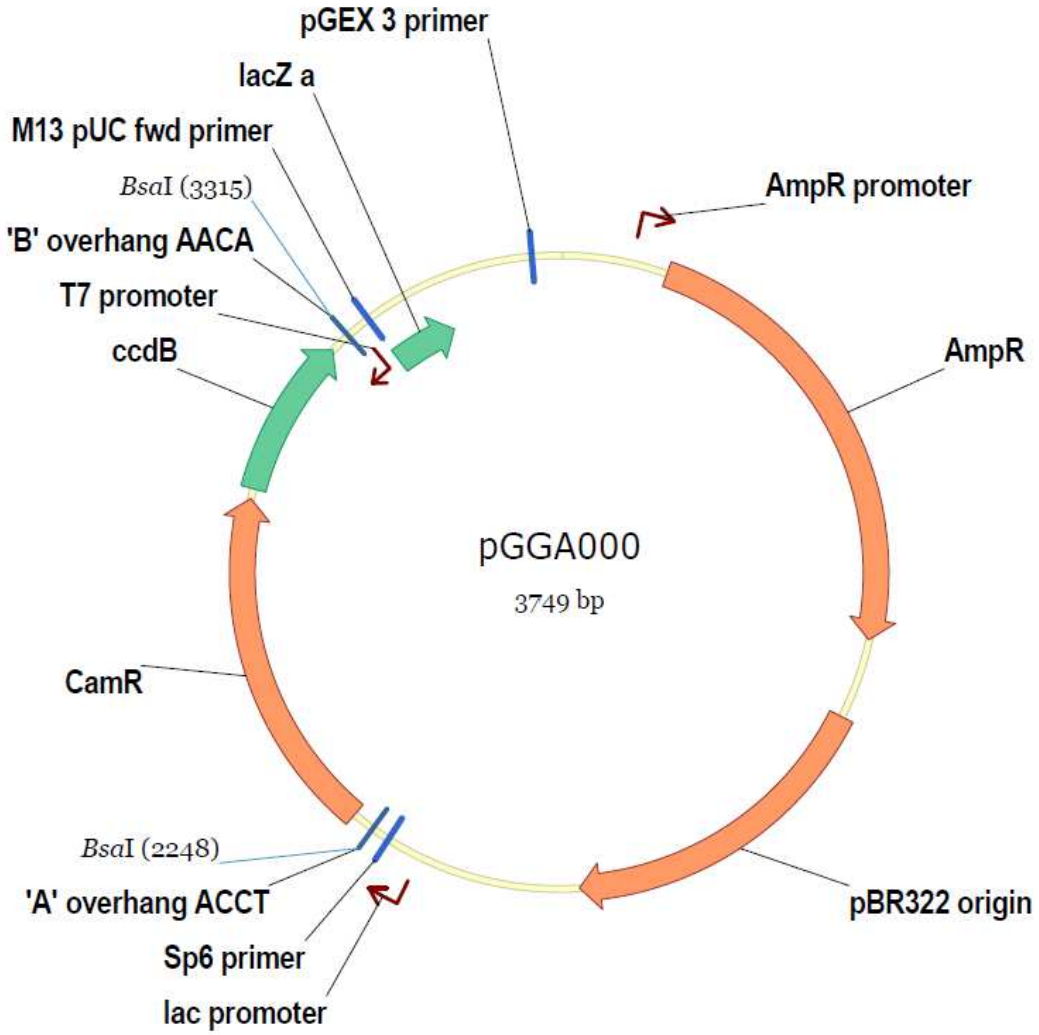

Figure A-1: Exemplary empty GreenGate pGGA000 entry vector. Exemplary plasmid map of the empty pGGA000 entry vector, thought to harbour the upstream regulatory sequence of a gene of interest (GOI). AmpR: Ampicillin resistance; pBR322 origin: origin of replicate; lac promoter: lactose promoter; CamR: Chloramphenicol resistance; *ccdB*: encodes a cytotoxic gene as a negative selection marker; *lacZ*: encodes β-galactosidase coding gene. Two *Bsa*I recognition sites, 'A' overhang ACCT and 'B' overhang AACA for the directed integration of desired DNA-fragment with restriction digest/ligation. Sp6 primer, T7 primer, M13 pUC fwd primer and pGEX 3 primer are commonly used primers for sequencing.

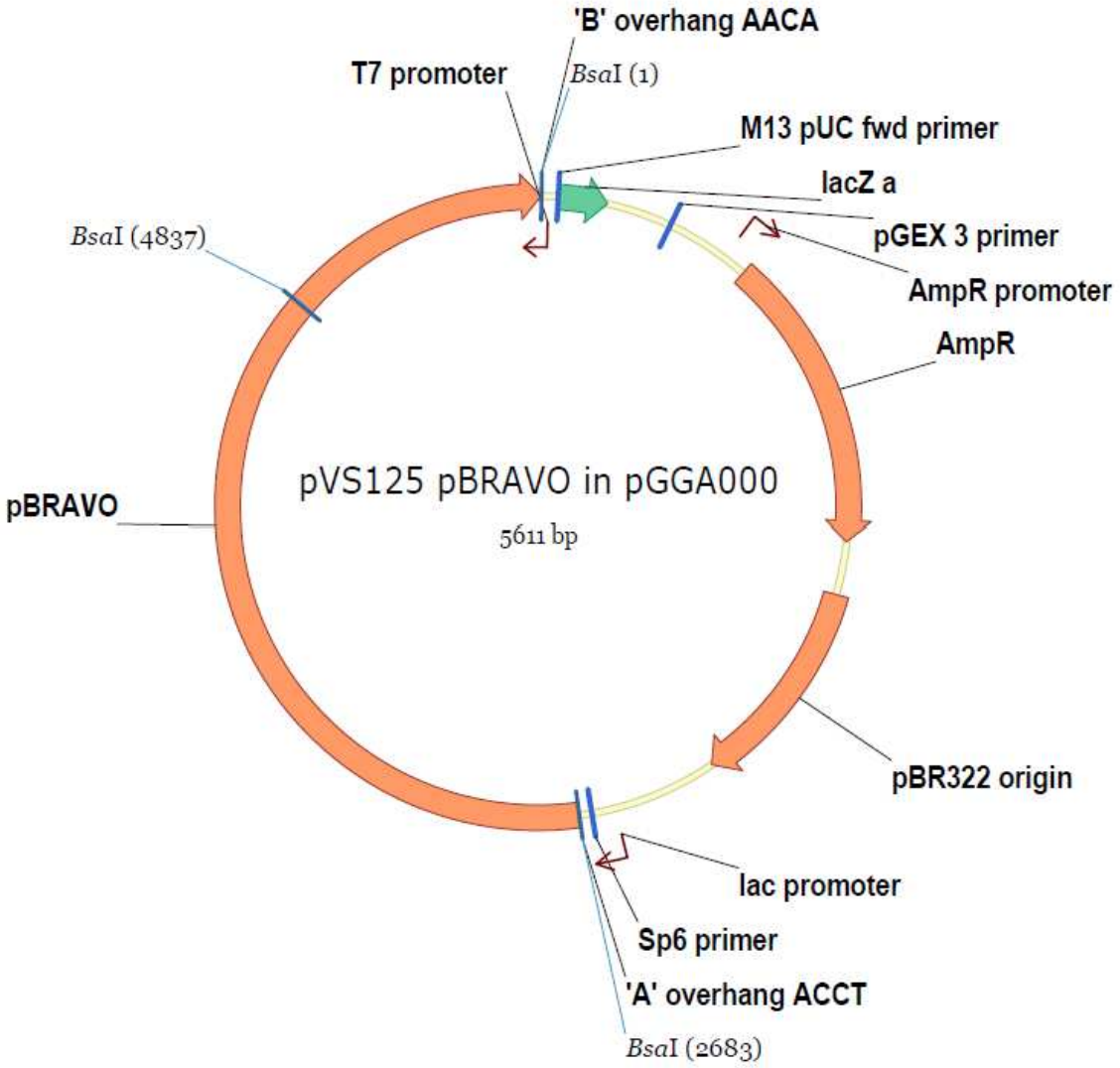

Figure A-2: GreenGate entry vector harbouring the *BRAVO* promoter (*pBRAVO*) sequence. Used together with six other GreenGate entry modules to create a plant expression cassette in the GreenGate destination vector. BRAVO: BRASSINOSTEROIDS AT VASCULATURE AND ORGANIZING CENTER; AmpR: Ampicillin resistance; pBR322 origin: origin of replicate; lac promoter: lactose promoter; *lacZ*: encodes β-galactosidase coding gene. Two *Bsa*I recognition sites, 'A' overhang ACCT and 'B' overhang AACA were used to replace the chloramphenicol resistance as well as the *ccdB* gene with *BRAVO* promoter sequence. Sp6 primer, T7 primer, M13 pUC fwd primer and pGEX 3 primer are commonly used primers for sequencing.

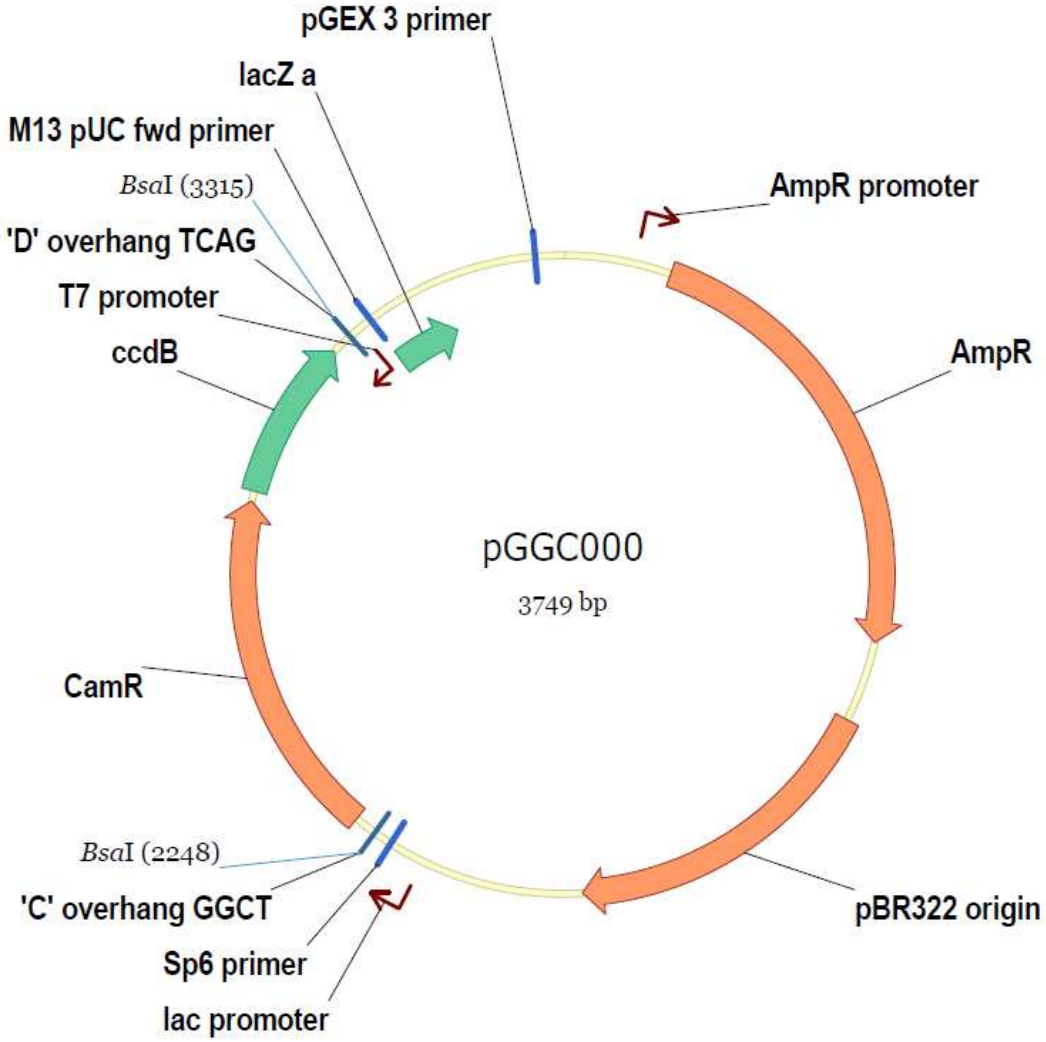

Figure A-3: Exemplary empty GreenGate pGGC000 entry vector. Exemplary plasmid map of the empty pGGA000 entry vector, thought to harbour the coding sequence (CDS) of a protein of interest (POI). AmpR: Ampicillin resistance; pBR322 origin: origin of replicate; lac promoter: lactose promoter; CamR: Chloramphenicol resistance; *ccdB*: encodes a cytotoxic gene as a negative selection marker; *lacZ*: encodes β-galactosidase coding gene. Two *Bsa*I recognition sites, 'C' overhang GGCT and 'D' overhang TCAG for the directed integration of desired DNA-fragment with restriction digest/ligation. Sp6 primer, T7 primer, M13 pUC fwd primer and pGEX 3 primer are commonly used primers for sequencing.

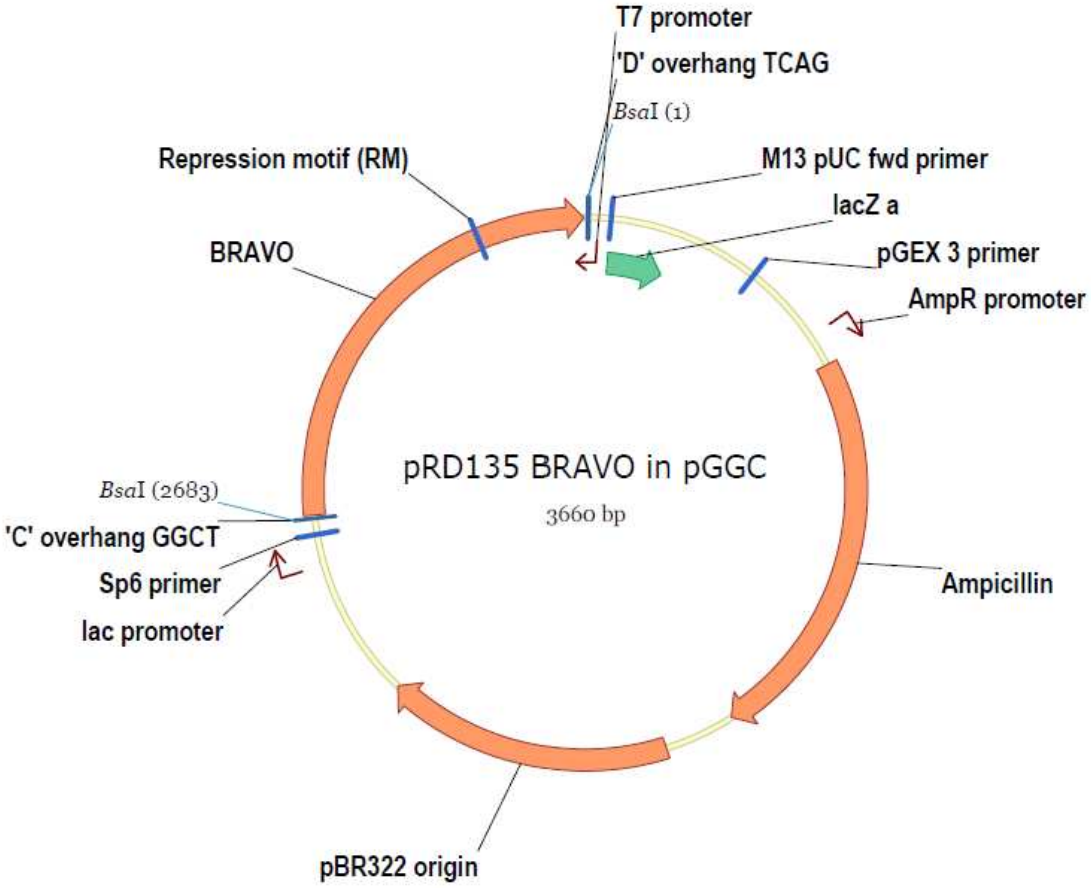

Figure A-4: GreenGate entry vector harbouring the BRAVO CDS. Used together with six other GreenGate entry modules to create a plant expression cassette in the GreenGate destination vector. BRAVO: BRASSINOSTEROIDS AT VASCULATURE AND ORGANIZING CENTER; AmpR: Ampicillin resistance; pBR322 origin: origin of replicate; lac promoter: lactose promoter; *lacZ*: encodes β-galactosidase coding gene. Two *Bsa*I recognition sites, 'C' overhang GGCT and 'D' overhang TCAG were used to replace the chloramphenicol resistance as well as the *ccdB* gene with BRAVO CDS. Sp6 primer, T7 primer, M13 pUC fwd primer and pGEX 3 primer are commonly used primers for sequencing.

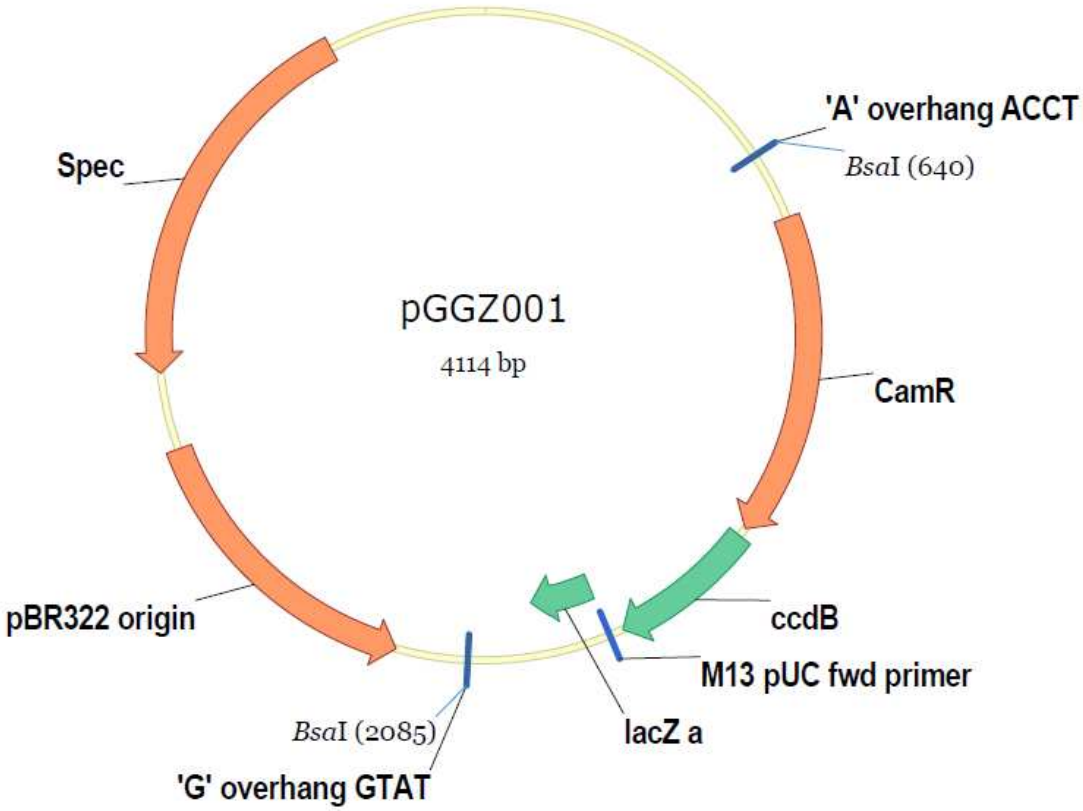

Figure A-5: Exemplary empty GreenGate pGGZ001 destination vector. Plasmid map of the empty GreenGate destination vector pGGZ001 for the integration of an expression cassette. Spec: Spectinomycin resistance; pBR322 origin: origin of replicate; CamR: Chloramphenicol resistance; *ccdB*: encodes a cytotoxic gene as a negative selection marker; *lacZ*: encodes β-galactosidase coding gene. Two *Bsa*I recognition sites, 'A' overhang ACCT and 'G' overhang GTAT for the directed integration of the desired DNA-fragments with restriction digest/ligation. M13 pUC fwd primer is commonly used for sequencing.

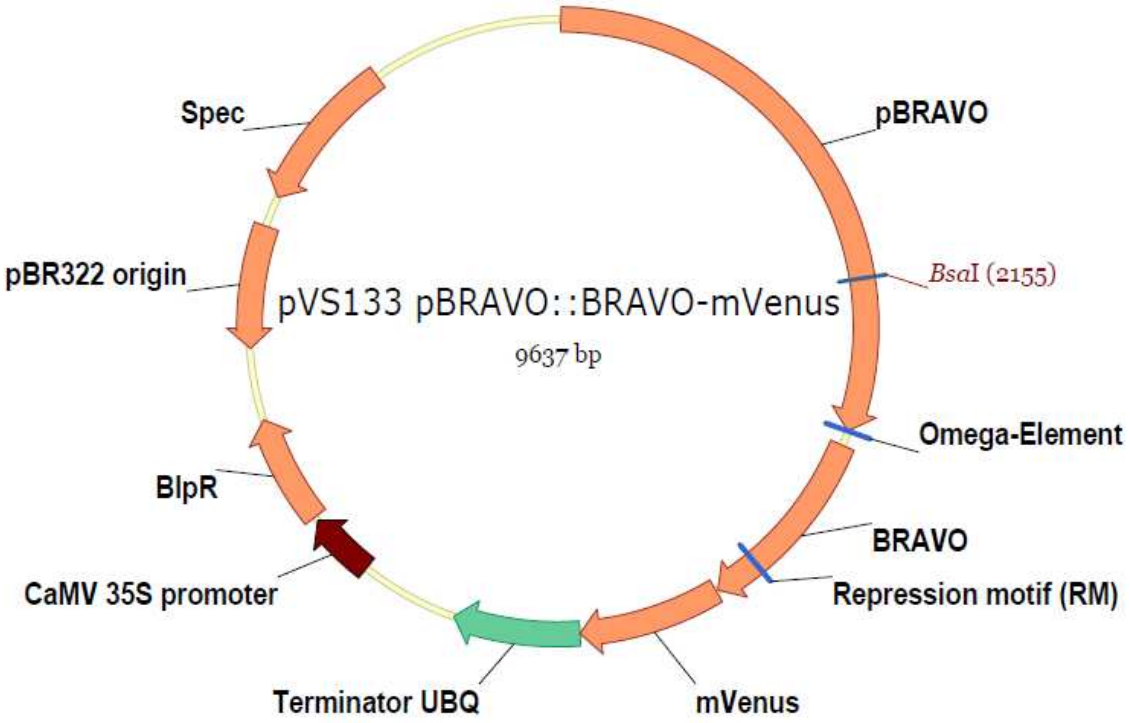

Figure A-6: Exemplary GreenGate pGGZ001 destination vector with *pBRAVO::BRAVO-mVenus*. Spec: Spectinomycin resistance; pBR322 origin: origin of replicate; *pBRAVO*: *BRAVO* promoter sequence; Omega-element: translational enhancer; BRAVO: BRAVO CDS; mVenus: fluorescent protein for microscopic visualization; Terminator UBQ: UBIQUITIN 10 terminator; *CaMV 35S* promoter: consecutive promoter from cauli flower mosaic virus used to drive the expression of BlpR: bialaphos resistance conferring resistance to the herbicide BASTA (containing phosphinothricin) for plant selection.

3. List of figures

4. List of tables

5. List of supplementary figures

6. List of supplementary tables

Acknowledgements

First and most importantly, I want to thank Yvonne for the opportunity to do my PhD with her. Thank you for your guidance during my master's thesis and during my PhD and for always supporting me even when times were tough. Thanks for always believing in me, especially when I did not. I could not have wished for a better supervisor. Thank you!

Thanks also to Rüdiger for being my co-supervisor and for providing the lab and office space (also after my PhD), as well as for insightful discussions and conversations, sometimes science related, sometimes about life.

Thanks to all members of the Center for Advanced Imaging (CAi), for taking care of the microscopes and for your support in all matters, whether related to microscopy or how to efficiently handle the massive amount of data. Special thanks go to Steffi and Sepp, who were always there when the microscope had other plans than me.

A big thank you to all former and current AG Stahl and AG Simon lab members, who have been along the way. It may not have seemed like it in the end, but you made these years one of the best times of my life. Thanks to Jenia and Paddy: Believe it or not, you made me want to start my PhD.

Special thanks to the master's and bachelor's students Perli, Sascha and Vanessa, whom I supervised during my time and who accompanied me on this journey.

Thanks to Cornelia, Carin and Silke for keeping the lab equipped and tidy and for your support with my big genotyping experiments.

A big thank you to Karine, Anika, Jan and Isaia: I really enjoy your company, both inside and outside the lab. Karine, thank you for taking care of literally everything. I am pretty sure the lab would fall apart if you left. Thank you, Anika, for the numerous coffee and tea breaks and your sympathetic ear. Someday I may master latté art like you. Jan, thank you for broadening my culinary horizons and for always being there on the dance floor with us. Thanks to Isaia. We have started this journey together and it was always comforting to have someone next to me who knows exactly what I was going through. We are almost there!

A huge thank you goes to Meik. Words cannot describe what it means to me that you came to this lab a few years ago. I do not want to imagine it without you. I have found a lifetime friend in you.

I also want to thank my friends outside the lab, especially Lilith, Aline and Laura, who always supported me during the ups and downs of this adventure. Thank you for listening to the same problems over and over again and distracting me from them.

Außerdem möchte ich mich noch bei meiner Familie bedanken, bei dem Teil, der diesen Tag mit mir erleben kann, aber auch bei dem Teil, der das nicht kann. Ihr habt immer an mich geglaubt, auch wenn ihr nicht so richtig verstanden habt, was genau ich eigentlich mache. Das macht das Ganze eigentlich noch schöner. Danke!

‘And last but not least, I wanna thank me
I wanna thank me for believing in me
I wanna thank me for doing all this hard work
I wanna thank me for having no days off
I wanna thank me for never quitting’

Calvin Cordozar Broadus Jr., better known as Snoop Dogg